N° d'ordre :
Année : 2010

UNIVERSITE ABDEL MALEK ESSAADI
FACULTE DES SCIENCES
TETOUAN

THESE

Présentée

Pour l'obtention du

DOCTORAT EN SCIENCES

Par :

Bilal El Bakkari

Discipline : Physique

Spécialité : Physique Nucléaire

TITRE: Development of a new Monte Carlo burnup computer code – Application to the calculation of neutronics and burnup parameters of TRIGA MARK II Moroccan Research Reactor –

Soutenue le 12 juin 2010 devant le jury composé de :

Mr A. Kamili	Professeur	Faculté des Sciences - Tétouan	Président
Mr E. Chakir	Professeur	Faculté des Sciences - Kénitra	Rapporteur
Mr O. El Hajjaji	Professeur	Faculté des Sciences - Fès	Rapporteur
Mr H. Boukhal	Professeur	Faculté des Sciences - Tétouan	Rapporteur
Mr L. Erradi	Professeur	Faculté des Sciences – Rabat	Invité
Mr A. Jehouani	Professeur	Faculté des Sciences – Marrakech	Examinateur
Mr. B. Nacir	Ingénieur	CNESTEN-CENM	Invité
Mr T. El Bardouni	Professeur	Faculté des Sciences – Tétouan	Directeur

« الحمد لله الذي هدانا لهذا وما كنا لنهتدي لولا أن هدانا الله »

Préface

Le travail de recherche effectué par Monsieur Bilal El Bakkari constitue une contribution originale aux études neutroniques et aux études liées à l'évolution du combustible nucléaire des réacteurs refroidis à eau. Il s'est intéressé particulièrement au développement d'un code BUCAL-1 de calcul burnup permettant de résoudre les équations de combustion des chaînes de l'uranium, plutonium et du thorium, et de la production des différents précurseurs moyennant la méthode de Rung kutta. Il s'est intéressé spécialement à améliorer l'algorithme adopté en introduisant la technique Predictor-Corrector et élaborer un moyen numérique lui permettant de coupler son code à un code de calcul neutronique de référence international MCNP5 basé sur la méthode de Monte Carlo.

La validation et la vérification du système BUCAL1-MCNP5 a été réalisé en reproduisant les résultats disponibles dans la littérature qui sont obtenus pour des benchmarks consacrés au thème de la thèse. Le code permet de reproduire ses résultats avec une bonne précision. Ce qui a poussé le candidat à l'appliquer au réacteur de recherche marocain TRIGA MARK II du CENM de la Maâmora. Cet exercice permet de prévoir la durée de vie du combustible de ce réacteur et par conséquent l'étude actuelle sera la base de l'établissement d'un plan de gestion du fonctionnement du réacteur TRIGA afin de mieux exploiter le combustible actuellement disponible. Pour mener à bien ses prévisions sur le réacteur TRIGA, le candidat a contribué à l'amélioration du model MCNP de ce réacteur afin de tenir compte des données As-Built du constructeur Genaral Atomics. Ces améliorations ont permis de reproduire correctement les paramètres neutroniques de ce réacteur et par conséquent les prévisions du calcul burnup sont fiables.

L'originalité et la richesse de ce travail en résultats ont permis à Mr Bilal El Bakkari de présenter plusieurs communications nationales et internationales et de publier trois articles dans des revues internationales spécialisées; le quatrième article est accepté pour publication dans *Journal of Nuclear Radiation and Chemistry*. Il a, également, contribué à la co-rédaction de plusieurs autres papiers scientifiques dans le domaine de la physique des réacteurs nucléaires et participer à plusieurs communications (voir liste des communications et publications).

Mr Bilal El Bakkari a fait preuve de ses solides connaissances et compétence dans le domaine de la physique des réacteurs ainsi que les techniques numériques. Ce qui lui a permis

de réaliser un travail constituant un apport consistent et important dans son domaine. La clarté et la présentation structurée du manuscrit ainsi que sa richesse en références bibliographiques ont en fait un mémoire de qualité.

La thèse, ainsi présentée par Mr **Bilal EL BAKKARI**, pour obtenir le titre de Doctorat en Sciences, mérite d'être soutenue.

Pr T. EL BARDOUNI

LISTE DES PUBLICATIONS

P1. B. EL Bakkari et al., « Development of an MCNP-tally based burnup code and validation through PWR benchmark exercises», Annals of Nuclear Energy 36 (2009) p. 626-633.

P2. B. EL Bakkari et al., « Validation of a new continuous Monte Carlo burnup code using a MOX fuel assembly », Nuclear Engineering and Design 239 (2009) p. 1828–1838.

P3. B. EL Bakkari et al., « The Development of an MCNP-Tally based burnup code», *Int. J. Nuclear Energy Science and Technology, Vol. 4, No. 3, 2009.*

P4. B. EL Bakkari et al., « Benchmark analysis of the 2MW TRIGA MARK II Moroccan research reactor using the MCNP5 code and the latest nuclear data libraires », IAEA-TECDOC (*Article in press*).

P5. B. EL Bakkari et al., « Neutronic Analysis of the 2 MW TRIGA MARK II Moroccan research reactor», submitted to Annals of Nuclear Energy on Octobre 2009.

P6. O. Merroun, A. Al Mers, M.A. Veloso, T. El Bardouni, B. El Bakkari, E. Chakir, « Experimental validation of the thermal-hydraulic code SACATRI», Nuclear Engineering and Design (2009), Article in press.

P7. O. Merroun, A. Almers, T. El Bardouni, B. El Bakkari, E. Chakir, "Analytical benchmarks for verification of thermal-hydraulic codes based on sub-channel approach", Nuclear Engineering and Design 239 (2009) p.735–748.

LISTE DES COMMUNICATIONS

C1. « Etude de benchmarks Rapides et validation des bibliothèques de sections efficaces » 8ème journées de la recherche, Université ABDELMALEK ESSAADI (Maroc) 24, 25 Décembre 2004.
Auteurs: B. El Bakkari, T. El Bardouni, O. Merroun, E. Chakir.

C2. « Modélisation MCNP de benchmarks Rapides et qualification de nouvelles bibliothèques de sections efficaces », 3ème Journées National de la Physique des réacteurs (JNPR3), Faculté des Sciences DHAR ELMEHRAZ de Fès (Maroc) 14,15 Avril 2005.
Auteurs: B. El Bakkari, T. El Bardouni, O. Merroun, E. Chakir.

C3. « Constitution and validation of new neutron cross section libraries for MCNP code using NJOY system and some critical benchmarks » Mathematics and Computing, Supercomputing, Reactor Physics and Nuclear and Biological Applications Meeting, Palais des Papes, Avignon (French), 12-15 Septembre 2005.
Auteurs: T. El Bardouni, O. Meroun, B. El Bakkari, M. Azahra, L. Erradi, E. Chakir, T. El Khoukhi;

C4. « Elaboration et qualification de nouvelles bibliothèques de sections efficaces » 9ème Journée de la Recherche Scientifique Faculté des Sciences of Tétouan (Maroc), 22 Décembre 2005.
Auteurs: B. El Bakkari, T. El Bardouni, O. Merroun, E. Chakir.

C5. « Elaboration et qualification de nouvelles bibliothèques de sections efficaces » Journées Méditerranéennes de la physique, Faculté of Sciences of Tétouan (Maroc) 24,26 Novembre 2005.
Auteurs: B. El Bakkari, T. El Bardouni, O. Merroun, E. Chakir.

C6. « Performance assessment of new neutron cross section libraries using MCNP code and some critical benchmarks » First International Conference on Physics and Technology of Reactors and Applications (PHYTRA1) Marrakech (Morocco) 14, 16 Mars 2007.
Auteurs: B. El Bakkari, T. El Bardouni, L. Erradi, E. Chakir, O. Meroun, M. Azahra, H. Boukhal, T. El Khoukhi, A. Htet.

C7. « Etablissement d'un code de calcul Burnup et couplage avec le code MCNP » 4ième Journée Nationale sur la Physique des Réacteurs Nucléaires. Faculté des Sciences de AIN CHOK Casablanca (Maroc) 24, 25 Mai 2008.
Auteurs: B. El Bakkari,T. El Bardouni, O. Meroun, C. El Younoussi, Y.Boulaich, E.Chakir.

C8. « Benchmark analysis of the 2MW TRIGA MARK II Moroccan research reactor using the MCNP5 code and the latest nuclear data libraires », IAEA Technical meeting in collaboration with NEA on Specific Applications of Research Reactors: Provision of Nuclear Data, International Atomic Energy Agency, Vienne, Autrish, 12 – 16 Octobre 2009.
Auteurs: B. El Bakkari, B. Nacir, T. El Bardouni, A. Htet, C. El Younoussi, O. Merroun, Y. Boulaich, M. Chakir.

C9. « The study of Time dependent neutronics parameters of the 2MW TRIGA MARKII Moroccan research reactor using BUCAL1 computer code ». The 14th annual topical meeting on Research Reactor Fuel Management (RRFM2010), Marrakech – Morocco 21 – 25 Mars 2010.
Auteurs: B. El Bakkari, B. Nacir, T. El Bardouni, C. El Younoussi, Y. Boulaich, et al.

C10. « Modélisation MCNP du réacteur TRIGA MARK II du CENM et calcul de quelques paramètres neutroniques » Rencontre National sur le réacteur TRIGA Mark II du CENM : outil de recherche et du développement socio-économique 12, 13 juin 2006. Faculté des Scienes de Kénitra (Maroc).
Auteurs: O. Meroun, T. El Bardouni, B. El Bakkari, E. Chakir, M. Azahra, F. El Moussaoui.

C11. « Analysis of the CREOLE experiment on the reactivity temperature coefficient using the MCNP5 code and ENDF/B-VI neutron cross sections evaluation » First International Conference on Physics and Technology of Reactors and Applications (PHYTRA1) Marrakech (Morocco) 14, 16 Mars 2007.
Auteurs: Y. Boulaich, T. El Bardouni, L. Erradi, A.Santamarina, E. Chakir, C.El Younoussi, O. Meroun, B. El Bakkari.

C12. « Phoswich detector for RHIB (JRA9) » Three open combined EURISOL & EURONS town meeting days, hosted by the University of Jyväskylä and the Helsinki institute of Physics (Finland) 17, 19 Septembre 2007.
Auteurs: M. Turion, A. Perea, B. El Bakkari, O. Tengblad, R. Rodriguez, T. El Bardouni, M. J. G. Borge.

C13. « Thermalhydraulic modeling and analysis for a hot cannel of the Moroccan TRIGA MARK II Research Reactor » First International Conference on Physics and Technology of Reactors and Applications (PHYTRA1) Marrakech (Morocco) 14, 16 Mars 2007.
Auteurs: O. Meroun, A. El Mers, T. El Bardouni, L. Erradi, E. Chakir, B. El Bakkari, I. Chaoui, B. Nacir.

C14. « Contribution à la qualification des méthodes et données nucléaires utilisées dans le calcul du coefficient de température des réseaux des réacteurs à eau légère : Analyse des expériences CREOLE et KRITZ par la méthode de Monte Carlo et les bibliothèques ENDF/B,

JEFF et ENDL » 4ième Journée Nationale sur la Physique des Réacteurs Nucléaires. Faculté des Sciences de AIN CHOK Casablanca (Maroc) 24, 25 Mai 2008.
Auteurs: Y. Boulaich, T. El Bardouni, C. El Younoussi, B. El Bakkari, O. Merroun, L. Erradi, A. Santamarina, E. Chakir.

C15. « Caractérisation des positions d'irradiation dans le réacteur TRIGA MARK II moyennant le code MCNP5 », 4ième Journée Nationale sur la Physique des Réacteurs Nucléaires. Faculté des Sciences de AIN CHOK Casablanca (Maroc) 24, 25 Mai 2008.
Auteurs : C. El Younoussi, T. El Bardouni, M. Chakir, B. El Bakkari, Y. Boulaich, O. Merroun.

C16. « Verification and validation procedures in nuclear engineering: Application to thermalhydraulic analysis of triangular lattices of light water research reactor in natural circulation regime » 4ième Journée Nationale sur la Physique des Réacteurs Nucléaires. Faculté des Sciences de AIN CHOK Casablanca (Maroc) 24, 25 Mai 2008.
Auteurs: Meroun Ossama, Ahmed El Mers, Tarek El Bardouni, Bilal El Bakkari.

C17. « Analysis of the CREOLE experiment on the reactivity temperature coefficient using the MCNP5 code with ENDF/B-VII and JEFF-3.1 neutron cross section evaluations ». The 14th annual topical meeting on Research Reactor Fuel Management (RRFM2010), Marrakech – Morocco 21 – 25 Mars 2010.
Auteurs: Y. Boulaich, T. El Bardouni, C. El Younoussi, B. El Bakkari, et al.

C18. « Computational analysis of neutronic parameters of CENM TRIGA MARK II research reactor ». The 14th annual topical meeting on Research Reactor Fuel Management (RRFM2010), Marrakech – Morocco 21 – 25 March 2010.
Auteurs: C. El Younoussi, B. El Bakkari, B. Nacir, Y. Boulaich, T. El Bardouni, M. Ossama, E.Chakir

Scientific Activities

List of publications

P1. B. EL Bakkari et al., « *Development of an MCNP-tally based burnup code and validation through PWR benchmark exercises* », Annals of Nuclear Energy 36 (2009) p. 626-633.

P2. B. EL Bakkari et al., « *Validation of a new continuous Monte Carlo burnup code using a MOX fuel assembly* », Nuclear Engineering and Design 239 (2009) p. 1828–1838.

P3. B. EL Bakkari et al., « *The Development of an MCNP-Tally based burnup code* », Int. J. Nuclear Energy Science and Technology, Vol. 4, No. 3, 2009.

P4. B. EL Bakkari et al., « *Benchmark analysis of the 2MW TRIGA MARK II Moroccan research reactor using the MCNP5 code and the latest nuclear data libraires* », IAEA-TECDOC (*Article in press*).

P5. B. EL Bakkari et al., « *Monte Carlo Modelling of TRIGA research reactor* », Nuclear Radiation and Chemistry, accepted 14 April 2010 (*article in press*).

P6. O. Merroun, A. Al Mers, M.A. Veloso, T. El Bardouni, B. El Bakkari, E. Chakir, « *Experimental validation of the thermal-hydraulic code SACATRI* », Nuclear Engineering and Design (2009), Article in press.

P7. O. Merroun, A. Almers, T. El Bardouni, B. El Bakkari, E. Chakir, « *Analytical benchmarks for verification of thermal-hydraulic codes based on sub-channel approach* », Nuclear Engineering and Design 239 (2009) p.735–748.

List of communications

C1. « *Etude de benchmarks Rapides et validation des bibliothèques de sections efficaces* » 8ème journées de la recherche, University ABDELMALEK ESSAADI (Morocco) 24, 25 December.
Authors: B. El Bakkari, T. El Bardouni, O. Merroun, E. Chakir.

C2. « *Modélisation MCNP de benchmarks Rapides et qualification de nouvelles bibliothèques de sections efficaces* », 3ème Journées National de la Physique des réacteurs (JNPR3), Faculty of Sciences DHAR ELMEHRAZ of Fès (Morocco) 14,15 April 2005.
Authors: B. El Bakkari, T. El Bardouni, O. Merroun, E. Chakir.

C3. « *Constitution and validation of new neutron cross section libraries for MCNP code using NJOY system and some critical benchmarks* » Mathematics and Computing, Supercomputing, Reactor Physics and Nuclear and Biological Applications Meeting, Palais des Papes, Avignon (French), 12-15 September 2005.
Authors: T. El Bardouni, O. Meroun, B. El Bakkari, M. Azahra, L. Erradi, E. Chakir, T. El Khoukhi;

C4. « *Elaboration et qualification de nouvelles bibliothèques de sections efficaces* » 9ème Journée de la Recherche Scientifique Faculty of Sciences of Tetuan (Morocco), 22 December 2005.
Authors: B. El Bakkari, T. El Bardouni, O. Merroun, E. Chakir.

C5. « *Elaboration et qualification de nouvelles bibliothèques de sections efficaces* » Journées Méditerranéennes de la physique, Faculty of Sciences of Tetuan (Morocco) 24,26 Novembre 2005.
Authors: B. El Bakkari, T. El Bardouni, O. Merroun, E. Chakir.

C6. « *Performance assessment of new neutron cross section libraries using MCNP code and some critical benchmarks* » First International Conference on Physics and Technology of Reactors and Applications (PHYTRA1) Marrakech (Morocco) 14, 16 March 2007.
Authors: B. El Bakkari, T. El Bardouni, L. Erradi, E. Chakir, O. Meroun, M. Azahra, H. Boukhal, T. El Khoukhi, A. Htet.

C7. « *Etablissement d'un code de calcul Burnup et couplage avec le code MCNP* » 4ième Journée Nationale sur la Physique des Réacteurs Nucléaires. Faculty of Sciences of AIN CHOK Casablanca (Morocco) 24,25 Mai 2008.
Authors: B. El Bakkari,T. El Bardouni, O. Meroun, C. El Younoussi, Y.Boulaich, E.Chakir.

C8. « *Benchmark analysis of the 2MW TRIGA MARK II Moroccan research reactor using the MCNP5 code and the latest nuclear data libraires* », IAEA Technical meeting in collaboration with NEA on Specific Applications of Research Reactors: Provision of Nuclear Data, International Atomic Energy Agency, Vienna, Austeria, 12 – 16 October 2009.
Authors: B. El Bakkari, B. Nacir, T. El Bardouni, A. Htet, C. El Younoussi, O. Merroun, Y. Boulaich, M. Chakir.

C9. « *The study of Time dependent neutronics parameters of the 2MW TRIGA MARKII Moroccan research reactor using BUCAL1 computer code* ». The 14th annual topical meeting on Research Reactor Fuel Management (RRFM2010), Marrakech – Morocco 21 – 25 March 2010.
Authors: B. El Bakkari, B. Nacir, T. El Bardouni, C. El Younoussi, Y. Boulaich, et al.

C10. « *Modélisation MCNP du réacteur TRIGA MARK II du CENM et calcul de quelques parameters neutroniques* » National meeting on CENM TRIGA Mark II reactor: Tools of research and socio-economic development 12, 13 juin 2006. Faculty of Scienes of Kénitra (Morocco).
Authors: O. Meroun, T. El Bardouni, B. El Bakkari, E. Chakir, M. Azahra, F. El Moussaoui.

C11. « *Analysis of the CREOLE experiment on the reactivity temperature coefficient using the MCNP5 code and ENDF/B-VI neutron cross sections evaluation* » First International Conference on Physics and Technology of Reactors and Applications (PHYTRA1) Marrakech (Morocco) 14, 16 March 2007.
Authors: Y. Boulaich, T. El Bardouni, L. Erradi, A.Santamarina, E. Chakir, C.El Younoussi, O. Meroun, B. El Bakkari.

C12. « *Phoswich detector for RHIB (JRA9)* » Three open combined EURISOL & EURONS town meeting days, hosted by the University of Jyväskylä and the Helsinki institute of Physics (Finland) 17, 19 September 2007.
Authors: M. Turion, A. Perea, B. El Bakkari, O. Tengblad, R. Rodriguez, T. El Bardouni, M. J. G. Borge.

C13. « *Analysis of the CREOLE experiment on the reactivity temperature coefficient using the MCNP5 code with ENDF/B-VII and JEFF-3.1 neutron cross section evaluations* ». The 14th annual topical meeting on Research Reactor Fuel Management (RRFM2010), Marrakech – Morocco 21 – 25 March 2010.
Authors: Y. Boulaich, T. El Bardouni, C. El Younoussi, B. El Bakkari, et al.

C14. « Computational analysis of neutronic parameters of CENM TRIGA MARK II research reactor ». The 14th annual topical meeting on Research Reactor Fuel Management (RRFM2010), Marrakech – Morocco 21 – 25 March 2010.

Authors: C. El Younoussi, B. El Bakkari, B. Nacir, Y. Boulaich, T. El Bardouni, M. Ossama, E.Chakir

This works is dedicated:

To my Mother and Father

To my brothers and sister

To my family

And To my best friends

ACKNOWLEDGMENTS

This research is the result of the efforts of many individuals to whom I owe the utmost appreciation.

I must first sincerely thank my research chair, Professor Tarek El Bardouni. Dr. Tarek has guided me over the long duration of my research. His patience throughout is not only a sign of wisdom, but is a reflection upon his character. Without his competence and expertise, I would have been lost. I will never forget the moments he spent with me in the laboratory (weekends, nights, summers …) helping me to overcome all the problems I have encountered, thank you infinitely.

My special and sincere thanks to Professor El Mahjoub Chakir, from the *Faculty of Sciences of Kenitra*, for his continuing guidance, support and assistance in every aspect from the beginning to the end. And also for the participation on the correction of a big part of this thesis, thank you very much.

I would like to express my sincere thanks to Professor Hamid Boukhal for his assistance, motivations and encouragement.

I also extend sincere gratitude to the members of my committee, Dr. Abderahman Kamili Professor at the *Faculty of Sciences of Tetuan*, Dr. Lhoucine Erradi Professor at the *Faculty of Sciences of Rabat,* Dr. Hajjaji Otman Professor at the *Faculty of Sciences of Fés,* Dr. Abderahim Htet from *CNESTEN* and Dr. Jehouani Abdellatif Professor at the *Faculty of Sciences of Marrakech* for their valuable input.

Thanks should also be given to Engineer Bouzekri Nacir, the chief of the *Reactor Operating Unit at Centre of Nuclear Studies of Maâmora (CENM)* for his help, discussions and for putting in my hand all the documents of TRIGA reactor that were needed for the preparation of the last chapter of this thesis.

I would like to extend my thanks to CNRST for attributing me the fellowship of excellence during three years that was very helpful for achieving the aims of this thesis.

I would also like to thank and gratefully acknowledge the help of my colleagues Chafik El Younoussi, Yassine Boulaich, Meroun Ossama, Lamyae El Gonnouni and my little sister Mariam Zoubair, at the *Laboratory of Radiations and Nuclear Systems at the Faculty of Sciences of Tetuan*, I wish you the best.

I would like to express my thanks to all the people at *Reactor Operating Unit of CENM* specially Driss Riyach, Said Otmani, Ismail Marrhich and Khadija Laabouki for all their help and support.

Finally, my special thanks to my parents for their boundless love, support, and encouragement during this work and in all other aspects of my life. My sincere thanks are extended to all my family, and friends, who somehow touched my life.

Abstract

Numerical applications implemented on the Monte Carlo method have developed in line with the increase of computer power; nowadays, in the field of nuclear reactor physics, the required computing time can be abundantly reduced by taking advantage of a computer cluster. This thesis present a new elaborated burnup computer code called “BUCAL1”. The code uses MCNP tally information directly in the computation; this approach allows performing straightforward and accurate calculation without having to use the calculated group fluxes to perform transmutation analysis in a separate code. The Validation process of BUCAL1 was done using code–to–code comparisons of calculated results of different benchmark fuels from the Nuclear Agency Energy (NEA). Analysis of the results obtained showed that BUCAL1 is precise enough to do burnup calculations for the widely used nuclear fuels (UO2, UO2-ThO2, U-ZrH and MOX).

Then, BUCAL1 was used to study the time-dependent neutronic parameters of the 2MW TRIGA MARK II Moroccan research reactor. For the purpose of this study a full 3-D model of the TRIGA reactor was elaborated using the maximum data provided by the constructor General Atomics (GA) of USA and validated by benchmarking the TRIGA reactivity experiments.

Keywords: MCNP, BUCAL1, burnup, UO2, UO2-ThO2, U-ZrH, MOX and TRIGA MARK II.

Table of contents

List of Figures

List of Tables

Introduction

In the last few years, interest in burnup calculations using Monte Carlo methods has increased. Previous burnup codes have used diffusion theory for the neutronic portion of the codes. Diffusion theory works well for most reactors. However, diffusion theory does not produce accurate results in burnup problems that include strong absorbers or large voids. Also, diffusion theory codes are geometry-limited (rectangular, hexagonal, cylindrical, and spherical coordinates). Monte Carlo methods are ideal to solve very heterogeneous reactors and/or lattices/assemblies in which considerable burnable poisons are used. The key feature of this approach is that Monte Carlo methods permit essentially “exact” modeling of all geometrical details, without resort to energy and spatial homogenization of neutron cross sections. Several codes, or combinations of codes, have been developed to perform Monte Carlo depletion analysis using multigroup approximation. Basically, these codes were developed with the idea of solving the burnup problem for unit cells and/or fuel assemblies/lattices.

This thesis presents a new elaborated Monte Carlo bunup computer code called “BUCAL1”. The code uses neutron absorption and fission reaction data generated directly by the Monte Carlo neutronics code MCNP to determine the isotopic inventory as a function of time and power density. This feature allows to benefit of the full capabilities provided by MCNP and to incorporate them into burnup calculations in the aim to perform more accurate and robust treatment of the problem without post-processing and additional manipulation of neutron flux and cross-sections set. This new code is intended for entire reactor cores as well as for unit cells and assemblies/lattices. The code has the capability to do burnup calculations with multi fuel cycles including fuel shuffling using for more than 900 fission products and actinides.

The use of neutron absorption and fission reaction MCNP tallies in BUCAL1 allows the integration of all the neutron flux information into the calculations. Also, using MCNP and continuous-energy cross sections allow neutron cross section manipulations to be avoided. These advantages permit straightforward and accurate calculations to be performed without having to use calculated group fluxes to perform transmutation analysis in a separate code such other burnup codes do.

The validation process of BUCAL1 is performed by a series of code–to–code comparisons using several burnup computer codes and for a wide variety of benchmark fuels, such as UO2, UO2-ThO2 and MOX fuels. The benchmarks studied are of different geometries (pin-cells and assemblies) and with different operating conditions, such as: different temperatures, benchmarks with different fuel compositions, etc...

As an application of our new elaborated burnup code BUCAL1, we will use it in determining the core life time and the time-dependent neutronics parameters of the 2MW TRIGA MARK II Moroccan research reactor at Centre d'Etude Nucléaire de la Maâmora (CENM). In this study, a full model of the TRIGA reactor is elaborated using the 3-D continuous energy Monte Carlo code MCNP5 and validated by benchmarking of some reactivity experiments. The model represents in details all the components of the reactor using the geometrical and material data provided by the reactor manufacturer General Atomics of USA throughout the fabrication shipment documents and enhanced by use of "as-built" data.

Continuous energy cross section data from the more recent nuclear data evaluations (ENDF/B-VI.8, ENDF/B-VII.0, JEFF-3.1, and JENDL-3.3) as well as S(α, β) thermal neutron scattering functions distributed with the MCNP5 code are used in this work. The cross section libraries in ACE format are generated by using the NJOY99 modular system updated to its more recent patch file "up259". The consistency and accuracy of the MCNP model of the TRIGA reactor are established by benchmarking the TRIGA experiments.

Thus the flow sheet of this thesis is as follow:

In the first chapter, the basic neutron nucleus reactions of importance in nuclear reactors and the nuclear data used in reactor physics calculations are described.

The second chapter is designated to describe the change in fuel composition due to burnup in an operating reactor and their effects on the reactor

A brief description of the MCNP5 code and its methodology as well as the adopted procedures for processing and validation of nuclear data to be used with the MCNP code are described in the third chapter of this thesis.

The fourth chapter of this thesis is dedicated to describe the mathematical procedure adopted in the development of the new Monte Carlo burnup computer code called BUCAL1. The process of its validation is also described in this chapter.

The fifth chapter is reserved to the MCNP modelling and the study of the time-dependent neutronic parameters of the 2MW TRIGA MARK II Moroccan research reactor at Centre d'Etude Nucléaire de la Maâmora (CENM).

1. Basic reactor physics

The physics of nuclear reactors is determined by the transport of neutrons and their interaction with matter within a reactor. The basic neutron nucleus reactions of importance in nuclear reactors and the nuclear data used in reactor physics calculations are described in this chapter

1. Neutron interactions

A nuclear reactor will not operate without neutrons, that induce the fission reaction, which produces the heat in nuclear reactors, and fission creates more neutrons, that engage in other reactions, and so on. It is important to know about these neutron interactions.

Most of the neutrons in a nuclear reactor come directly from fission. About 0.5% of the neutrons in a reactor at power are emitted as part of fission product decay. These two important types of neutrons, known as prompt and delayed neutrons respectively.

This section introduces five reactions that can occur when a neutron interacts with a nucleus. In the first two, known as scattering reactions, a neutron emerges from the reaction. In the remaining reactions, known as absorption reactions, the neutron is absorbed into the nucleus and something different emerges.

1.1. Elastic scattering (n,n)

Elastic scattering resembles a billiard ball collision. A neutron collides with a nucleus, transfers some energy to it, and bounces off in a different direction. (Sometimes it absorbs the neutron and then reemits it conserving kinetic energy, this phenomenon is known as the resonance scattering.) The fraction of its initial energy lost depends on whether it hits the target nucleus dead-on or at an angle - exactly like the cue ball striking a ball on the billiard table. The target nucleus gains the energy lost by the neutron, and then moves at an increased speed.

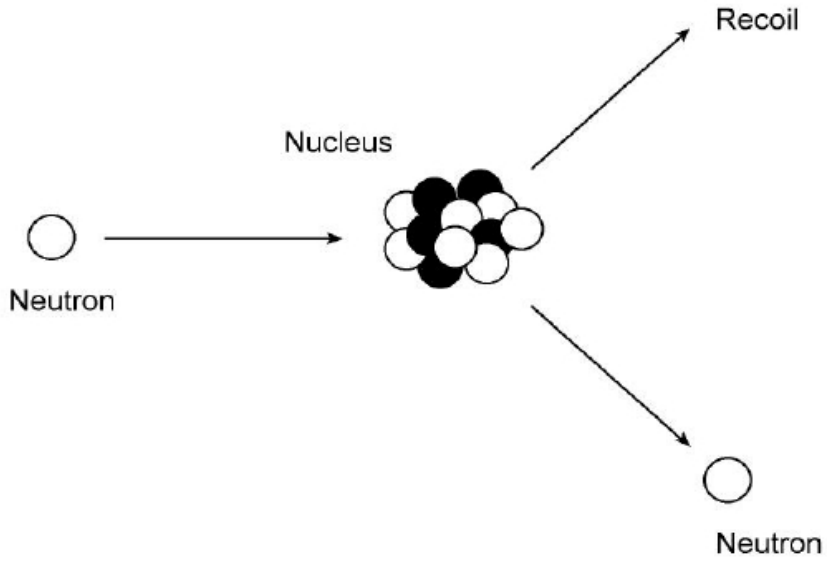

Figure 1.1- Elastic scattering.

Light nuclei are the most effective for slowing neutrons. A neutron colliding with a heavy nucleus rebounds with little loss of speed and transfers very little energy -rather like firing the cue ball at a cannon ball. On the other hand, neutrons will not be scattered by the light electron clouds surrounding the nucleus, but will travel straight on-much like baseballs through a fog.

1.2. Inelastic scattering (n, n'γ)

A neutron may strike a nucleus and be temporarily absorbed, forming a compound nucleus. This will be in an excited state. It may de-excite by emitting another neutron of lower energy, together with a gamma photon, which takes the remaining energy. This process is called inelastic scattering. It generally happens only when high-energy neutrons interact with heavy nuclei and has little practical importance for reactor operation.

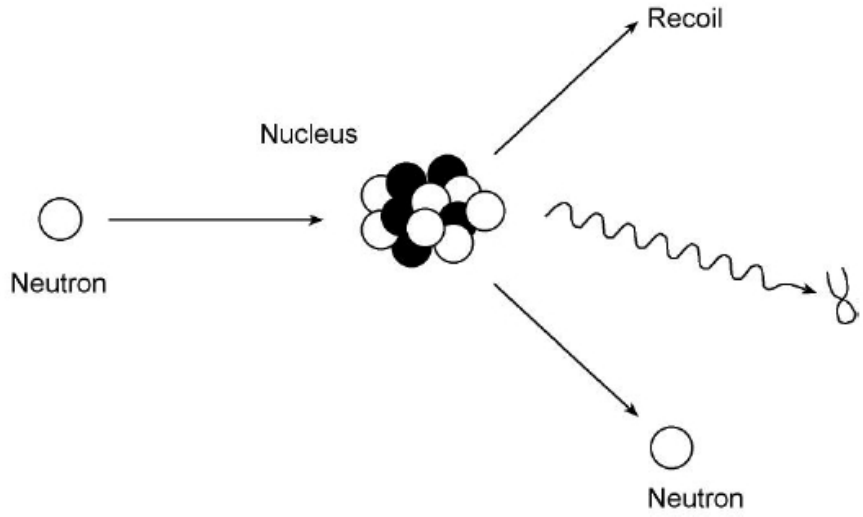

Figure 1.2- Inelastic scattering.

1.3. Radiative capture (n, γ)

This is the most common nuclear reaction. The compound nucleus formed emits only a gamma photon. In other words, the product nucleus is an isotope of the same element as the original nucleus. Its mass number increases by one.

The simplest radiative capture occurs when hydrogen absorbs a neutron to produce deuterium (heavy Hydrogen);

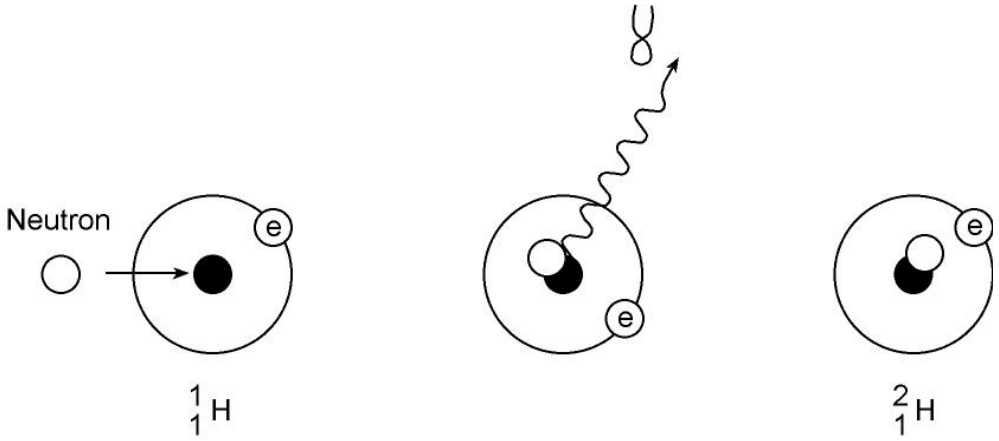

Figure 1.3- Radiative capture in hydrogen-1.

The deuterium formed is a stable nuclide. However, many radiative capture products are radioactive and are beta-gamma emitters.

1.4. Transmutation (n, p), (n, α)

A nucleus may absorb a neutron forming a compound nucleus, which then de-energizes by emitting a charged particle, either a proton or an alpha particle. This produces a nucleus of a different element. Such a reaction is called a transmutation.

Transmutation is the transformation of one element into another by a nuclear reaction.

Examples:

1.4.1. Neutron-Proton reaction (n, p)

Oxygen-16 captures a neutron and emits a proton to form nitrogen-16:

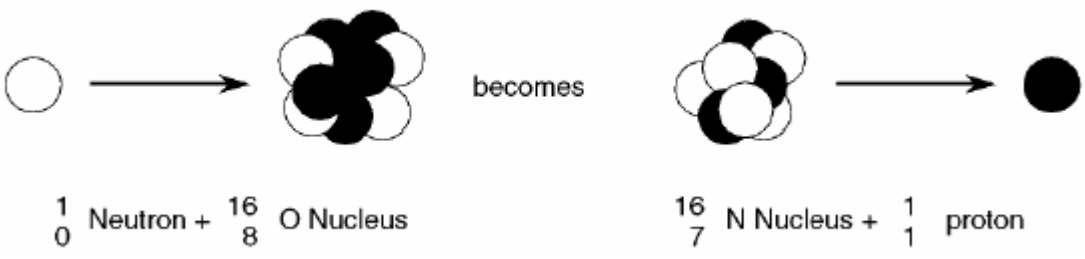

Figure 1.4- Neutron-Proton reaction.

The product, nitrogen-16, is radioactive with a half-life of 7.1 seconds so this example is an activation reaction. N-16 is a beta emitter, but more important, it also emits very penetrating, high-energy gamma rays.

1.4.2. Neutron Alpha reaction (n, α)

Neutrons captured by boron-10 cause the following reaction:

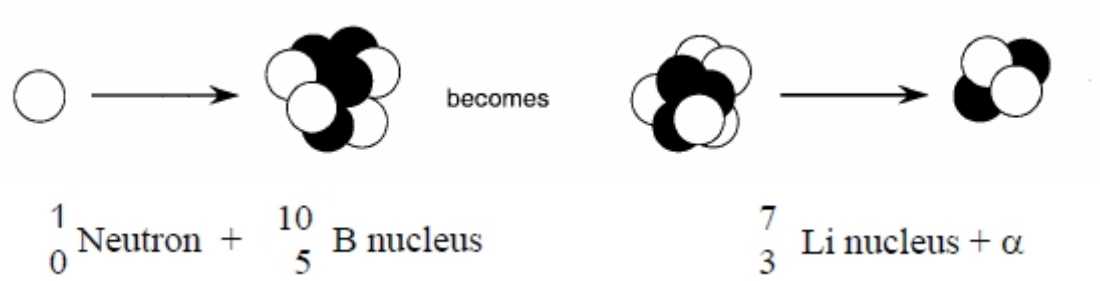

Figure 1.5- Neutron-Alpha reaction.

1.5. Fission

In the fission reaction the incident neutron enters the heavy target nucleus, forming a compound nucleus that is excited to such a high energy level ($E_{exc} > E_{crit}$) that the nucleus "splits" (fissions) into two large fragments plus an average of 2.5 neutrons. An example of a typical fission reaction is shown below.

$$^{1}_{0}n + {}^{235}_{92}U \rightarrow \left({}^{236}_{92}U\right)^{*} \rightarrow {}^{140}_{55}Cs + {}^{93}_{37}Rb + 3\left({}^{1}_{0}n\right)$$

A large amount of energy is released in the form of radiation and fragment kinetic energy.

An important factor affecting whether or not an atom wills fission is the speed at which the bombarding neutron is moving. If the neutron is highly energetic (and thus moving very quickly), it can cause fission in some elements that a slower neutron would not. For example, thorium-232 requires a very fast neutron to induce fission. However, uranium-235 needs slower neutrons. If a neutron is too fast, it will pass right through a ^{235}U atom without affecting it at all.

2. Fundamental basis

2.1. Neutron flux

Prior to absorption, a typical neutron will undergo many elastic scattering collisions with nuclei in a reactor. As a result, a neutron path consists of many straight line segments joining

the points of collision. The combined effect of billions of neutrons darting in all directions is a cloudlike diffusion of neutrons throughout the reactor material.

Neutron flux is simply a term used to describe the neutron cloud. Neutron flux f is defined as the number of neutrons in 1 cubic centimetre multiplied by their average velocity.

$$f = nv = \frac{neutrons}{cm^3} * \frac{cm}{s} = \frac{neutrons}{cm^2.s} \tag{1.1}$$

Neutron flux is sometimes simply called *nv*. A clear theoretical picture of neutron flux may be had by considering a beam of neutrons of one square centimetre cross section all travelling in the same direction. Then the number of neutrons contained in one centimetre of length of the beam is *n*, and *v* is the length of the beam passing a plane in one second. Hence, flux is the number of neutrons passing through one square centimetre of the plane in one second.

(However, remember that in reality the motion of the neutrons in a reactor is random, therefore, the above explanation is not really valid, but is a useful concept to help explain neutron flux.)

2.2. Neutron cross section

The probability of a neutron interacting with a nucleus for a particular reaction is dependent upon not only the kind of nucleus involved, but also the energy of the neutron. Accordingly, the absorption of a thermal neutron in most materials is much more probable than the absorption of a fast neutron. Also, the probability of interaction will vary depending upon the type of reaction involved.

The probability of a particular reaction occurring between a neutron and a nucleus is called the microscopic cross section (s) of the nucleus for the particular reaction. This cross section will vary with the energy of the neutron. The microscopic cross section may also be regarded as the effective area the nucleus presents to the neutron for the particular reaction. The larger the effective area, the greater the probability for reaction.

Because the microscopic cross section is an area, it is expressed in units of area, or square centimeter. A square centimeter is tremendously large in comparison to the effective area of a nucleus, and it has been suggested that a physicist once referred to the measure of a square centimeter as being "as big as a barn" when applied to nuclear processes. The name has

persisted and microscopic cross sections are expressed in terms of barns. The relationship between barns and cm^2 is shown below.

$$1 \text{ barn} = 10^{-24} cm^2$$

Whether a neutron will interact with a certain volume of material depends not only on the microscopic cross section of the individual nuclei but also on the number of nuclei within that volume. Therefore, it is necessary to define another kind of cross section known as the macroscopic cross section (Σ). The macroscopic cross section is the probability of a given reaction occurring per unit travel of the neutron. Σ is related to the microscopic cross section (s) by the relationship shown below.

$$\Sigma = Ns \tag{1.2}$$

where, Σ is the macroscopic cross section (cm^{-1}), N is the atom density of the material (at/cm^3) and s is the microscopic cross section (cm^2).

The difference between the microscopic and macroscopic cross sections is extremely important and is restated for clarity. The microscopic cross section (s) represents the effective target area that a single nucleus presents to a bombarding particle. The units are given in barns or cm^2. The macroscopic cross section (Σ) represents the effective target area that is presented by all of the nuclei contained in 1 cm^3 of the material.

A neutron interacts with an atom of the material it enters in two basic ways. It will either interact through a scattering interaction or through an absorption reaction. The probability of a neutron being absorbed by a particular atom is the microscopic cross section for absorption, s_a. The probability of a neutron scattering off of a particular nucleus is the microscopic cross section for scattering, s_s. The sum of the microscopic cross section for absorption and the microscopic cross section for scattering is the total microscopic cross section, s_T.

$$s_T = s_a + s_s \tag{1.3}$$

Both the absorption and the scattering microscopic cross sections can be further divided. For instance, the scattering cross section is the sum of the elastic scattering cross section (s_{se}) and the inelastic scattering cross section (s_{si}).

$$s_s = s_{se} + s_{si} \tag{1.4}$$

The microscopic absorption cross section (s_a) includes all reactions except scattering. However, for most purposes it is sufficient to merely separate it into two categories, fission (s_f) and capture (s_c).

$$s_a = s_f + s_c \tag{1.5}$$

The variation of absorption cross sections with neutron energy is often complicated. For many elements the absorption cross sections are small, ranging from a fraction of a barn to a few barns for slow (or thermal) neutrons.

2.3. Mean free path

If a neutron has a certain probability of undergoing a particular interaction in one centimeter of travel, then the inverse of this value describes how far the neutron will travel (in the average case) before undergoing an interaction. This average distance traveled by a neutron before interaction is known as the mean free path for that interaction and is represented by the symbol l . The relationship between the mean free path (l) and the macroscopic cross section (Σ) is shown below.

$$l = \frac{1}{\Sigma} \tag{1.6}$$

2.4. Reaction rates

If the total path length of all the neutrons in a cubic centimeter in a second is known, (neutron flux (f)), and if the probability of having an interaction per centimeter path length is also known (macroscopic cross section (Σ)), multiply them together to get the number of interactions taking place in that cubic centimeter in one second. This value is known as the reaction rate and is denoted by the symbol *R*. The reaction rate can be calculated by the equation shown below.

$$R = \Sigma.f \tag{1.7}$$

where

R = reaction rate (reaction/sec)

f = neutron flux (neutron/cm^2-sec)

Σ = macroscopic cross section (cm^{-1})

Substituting the fact that $\Sigma = Ns$ into Equation (1.7) yields the equation below.

$$R = Nsf \tag{1.8}$$

where

N = atom density (atom/cm^3)

s = microscopic cross section (cm^{-2})

The reaction rate calculated will depend on which macroscopic cross section is used in the calculation. Normally, the reaction rate of greatest interest is the fission reaction rate.

3. Neutron life cycle

3.1. Multiplication factor

The average lifetime of a single neutron in the reactor neutron cloud may be as small as one ten-millionth of a second. This means that in order for the cloud to remain in existence, each neutron must be responsible for producing another neutron in less than one ten millionth of second. Thus, one second after a neutron is born, its ten-millionth generation descendent is born. (The term neutron generation will be used to refer to the "life" of a group of neutrons from birth to the time they cause fission and produce new neutrons). However, not all of the neutrons produced by fission will have the opportunity to cause new fissions because some will be absorbed by non-fissile material and others will leak out of the reactor. The number of neutrons absorbed or leaking out of the reactor will determine whether a new generation of neutrons is larger, smaller, or the same size as its predecessor.

A measure of the increase or decrease in size of the neutron cloud is the ratio of the neutrons produced to the sum of the neutrons absorbed in fission or non-fission reactions, plus those lost in any one generation. This ratio is called the effective multiplication factor and may be expressed mathematically by

$$keff = \frac{production}{absorption + leakage} \tag{1.9}$$

If the production of neutrons by one generation is greater than the sum of its absorption and the leakage, *keff* will be greater than 1.0, e.g., 1.1, and the neutron flux will increase with each generation. If, on the other hand, *keff* is less than 1.0, perhaps 0.9, the flux will decrease with each generation. If the size of each successive generation is the same then the production exactly equals the losses by absorption and leakage. *keff* is then exactly 1.0 and the reactor is said to be critical. The multiplication factor can, therefore, also be defined as:

$$keff = \frac{\text{number of neutrons in one generation}}{\text{number of neutrons in preceding generation}} \tag{1.10}$$

Changes in the neutron flux cause changes in the power level of the reactor. Since the change in power level is directly affected by the multiplication factor, it is necessary to know more about how this factor depends upon the contents and construction of the reactor.

The balance between the production of neutrons, on the one hand, and their absorption in the core and leakage out of the core, on the other hand, determines the value of the multiplication factor. If the leakage is small enough to be neglected, the multiplication factor depends only upon the balance between production and absorption and is called the infinite multiplication factor, k_∞ (an infinitely large core can have no leakage). When the leakage is included, the factor is called the effective multiplication factor (*keff*). Each will be considered. (By definition, the multiplication constants *keff* and k_∞ are dimensionless numbers.)

3.2. Infinite multiplication factor

The infinite multiplication factor, since it assumes no leakage, may be expressed as

$$k_\infty = \frac{production}{absorption} \tag{1.11}$$

The infinite multiplication factor also represents the average number of neutrons in a generation resulting from a single neutron in the preceding generation in an infinite reactor. We will analyse the infinite multiplication factor from this second viewpoint.

A group of newly produced fast neutrons can enter into several reactions. Some of these reactions reduce the neutron flux; others allow the group to increase or produce a second generation. One way to analyse the infinite multiplication factor is to describe these various possible reactions by means of a product of factors, each factor representing one of the types of events that may occur. Expressed mathematically,

$$k_\infty = epfn \tag{1.12}$$

where

e = fast fission factor

p = resonance escape probability

f = thermal utilization factor

n = reproduction factor

This equation is called the four-factor equation. The factors will be explained briefly by tracing a group of fast neutrons, just born, through a complete generation. Figure (1.5) will be extremely helpful in learning the significance of each factor.

3.3. Fast fission factor

Fission of ^{235}U is usually caused by a slow or thermal neutron, a neutron that has lost much of the energy since it was slowed due to collisions with light (moderator) nuclei. However, fission of ^{238}U may be caused by a fast neutron. Therefore, if some of fast neutrons cause fission of a few ^{238}U atoms, the group of fast neutrons will be increased by a few additional fast neutrons. The total number of fast neutrons compared to the number in the original group is called the fast fission factor, e .

$$e = \frac{\int_{fuel} dV \int_0^{+\infty} dEu \sum_f (r,E)\Phi(r,E)}{\int_{fuel} dV \int_0^{E_2} dEu \sum_f (r,E)\Phi(r,E)} \tag{1.13}$$

where, $E2$ is a cutoff energy separating the thermal region (where up-scattering is important) and the fast region.

3.4. Resonance escape probability

Having increased in number as a result of some fast fissions, the group of neutrons continues to diffuse or wander through the reactor. As the neutrons move, they collide with nuclei of non-fuel material in the reactor, losing part of their energy in each collision and slowing down.

Now ^{238}U has some very large resonances in its absorption cross section and if the neutron is slowed to the energy of one of these resonances, then it has a high probability of being captured. This process is called resonance absorption. The number of neutrons that escape resonance absorption compared to the number of neutrons that begin to slow down is the resonance escape probability factor, p.

$$p = \frac{\int_{cell} dV \int_0^{E_2} dE \sum_a (r,E)\Phi(r,E)}{\int_{cell} dV \int_0^{+\infty} dE \sum_a (r,E)\Phi(r,E)} \tag{1.14}$$

3.5. Thermal utilization factor

The thermal or slow neutrons are those that have completed the slowing down process without being absorbed are finally available for absorption in fuel. They, like the fast neutrons, diffuse through the reactor, but at slower speeds, and travel over less area. As thermal neutrons, they are subject to absorption by other materials in the reactor as well as by the fuel. Since only those neutrons absorbed in fuel have a chance of reproducing, it is necessary to know the fraction of all absorbed thermal neutrons that is absorbed in the fuel. The number of thermal neutrons absorbed in fuel compared with the number absorbed in all materials including fuel, is the thermal utilization factor, *f*.

$$f = \frac{\int_{fuel} dV \int_0^{E_2} dE \sum_a^{fuel}(r,E)\Phi(r,E)}{\int_{cell} dV \int_0^{E_2} dE \sum_a(r,E)\Phi(r,E)} \qquad (1.15)$$

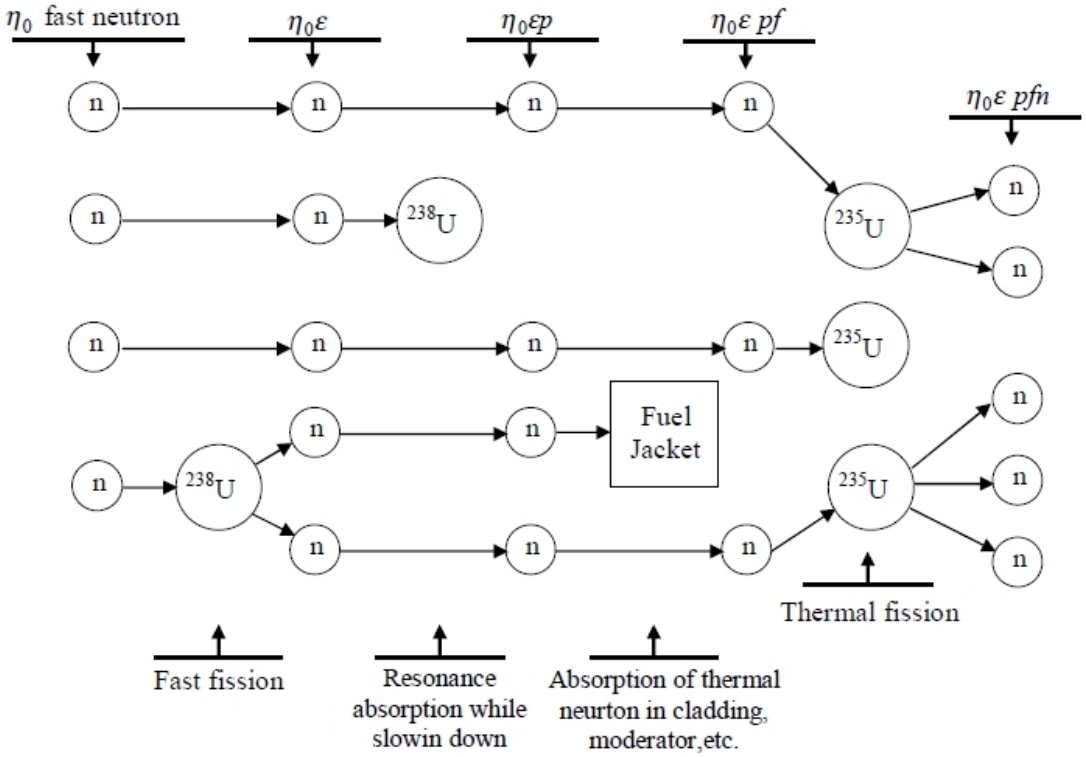

For this diagram only : $\varepsilon = \frac{5}{4}$; $p = \frac{4}{5}$; $f = \frac{3}{4}$; $\eta = \frac{5}{3}$

$$k_\infty = \frac{\eta_0 \varepsilon p f n}{\eta_0} = \frac{5}{4} = 1.25$$

Figure 1.6- Schematic diagram of one neutron generation.

3.6. Reproduction factor

Most of the neutrons absorbed in the fuel cause fission, but some do not. The average number of fission neutrons produced for each thermal neutron absorbed in the fuel is the reproduction factor, *n*.

$$n = \frac{\int_{fuel} dV \int_0^{E_2} dEu \sum_f (r,E)\Phi(r,E)}{\int_{fuel} dV \int_0^{E_2} dEu \sum_a^{fuel} (r,E)\Phi(r,E)} \tag{1.16}$$

With the birth of fast neutrons from fission, the cycle is complete. By multiplying these factors together the infinite multiplication factor can be found.

Figure (1.6) will be used to illustrate how each of the factors are determined, and to help in the understanding of k_∞. It pictures the life cycle of neutrons in chronological order with the various hazards they encounter from birth (fast neutrons), through life (while slowing down), until death (thermalized and absorbed either productively or non-productively).

The cycle starts with four fast neutrons. Of these four, one causes fast fission in ^{238}U, producing two more. Notice that the second column has five fast neutrons. Therefore, the fast fission factor (e) is represented as 5/4. While the five fast neutrons are slowing down, one of the five is absorbed (a resonance absorption) in ^{238}U. Column three shows that four neutrons slowed down and escaped resonance absorptions; therefore, the resonance escape probability (p) is 4/5. Of the four slow neutrons at this stage, one is absorbed in fuel jacket material, while three of them are absorbed in ^{235}U and cause fission. Therefore, the thermal utilization factor (f) is 3/4. These three slow neutrons that were absorbed in ^{235}U resulted in five fast neutrons being born during fission. Therefore, 5/3 would be the reproduction factor. When comparing the five fast neutrons just born to the four original fast neutrons, the result, 5/4, represents k_∞, the infinite multiplication factor. It should be evident that whenever a picture of this sort is given, each of the four factors and k_∞ can be found simply by counting the neutrons in each of the five vertical columns. (Notice that each neutron appears in each consecutive column until it is absorbed). Column 1 represents the initial number of fast neutrons under consideration or n_0. Column 2 represents the initial number of fast neutrons present as a result of fast fission, $n_0\varepsilon$; column 3 represents the number of neutrons which have escaped resonance absorption, $n_0\varepsilon p$; column 4 represents the number of neutrons which are absorbed in ^{235}U, $n_0\varepsilon pf$; column 5 represents the number of fast neutrons resulting from fission of ^{235}U, $n_0\varepsilon pf\eta$ or $n_0 k_\infty$.

3.7. Effective multiplication factor

The effective multiplication factor for a finite reactor may be expressed mathematically in terms of the infinite multiplication factor and two additional factors that allow for neutron leakage as:

$$keff = k_{\infty} x_f x_t \tag{1.17}$$

where, x_f is the fraction of fast neutrons in one generation that do not leak out of the core while slowing down, and x_t is the fraction of thermal neutrons that do not leak out. The product $x_f \; x_t$ represents the fraction of all the neutrons in one generation that do not leak out of the core and is known as the non-leakage probability. ([1 - $x_f \; x_t$] then, is the leakage probability.)

It should be pointed out that the four factors in the equation for k_∞ depend upon both the kind and quantity of fuel and other materials placed in the core and the control rod configuration, whereas the leakage factors depend not only on the contents but also on the size and shape of the reactor. These quantities play an extremely important part in reactor operation, since ***keff*** = (e ***pfn***) ($x_f x_t$), and the value of ***keff*** determines the behaviour of the reactor at a given time. A change in any one of these quantities simultaneously changes ***keff***.

4. Neutron transport theory

Calculation of the transport of neutrons and their interaction with matter are perhaps the fundamental topics of reactor physics. In this section, the major computational methods used for the transport of neutrons in nuclear reactors are described.

4.1. Neutron transport equation

The distribution of neutrons in space and angle is defined by the particle distribution function $N(r, \Omega, t)$, such that $N(r, \Omega, t)\, dr d\Omega$ is the number of neutrons in volume element dr at position r moving in the cone of directions $d\Omega$ about direction Ω, as depicted in Figure (1.7). An equation for $N(r, \Omega, t)$ can be derived by considering a balance on the differential cylindrical volume element of length $dl = v.dt$, where v is the neutron speed, and cross-section area dA surrounding the direction of neutron motion, as shown in Figure (1.8). The rate of change of $N(r, \Omega, t)$ within this differential volume is equal to the rate at which neutrons with direction Ω are flowing into the volume element (e.g., across the left face in Figure (1.8)) less

the rate at which they are flowing out of the volume element (e.g., across the right face), plus the rate at which neutrons traveling in direction Ω are being introduced into the volume element by scattering of neutrons within the volume element from different directions Ω' and by fission, plus the rate at which neutrons are being introduced into the volume element by an external source S_{ex}, minus the rate at which neutrons within the volume element traveling in direction Ω are being absorbed or being scattered into a different direction Ω':

$$\begin{aligned}\frac{\partial N}{\partial t}(r,\Omega,t)drd\Omega = v(N(r,\Omega,t) - N(r+\Omega dl,\Omega,t)dAd\Omega \\ + \int_0^{4p} d\Omega'\Sigma_s(r,\Omega'\to\Omega)vN(r,\Omega',t)drd\Omega \\ + \frac{1}{4p}\int_0^{4p} d\Omega' v\Sigma_f(r)vN(r,\Omega',t)drd\Omega \\ + S_{ex}(r,\Omega)drd\Omega - (\Sigma_a(r)+\Sigma_s(r))vN(r,\Omega,t)drd\Omega\end{aligned} \tag{1.18}$$

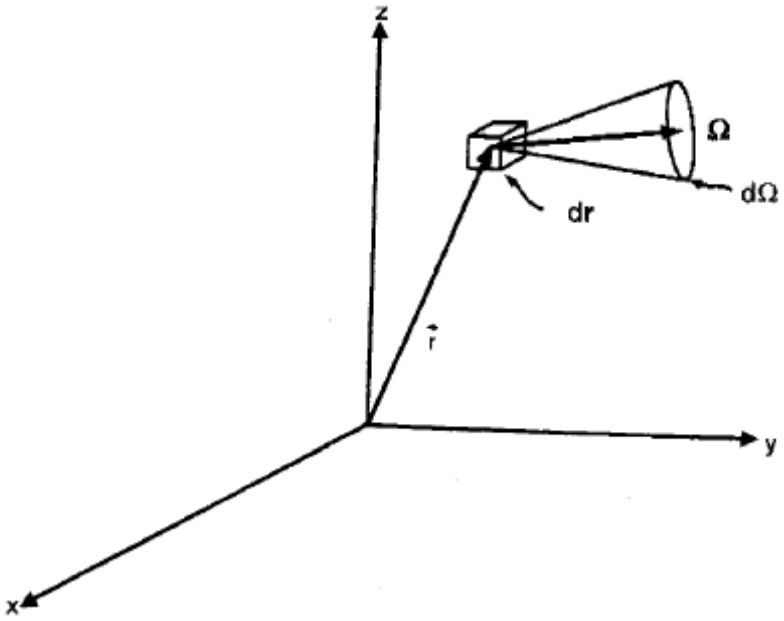

Figure 1.7- Particles in *dr* at location *r* moving in the cone *dΩ* about the direction *Ω*.

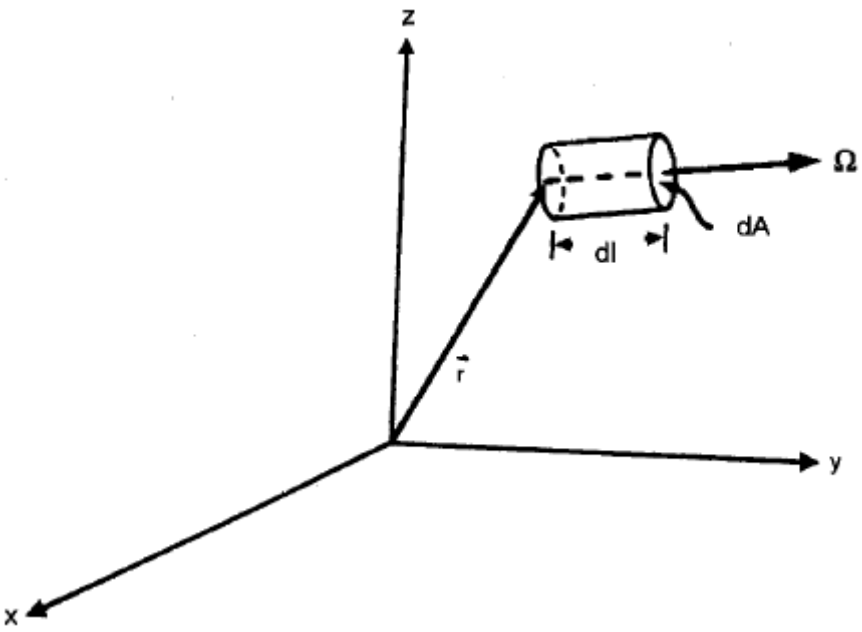

Figure 1.8-Incremental volume element for particles at location r moving in the direction Ω.

Making a Taylor's series expansion

$$N(r+\Omega dl,\Omega,t) = N(r,\Omega,t) + \frac{\partial N(r,\Omega,t)}{\partial t} dl + ... \\ = N(r,\Omega,t) + \Omega.\nabla N(r,\Omega,t) + ... \tag{1.19}$$

to evaluate the streaming term, defining the directional flux distribution

$$y\ (r,\Omega,t) \equiv vN(r,\Omega,t) \tag{1.20}$$

and taking note of the fact that the scattering from Ω' to Ω depends only on $\Omega \bullet \Omega' \equiv m_0$

$$\Sigma_s(r,\Omega' \to \Omega) = \frac{1}{2p}\Sigma_s(r,\Omega \bullet \Omega') \equiv \frac{1}{2p}\Sigma_s(r,m_0) \tag{1.21}$$

and writing $\Sigma_t = \Sigma_a + \Sigma_s$ leads to the neutron transport equation

$$\frac{1}{v}\frac{\partial y}{\partial t}(r,\Omega,t) + \Omega \bullet \nabla y\ (r,\Omega,t) + \Sigma_t(r) y\ (r,\Omega,t) \tag{1.22}$$
$$= \int_{-1}^{1} dm_0 \Sigma_s(r,m_0) y\ (r,\Omega',t) + \frac{1}{4p}\int_{\grave{a}}^{4p} d\Omega' u \Sigma_f(r) y\ (r,\Omega,t) + S_{ex}(r,\Omega) = S(r,\Omega)$$

The steady-state version of *Eq. (1.22)* may be written

$$\frac{d}{dR} y\ (r,\Omega) dr d\Omega + \Sigma_t(r) y\ (r,\Omega) dr d\Omega = S(r,\Omega) dr d\Omega \tag{1.23}$$

where, *dR* is the differential length along the direction Ω (i.e., $\Omega \bullet \nabla$ = *d/dR).* This equation may be integrated along the direction Ω from r_0 to r, to obtain the so called « integral transport theory »

$$y\,(r,\Omega)dr = e^{-a\,(r_0,r)}y\,(r_0,\Omega)dr_0 + \int_{r_0}^{r} e^{-a\,(r',r)}S(r',\Omega)dr' \qquad (1.24)$$

where, $a\,(r',r)$ is the optical path length along the direction Ω between r' and r:

$$a\,(r',r) = \left|\int_{r'}^{r} \Sigma_t(R)dR\right| \qquad (1.25)$$

4.2. Transport calculation techniques

Neutron histories are difficult to determine because of the large number of different possible interactions in materials. This difficulty is further increased when the composition of matter changes frequently along the path of a neutron. Criticality calculations can be done using deterministic methods such as “discrete ordinates techniques” considered as the fast and accurate iterative technique, or using stochastic methods such as “Monte Carlo technique”. Deterministic methods usually involve multi-group approaches while Monte Carlo can work with multi-group and continuous energy cross-section libraries.

4.2.1. Monte Carlo technique

The probability of a neutron interaction occurring is an important feature in the description of neutrons traveling through matter. Instead of trying to predict what an individual neutron may do, one can use procedures to predict what fraction of a large number of neutrons will behave in some manner of interest. Calculation techniques that, in simplistic terms, predict neutron events with “rolls of dice” (actually the generation of random numbers in a computer) are called Monte Carlo methods.

The Monte Carlo method can allow a detailed three-dimensional geometrical model to be constructed mathematically to simulate a physical situation. A neutron can be started at a selected location with a certain energy and direction. It travels distances that are consistent with the mean-free-path lengths in the materials, with random variations time the expected mean. At the end of each step in the neutron’s path, a decision may be made to simulate a certain interaction, with the decision based on the cross section for the interaction with that material at that neutron energy. If an interaction is selected, the results of the interaction are simulated and its consequences followed. Eventually, a point is reached where no further interest in the neutron exists and its history is terminated. This might occur with the escape of the neutron or its moderation to very low energy. The neutron might be absorbed followed by the emission of a gamma ray of no interest or it might undergo a multiplication event. If a multiplication event occurs the histories of the new neutrons are followed. In principle, the history of a simulated neutron is one that might actually occur with a real neutron.

By repeating this procedure for many thousands of neutrons and by keeping tallies of how many enter a detector region, how many cause fissions how many escape through a shield, or whatever else is of interest, an average behavior and its uncertainty are gradually deduced. Many specialized techniques may be used to get good average values with the fewest number of neutrons, but there are cases where even a fist computer cannot provide enough histories within the constraints of time and budget. Nonetheless, Monte Carlo techniques provide essential assistance in design work by closely modeling the actual geometry of a problem and by having imaginary neutrons that simulate the motions and interactions of real ones.

4.2.2. Discrete ordinates techniques

Analytical transport equations exist that describe the exact behavior of neutrons in matter. However, only approximate numerical solutions to these equations can be obtained for complicated systems. Procedures for obtaining these numeral solutions are classified as discrete ordinates techniques.

Some important differences distinguish discrete ordinates techniques from Monte Carlo techniques. Only one- or two-dimensional geometries are generally practical with a discrete ordinates process, and the neutrons are considered to be at discrete locations instead of moving freely through a three dimensional geometry. In a two dimensional discrete ordinates case, for example, it is as if the surface material were covered by a wire mesh and the neutrons existed only at the intersections of the wires. Furthermore, the energy of a neutron at any time must be selected from a finite set, in contrast to the continuously varying energy of a neutron in the Monte Carlo method.

Despite these disadvantages, discrete ordinates techniques can produce useful results in many cases. For problems involving large volumes and amounts of materials (such as reactor cores), the Monte Carlo technique can be too cumbersome and slow, a discrete ordinates solution might be feasible.

5. Nuclear reactor principles

5.1. Nuclear chain reaction

A nuclear chain reaction occurs when on average more than one neutron from a nuclear fission reaction causes another fission reaction, as show in Figure (1.9). The first self-sustaining nuclear chain reaction was initiated by a team led by Enrico Fermi below the bleachers of Stagg Field at the University of Chicago on December 2, 1942 during the Manhattan Project.

The rate of reactions will accelerate exponentially if left unmoderated. An uncontrolled chain reaction within a sufficiently large amount of fission fuel (critical mass) can lead to an explosive energy release and is the concept behind nuclear weapons. The chain reaction could also be adequately controlled and used as an energy source especially for nuclear reactors.

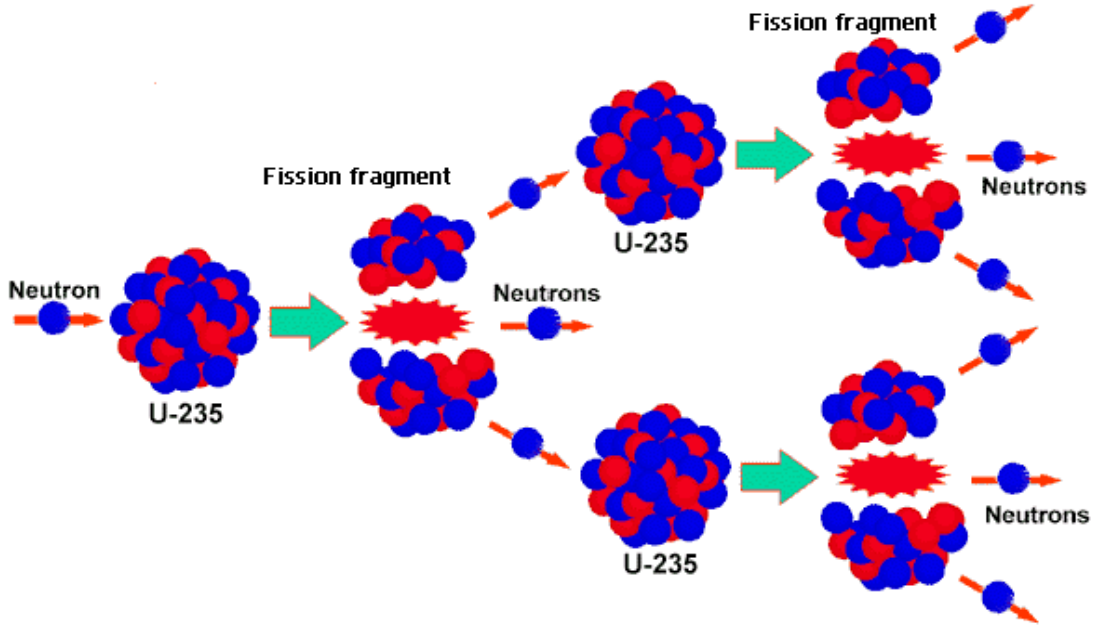

Figure 1.9- Nuclear chain reaction.

5.2. Moderators

Fission neutrons are produced at an average energy level of 2MeV, while those used to fission ^{235}U are thermal (~0.025eV). In natural uranium it is essential, and with enriched fuels it is usually desirable, to slow the neutrons down to thermal energies in some material other than the fuel. The material used to slow down neutrons is called the moderator.

The function of the moderator is to reduce neutrons of fission energy to thermal energy within the smallest space and with the least loss of neutrons. The descriptive term attached to a moderator, "slowing down power" can be given quantitative meaning in the following way. The moderator must be (1) efficient at slowing down the neutrons (i.e. to slow down in as few collisions as possible) and (2) it must be a poor absorber of neutrons. The first requirement indicates a light element, since the average relative energy loss per collision $\Delta E/E$ crudely varies inversely with the mass of the moderator nucleus (e.g., $\Delta E/E \approx 1.0$ for H and $\Delta E/E \approx 0.159$ for C). The second requirement eliminates such light elements as lithium and boron, and makes hydrogen unsuitable for use with natural uranium. Carbon and heavy water are usual moderators for natural uranium, while water or other hydrogen containing compounds are commonly used with enriched fuel.

5.3. Reflectors

In the discussion thus far, a reactor consisting only of fuel and moderator has been assumed. It has been further assumed that if a neutron leaves such a reactor, it will never return. Suppose, however, a good scattering material such as carbon is put around the reactor. Some of the neutrons that leave the reactor will now collide with carbon nuclei and be scattered back into the reactor. Such a layer of scattering material around a reactor is called a reflector. By reducing neutron leakage, the reflector increases *keff* and reduces the amount of fuel necessary to make the reactor critical.

The efficiency of a reflector is measured by the ratio of the number of neutrons reflected back into the reactor to the number entering the reflector. This ratio is called the albedo. The value of the albedo will depend on the composition and thickness of the reflector. An infinite reflector will have the maximum albedo, but for all practical purposes a reflector will suffice if it is about twice as thick as the average distance over which a thermal neutron diffuses. (In water, a thickness of ~2 inches makes such a reflector.) Values of the albedo for the usual scattering materials fall within the range of 0.8 to 0.9.

Figure (1.10) shows qualitatively the variation in neutron flux for a core with and without a reflector. When the reflector is in place, neutrons that would otherwise be lost are returned to the core. (In a large number of reactors, water serves as both moderator and reflector.) This figure also shows a peak in thermal flux within the reflector. This is because some of the fast neutrons that enter the reflector are reduced to thermal energy while being scattered in the reflector. Thermal neutrons are effectively being produced within the reflector. In addition, the absorption of thermal neutrons is much less in that reflector because of the fact that there is no fuel present with its large absorption cross section.

It is found that the fast flux does not show recovery peaks in the reflector near the core, but rather drops off sharply inside the moderator-reflector. However, in some cases it is found the fast flux becomes a significant portion of the total flux. This typically is the case outside thick shields which contain absorbers for thermal neutrons but otherwise have relatively little attenuation (moderation) for the fast flux.

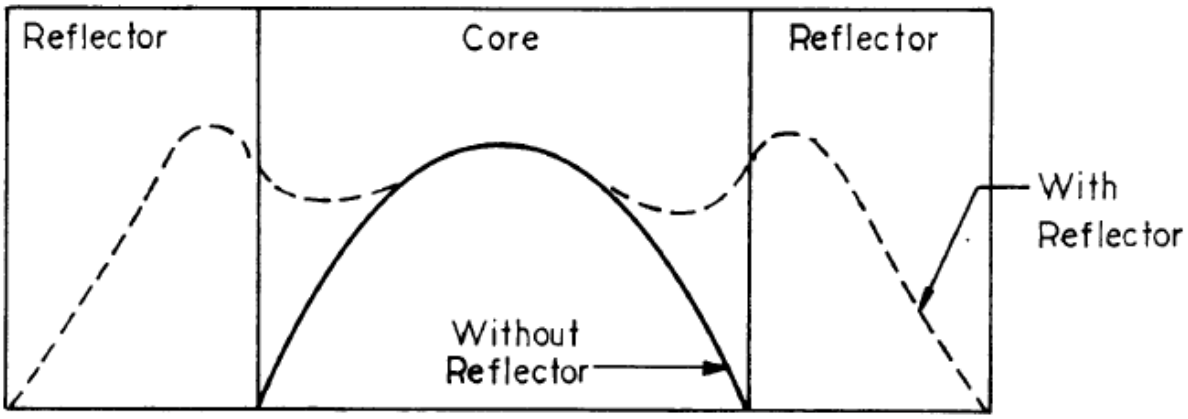

Figure 1.10- Radial thermal flux distribution with and without reflector.

5.4. Neutron flux distribution

It can be shown that the radial and axial flux distributions for bare (non-reflected) reactors are given by precise mathematical functions. These functions are dependent on the geometry and size of the reactor core. For example, in a cylindrical reactor the flux is given by:

$$f(r,z) = AJ_0(2.405r/R)\cos(pz/H) \tag{1.26}$$

where, R and H are the radius and the height of the core, respectively.

This means that the radial flux has the shape of the Bessel function J0 and the axial flux has the shape of a cosine (*Fig. 1.11*) below.

It should be emphasized that this is the flux shape for an ideal, homogeneous reactor core. Practical cores, with reflectors, lumped fuel elements, control rods, variable enrichments, variable burn-up, and fission product poisons have modified flux distributions. However, these cores still have very similar general flux distributions.

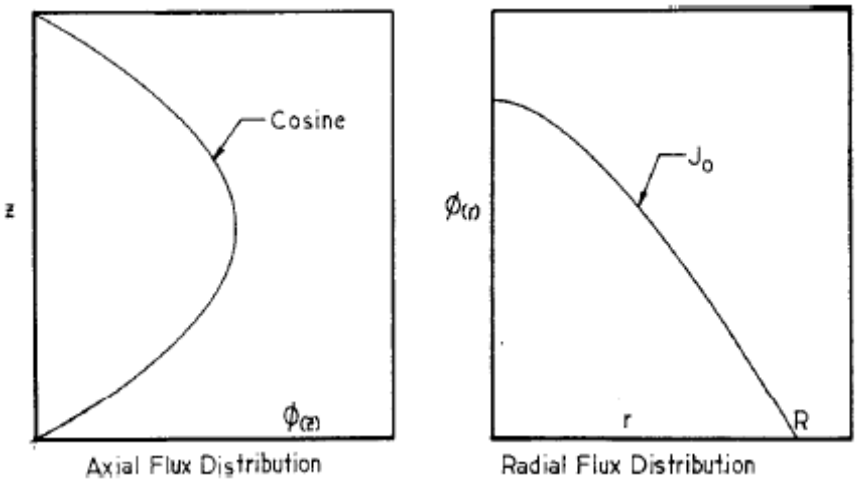

Figure 1.11- Axial and radial flux distribution.

In contrast to the overall flux shape, if the details of the distribution of the thermal neutron flux in and around a fuel element were studied, it would be found that the thermal neutron flux is at a minimum in the centre of the element. The reason for this is that the fuel readily absorbs thermal neutrons (to produce fast neutrons in fission), and so the outside of the fuel essentially shields the inside. This is known as self-shielding (*Fig. 1.12*).

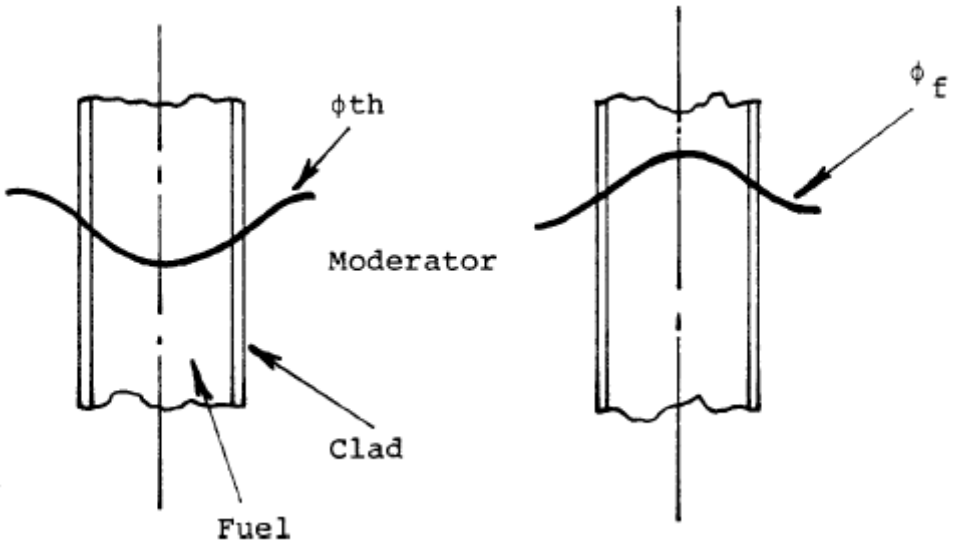

Figure 1.12- Thermal and fast flux distribution in fuel elements.

5.5. Control rods

The adjustment of neutron flux or power level in the reactor is achieved by movement of the control rods. They consist of a container filled with a strongly neutron-absorbing medium such as boron, cadmium, gadolinium, or hafnium. The rod has the property of reducing or increasing the *thermal utilization factor* (*f*) and thus changing *keff*, depending on whether the rod is inserted or withdrawn from the core. This change in *keff* results in a change in the reactivity of the core. The worth of a control rod is, therefore, directly related to its effect on reactivity and is usually measured in the same units.

The physical effects produced by a control rod can be visualized in the following way. If a thermal neutron, in the course of its diffusion through the core, enters the absorbing boron, for example, its chance of getting through is almost nil. For all practical purposes, boron is "black", i.e., a perfect absorber, for thermal neutrons, in that all neutrons that reach the surface are lost. Thus, the neutron flux and density effectively go to zero at the boundary of the absorber, as shown in Figure (1.13).

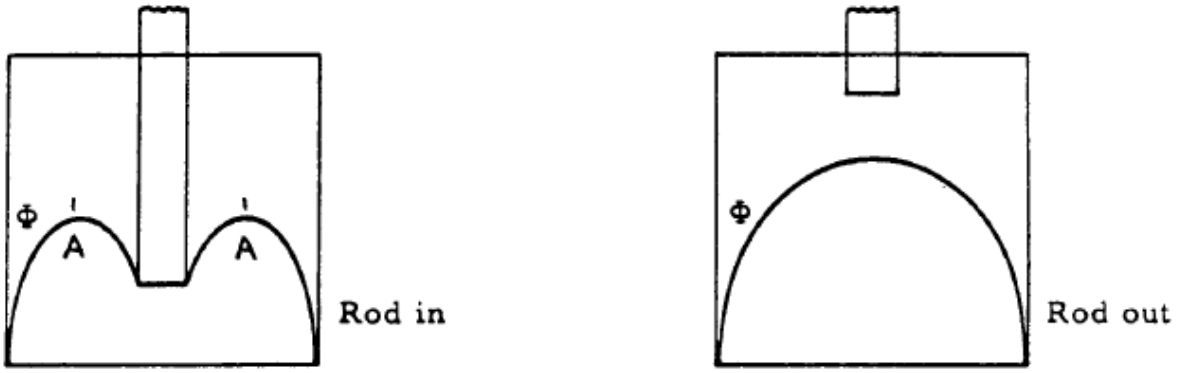

Figure 1.13- Effect of a single control rod on neutron flux.

The effectiveness, or worth, of a control rod depends largely upon the value of the neutron flux at the location of the rod. The control rod will have maximum effect if it is placed in the reactor where the flux is a maximum. If a reactor had only one control rod, the rod would be placed in the centre of the reactor. The effect of such a rod on the flux is indicated in Figure (1.13). If additional rods are added to this simple reactor, the most effective locations will again be where the flux is a maximum, i.e., at points A.

In a similar manner, the variation in the worth of the rod as it is inserted or withdrawn from the reactor is dependent on the axial flux shape. It can be seen from the earlier discussion (*Fig. 1.11*); that the flux is typically less at the top and bottom of the reactor than in the middle. Therefore, the control rod is worth less at the top and bottom than it is in the middle during insertion or withdrawal. This behavior is typically illustrated in the differential and integral rod worth curves as shown in Figure (1.14). The integral control rod worth curve is particularly important in research reactor operation.

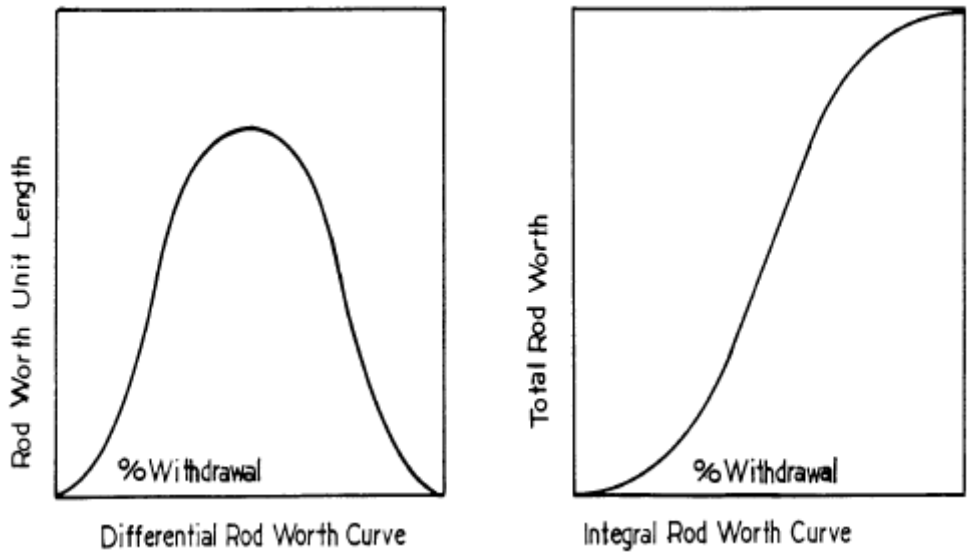

Figure 1.14- Differential and integral control rod worth curves.

5.6. Self-shielding

In some locations within the reactor, the flux level may be significantly lower than in other areas due to a phenomenon referred to as *neutron shadowing* or *self-shielding*. For example, the interior of a fuel pin or pellet will "see" a lower average flux level than the outer surfaces since an appreciable fraction of the neutrons will have been absorbed and therefore cannot reach the interior of the fuel pin. This is especially important at resonance energies, where the absorption cross sections are large.

5.7. Fast and thermal reactors spectra

Figure (1.15) shows typical neutron spectra plotted as $E_j\,(E)$ for a sodium-cooled fast reactor and for a water-cooled thermal reactor. Several features are noteworthy. Fast reactor spectra are concentrated in the keV and MeV range with nearly all of the neutrons absorbed before slowing down to energies less than a keV. Fast reactor cores contain intermediate weight elements, such as sodium coolant and iron used for structural purposes. These intermediate atomic weight elements have large resonances in their elastic scattering cross sections in the keV and MeV energy range. Thus the fast spectra are quite jagged in appearance, resulting from the energy self-shielding phenomenon, in which the flux is inversely proportional to the total cross section.

Thermal reactor spectra have a more modest peak in the MeV range where fission neutrons are born. The spectra over higher energies are somewhat smoother as a result of the prominent role played by the lightweight moderator materials; moderators have no resonances at those energies. Moving downward through the keV range, we see that the spectrum is nearly flat. Here there is very little absorption, resulting in a nearly *1/E* [or constant $E_j\,(E)$] spectrum with the constant slowing down density. The thermal reactor spectra do decrease with decreasing energy going from 100 and 1.0 eV, accentuated by sharp dips in the flux. Although barely visible in the figure, resonance absorption in uranium over this energy range causes the slowing down density to decrease and the self-shielding to become more pronounced. Below 1.0 eV, the characteristic thermal peak occurs as a result of thermal neutron absorption in the fuel and moderator.

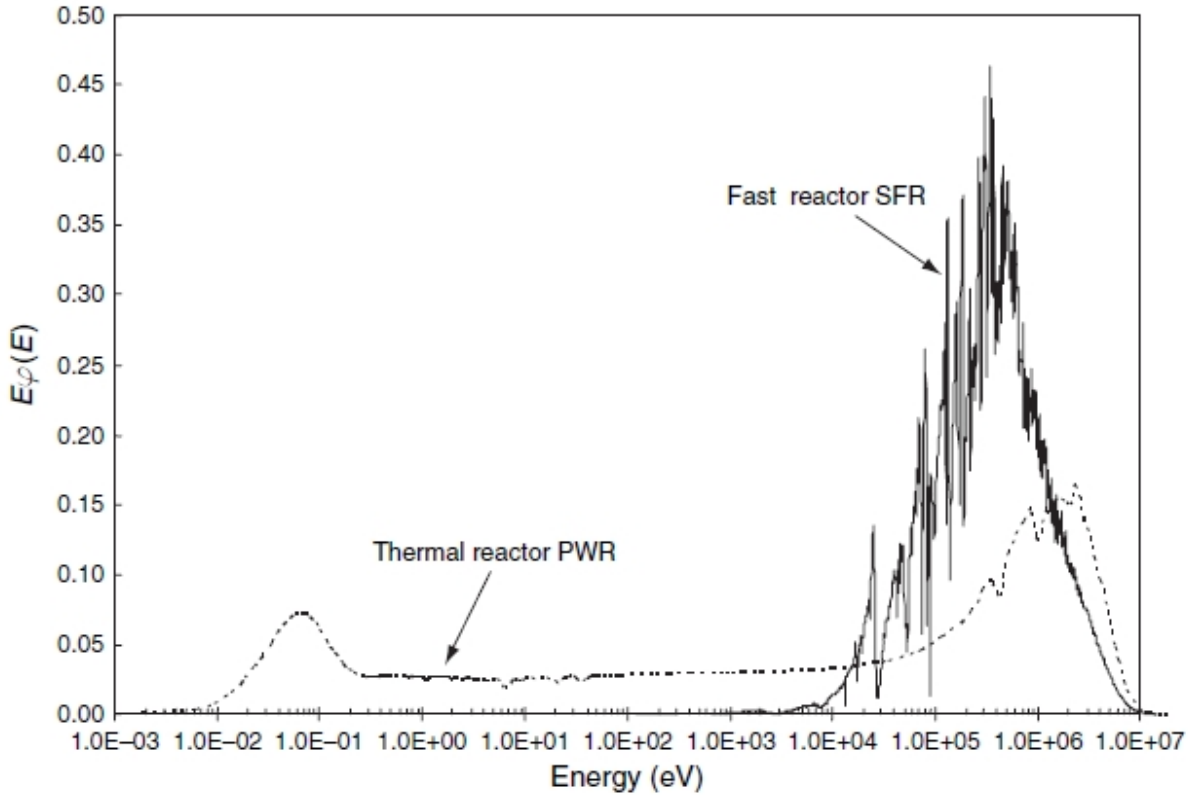

Figure 1.15- Neutron flux spectra from thermal (pressurized water) and fast (sodium-cooled) reactors.

5.8. Delayed neutrons

One of the most important aspects of the fission process from the viewpoint of reactor control is the presence of delayed neutrons. A delayed neutron is a neutron emitted by an excited fission product nucleus during beta disintegration some appreciable time after the fission. How long afterward, is dependent on the half-life of the delayed neutron precursor, since the neutron emission itself occurs in a very short time. The symbol b is used to denote the total fraction of delayed neutrons.

There are many decay chains which are of significance in the emission of delayed neutrons. (Not all of these chains have been positively identified.) Correspondingly, delayed neutrons are commonly discussed as being in six groups. Each of these groups (i) is characterized by a fractional yield b_i and a decay constant l_i.

Table (1.1) lists the properties of the six known groups of delayed neutrons emitted during the fission of ^{235}U. The fractional yield b_i is the number of delayed neutrons in a reactor operating at steady state, which are due to neutron emission from decay of fission products (precursors) in group i. The total yield of delayed neutrons is the sum of the fractional values b_i over all groups i. In general, delayed neutrons are more effective than prompt neutrons because they

are born at somewhat lower energy compared to prompt (fission) neutrons. Thus they have a better chance to survive leakage and resonance absorption. This is accounted for by giving the delayed neutrons a higher "weight", which is realized by an upward adjustment of the yield values. The effective total delayed neutron fraction is designated b_{eff}. The value of b_{eff}, for a given fuel, will vary with the average energy of the neutrons producing fission. [b_{eff} for the TRIGA using $^{235}U = 0.007$.]

Table 1.1- Delayed neutrons from thermal fission of ^{235}U.

Group	Probable precursor	Half-life (s)	Effective yield b_i	% of delayed neutrons $100\, b_i / b = f_i$	Number of fission neutrons delayed per fission
1	^{87}Br	55.72	0.00021	3.23	0.00052
2	^{137}I	22.72	0.00141	21.7	0.00346
3	^{89}Br	6.22	0.00127	19.55	0.00310
4	^{139}I	2.30	0.00255	39.3	0.00624
5	^{85}As	0.61	0.00074	11.4	0.00182
6	^{9}Li	0.23	0.00027	4.16	0.00066
Total delayed					0.00158
Fraction delayed b			0.0065		
Weighted mean life (t) = 12.3 s			l_i = decay constant = $\ln 2/t_{1/2}$		
Total fission neutrons = 2.43			Ti = mean life = $t_{1/2}/\ln 2$		

6. Reactivity

6.1. Definition of reactivity

Reactivity is the measure of the departure of a reactor from criticality. The effective multiplication factor, ***keff***, determines whether the neutron density within a reactor will remain constant or change. Since the power level is directly proportional to the neutron density, whenever ***keff*** = 1.0, the reactor is critical and operates at a constant power level. If ***keff*** < 1.0, the reactor is subcritical and the power level is decreasing. If ***keff*** > 1.0, the reactor is supercritical and the power level is rising. (Notice that the power level, neutron density, etc., are constantly changing whenever ***keff*** is not equal to 1.0.) The difference between a given value of ***keff*** and 1.0 is known as the "excess" multiplication factor, d k:

$$keff - 1 = d\,k = k_{excess} \qquad (1.27)$$

and d k may be either positive or negative, depending upon whether ***keff*** is greater or less than 1.0. A useful quantity known as reactivity is given by the symbol r (rho) and is related to d k as follows:

$$r = \frac{keff - 1}{keff} = \frac{dk}{keff} \tag{1.28}$$

NOTE:

r and d k are equal to "0" whenever a reactor is exactly critical, and have almost the same value whenever ***keff*** is slightly larger or smaller than 1.0.

6.2. Reactivity effects

6.2.1. Reactivity coefficients and reactivity defects

The amount of reactivity (r) in a reactor core determines what the neutron populations, and consequently the reactor power, are doing at any given time. The reactivity can be affected by many factors (for example, fuel depletion, temperature, pressure, or poisons).

To quantify the effect that a variation in parameter (that is, increase in temperature, control rod insertion, increase in neutron poison) will have on the reactivity of the core, ***reactivity coefficients*** are used. Reactivity coefficients are the amount that the reactivity will change for a given change in the parameter. For instance, an increase in moderator temperature will cause a decrease in the reactivity of the core. The amount of reactivity change per degree change in the moderator temperature is the moderator temperature coefficient. Typical units for the moderator temperature coefficient are pcm/°C. Reactivity coefficients are generally symbolized by a_x, where x represents some variable reactor parameter that affects reactivity. The definition of a reactivity coefficient in equation format is shown below.

$$a_x = \frac{\Delta r}{\Delta x} \tag{1.29}$$

If the parameter x increases and positive reactivity is added, then a_x is positive. If the parameter x increases and negative reactivity is added, then a_x is negative.

Reactivity defects (Δr) are the total reactivity change caused by a variation in a parameter. Reactivity defects can be determined by multiplying the change in the parameter by the average value of the reactivity coefficient for that parameter. The equation below shows the general method for relating reactivity coefficients to reactivity defects.

$$\Delta r = a_x \Delta x \tag{1.30}$$

6.2.2. Temperature coefficient of reactivity

The temperature coefficient of reactivity is defined as the change in reactivity for a unit change in temperature and is represented by a_T.

In an operating reactor, the temperature changes as the power varies. Let us consider a power increase. A power-level increase is a direct result of more fissions releasing more heat. As the average temperature of the reactor contents rises, the coolant and moderator expand and become less dense. Because there are now fewer molecules per unit volume, the moderator is less effective in slowing down neutrons and more leakage is observed. The overall effect is a reduction in *keff* or the addition of negative reactivity. Reactivity and temperature change are related thus:

$$dk_T = a_T(T_2 - T_1) = a_T \Delta T \tag{1.31}$$

where

dK_T = the reactivity change resulting from temperature change,

a_T = temperature coefficient,

T_2 = final temperature,

T_1 = initial temperature,

ΔT = temperature change.

Notice from the equation that whenever the reactivity and the temperature change move in the same direction, a_T is positive and is known as a "positive temperature coefficient". If the reactivity and the temperature change move in opposite directions, a_T is negative and is, of course, a "negative temperature coefficient." Any reactor having a positive temperature coefficient is unstable and can be difficult to control.

6.2.3. Pressure coefficient

The reactivity in a reactor core can be affected by the system pressure. The ***pressure coefficient*** of reactivity is defined as the change in reactivity per unit change in pressure. The pressure coefficient of reactivity for the reactor is the result of the effect of pressure on the density of the moderator. For this reason, it is sometimes referred to as the moderator density reactivity coefficient. As pressure increases, density correspondingly increases, which increases the moderator-to-fuel ratio in the core. In the typical under moderated core the increase in the moderator-to-fuel ratio will result in a positive reactivity addition. In reactors that use water as a moderator, the absolute value of the pressure reactivity coefficient is

seldom a major factor because it is very small compared to the moderator temperature coefficient of reactivity.

6.2.4. Void coefficient

In systems with boiling conditions, such as boiling water reactors (BWR), the pressure coefficient becomes an important factor due to the larger density changes that occur when the vapor phase of water undergoes a pressure change. Of prime importance during operation of a BWR, and a factor in some other water-moderated reactors, is the void coefficient. The void coefficient is caused by the formation of steam voids in the moderator. The *void coefficient* of reactivity is defined as the change in reactivity per percent change in void volume. As the reactor power is raised to the point where the steam voids start to form, voids displace moderator from the coolant channels within the core. This displacement reduces the moderator-to-fuel ratio, and in an under moderated core, results in a negative reactivity addition, thereby limiting reactor power rise. The void coefficient is significant in water-moderated reactors that operate at or near saturated conditions.

2. Nuclear fuel burnup

(Weston M. Stacey, 2007)

The long-term changes in the properties of a nuclear reactor over its lifetime are determined by the changes in composition due to fuel burnup and the manner in which these are compensated. The economics of nuclear power is strongly affected by the efficiency of fuel utilization to produce power, which in turn is affected by these long-term changes associated with fuel burnup. In this chapter we describe the changes in fuel composition that take place in an operating reactor and their effects on the reactor, the effects of the samarium and xenon fission products with large thermal neutron cross sections, the conversion of fertile material to fissionable material by neutron transmutation, the effects of using plutonium from spent fuel and from weapons surplus as fuel, the production of radioactive waste, the extraction of the residual energy from spent fuel, and the destruction of long-lived actinides.

1. Changes in fuel composition

The initial composition of a fuel element will depend on the source of the fuel. For reactors operating on the uranium cycle, fuel developed directly from natural uranium will contain a mixture of ^{234}U, ^{235}U and ^{238}U, with the fissile ^{235}U content varying from 0.72% (for natural uranium) to more than 90%, depending on the enrichment. Recycled fuel from reprocessing plants will also contain the various isotopes produced in the transmutation-decay process of uranium. Reactors operating on the thorium cycle will contain ^{232}Th and ^{233}U or ^{235}U, and if the fuel is from a reprocessing plant, isotopes produced in the transmutation-decay process of thorium.

During the operation of a nuclear reactor a number of changes occur in the composition of the fuel. The various fuel nuclei are transmuted by neutron capture and subsequent decay. For a uranium-fueled reactor, this process produces a variety of transuranic elements in the actinide series of the periodic table. For a thorium fueled reactor, a number of uranium isotopes are produced. The fission event destroys a fissile nucleus, of course, and in the process produces two intermediate mass fission products. The fission products tend to be neutron-rich and subsequently decay by beta or neutron emission (usually accompanied by gamma emission) and undergo neutron capture to be transmuted into a heavier isotope, which itself undergoes radioactive decay and neutron transmutation, and so on. The fissile nuclei also undergo neutron transmutation via radiative capture followed by decay or further transmutation.

1.1. Fuel transmutation-decay chains

Uranium-235, present 0.72% in natural uranium, is the only naturally occurring isotope that is fissionable by thermal neutrons. However, three other fissile (fissionable by thermal neutrons)

isotopes of major interest as nuclear reactor fuel are produced as the result of transmutation-decay chains. Isotopes that can be converted to fissile isotopes by

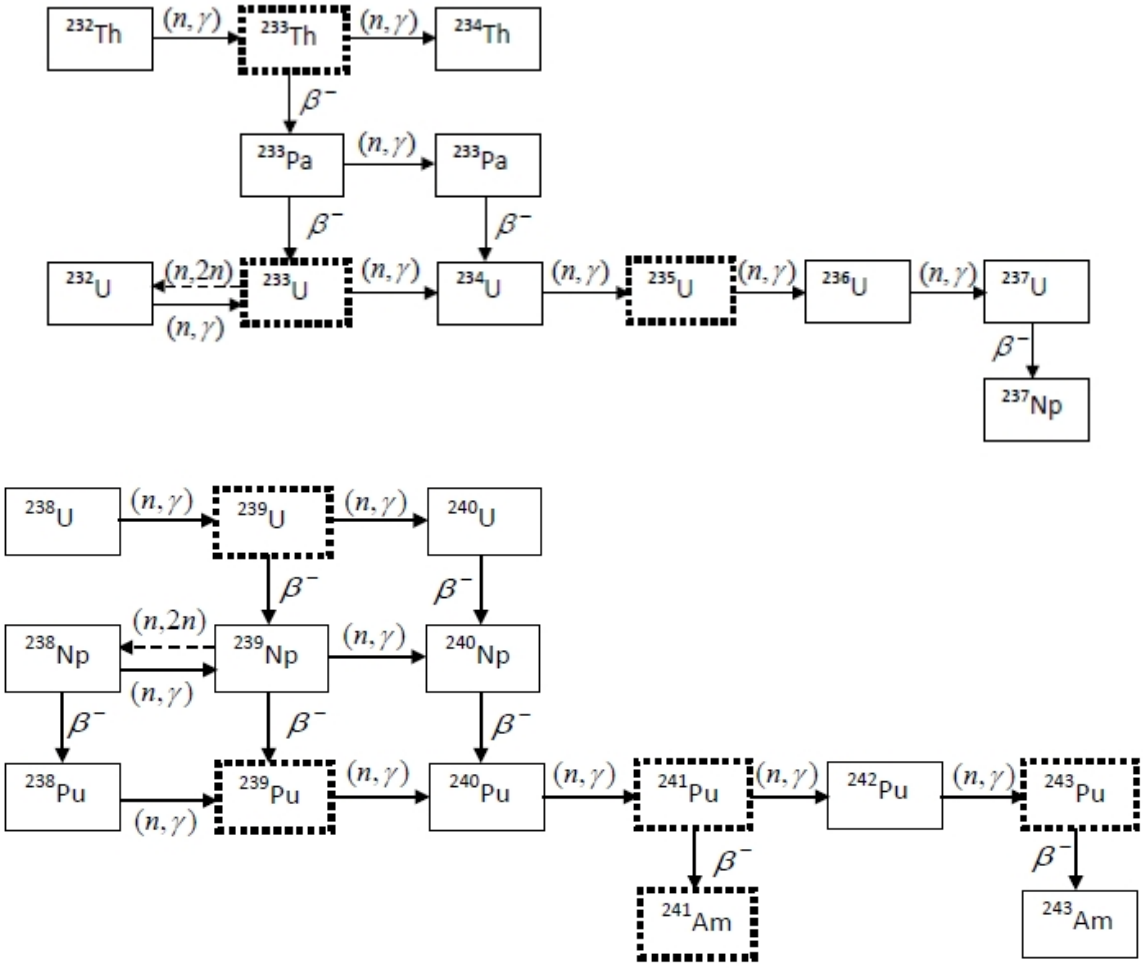

Figure 2.1- Transmutation-decay chains for ^{232}Th and ^{238}U isotopes.

neutron transmutation and decay are known as fertile isotopes. ^{239}Pu and ^{241}Pu are products of the transmutation-decay chain beginning with the fertile isotope ^{238}U, and ^{233}U is a product of the transmutation-decay chain beginning with the fertile isotope ^{232}Th. These two transmutation-decay chains are shown in Figure (2.1). Isotopes are in rows with horizontal arrows representing (n,g) transmutation reactions. Downward arrows indicate b-decay. Thermal neutron fission is represented by a dashed diagonal arrow.

1.2. Fuel depletion-transmutation-decay equations

Concentrations of the various fuel isotopes in a reactor are described by a coupled set of production-destruction equations. We adopt the two-digit superscript convention for identifying isotopes in which the first digit is the last digit in the atomic number and the second digit is the last digit in the atomic mass. We represent the neutron reaction rate by

$s_X^{nm} fn^{nm}$, although the actual calculation may involve a sum over energy groups of such terms.

For reactors operating on the uranium cycle, the isotopic concentrations are described by:

$$\frac{\partial n^{24}}{\partial t} = -s_a^{24} fn^{24}$$

$$\frac{\partial n^{25}}{\partial t} = s_g^{24} fn^{24} - s_a^{25} fn^{25} \qquad (2.1)$$

$$\frac{\partial n^{26}}{\partial t} = s_g^{26} fn^{26} + l_{ec}^{36} n^{36} - s_a^{26} fn^{26}$$

$$\frac{\partial n^{27}}{\partial t} = s_g^{26} fn^{26} + s_{n,2n}^{28} fn^{28} - l^{27} n^{27}$$

$$\frac{\partial n^{28}}{\partial t} = -s_a^{28} fn^{28}$$

$$\frac{\partial n^{29}}{\partial t} = s_g^{28} fn^{28} - (l^{29} + s_a^{29} f) n^{29}$$

$$\frac{\partial n^{36}}{\partial t} = s_{n,2n}^{37} fn^{37} - (l^{36} + s_a^{36} f) n^{36}$$

$$\frac{\partial n^{37}}{\partial t} = l^{27} n^{27} - s_a^{37} fn^{37}$$

$$\frac{\partial n^{38}}{\partial t} = s_g^{37} fn^{37} - (l^{38} + s_a^{38} f) n^{38}$$

$$\frac{\partial n^{39}}{\partial t} = l^{29} n^{29} - (l^{39} + s_a^{39} f) n^{39}$$

$$\frac{\partial n^{48}}{\partial t} = l^{38} n^{38} - s_a^{48} fn^{48}$$

$$\frac{\partial n^{49}}{\partial t} = l^{39} n^{39} - s_a^{49} fn^{49} + s_g^{48} fn^{48}$$

$$\frac{\partial n^{40}}{\partial t} = s_g^{49} fn^{49} - s_a^{40} fn^{40} + s_g^{29} fn^{29} + s_g^{39} fn^{39}$$

$$\frac{\partial n^{41}}{\partial t} = s_{g}^{40} f n^{40} - (l^{41} + s_{a}^{41} f) n^{41}$$

$$\frac{\partial n^{42}}{\partial t} = s_{g}^{41} f n^{41} - s_{a}^{42} f n^{42}$$

$$\frac{\partial n^{43}}{\partial t} = s_{g}^{42} f n^{42} - (l^{43} + s_{a}^{43} f) n^{43}$$

$$\frac{\partial n^{51}}{\partial t} = l^{41} n^{41} - (l^{51} + s_{a}^{51} f) n^{51}$$

$$\frac{\partial n^{52}}{\partial t} = s_{g}^{51} f n^{51} - s_{a}^{52} f n^{52}$$

$$\frac{\partial n^{53}}{\partial t} = l^{43} n^{43} - s_{a}^{53} f n^{53} + s_{g}^{52} f n^{52}$$

With respect to Figure (2.1), a few approximations have been made in writing *Eq. (2.1)*. The neutron capture in ^{239}U to produce ^{240}U followed by the decay ($t_{1/2}$= 14h) into ^{240}Np and the subsequent decay ($t_{1/2}$= 7 min) into ^{240}Pu is treated as the direct production of ^{240}Pu by neutron capture in ^{239}U and the production of ^{240}Np by neutron capture in ^{239}Np followed by the subsequent decay ($t_{1/2}$ = 7 min) of ^{240}Np into ^{240}Pu is treated as the direct production of ^{240}Pu by neutron capture in ^{239}Np. These approximations have the beneficial effect for numerical solution techniques of removing short time scales from the set of equations, without sacrificing information of interest on the longer time scale of fuel burnup.

For reactors operating on the thorium cycle, the isotopic concentrations are described by:

$$\frac{\partial n^{02}}{\partial t} = -s_{a}^{02} f n^{02}$$

$$\frac{\partial n^{03}}{\partial t} = s_{g}^{02} f n^{02} - (l^{03} + s_{a}^{03} f) n^{03} \qquad (2.2)$$

$$\frac{\partial n^{13}}{\partial t} = l^{03} n^{03} - (l^{13} + s_{a}^{13} f) n^{13}$$

$$\frac{\partial n^{22}}{\partial t} = -(l^{22} + s_{a}^{22} f) n^{22}$$

$$\frac{\partial n^{23}}{\partial t} = s_{g}^{22} f n^{22} + l^{13} n^{13} - s_{a}^{23} f n^{23}$$

$$\frac{\partial n^{24}}{\partial t} = s_{g}^{23} f n^{23} - s_{a}^{24} f n^{24} + s_{g}^{13} f n^{13}$$

$$\frac{\partial n^{25}}{\partial t} = s_{g}^{24} f n^{24} - s_{a}^{25} f n^{25}$$

$$\frac{\partial n^{26}}{\partial t} = s_{g}^{25} f n^{25} - s_{a}^{26} f n^{26}$$

$$\frac{\partial n^{27}}{\partial t} = s_{g}^{26} f n^{26} - (l^{27} + s_{a}^{27} f) n^{27}$$

$$\frac{\partial n^{37}}{\partial t} = l^{27} n^{27} - s_{a}^{37} f n^{37}$$

Another short-time-scale elimination approximation that neutron capture in ^{233}Pa leads directly to ^{234}U has been made.

1.3. Fission products

The fission event usually produces two intermediate mass nuclei, in addition to releasing two or three neutrons. Interestingly, the fission product masses are not usually equal to about half the mass of the fissioning species, but are distributed in mass with peaks at about 100 and 140amu, as shown in Figure (2.2). The isotopes produced by fission tend to be neutron-rich and undergo radioactive decay. They also undergo neutron capture, with cross sections ranging from a few tenths of a barn to millions of barns. The general production-destruction equation satisfied by a fission product species j is:

$$\frac{dn_j}{dt} = g_j \Sigma_f f + \sum_i (l^{i \to j} + s^{i \to j} f) n_i - (l^j + s_a^j f) n_j \qquad (2.3)$$

where g_j is the fraction of fission events that produces a fission product species j, $l^{i \to j}$ is the decay rate of isotope i to produce isotope j (beta, alpha, neutron, etc., decay) and $s^{i \to j}$ is the transmutation cross section for the production of isotope j by neutron capture in isotope i. Even though the fission products undergo transmutation and decay, the total inventory of direct fission products plus their progeny increases in time as

$$\frac{dn_{fp}}{dt} = \sum_j \frac{dn_j}{dt} = \sum_j g_j \Sigma_f f \qquad (2.4)$$

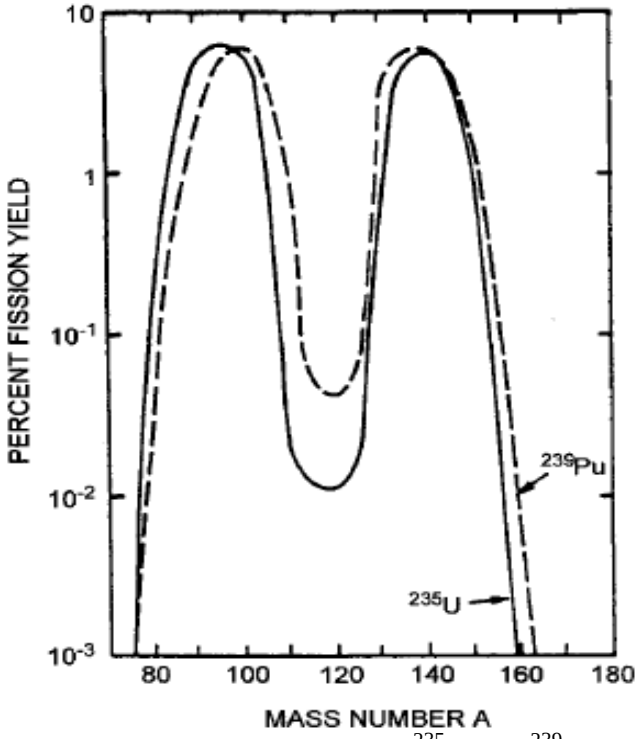

Figure 2.2- Fission yields for ^{235}U and ^{239}Pu.

1.4. Solution of the depletion equations

The equations above can be integrated to determine composition changes over the lifetime of the reactor core loading if the time dependence of the flux is known. However, the flux distribution depends on the composition. In practice, a neutron flux distribution is calculated for the beginning-of-cycle composition and critical control rod position or soluble boron concentration (PWR), and this flux distribution is used to integrate the composition equations above over a depletion-time step, Δt_{burn}. Then the new critical control rod position or soluble boron concentration is determined (by trial and error) and the flux distribution is recalculated for use in integrating the production-destruction equations over the next depletion time step, and so on, until the end of cycle is reached. The maximum value of Δt_{burn} depends on how fast the composition is changing and the effect of that composition change on the neutron flux distribution and on the accuracy of the numerical integration scheme. Excluding, for the moment, the relatively short time scale phenomena associated with the xenon and samarium fission products, the time scale of significant composition and flux changes is typically several hundred hours or more.

The typical process of advancing the depletion solution from time t_i, at which the composition is known, to time t_{i+1}, is: (1) determine the multigroup constants appropriate for the composition at t_i, (2) determine the critical control rod positions or soluble poison

concentration by solving the multigroup diffusion equations for the flux at t_i (adjusting the control rod positions or boron concentration until the reactor is critical), and (3) integrate the various fuel and fission product production destruction equations from t_i to t_{i+1}. (The neutron flux solution could be made with a multigroup transport calculation or with multigroup or continuous-energy Monte Carlo calculation, and the preparation of cross sections could involve infinite media spectra and unit cell homogenization calculations or could be based on fitted, precomputed constants.) The integration of the production-destruction equations can be for a large number of points, using the neutron flux at each point; for each fuel pin, using the average flux in the fuel pin; for each fuel assembly, using the average flux over the fuel assembly; and so on.

Assuming that the flux is constant in the interval $t_i < t < t_{i+1}$, the production destruction equations can be written in matrix notation as

$$\frac{dN(t)}{dt} = A(f(t_i))N(t) + F(f(t_i)), \quad t_i \le t \le t_{i+1} \tag{2.5}$$

Eq. (2.5) may be solved using a variety of numerical techniques (Rung kutta methods, Taylor series, matrix exponential method, etc …). The accuracy of the solution depends on a lot of parameters participating on the solution of the production-destruction equation, such as, the solution technique chosen, nuclear data, time steps sizes, etc … .

1.5. Measure of fuel burnup

The most commonly used measure of fuel burnup is the fission energy release per unit mass of fuel. The fission energy release in megawatt-days divided by the total mass (in units of 1000 kg or 1 tonne) of fuel nuclei (fissile plus fertile) in the initial loading is referred to as megawatt-days per tonne (MWd/T). An equivalent unit is MWd/kg - 10^3 MWd/T. For example, a reactor with 100,000 kg of fuel operating at 3000MW power level for 1000 days would have a burnup of 30,000 MWd/T. For LWRs the typical fuel burnup is 30,000 to 50,000 MWd/T. Fuel burnup in fast reactors is projected up to be about 100,000 to 150,000 MWd/T.

1.6. Fuel composition changes with burnup

The original fissionable isotope (e.g., ^{235}U) naturally decreases as the reactor operates. However, the neutron transmutation of the fertile isotope (e.g., ^{238}U) reduces the fissionable isotope ^{239}Pu, which in turn is transmuted by neutron capture into ^{240}Pu and higher actinide

isotopes. The buildup of the various Pu isotopes as a function of fuel burnup for a typical LWR is shown in Figure (2.3). Compositions of spent fuel discharged from representative LWR and LMFBR designs are given in Table (2.1). The units are densities (cgs units) times which allow construction of macroscopic cross section upon multiplication by the microscopic cross section in barns. The composition for the average enrichment and burnup of PWR spent fuel is shown in the first column for fuel discharged before 1995 and in the second column for fuel discharged after 1995.

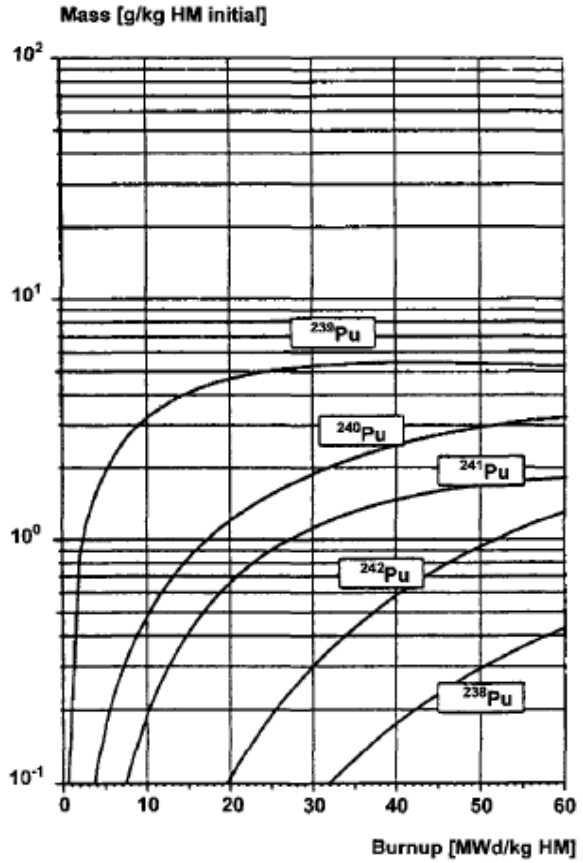

Figure 2.3- Buildup of Pu isotopes in 4 wt % enriched UO2 in an LWR (*Weston M. Stacey, 2007*).

Table 2.1- Heavy metal composition of spent UO2 fuel at discharge (*Weston M. Stacey, 2007*).

Reactor Type	**LWR**	**LWR**	**LMFBR**	**LMFBR**
Initial enrichment (wt%)	3.13	4.11	20	20
Power (MW/MTU)	21.90	27.99	54.76	54.76
Burnup (GWd/T)	32	46	100	150
Actinides ($10^{24}cm^3$)				
^{234}U	$3.92x10^{-6}$	4.51×10^{-6}	3.37×10^{-5}	2.88×10^{5}
^{235}U	1.92×10^{-4}	1.72×10^{-4}	2.17×10^{-3}	1.37×10^{-3}
^{236}U	8.73×10^{-5}	1.23×10^{-4}	4.58×10^{-4}	5.62×10^{-4}
^{237}U	-	2.48×10^{-7}	5.71×10^{-7}	7.89×10^{-7}
^{238}U	2.12×10^{-2}	2.08×10^{-2}	1.63×10^{-2}	1.53×10^{-2}
^{237}Np	1.01×10^{-5}	1.64×10^{-5}	5.11×10^{-5}	1.01×10^{-4}
^{239}Np	$1.25 x10^{-6}$	1.55×10^{-6}	2.93×10^{-6}	3.16×10^{-6}
^{238}Pu	3.36×10^{-6}	6.56×10^{-6}	3.84×10^{-6}	1.20×10^{-5}
^{239}Pu	1.23×10^{-4}	1.23×10^{-4}	1.04×10^{-3}	1.36×10^{-3}
^{240}Pu	4.05×10^{-5}	4.28×10^{-5}	7.83×10^{-5}	1.71×10^{-4}
^{241}Pu	3.44×10^{-5}	4.07×10^{-5}	2.60×10^{-6}	8.37×10^{-6}
^{242}Pu	1.05×10^{-5}	1.69×10^{-5}	-	4.70×10^{-7}
^{241}AM	1.45×10^{-6}	$1.62 x10^{-6}$	1.50×10^{-7}	6.87×10^{-7}
^{243}AM	2.12×10^{-6}	4.46×10^{-6}	-	-
^{242}CM	3.71×10^{-7}	5.66×10^{-7}	-	-
^{244}CM	4.81×10^{-7}	1.39×10^{-6}	-	-

1.7. Reactivity effects of fuel composition changes

There are many of reactivity effects associated with the change in fuel composition. The fission of fuel nuclei produces two negative reactivity effects; the number of fuel nuclei is reduced and fission products are created, many of which have large neutron capture cross sections. The transmutation-decay chain of fertile fuel nuclei of a given species produces a sequence of actinides (uranium-fueled reactor) or uranium isotopes (thorium-fueled reactor), some of which are fissile. The transmutation of one fertile isotope into another non fissile isotope can have a positive or negative reactivity effect, depending on the cross sections for the isotopes involved, but the transmutation of a fertile isotope into a fissile isotope has a positive reactivity effect. Depending on the initial enrichment, the transmutation-decay process generally produces more fissile nuclei than are destroyed early in the cycle, causing a positive reactivity effect, until the concentration of transmuted fissile nuclei comes into equilibrium.

The buildup of ^{239}Pu early in life of a uranium-fueled reactor produces a large positive reactivity effect which may be greater than the negative reactivity effect of ^{235}U depletion and fission product buildup. For thermal reactors, $\eta^{49} < \eta^{25}$, so the buildup of ^{239}Pu must exceed the burnup of ^{235}U in order for a positive reactivity effect. For fast reactors, $\eta^{49} > \eta^{25}$ for neutron energies in excess of about 10keV, and there can be an initial positive reactivity effect even if the decrease in ^{235}U is greater than the buildup of ^{239}Pu. However, the ^{239}Pu concentration will saturate at a value determined by the balance between the ^{238}U transmutation rate and the ^{239}Pu depletion rate, at which point the continued depletion of ^{235}U and buildup of fission products produce a negative reactivity effect that accrues over the lifetime of the fuel in the reactor.

1.8. Compensating for fuel-depletion reactivity effects

The reactivity effects of fuel depletion must be compensated to maintain criticality over the fuel burnup cycle. The major compensating elements are the control rods, which can be inserted to compensate positive depletion reactivity effects and withdrawn to compensate negative depletion reactivity effects. Adjustment of the concentration of a neutron absorber (e.g., boron in the form of boric acid) in the water coolant is another means used to compensate for fuel-depletion reactivity effects. Soluble poisons are used to compensate fuel-depletion reactivity in PWRs but not in BWRs, because of the possibility that they will plate out on boiling surfaces. Since a soluble poison introduces a positive coolant temperature reactivity coefficient because an increase in temperature decreases the density of the soluble neutron absorber, the maximum concentration (hence the amount of fuel depletion reactivity that can be compensated) is limited.

Burnable poisons (e.g., boron, erbium, or gadolinium elements located in the fuel lattice), which themselves deplete over time, can be used to compensate the negative reactivity effects of fuel depletion. The concentration of burnable poison can be described by

$$\frac{dn^{bp}}{dt} = -f_{bp} n^{bp} s_{bp} f \qquad (2.6)$$

where, f_{bp} is the self-shielding of the poison element (i.e., the ratio of the neutron flux in the poison element to the neutron flux in the adjacent fuel assembly). The poison concentration is chosen so that the spatial self-shielding of the poison elements is large enough ($f_{bp} << 1$) early in the burnup cycle to shield the poison from neutron capture, and the neutron capture rate remains constant in time. After a certain time the concentration of the poison nuclei is sufficiently reduced that f_{bp} increases and the poison burns out, resulting in an increasing

reactivity. If the poison starts to burn out at about the same time that the overall fuel depletion reactivity effect starts to become progressively more negative (i.e., when the ^{239}Pu concentration saturates), the burnout of the poison will at least partially compensate the fuel-depletion reactivity decrease.

1.9. Reactivity penalty

The buildup of actinides in the ^{238}U transmutation-decay process introduces a fuel reactivity penalty because some of actinides act primarily as parasitic absorbers.

While ^{239}Pu and ^{241}Pu are fissionable in a thermal reactor, and ^{240}Pu transmutes into ^{241}Pu, ^{242}Pu transmutes into ^{243}Pu with a rather small cross section, and ^{243}Pu has a rather small fission cross section, so that ^{242}Pu is effectively a parasitic absorber that builds up in time. The ^{243}Am also accumulates and acts primarily as a parasitic absorber. Whereas the ^{243}Am, which is produced by the decay of ^{243}Pu can, be separated readily, it is difficult to separate the different plutonium isotopes from each other, so the negative ^{242}Pu reactivity effect is exacerbated if the plutonium is recycled with uranium. A similar problem arises with the ^{236}U produced by radiative capture in ^{235}U as shown in Figure (2.4), which is difficult to separate from ^{235}U, and with ^{237}Np which is produced by transmutation of ^{236}U into ^{237}U followed by beta decay. The ^{237}Np can be separated readily, however, and does not need to accumulate in recycled fuel.

End-of-cycle reactivity penalties calculated for the recycle of BWR fuel are shown in Table (2.2) after one, two, and three cycles. It was assumed that the ^{237}Np and ^{243}Am were removed between cycles, but there was a cycle-to-cycle increase in the ^{237}Np and ^{243}Am reactivity penalties due to the accumulation of ^{236}U and ^{242}Pu, respectively.

1.10. Effects of fuel depletion on the power distribution

Fuel depletion and the compensating control actions affect the reactor power distribution over the lifetime of the fuel in the core. Depletion of fuel will be greatest where the power is greatest. The initial positive reactivity effect of depletion will then enhance the power peaking. At later times, the negative reactivity effects will cause the power to shift away to regions with higher k_∞. Any strong tendency of the power distribution to peak as a result of fuel depletion must be compensated by control rod movement. However, the control rod movement to offset fuel depletion reactivity effects itself produces power peaking; the presence of the rods shields the nearby fuel from depletion and when the rods are withdrawn, the higher local k_∞, causes power peaking. Similarly, burnable poisons shield the nearby fuel,

producing local regions of higher k_∞, and power peaking when they burn out. Determination of the proper fuel concentration zoning and distribution of burnable poisons and of the proper control rod motion to compensate fuel depletion reactivity effects without unduly large power peaking is a major nuclear analysis task.

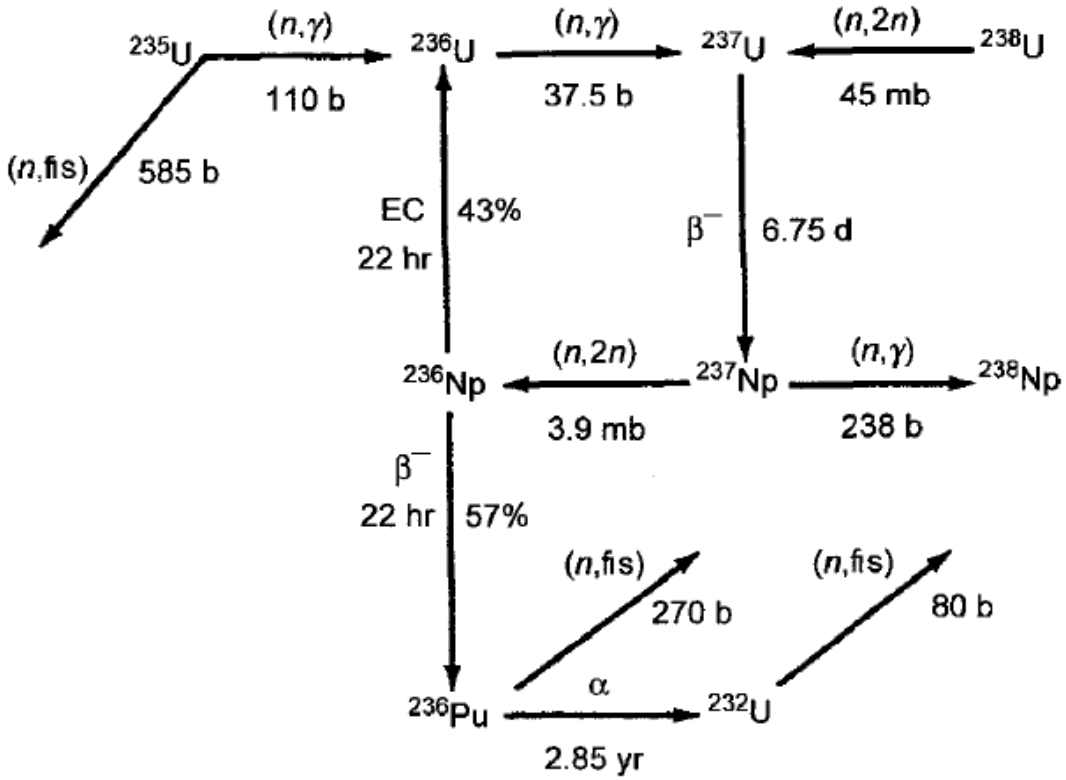

Figure 2.4- ^{235}U neutron transmutation-decay chain.

Table 2.2- Reactivity penalty with recycled BWR fuel ($\%\Delta k/k$) (*Weston M. Stacey, 2007*).

End of Cycle	^{236}U	^{237}Np	^{242}Pu	^{243}Am
1	0.62	0.13	0.65	0.36
2	0.90	0.59	1.53	0.57
3	1.12	0.73	2.04	0.89

1.11. In-core fuel management

At any given time, the fuel in a reactor core will consist of several batches that have been in the core for different lengths of time. The choice of the number of batches is made on the basis of a trade-off between maximizing fuel burnup and minimizing the number of shutdowns for refueling, which reduces the plant capacity factor. At each refueling, the batch of fuel with the highest burnup is discharged, the batches with lower burnup may be moved to different locations, and a fresh or partially depleted batch is added to replace the discharged

batch. The analysis leading to determination of the distribution of the fuel batches within the core to meet the safety, power distribution and burnup, or cycle length constraints for fuel burn cycle is known as fuel management analysis. Although fuel management may be planned in advance, it must be updated online to adjust to higher or lower capacity factors than planned (which result in lower or higher reactivity than planned at the planned refueling time) and unforeseen outages (which result in higher reactivity than planned at the planned refueling time).

Typically, a PWR will have three fuel batches, and a BWR will have four fuel batches in the core at any given time and will refuel every 12 to 18 months. A number of different loading patterns have been considered, with the general conclusion that more energy is extracted from the fuel when the power distribution in the core is as flat as possible. In the in-out loading pattern, the reactor is divided into concentric annular regions loaded with different fuel batches. The fresh fuel batch is placed at the periphery, the highest burnup batch is placed at the center, and intermediate burnup batches are placed in between to counter the natural tendency of power to peak in the center of the core. At refueling, the central batch is discharged, the other batches are shifted inward, and a fresh batch is loaded on the periphery. The in-out loading pattern has been found to go too far in the sense that the power distribution is depressed in the center and peaked at the periphery. An additional difficulty is the production of a large number of fast neutrons at the periphery that leak from the core and damage the pressure vessel.

In the scatter loading pattern the reactor core is divided into many small regions of four to six assemblies from different batches. At refueling, the assemblies within each region with the highest burnup are discharged and replaced by fresh fuel assemblies. This loading pattern has been found to produce a more uniform power distribution and to result in less fast neutron leakage than the in-out pattern.

Since the pressure vessel damage by fast neutrons became recognized as a significant problem, a number of different loading patterns have been developed with the specific objective of minimizing neutron damage to the pressure vessel. These include placement of only partially depleted assemblies at the core periphery, placement of highly depleted assemblies near welds and other critical locations, using burnable poisons in peripheral assemblies, replacing peripheral fuel assemblies with dummy assemblies, and others.

Better utilization of resources argues for the highest possible fuel burnup consistent with materials damage limitations and a new higher enrichment fuel has been developed that can achieve burnups of up to 50,000MWd/T in LWRs. The higher fuel burnup produces more

actinides and fission products with large thermal neutron cross sections, which compete more effectively with control rods for thermal neutrons and reduces control rod worth, and which produces larger coolant temperature reactivity coefficients. The higher-enrichment higher-burnup fuel also provides the possibility of longer refueling cycles, which improves plant capacity factor and reduces power costs.

2. Samarium and xenon

The short-term time dependence of two fission product progeny, ^{149}Sm and ^{135}Xe, which have very large absorption cross sections, introduces some interesting reactivity transients when the reactor power level is changed.

2.1. Samarium poisoning

Samarium-149 is produced by the beta decay of the fission product ^{149}Nd, as described in Figure (2.5). It has a thermal neutron absorption cross section of 4 x 10^4 barns and a large epithermal absorption resonance. The 1.7-h half-life of ^{149}Nd is sufficiently short that ^{149}Pm can be assumed to be formed directly from fission in writing the production destruction equations for ^{149}Pm:

$$\begin{aligned} \frac{dP}{dt} &= g^{Nd} \Sigma_f f - l^P P \\ \frac{dS}{dt} &= l^P P - s_a^S f S \end{aligned} \qquad (2.7)$$

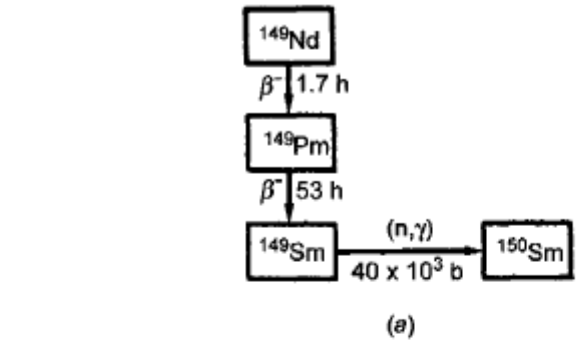

FISSILE NUCLIDE	γ^{Nd}
^{233}U	0.0066
^{235}U	0.0113
^{239}Pu	0.0190

(b)

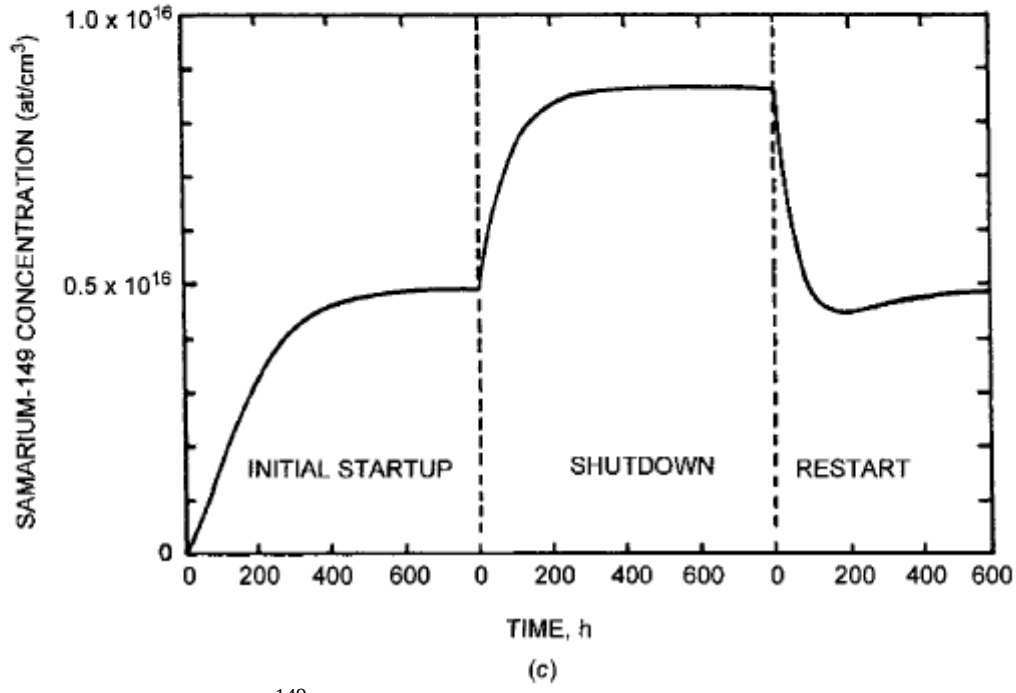

Figure 2.5- Characteristics of ^{149}Sm under representative LWR conditions: (a) transmutation-decay chain; (b) fission yields; (c) time dependence.

where, P and S refer to ^{149}Pm and ^{149}Sm, respectively. These equations have the solution, for constant f ,

$$P(t) = \frac{g^{Nd}\Sigma_f f}{l^P}(1-\exp(-l^P t) + P(0)\exp(-l^P t) \tag{2.8}$$

$$S(t) = S(0)\exp(-s_a^S f t) + \frac{g^{Nd}\Sigma_f}{s_a^S}(1-\exp(-s_a^S f t) - \frac{g^{Nd}\Sigma_f f - l^P P(0)}{l^P - s_a^S f}(\exp(-s_a^S f t) - \exp(-l^P t))$$

At the beginning of life in a fresh core, P(0) = S(0) = 0, and the promethium and samarium concentrations build up to equilibrium values:

$$P_{eq} = \frac{g^{Nd}\Sigma_f f}{l^P}, \quad S_{eq} = \frac{g^{Nd}\Sigma_f}{s_a^S} \tag{2.9}$$

The equilibrium value of ^{149}Pm depends on the neutron flux level. However, the equilibrium value of ^{149}Sm is determined by a balance between the fission production rate of ^{149}Pm and the neutron transmutation rate of ^{149}Sm, both of which are proportional to the neutron flux, and consequently, does not depend on the neutron flux level. The time required for the achievement of equilibrium concentrations depends on f, s_a^S and l^P. For typical thermal reactor flux levels (e.g., 5x10^{13} n/cm^2.s), equilibrium levels are achieved in a few hundred hours.

When a reactor is shut down after running sufficiently long to build up equilibrium concentrations, the solutions of *Eqs.(2.8)* with P(0) = P_{eq}, S(0) = S_{eq}, and f =0 are indicating that the ^{149}Sm concentration will increase to S_{eq} + P_{eq}, as the ^{149}Pm decays into ^{149}Sm with time constant 1/ l^P = 78 h.

$$P(t) = P_{eq}\exp(-l^P t)$$

$$S(t) = S_{eq} + P_{eq}(1-\exp(-l^P t)) \rightarrow S_{eq} + P_{eq} \tag{2.10}$$

If the reactor is restarted, the ^{149}Sm burns out until the ^{149}Pm builds up; then the ^{149}Sm returns to its equilibrium value. This time dependence of the samarium concentration is illustrated in Figure (2.5).

The perturbation theory estimate for the reactivity worth of ^{149}Sm is

$$r_{Sm}^{(t)} = -\frac{S(t)s_a^S}{\Sigma_a} \tag{2.11}$$

which for the equilibrium concentration becomes

$$r_{Sm}^{eq} = -\frac{g^{Nd}\Sigma_f}{s_a^S}\frac{s_a^S}{\Sigma_a} = -g^{Nd}\frac{\Sigma_f}{\Sigma_a} = -\frac{g^{Nd}}{u} \tag{2.12}$$

where we have used the approximation that $k \approx u\frac{\Sigma_f}{\Sigma_a} = 1$. For a ^{235}U-fueled reactor, $r_{Sm}^{eq} \approx 0.0045$.

2.2. Xenon poisoning

Xenon-135 has a thermal absorption cross section of 2.6x10^6 barns. It is produced directly from fission, with yield g^{Xe}, and from the decay of ^{135}I, which in turn is produced by the decay of the direct fission product ^{135}Te, with yield g^{Te}, as indicated in Figure (2.6). The

production-destruction equations may be written, with the assumption that ^{135}I is produced directly from fission with yield g^{Te},

$$\frac{dI(t)}{dt} = g^{Te}\Sigma_f f - l^I I \tag{2.13}$$

$$\frac{dX(t)}{dt} = g^{Xe}\Sigma_f f + l^I I - (l^X + s_a^X f)X$$

These equations have the solutions

$$I(t) = \frac{g^{Te}\Sigma_f f}{l^I}(1-\exp(-l^I t)) + I(0)\exp(-l^I t) \tag{2.14}$$

$$X(t) = \frac{(g^{Te}+g^{Xe})\Sigma_f f}{l^X + s_a^X f}[1-\exp(-(l^X + s_a^X f)t)] + \frac{g^{Te}\Sigma_f f - l^I I(0)}{l^X - l^I + s_a^X f}[\exp(-(l^X + s_a^X f)t) - \exp(-l^I t)]$$
$$+ X(0)\exp(-(l^X + s_a^X f)t)$$

When the reactor is started up from a clean condition in which X(0) = I(0) = 0, or the reactor power level is changed, the ^{135}I and ^{135}Xe concentrations approach equilibrium values:

$$I_{eq} = \frac{g^{Te}\Sigma_f f}{l^I}, \quad X_{eq} = \frac{(g^{Te}+g^{Xe})\Sigma_f f}{l^X + s_a^X f} \tag{2.15}$$

with time constants $1/l^I \approx 0.1h$ and $1/(l^X + s_a^x f) \approx 30h$, respectively. The perturbation theory estimate of the reactivity worth of equilibrium xenon is

$$r_{Xe}^{eq} = -\frac{s_a^X (g^{Te}+g^{Xe})\Sigma_f f}{\Sigma_a (l^X - s_a^X f)} \approx -\frac{g^{Te}+g^{Xe}}{u(1+l^X/s_a^X f)} = \frac{0.026}{1+(0.756.10^{13})/f} \tag{2.16}$$

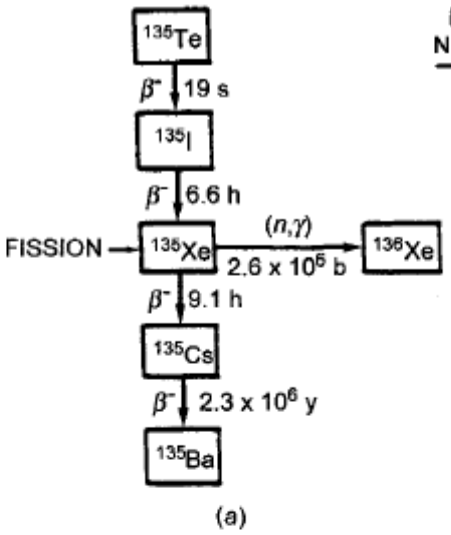

FISSILE NUCLIDE	γ(135Te)	γ(135Xe)
233U	0.051	
235U	0.061	0.003
239Pu	0.055	

(b)

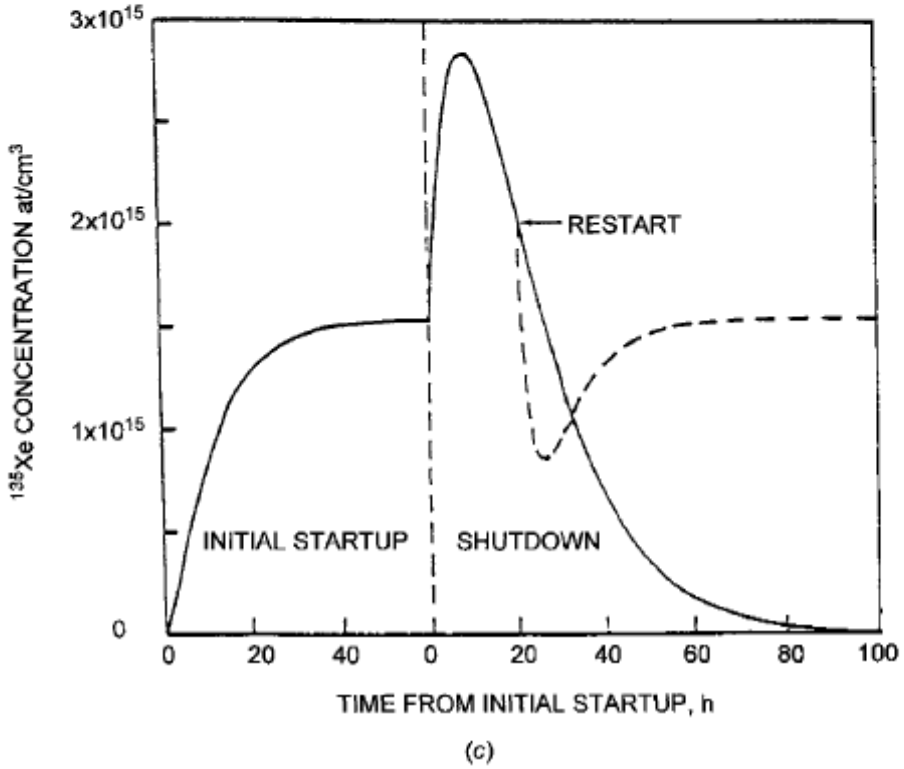

(c)

Figure 2.6- Characteristics of ^{135}Xe under representative LWR conditions: (a) transmutation-decay chain; (b) fission yields; (c) time dependence.

2.3. Peak xenon

When a reactor is shut down from an equilibrium xenon condition, the iodine and xenon populations satisfy *Eqs. (2.14)* with I(0) =I_{eq}, X(0) =X_{eq}, and $f = 0$:

$$I(t) = I_{eq} \exp(-l^I t)$$
$$X(t) = X_{eq} \exp(-l^X t) + I_{eq} \frac{l^I}{l^I - l^X} (\exp(-l^X t) - \exp(-l^I t)) \quad (2.17)$$

If $f > (g^X / g^{Te})(l^X / s_a^X)$, xenon will build up after shutdown to a peak value at time

$$t_{PK} = \frac{1}{l^I - l^X} \ln \frac{l^I / l^X}{1 + (l^X / l^I)(l^X / l^I - 1)(X_{eq} / I_{eq})} \tag{2.18}$$

and then decay to zero unless the reactor is restarted. For ^{235}U and ^{233}U-fueled reactors f >4x10^{11} and 3x10^{12} n/cm^2.s, respectively, is sufficient for an increase in the xenon concentration following shutdown. Typical flux values (e.g., 5x10^{13} n/cm^2-s) in thermal reactors are well above these threshold levels, and for typical flux values, *Eq. (2.18)* yields a peak xenon time of ≈ 11.6 h. If the reactor is restarted before the xenon has entirely decayed, the xenon concentration will initially decrease because of the burnout of xenon and then gradually build up again because of the decay of a growing iodine concentration, returning to values of I_{eq} and X_{eq}, for the new power level. This time dependence of the xenon concentration is illustrated in Figure (2.6).

2.4. Effect of power-level changes

When the power level changes in a reactor (e.g., in load following) the xenon concentration will change. Consider a reactor operating at equilibrium iodine $I_{eq}(f_0)$ and xenon $X_{eq}(f_0)$ at flux level f_0. At t = t$_0$ the flux changes from f_0 to f_1. *Eqs. (2.15)* can be written

$$I(t) = I_{eq}(f_1)\left(1 - \frac{f_1 - f_0}{f_1}\exp(-l^I t)\right)$$

$$X(t) = X_{eq}(f_1)\left(1 - \frac{f_1 - f_0}{f_1}\left\{\begin{array}{l} \dfrac{l^X}{l^X + s_a^X f_0}\exp(-(l^X + s_a^X f)t) + \\ \dfrac{g^{Te}}{g^{Te} + g^{Xe}}\dfrac{l^X + s_a^X f_1}{l^X - l^I + s_a^X f_1}(\exp(-l^I t) - \exp(-(l^X + s_a^X f)t) \end{array}\right\}\right) \tag{2.19}$$

The xenon concentration during a transient of this type is shown in Figure (2.7). The perturbation theory estimate for the reactivity worth of xenon at any time during the transient discussed above is

$$r_{Xe}(t) = -\frac{s_a^X X(t)}{\Sigma_a} \approx -\frac{s_a^X X(t)}{u\,\Sigma_f} \tag{2.20}$$

Example: Xenon Reactivity Worth. As an example of xenon buildup, consider a ^{235}U-fueled reactor that has operated at a thermal flux level of 5×10^{13}cm^{-2}s^{-1} for two months such that equilibrium xenon and iodine have built in to the levels given by *Eqs. (2.15)*. Using $s_a^X = 2.6 \times 10^{-18}$ cm^2, $t_{1/2}^I = 6.6$ h, $t_{1/2}^X = 9.1$ h, $l = \ln 2/t_{1/2}$, $g_{Te} = 0.061$, and $g_{Xe} = 0.003$, the equilibrium values of xenon and iodine are $X^{eq} = 0.0203\times10^{18}\sum_f cm^{-3}$ and $I^{eq} = 0.1051\times10^{18}\sum_f cm^{-3}$. The reactivity worth of equilibrium xenon is $r_{Xe}^{eq} \approx s_a^X X^{eq}/\sum_a \approx 0.022\Delta k/k$, where the approximate criticality condition $u\sum_f/\sum_a$, has been used.

If the reactor is shut down for 6 h and then restarted, the xenon reactivity worth that must be compensated is, from *Eqs. (2.15)* and *(2.20)*,

$$r_{Xe}(t=6h) \approx s_a^X X(t=6h)/u\sum_f = (0.634X^{eq} + 0.367I^{eq})\times s_a^X/u\sum_f$$
$$= 0.0171 + 0.04 = 0.0571\Delta k/k$$

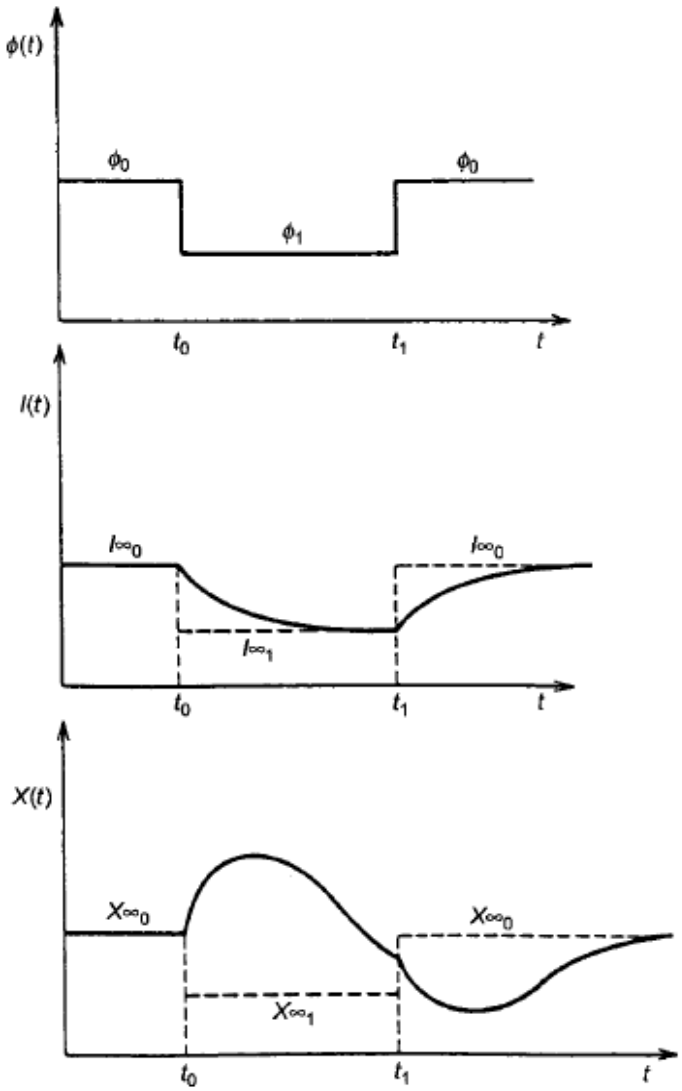

Figure 2.7- Xenon concentration following power-level changes.

The largest contribution to the xenon worth at 6 h after shutdown clearly comes from buildup of xenon from the decay of the iodine concentration at shutdown at a faster rate than the resulting xenon decays.

3. Fertile–to–fissile conversion and breeding

3.1. Availability of neutrons

The transmutation-decay processes depicted in Figure (2.1) hold out the potential for increasing the recoverable energy content from the world's uranium and thorium resources by almost two orders of magnitude by converting the fertile isotopes ^{238}U and ^{232}Th, which only fission at very high neutron energies, into fissile isotopes, ^{239}Pu and ^{241}Pu in the case of ^{238}U, and ^{233}U in the case of ^{232}Th, which have large fission cross sections for thermal neutrons and substantial fission cross sections for fast neutrons. The rate of transmutation of fertile-to-fissile isotopes depends on the number of neutrons in excess of those needed to maintain the chain fission reaction that are available. In the absence of neutron absorption by anything other than fuel and in the absence of leakage, the number of excess neutrons is η-1. The quantity η is plotted in Figure (2.8) for the principal fissile isotopes.

The fertile-to-fissile conversion characteristics depend on the fuel cycle and the neutron energy spectrum. For a thermal neutron spectrum (E < 1 eV), ^{233}U has the largest value of η of the fissile nuclei. Thus the best possibility for fertile-to-fissile conversion in a thermal spectrum is with the ^{232}Th – ^{233}U fuel cycle. For a fast neutron spectrum (E > $5x10^4$eV), ^{239}Pu and ^{241}Pu have the largest values of *h* of the fissile nuclei. The LMFBR, based on the ^{238}U–^{239}Pu fuel cycle, is intended to take advantage of the increase of η^{49} at high neutron energy.

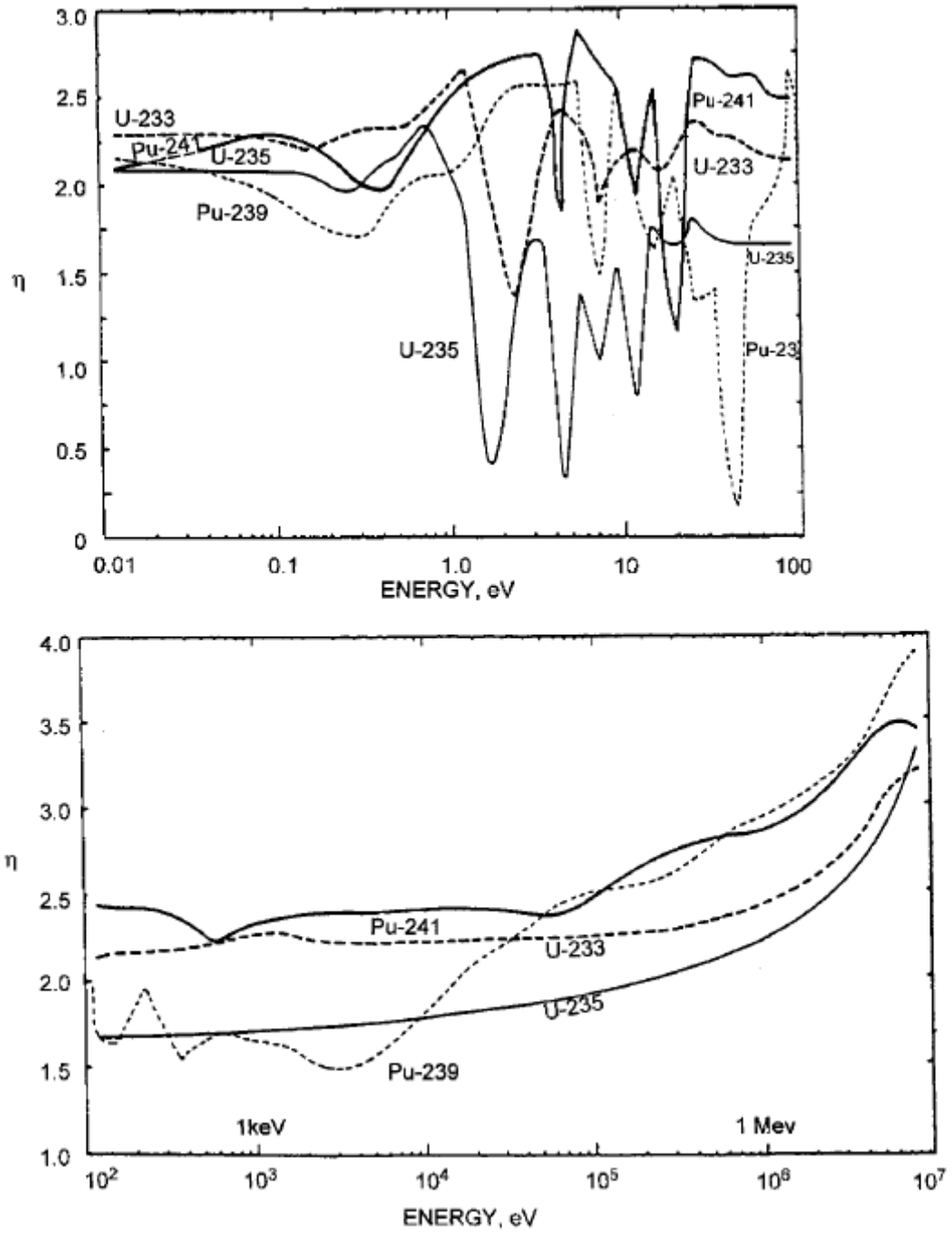

Figure 2.8- Parameter η for the principal fissile nuclei (*Weston M. Stacey, 2007*).

3.2. Conversion and breeding ratios

The instantaneous conversion ratio is defined as the ratio of the rate of creation of new fissile isotopes to the rate of destruction of fissile isotopes. When this ratio is greater than unity, it is conventional to speak of a breeding ratio, because the reactor would then be producing more fissile material than it was consuming. Average conversion or breeding ratios calculated for reference reactor designs of various types are shown in Table (2.3).

The values of the conversion ratios for the PWR and BWR are the same because of design similarities. The HTGR conversion ratio is somewhat higher because of the higher value of η for ^{233}U than for ^{235}U. The improved conversion ratio for the CANDU-PHWR is due to the better neutron economy provided by online refueling and consequent reduced requirements for control poisons to compensate excess reactivity.

The breeding ratio in an LMFBR can vary over a rather wide range, depending on the neutron energy spectrum. Achieving a large value of η and hence a large breeding ratio favors a hard neutron spectrum. However, a softer spectrum is favored for safety reasons-the lower-energy neutrons which are subject to resonance absorption become more likely to be radiatively captured than to cause fission as the neutron energy is reduced.

Table 2.3- Conversion/Breeding ratios in different reactor systems (*Weston M. Stacey, 2007*).

Reactor system	Initial Fuel	Conversion cycle	Conversion ratio
BWR	2 – 4 wt% ^{235}U	^{238}U – ^{239}Pu	0.6
PWR	2 – 4 wt% ^{235}U	^{238}U – ^{239}Pu	0.6
PHWR	Natural U	^{238}U – ^{239}Pu	0.8
HTGR	≈ 5 wt% ^{235}U	^{232}Th – ^{233}U	0.8
LMFBR	10 – 20 wt % Pu	^{238}U – ^{239}Pu	1.0 – 1.6

4. Simple model of fuel depletion

The concepts involved in fuel depletion and the compensating control adjustment can be illustrated by a simple model in which the criticality requirement is written as

$$k = hf = \frac{h\sum_a^F(t)}{\sum_a^F(t)+\sum_a^M+\sum_a^{fp}(t)+\sum_c(t)} = 1 \tag{2.21}$$

where, $\sum_a^F$ is the fuel macroscopic absorption cross section, $\sum_a^M$ the moderator macroscopic absorption cross section, and $\sum_a^C$ the combined (soluble and burnable poisons plus control rod) control absorption cross section. Assuming that the reactor operates at constant power $u\sum_f^F(t)f(t) = u\sum_f^F(0)f(0)$ and that $h = u\sum_f^F \Big/ \sum_a^F$ is constant in time, the fuel macroscopic absorption cross section at any time is

$$\begin{aligned}\sum_a^F(t) = N_F(t)s_a^F &= s_a^F\left[N_F(0) - es_a^F\int_0^t N_F(t')f(t')dt'\right] \\ &= N_F(0)s_a^F\left[1-ef(0)s_a^F t\right]\end{aligned} \tag{2.22}$$

The neutron flux is related to the beginning-of-cycle neutron flux by

$$f(t) = \frac{f(0)}{1 - e s_a^F f(0) t} \tag{2.23}$$

where, ε <1 is a factor that accounts for the production of new fissionable nuclei via transmutation-decay.

The fission product cross section is the sum of the equilibrium xenon and samarium cross sections constructed using *Eqs. (2.15)* and *(2.9)*, respectively, and an effective cross section for the other fission products,

$$\Sigma_{fp'} = s_{fp'} g_{fp'} \Sigma_f(t) f(t) t = s_{fp'} g_{fp'} \Sigma_f(0) f(0) t \tag{2.24}$$

Which accumulate in time from fission with yield $g_{fp'}$. The quantity $g_{fp'} s_{fp'}$ is about 40 to 50 barns per fission. Using these results, *Eq. (2.21)* can be solved for the value of the control cross section that is necessary to maintain criticality:

$$\begin{aligned} \Sigma_c(t) = (h-1)\Sigma_a^F(0)\left[1 - s_a^F e f(0) t\right] - \Sigma_a^M - \frac{(g^{Te} + g^{Xe})\Sigma_f(0) f(0)}{l^X / s_a^X + f(t)} \\ - g^{Nd} \Sigma_f(0)\left[1 - e s_a^F f(0) t\right] - s_{fp'} g_{fp'} \Sigma_f(0) f(0) t \end{aligned} \tag{2.25}$$

The soluble poison will be removed by the end of cycle, and the burnable poisons should be fully depleted by that time. Thus the lifetime, or cycle time, is the time at which the reactor can no longer be maintained critical with the control rods withdrawn as fully as allowed by safety considerations. This minimum control cross section is small, and we set it to zero. The end-of-cycle time can be determined from *Eq. (2.25)* by setting $\Sigma_a^C = 0$ and solving for t_{EOC}:

$$t_{EOC} = \begin{cases} \dfrac{h r_{ex}(1+a) - (g^{Te} + g^{Xe}) f(0) s_a^X / l^X - g^{Nd}}{[(h-1)(1+a) s_a^F - g^{Nd} s_a^F + g_{fp'}] f(0)}, & f(t) \text{ pp } \dfrac{l^X}{s_a^X} \\ \dfrac{h r_{ex}(1+a) - (g^{Te} + g^{Xe} + g^{Nd})}{[(h-1)(1+a) s_a^F - (g^{Te} + g^{Xe} + g^{Nd}) s_a^F + g_{fp'} s_{fp'}] f(0)}, & f(t) \text{ ff } \dfrac{l^X}{s_a^F} \end{cases} \tag{2.26}$$

where α is the capture-to-fission ratio for the fuel, and

$$r_{ex} \equiv \frac{k_\infty(0) - 1}{k_\infty(0)} \tag{2.27}$$

is the excess reactivity at beginning-of-cycle without xenon, samarium, fission products, or control cross section. The initial control cross section (including soluble and burnable poisons) must be able to produce a negative reactivity greater than r_{ex}. It is clear from *Eq. (2.26)* that the cycle lifetime is inversely proportional to the power, or flux, level.

5. Fuel reprocessing and recycling

A substantial amount of plutonium is produced by neutron transmutation of ^{238}U in LWRs. About 220 kg of fissionable plutonium (mainly ^{239}Pu and ^{241}Pu) is present in the spent fuel discharged from an LWR at a burnup of 45 MWd/T. The spent fuel can be reprocessed to recover the plutonium (and remaining enriched uranium) for recycling as new fuel.

5.1. Composition of recycled LWR fuel

The potential energy content of the fissile and fertile isotopes remaining in spent reactor fuel (*Tab. 2.1*) constitutes a substantial fraction of the potential energy content of the initial fuel loading, providing an incentive to recover the uranium and plutonium isotopes for reuse as reactor fuel. The recycled plutonium concentrations calculated for successive core reloads of a PWR are shown in Table (2.4). The initial core loading and the first reload were slightly enriched UO2. The plutonium discharged from the first cycle was recycled in the third cycle, that in the second cycle in the fourth cycle, and so on, in separate mixed oxide (MOX) UPuO2 pins. The proportion of MOX increases from about 18% in the second reload to just under 30% in the sixth and subsequent reloads, for which reloads the plutonium recovered from spent MOX and UO2 fuel is about the same as was loaded into this fuel at beginning-of-cycle (i.e., the plutonium concentration reaches equilibrium). The percentage of plutonium in MOX increases from less than 5% on the initial recycle load to about 8% in equilibrium, in order to offset the reactivity penalty.

Table 2.4- Plutonium concentrations in a PWR recycling only self-generated plutonium (wt %) (*Weston M. Stacey, 2007*).

Loading Recycle	**1**	**2**	**3** **1**	**4** **2**	**5** **3**	**6** **4**	**7** **5**
^{235}U in UO_2	2.14	3.0	3.0	3.0	3.0	3.0	3.0
Pu in MOX	-	-	4.72	5.83	6.89	7.51	8.05
MOX of fuel	-	-	18.4	23.4	26.5	27.8	28.8
^{235}U discharged	0.83	-	-	-	-	-	-
Discharged Pu							
^{239}Pu	56.8	56.8	49.7	44.6	42.1	40.9	40.0
^{240}Pu	23.8	23.8	27.0	38.7	29.4	29.6	29.8
^{241}Pu	14.3	14.3	16.2	17.2	17.4	17.4	17.3
^{242}Pu	5.1	5.1	7.1	9.5	11.1	12.1	12.9

5.2. Physics differences of MOX cores

The use of MOX fuels in PWRs changes the physics characteristics in several ways. The variation with energy of the cross sections for the plutonium isotopes is more complex than for the uranium isotopes, as shown in Figure (2.9). The absorption cross sections for the plutonium isotopes are about twice those of the uranium isotopes in a thermal spectrum and are characterized by large absorption resonances in the epithermal (0.3 to 1.5eV) range and by overlapping resonances. Representative thermal neutron spectra in UO2 and MOX fuel cells are compared in Figure (2.10). Thermal parameters for ^{235}U and ^{239}Pu, averaged over a representative LWR thermal neutron energy distribution, are given in Table (2.5). Because of the larger thermal absorption cross section for ^{239}Pu the, reactivity worth of control rods,

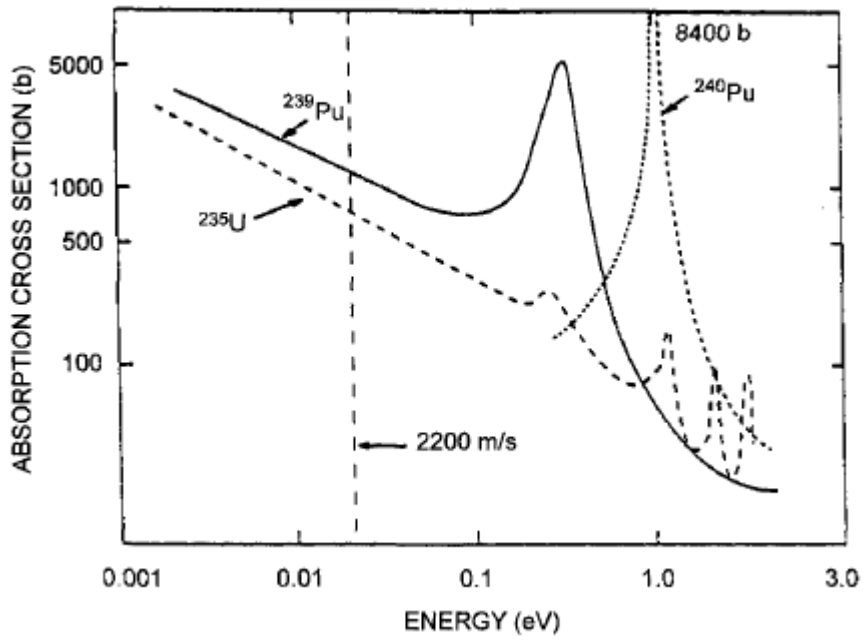

Figure 2.9- Thermal absorption cross section for ^{239}Pu (*Weston M. Stacey, 2007*).

burnable poisons, and soluble poisons (PWRs) will be less with MOX fuel than with UO2, unless the MOX rods can be placed well away from control rods and burnable poisons. The higher ^{239}Pu fission cross section will lead to greater power peaking with MOX than with UO2, unless the MOX rods are placed well away from water gaps.

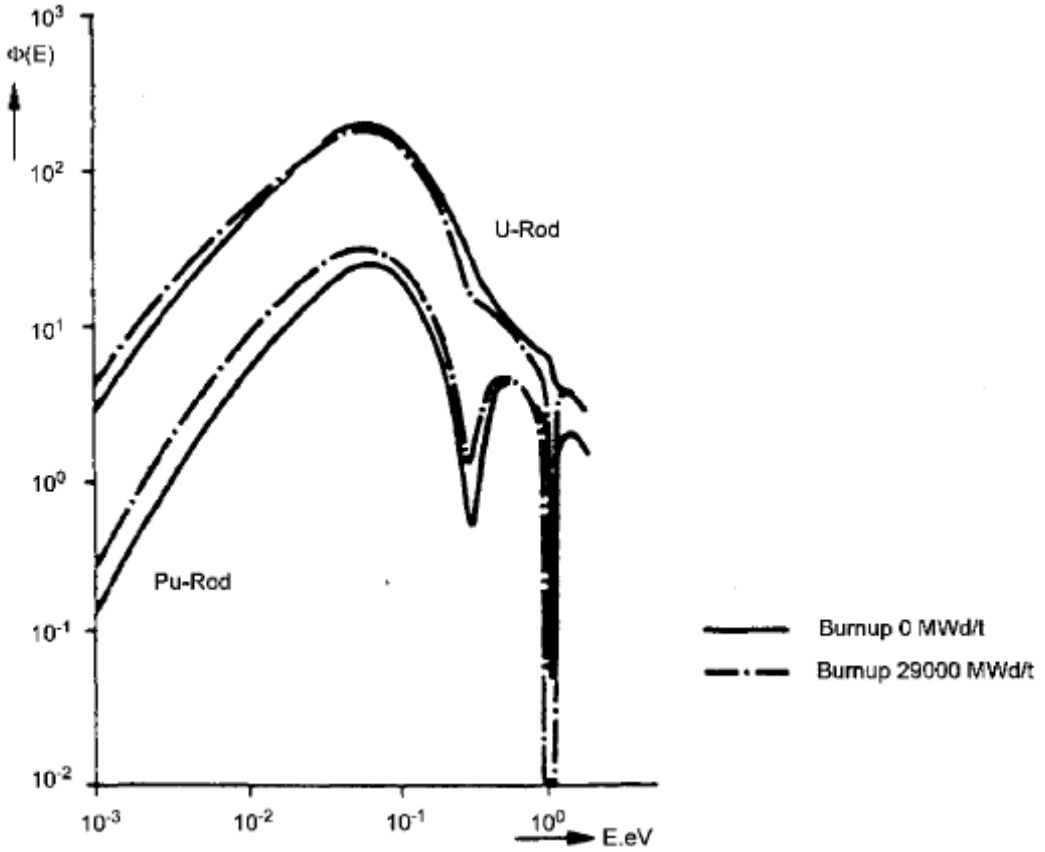

Figure 2.10- Thermal neutron spectra in UO2 and MOX PWR fuel cells (*Weston M. Stacey, 2007*).

Table 2.5- Thermal parameters for ^{235}U and ^{239}Pu in a LWR (*Weston M. Stacey, 2007*).

Parameter	**^{235}U**	**^{239}Pu**
Fission cross section s_f (barns)	365	610
Absorption cross section s_a (barns)	430	915
Nu-fisssion to absorption h	2.07	1.90
Delayed neutron fraction b	0.0065	0.0021
Generation time Λ (s)	4.7×10^{-5}	2.7×10^{-5}

There are reactivity differences between MOX and UO2. The buildup of ^{240}Pu and ^{242}Pu with the recycling MOX fuel accumulates parasitic absorbers that result in a reactivity penalty, as discussed above. The average thermal value of η is less for ^{239}Pu than for ^{235}U, which requires a larger fissile loading to achieve the same initial excess reactivity with MOX as with UO2. Furthermore, the temperature defect is greater for MOX because of the large low-energy resonances in ^{239}Pu and ^{240}Pu shown in Figure (2.9). However, the reactivity decrease with burnup is less for MOX than for UO2, because of the lower η for ^{239}Pu than for ^{235}U**,** and

because of the transmutation of ^{240}Pu into fissionable ^{241}Pu, so that less excess reactivity is needed.

The delayed neutron fractions for ^{239}Pu, ^{241}Pu, and ^{235}U are in the ratio 0.0020/0.0054/0.0064, which means that the reactivity insertion required to reach prompt critical runaway conditions is less for MOX than for UO2 by a factor that depends on the ^{239}Pu/^{241}Pu/^{235}U ratio. As the ^{241}Pu builds up with repeated recycle, the difference between MOX and UO2 decreases. The neutron generation time is also shorter for MOX than for UO2, so that any prompt supercritical excursion would have a shorter period. The fission spectrum neutrons are more energetic for ^{239}Pu than for ^{235}U. On the other hand, because of the large epithermal absorption resonances in the plutonium isotopes, the moderator and fuel Doppler temperature coefficients of reactivity tend to be more negative for MOX cores than for UO2 cores. Accumulation of actinides, which are strong emitters of energetic alpha particles, leads to higher radioactive decay heat removal requirements with MOX. These considerations would tend to limit the MOX fraction in a reload core.

The yield of ^{135}Xe is about the same for the fission of plutonium as for the fission of uranium. Due to the higher thermal absorption cross section of the plutonium isotopes, the excess reactivity needed to start up at peak xenon conditions and the propensity for spatial flux oscillations driven by xenon oscillations are less in a MOX than a UO2 core.

For plutonium recycle in other reactor types, similar types of physics considerations would enter. However, the different relative values of η for ^{235}U and ^{239}Pu in different spectra (e.g., the epithermal spectrum of a HTGR and the fast spectrum of a LMFBR) would lead to different conclusions about reactivity penalties. In fact, LMFBRs have been designed from the outset with the concept of switching from ^{235}U to ^{239}Pu as the latter was bred.

5.3. Physics considerations with uranium recycle

Although it is relatively straightforward to separate uranium from other chemically distinct isotopes, it is impractical to separate the various uranium isotopes from each other in the reprocessing step. So recycling uranium means recycling all of the uranium isotopes, some of which are just parasitic absorbers and another of which leads through subsequent decay to the emission of an energetic gamma.

Two isotopes present in relatively small concentrations in fresh fuel (^{234}U and ^{236}U) necessitate adding ^{235}U to enrich reprocessed uranium to a higher enrichment than is required with fresh uranium fuel. Uranium-234 has a large absorption resonance integral and, while only a tiny fraction in natural uranium, will tend to be enriched along with ^{235}U. Uranium-

236 is produced by neutron capture in ^{235}U and by electron capture in ^{236}Np, as shown in Figure (2.4), and is a parasitic neutron absorber with a significant capture resonance integral. Reprocessed uranium is made difficult to handle by the decay product ^{208}Tl, which emits a 2.6-MeV gamma with $t_{1/2}$= 3.1 min. This radioisotope is produced by a series of alpha decays of ^{232}U, which is produced by the chain shown in Figure (2.4).

5.4. Physics considerations with plutonium recycle

The same type of difficulties exists for plutonium reprocessing as discussed for uranium-all of the plutonium isotopes must be recycled. Plutonium-236 decays into ^{232}U, which leads to the emission of a 2.6-MeV gamma, as described above. Plutonium-238 is produced through neutron transmutation of ^{237}Np; it alpha-decays with $t_{1/2}$ = 88 years and constitutes a large shutdown heat source if present in sufficient quantity. Plutonium-240 has an enormous capture resonance integral. Both ^{238}Pu and ^{240}Pu contribute a large spontaneous fission neutron source. Plutonium-241, while having a large fission cross section, also decays into ^{241}Am, which has a large thermal capture cross section and a large capture resonance integral. Americium-241 also decays into daughter products which are energetic gamma emitters. Stored plutonium loses its potency as a fuel over time because of the decay of ^{241}Pu into ^{241}Am. Plutonium from spent LWR fuel at a typical burnup of about 35,000 MWd/T must be utilized within 3 years after discharge or it will be necessary to reprocess it again to remove the ^{241}Am and daughter products.

5.6. Reactor fueling characteristics

Nuclear fuel cycles with plutonium recycle have been studied extensively (*Weston M. Stacy, 2007*). Representative equilibrium fueling characteristics for LWRs operating on the ^{238}U-^{239}Pu and ^{232}Th – ^{233}U fuel cycles and for a LMFBR operating on the ^{238}U-^{239}Pu fuel cycle are shown in Table (2.6). Fuel is partially discharged and replenished each year (annual discharge and annual reload), requiring a net amount of new fuel (annual makeup) from outside sources. In the absence of reprocessing and recycling, the annual reload would have to be supplied from outside sources. The LMFBR produces more fuel than it uses and could provide the extra fuel needed by the LWRs from the transmutation of ^{238}U if LMFBRs and LWRs were deployed in the ratio of about 7/5.

Table 2.6- Representative fueling characteristics of 1000-MWt reactors (*Weston M. Stacey, 2007*).

Characteristic	Reactor type		
	LWR	**LWR**	**LMFBR**
Fuel cycle	^{232}Th-^{233}U	^{238}U-^{239}Pu	^{238}U-^{239}Pu
Conversion ratio	0.78	0.71	1.32
Initial core load (kg)	1580	2150	3160
Burnup (MWd/T)	35000	33000	100000
Annual reload (kg)	720	1000	1480
Annual discharge (kg)	435	650	1690
Annual makeup (kg)	285	350	(-210)

3. Nuclear data processing and validation

The MCNP code, which is considered as a reference code has been adopted in our neutronics calculations. This code needs data in an appropriated format called ACE format (A Compact ENDF). The ACE format has evolved to include all the details of the ENDF (Evaluated Nuclear Data Files) representations for neutron and photon data. The only solution to process data in ACE format is to use specific modules of the NJOY system. However, the processing of data in ACE format from that in ENDF is a complicated task.

In this chapter we describe briefly the MCNP5 code and its methodology also we explain our adopted procedure for processing and validation of nuclear data to be used with the MCNP code.

1. Monte Carlo N-Particle Transport Code (MCNP5)

The problem of simulating the interaction of radiation with matter has a long history, spanning decades, of applications in physics, medicine and engineering. Two approaches have been developed for this purpose, namely, Monte Carlo and Deterministic methods. Deterministic methods are linked to the integro-differential Boltzmann equation, which describes the radiation transport process. This is a discretized process and the resulting system of algebraic equations is solved. On the other hand Monte Carlo techniques are linked to the physics of radiation transport. The random history of individual particles is simulated and the results are averaged over many particles. The fundamental advantage of Monte Carlo techniques over deterministic techniques is that Monte Carlo techniques represent the geometry and the nuclear data more accurately than Deterministic techniques. Deterministic methods require reasonably simple geometries for the numerical technique to work and use the multigroup approximation to cross section data. The Monte Carlo technique can handle complex geometry, and continuous as well as multigroup cross section data.

1.1. Monte Carlo Methodology

Monte Carlo methods are stochastic techniques; they are based on the use of random numbers and probability density functions to investigate a variety of physical problems. They provide solutions to these problems by performing statistical sampling experiments on a computer. If one could determine the exact path of each particle follows and its energy, assuming it passes through a medium in a random walk fashion, one could in principle simulate a large number of individual particle histories so as to minimize the stochastic effects of the individual particle interactions. This concept of using a large number of randomly generated particle

histories to estimate some average particle behavior is an essential feature of Monte Carlo Methods.

The particle tracks (histories) are generated by simulating the random nature of particle interaction with the medium. To do this, one requires mathematical expressions for the probability relationship which governs the track-length of an individual particle between the points of interaction. The choice of a new energy and new direction, if the interaction is one of a scattering type and the possible production of additional particles is random; therefore, the entire variables are stochastic. In order to make selection of the specific values for these variables, one needs a complete understanding of the physics of the various processes a particle undergoes in its lifetime from the time it is created in the source until it is absorbed or leaves the system under consideration. In some cases, there are equations that adequately describe the behavior of such systems and that can be solved either analytically or numerically. Monte Carlo methods are used in nuclear reactor calculations and also for radiation transport applications such as dosimetry, shielding, detector response analysis, etc.

Assume that N neutron histories are generated and that n of the histories terminate in the escape of the neutron from the system. To calculate an estimate for the probability that any single neutron escapes, a score Si is assigned to each neutron *i* as follows: $Si = 0$ if the neutron is absorbed within the system and $Si = 1$ if the neutron escapes. Then the estimated probability of the escape is given by the mean score:

$$\bar{S} = \frac{1}{N}\sum S_i = \frac{n}{N} \tag{3.1}$$

The relative error (relative statistical uncertainty) indicates the precision of the tally, not its accuracy. Relative error in this probability estimation is related to the variance of the *Si*, *Var(Si)*, which can be approximated when N is large enough by:

$$Var(S_i) \approx \frac{1}{N}\sum_i S_i^2 - (\frac{1}{N}\sum_i S_i)^2 = \frac{n(N-n)}{N^2} \tag{3.2}$$

Then the relative error in the probability estimation is given by

$$\frac{1}{S}\sqrt{\frac{Var(S_i)}{N}} = \sqrt{\frac{(N-n)}{Nn}} \tag{3.3}$$

1.2. MCNP code

MCNP (Los Alamos National Laboratory − LANL, USA) is a coupled neutron, photon, and electron Monte Carlo transport code. It is considered as reference code for criticality

calculations. In this thesis, we have used the version 5 of the release 1.4 of MCNP (*X-5 Monte Carlo Team, 2003*). The user creates an input file that specifies the geometry, materials, location and type of source, the type of answers desired and any variance reduction techniques to be used to improve efficiency. The Monte Carlo method is useful to solve complex problems. A particle is created with characteristics specified by the user. A random number is generated to determine the distance this particle will travel given the materials that make up the problem. Another random number is generated to determine what type of interaction the particle will have. This continues until the particle is absorbed or escapes the boundaries set by the inputs. This process constitutes one history. As more histories are run, the particles distributions are better known.

The quantities of interest specified by the user are tallied along with an estimation of the corresponding error. The primary source of the continuous energy nuclear libraries comes from the Evaluated Nuclear Data File (ENDF) system. Data exists for neutron interactions, neutron induced photons, photon interactions and thermal particle scattering S(α, β). The S(α, β) treatment is particularly important for this thesis since it describes the properties of moderators and other materials (ZrH, H_2O, graphite, etc.). This scattering treatment includes molecular binding and crystalline effects that become particularly important for neutrons with low energy. All of these cross section data are important for accurately describing the problem at hand so that the correct solution can be reached. Answers that are specified by the user can be tallied by MCNP. These tallies include: particle current, flux, and energy deposition are normalized to be per source particle with the exception of criticality calculations. For MCNP, the criticality is defined as the number of fission neutrons in the current generation divided by the previous generation. MCNP will also print out the estimated relative error which is defined as one standard deviation of the mean divided by the mean. This informs the user about the degree of confidence there is in the answer calculated by MCNP.

The input file is formatted as follows:

- Title
- Cell cards
- Surface cards
- Data cards

2. Nuclear data

Nuclear data are fundamental to the development and application of all nuclear sciences and technologies. Basic nuclear data, whether measured or calculated, follow a complex process of evaluation, correction and analysis before becoming “directly” available in application.

2.1. Data evaluation

As there are no predictive theories for neutron-induced reactions in the resonance energy range, the basic nuclear data have to be obtained through measurements at dedicated experimental facilities, such as linear particle accelerators for example. The measured raw data are then corrected for the experimental conditions, such as sample impurities, background effects, room temperature, sample geometry, detector efficiencies …

However, the experimental data obtained are not directly suitable for application calculations. A thorough analysis of the data is necessary to produce a coherent set of usable one. Data evaluation is very difficult and long step to produce the coherent set of data for each nuclide. An evaluation is the process of analyzing experimentally measured cross sections, combining them with the predictions of nuclear model calculations and attempting to extract the “true” value of a cross section (at 0 Kelvin). Parameterization and reduction of the data to tabular form produce an evaluated data set. If a written description of the preparation of a unique data set from the data sources is available, the data set is referred to as a documented evaluation.

2.2. The evaluated nuclear data file (ENDF) format

Few countries, few experts carry out this painful work. But, since the end of the cold war, a cooperative effort of national laboratories, industry and universities leads to choose the ENDF formats and libraries for nuclear data. The ENDF formats (*M. Herman, 2005*) are decided by the Cross Section Evaluation Working Group (CSEWG) and are maintained by the National Nuclear Data Center (NNDC) in US. In the different countries which are doing data evaluation, the scientific community have accepted the ENDF format as the only one format.

2.3. What is the ENDF format?

The ENDF format provides representations for neutron cross sections and angular distributions, photon production from neutron reactions, a limited amount of charged-particle production from neutron reactions, photo-atomic interaction data, thermal neutron scattering data and radionuclide production and decay data (including fission products). In the last past

decade, a new version of the format had delivered: the version 6 (ENDF-6 which allows higher incident energies, adds more complete descriptions of the distributions of emitted particles and provides for incident charged particles and photo-nuclear data partitioning the ENDF library into sub-libraries. Decay data, fission product yield data, thermal scattering data and photo-atomic data have also been formally placed in sub-libraries.

The ENDF system was developed for the storage and retrieval of evaluated nuclear data to be used for applications of nuclear technology. These applications control many features of the system including the choice of materials to be included, the data used, the formats used and the testing required before a library is released. An important consequence of this is that each evaluation must be complete for its intended application. If required data are not available for particular reactions, the evaluators should supply them by using systematic nuclear models.

The ENDF system is logically divided into formats and procedures. Formats describe how the data are arranged in the libraries and give the formulas needed to reconstruct physical quantities such as cross sections and angular distribution from the parameters in the library. Procedures are the more restrictive rules that specify what data types must be included, which format can be used in particular circumstances and so on. Procedures are, generally, imposed by a particular organization and library sanctioned by the CSEWG is referred to as ENDF/B. Other organizations may use somewhat different procedures, if necessary, but they face the risk that their libraries will not work with processing codes sanctioned by CSEWG.

2.4. What append after the ENDF format?

Once the evaluated data sets have been prepared in ENDF format, they can be converted to appropriate forms for testing and actual applications using processing codes. Processing codes that generate group-averaged cross sections for use in neutronics calculations from the ENDF library have been written. These codes include such functions as resonance reconstruction, Doppler broadening multigroup averaging, and/or rearrangement into specified interfaces. It is typically the case for the PREPRO code (*Dermott E. Cullen, 2007*) or NJOY code (*MacFarlane, 1999*).

2.5. How to process data into ENDF format?

The present section focuses only on how to process data in ENDF format into the adaptated data format for the MCNP code.

MCNP code needs data in an appropriate format called ACE format (A Compact ENDF). The ACE format has evolved to include all the details of the ENDF representations for neutron

and photon data. However, for sake of efficiency, the representation of data in ACE is quite different from that in ENDF. The fundamental difference is the use of random access with pointers to the various parts of the data. Other key differences include the use of union energy grids, equal-probability bins, and cumulative probability distributions (more details can be found in the MCNP and NJOY user manuals). MCNP requires that all the cross-sections are given on a single union energy grid suitable for linear interpolation. The only solution to produce data in ACE format is to use specific modules of NJOY code. MCNP code needs also data process at specific temperature. These data are produced with the NJOY code only from the adopted ENDF data format. So, how to convert nuclear data into the appropriate format for my application?

3. NJOY99 nuclear data processing system

For generating ACE files for MCNP: build the NJOY99 input file and run NJOY99. The user can think that there is no physics in NJOY99, but it is not the truth, there is physics.

3.1. NJOY99 code

The NJOY99 (*R. E. MacFarlane, 1999*) nuclear data processing system is a modular computer code used for converting evaluated nuclear data in the ENDF format into libraries useful for neutronics codes. Because ENDF is used all around the world, ENDF/B-VI (*P. F. Rose, 1991*) and ENDF/B-VII (*M. B. CHadwik, P. Oblozinsky, M. Herman et al., 2006*) in the US, JEFF-3.1 (*A. Koning et al., 2006*) in Europe, JENDL-3.3 (*K. Shibata et al., 2002*) in Japan, etc …. NJOY99 gives access to a wide variety of the most up-to-date nuclear data. These libraries represent the underlying nuclear data from a physics point of view, but practical calculations usually require special libraries. NJOY99 provides comprehensive capabilities for processing evaluated data and it can serve applications ranging from continous-energy Monte Carlo code (like MCNP), to deterministic transport code (like WIMS). This is the mission of NJOY99 – to take the basic data from the nuclear data library and convert it into the forms needed for applications.

NJOY99 handles a wide variety of nuclear effects, including resonances, Doppler broadening, heating (KERM: Kinetic Energy Release in Material), radiation damage, thermal scattering (even cold moderators), gas production, neutrons and charged particles, photo-atomic interactions, self-shielding, probability tables, photon productions, and high-energy interactions (up to 150 MeV). Output can include printed listings, special library files for

applications and Postscript graphics. It is continuously updated within published patches available on its official web site.

NJOY99 consists of a set of modules, each performing a well-defined processing task. Each of these modules is essentially a separate computer program linked to others by input and output files and a few common constants. The NJOY99 modules are:

- **MODER**: Converts between ENDF/B standard coded mode and the NJOY99 blocked binary mode.
- **RECONR:** Reconstructs pointwise cross sections from ENDF resonance parameters and interpolation schemes.
- **BROADR**: Doppler-broadens and thins pointwise cross sections.
- **HEATR:** Generates pointwise heat production cross section (KERMA factors) and radiation damage production cross sections.
- **GASPR:** Adds gas production to PENDF.
- **THERMR:** Generates neutron scattering cross sections and point-to-point scattering kernels in the thermal range for free or bound atoms.
- **PURR:** Prepares unresolved region probability tables for the MCNP continuous energy Monte Carlo code.
- **ACER:** Prepares libraries in ACE format for the Los Alamos continuous energy Monte Carlo code MCNP.

For each material the processing sequence can be divided into two calculations:

- First calculation, to produce point-wise data in ENDF format (MODER to PURR modules)
- Second calculation, the module ACER generates the ACE formatted file that can be directly used in MCNP calculations. Here, error checking and consistency checks are also performed.

3.2. Processing evaluated nuclear data to ACE format.

In this section we describe the job elaborated by the most important NJOY99 modules.

3.2.1. Reconr

Most NJOY processing sequences start with RECONR. It fills two roles. First, it goes through all the reactions included on the ENDF tape and chooses a union grid that allows all cross sections to be represented using linear interpolation to a specified accuracy. This step removes any nonlinear interpolation ranges (***e.g.,*** log-log, linear-log). It also makes it possible for all

summation reactions to be reconstructed as the sum of their parts (*e.g.*, total, total inelastic, total fission). Second, for resonance materials, it reconstructs the resonance cross sections (elastic, fission, capture) on a union grid that allows them all to be represented within certain accuracy criteria, and then combines the resonance data with the other linearized and unionized cross sections. The results are written in PENDF (Point ENDF) format.

3.2.2. Broadr

BROADR adds temperature dependence to the pointwise cross sections generated by the RECONR module. It can also be used to rebroaden the results of a previous BROADR run to a higher temperature.

$$P(v',T)dv' = \frac{a^{3/2}}{p^{3/2}}\exp(-a\,v'^{2})dv' \tag{3.4}$$

In a material at temperature T, the target atoms and molecules are moving around randomly with a distribution of velocities given by the Maxwell-Boltzman function:

$$v\bar{s}(v,T) = \int dv' \left|v - v'\right| s\,(\left|v - v'\right|)P(v',T) \tag{3.5}$$

where

v' = the velocity of the incident particles,

s = the cross section of the stationary nuclei,

$P(v',T)$ = the distribution of target velocities in the laboratory system,

$\bar{s}$ = the Doppler-broadened cross section,

$a = M/kT$, with M is the target mass and k represents the Boltzmann's constant.

The basic cross sections are obtained from a PENDF tape generated by RECONR or produced in a previous BROADR run. The Doppler-broadened effective cross sections are written out as a multi-temperature PENDF tape.

The effect of temperature on typical cross sections is best illustrated by giving several examples. Figure (3.1) gives the (n,α) cross section for B-10 shown for temperatures of 0K, 3000K, and 3000000K. This shows that a 1/*v* cross section is invariant under Doppler broadening.

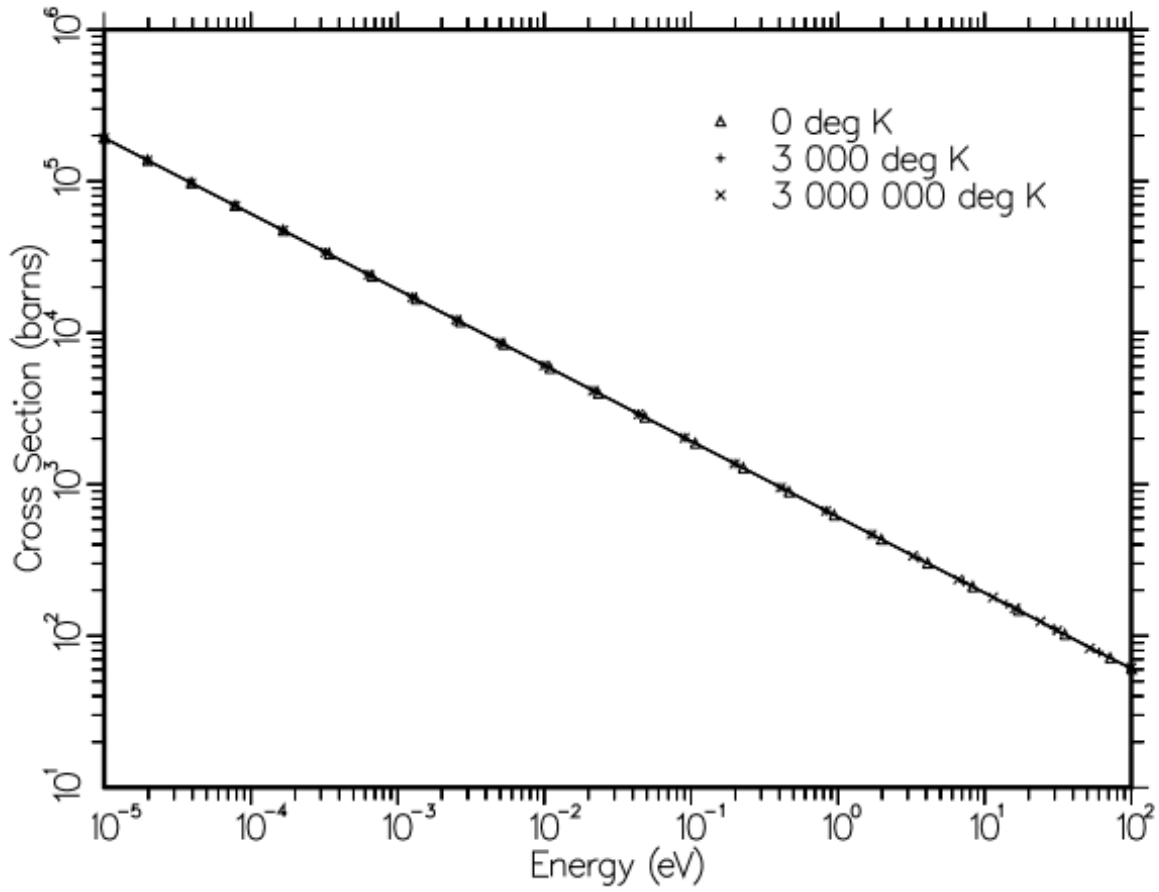

Figure 3.1- B-10 (n,α) cross section at various temperatures.

Figure (3.2) gives the elastic cross section for carbon shown for temperatures of 0K, 300K, 3000K, and 30000K. This shows that a constant cross section will develop a 1/*v* tail under Doppler broadening.

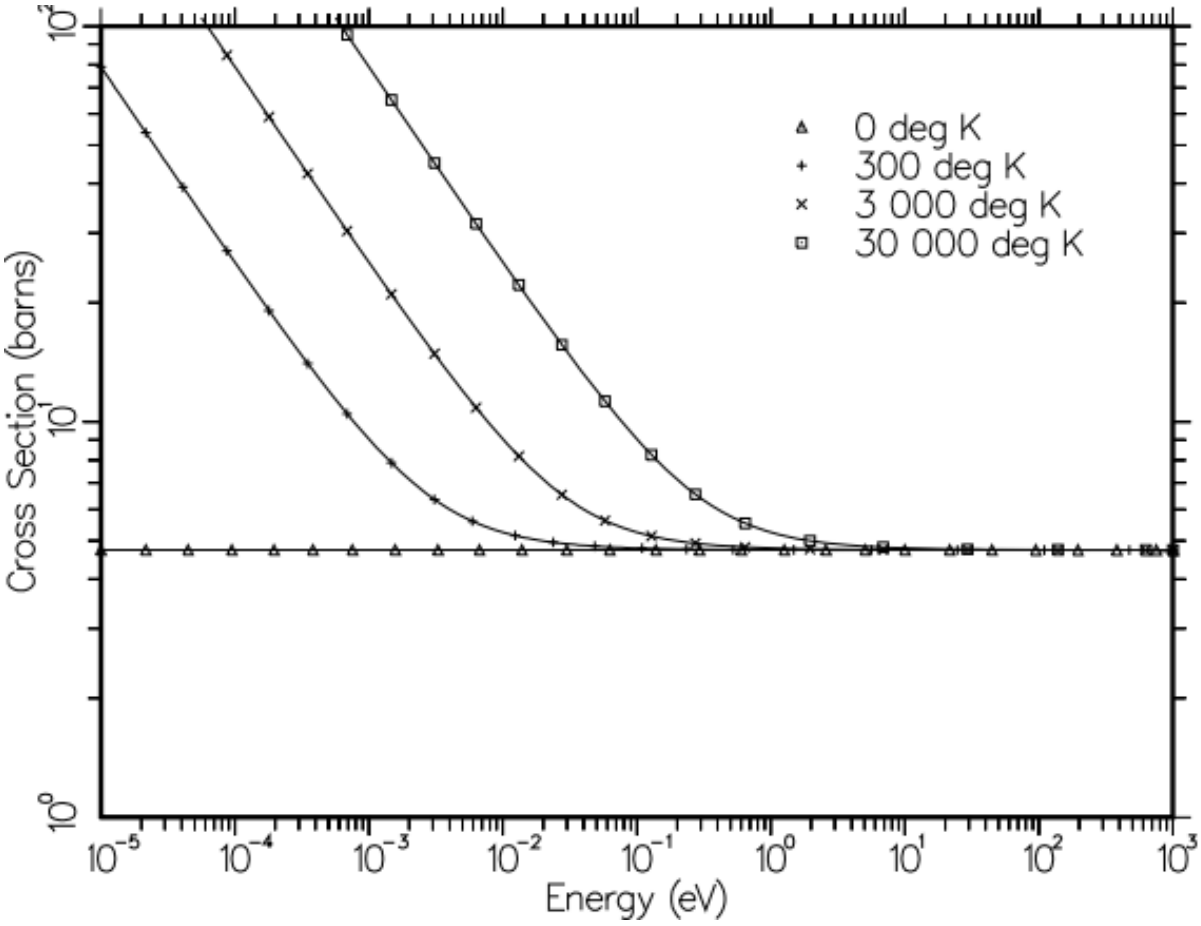

Figure 3.2- Elastic cross section for C-12 at various temperatures.

Finally, Figure (3.3) shows how resonance cross section is behaved under Doppler broadening. The (n,gamma) cross section for Pu-240 is shown for temperatures of 0K, 30000K, and 300000K. Resonances with energies larger than *kT/A* broaden symmetrically (and their areas tend to remain constant). Low energy resonances develop an additional 1/*v* tail, and their areas do not remain constant under Doppler broadening.

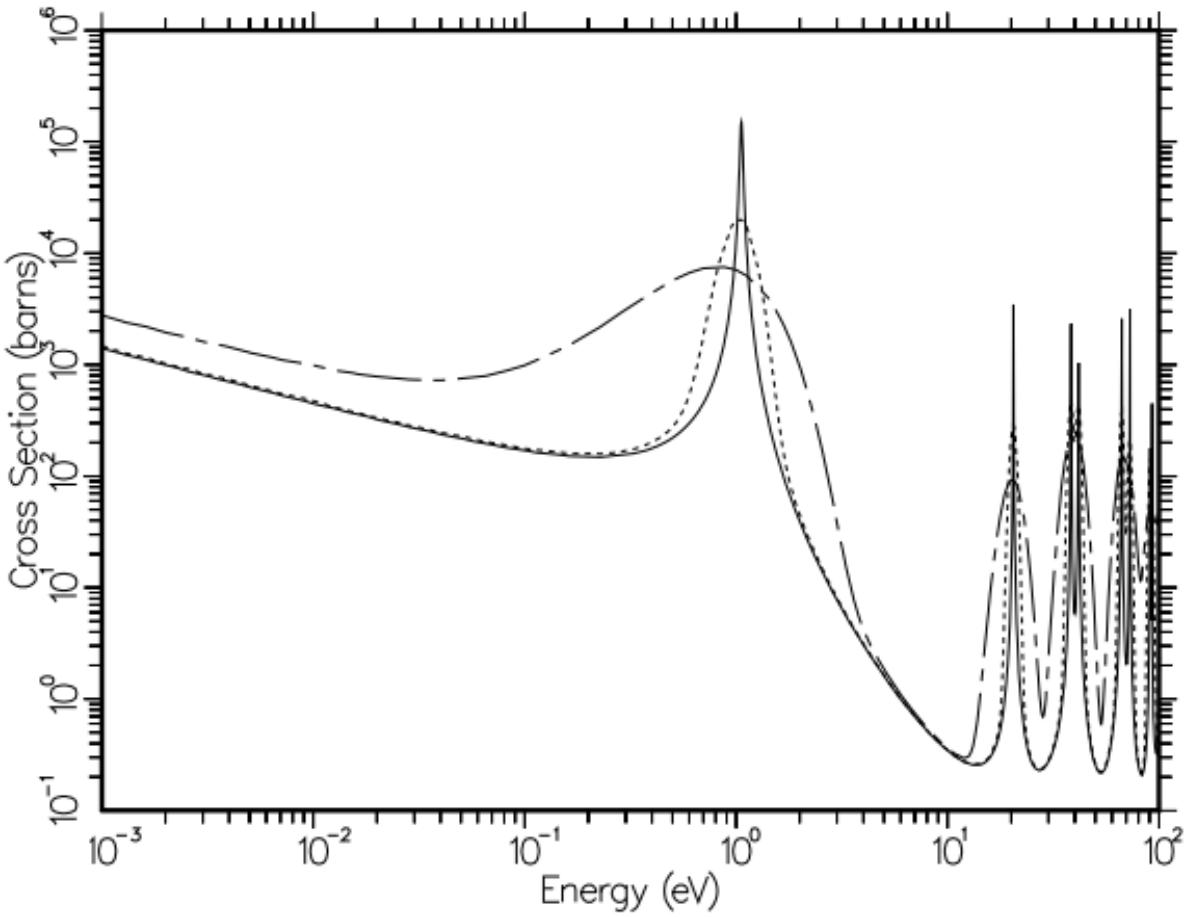

Figure 3.3- (n, gamma) cross section for Pu-240 at various temperatures.

These effects are best understood by noting that Doppler broadening preserves the reaction rate $v*\sigma(v)$, and a finite reaction rate is expected for T larger than zero even as v goes to zero.

3.2.3. Heatr

Nuclear heating results from the slowing down of energetic charged particles produced in nuclear reactions, including the recoil nucleus from scattering reactions. It is a very important quantity. Sometimes it is the product being sold (as in power reactors), and sometimes it is a damaging corollary of the nuclear reactions (as in melting of important structural elements). The HEATR module of NJOY can be used to compute estimates of energy-deposition cross sections for neutrons that can be combined with calculations of neutron fluxes in nuclear systems to compute the neutronics contributions to nuclear heating. The heating due to the photon flux in a nuclear system is usually even more important.

3.2.4. Thermr

At thermal energies, e.g., up to about 0.5 eV for temperatures around room temperature and maybe up to as high as 4 eV for hotter materials, the energy transferred by the scattering of a

neutron is similar to the kinetic energies of motion of the atoms in liquids and to the energies of excitations in molecules and crystalline lattices. Therefore, you cannot picture the target atoms as being initially stationary and recoiling freely as is normally done for higher neutron energies. The motion of the target atoms and their binding in liquids and solids affects both cross sections and the distribution in energy and angle of the scattered neutrons. The THERMR module of NJOY99 is used to compute these effects and add them to a PENDF tape for use by other modules.

For free-gas scattering, where only the thermal motion of the targets is taken into account, not internal modes of excitation, THERMR can generate the cross sections and scattering distributions using analytic formulas. For real bound scattering, it uses an input scattering function and other parameters from the ENDF-format thermal evaluation. A number of such evaluations for common moderator materials have been available for years in various ENDF-format libraries, and new ones have been produced recently using the LEAPR (see NJOY user manual) module of NJOY. The results of THERMR's work are stored into the new PENDF tape using a special set of MT numbers:

Table 3.1- MT numbers.

MT	Moderator
221	free gas
222	H in H_2O
223,224	H in polyethylene
225,226	H in ZrH_n
227	benzine
227	D in D_2O
229,230	C in graphite
231,232	Be
233,234	BeO
235,236	Zr in ZrH_n

As will be discussed below, the lines with two MT values refer to the inelastic and elastic components of scattering, respectively.

a) Incoherent inelastic scattering

The most interesting component of thermal scattering is called "incoherent inelastic" because the neutron exchanges energy with the target molecule or crystalline lattice and all the scattered waves are assumed to combine incoherently without interference effects. This component is described in terms of a scattering function called "S of alpha and beta," where alpha and beta are reduced values for momentum transfer and energy transfer, respectively:

$$s^{inc}(E,E',m)=\frac{s_b}{2kT}\sqrt{\frac{E'}{E}}e^{-b/2}S(a,b) \tag{3.6}$$

$$b=\frac{E'-E}{kT} \tag{3.7}$$

$$a=\frac{E'+E-2m\sqrt{EE'}}{AkT} \tag{3.8}$$

$$s_b=s_f\frac{(A+1)^2}{A^2} \tag{3.9}$$

Here, s_b is the bound scattering cross section, s_f is the free scattering cross section, E and E' are initial and final neutron energies, m is the scattering cosine, A is the ratio of the target mass to the neutron mass, a is the dimensionless momentum transfer and b is the dimensionless energy transfer.

The scattering function for a gas of particles with no internal structure (free gas) is given by

$$S(a,b=\frac{1}{\sqrt{4pa}}\exp(-\frac{a^2+b^2}{4a}) \tag{3.10}$$

b) Coherent elastic scattering

In crystalline materials consisting of coherent scatterers (e.g., graphite, beryllium, beryllium oxide), the scattering from different planes of atoms can interfere, leading to a series of "Bragg edges" as the neutron wavelength hits various possible atomic spacings. The thermal elastic cross section of graphite is shown in Figure (3.4).

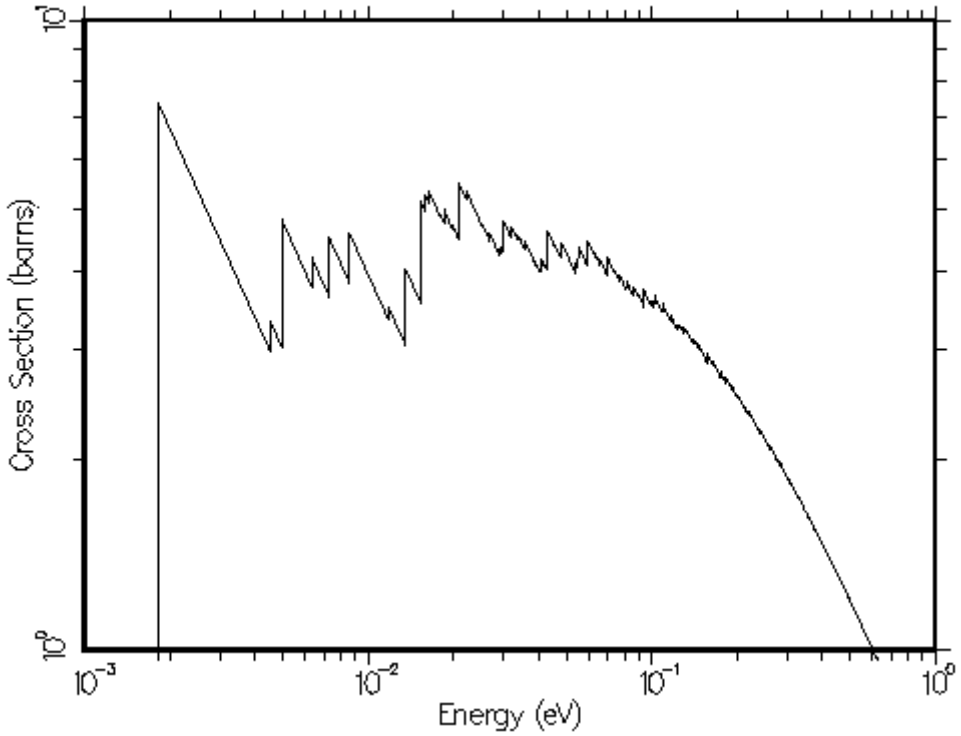

Figure 3.4- Thermal elastic cross section for graphite.

The mathematical express of the energy-angle distribution and integrated cross section for coherent elastic scattering is as follows:

$$s^{coh}(E,E',m) = \frac{s_c}{E}\sum_{Ei<E} f_i e^{-2WE_i} d(m-m_0) d(E-E') \tag{3.11}$$

$$m_0 = 1 - \frac{E_i}{E} \tag{3.12}$$

$$s^{coh} = \frac{s_c}{E}\sum_{E_i>E} f_i e^{-2WE_i} \tag{3.13}$$

where, s_c is the characteristic coherent cross section for the material, W is the effective Debye-Waller coefficient, E_i are the so-called "Bragg edges" and f_i are related to the crystallographic structure factors.

Note that the scattering distribution is completely defined by the energy locations and sizes of the steps in the integrated cross section. The MCNP Monte Carlo code takes advantage of this feature.

c) Incoherent elastic scattering

In solids containing hydrogen, such as polyethylene or frozen methane, the strong incoherence of the scattering from hydrogen simplifies the elastic term:

$$s^{iel}(E,E',m) = \frac{s_b}{2} e^{-2WE(1-m)} d(E-E') \tag{3.14}$$

$$s^{iel}(E) = \frac{s_b}{2}\left\{\frac{1-e^{-4WE}}{2WE}\right\} \tag{3.15}$$

where, s^{iel} is the differential cross section.

The cross section only depends on the bound scattering cross section and the Debye-Waller coefficient, W, which is computed from the excitation spectrum for the solid. Figure (3.5) shows an example of the elastic (dashed) and inelastic (solid) terms for frozen methane at 20K:

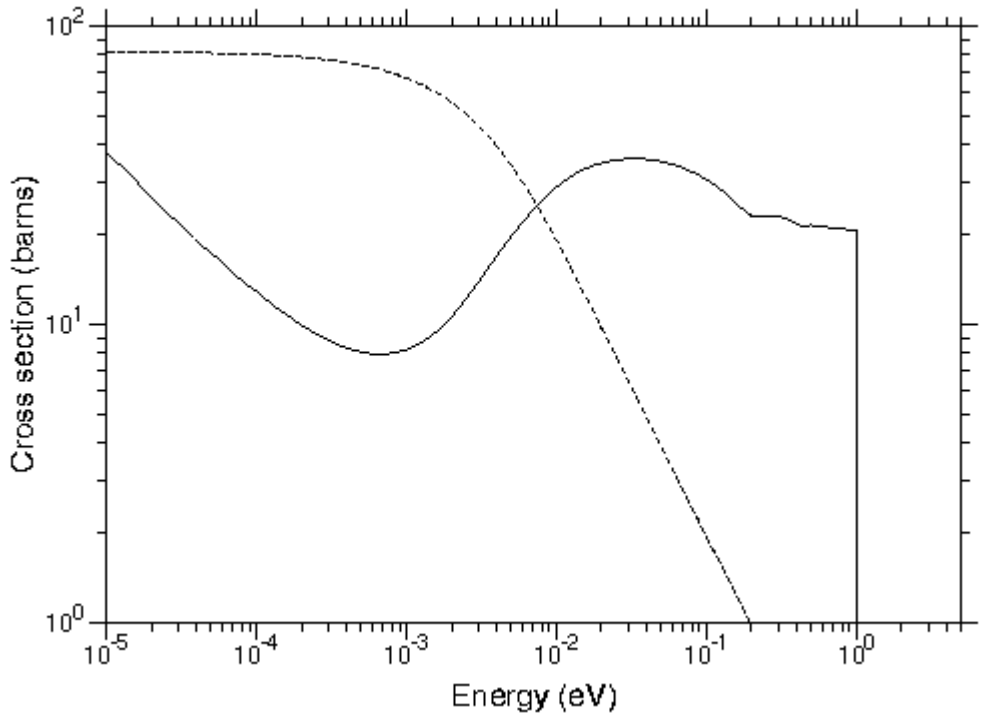

Figure 3.5-Elastic (dashed) and inelastic (solid) cross sections for frozen methane at 20K.

3.2.5. Gaspr

In many practical applications, it is important to know the total production of protons (hydrogen), alphas (helium), and other light charged particles resulting from the neutron flux. Therefore, it is convenient to have a set of special "gas production" or "charged-particle

production" cross sections that can be used in application codes. The ENDF format provides a set of MT numbers for these quantities, but only a few evaluators have added them to their files:

- MT=203 -- total proton production
- MT=204 -- total deuteron production
- MT=205 -- total triton production
- MT=206 -- total He-3 production
- MT=207 -- total alpha production

The GASPR module goes through all of the reactions given in an ENDF-format evaluation, determines which charged particles would be produced by the reaction, and adds up the particle yield times the reaction cross section to produce the desired gas production cross sections. It uses data from an input ENDF tape and an input PENDF tape, and it writes the results on an output PENDF tape. They are then available for plotting, multigroup averaging, or reformatting for the MCNP Monte Carlo code.

3.2.6. Unresolved resonance self shielding

At higher energies in heavier nuclei, the resonances get so close together that they cannot be given separately. Instead of giving individual resonances with their energies and characteristic widths, ENDF-format evaluations give average values for the resonance spacing and the various characteristic widths, together with the probability distributions needed to describe the quantities.

In this unresolved range, it is no longer possible to compute simple cross section versus energy tables; instead, you can calculate the effective cross section in the region of a given energy, which depends on the environment through self-shielding effects, or you can calculate probability distributions for the total cross section and the related elastic, fission, and capture distributions. The self-shielded cross sections are computed by UNRESR, and the probability tables are computed by PURR.

The effective self-shielded cross sections from UNRESR are normally used by the GROUPR module for generating self-shielded multigroup constants. The probability tables from PURR are usually processed by the ACER module and made available to the MCNP Monte Carlo code.

3.2.7. Formatted and binary mode

ENDF tapes received from ENDF/B, JEF, JENDL, CENDL, or BROND, come in a formatted ASCII mode that can be easily read or printed. However, this is not the most efficient form to

use for communicating between different processing modules in NJOY. Binary files are much more efficient because it is not necessary to repeatedly convert the data between the binary forms used in memory and the ASCII forms.

Although the ENDF format specifies a standard binary mode, NJOY uses a special blocked-binary mode that divides each ENDF "record" into one or more blocks of data of bounded size. The NJOY subroutines that read and write ENDF records know how to handle the binary mode and how to convert back and forth between binary and ASCII. NJOY normally uses a page size of 326 words for these binary blocks, which is small enough to use conveniently and large enough to reduce the total number of I/O operations to a reasonable value.

NJOY contains a special module called MODER for converting back and forth between the ASCII and binary forms. It uses negative unit numbers to indicate binary files.

3.2.8. Acer

In these days of inexpensive fast computers with huge memories, people are making more and more use of detailed Monte Carlo transport calculations. This approach is much more expensive than the multigroup approach, but it has two great advantages: detailed cross sections don't have to be approximated, and simplified models of the geometry do not have to be used. There are Monte Carlo codes (e.g., MORSE) that use multigroup data, and NJOY's multigroup data can be reformatted for these codes, but the most faithful physics modeling can be obtained by using a full continuous-energy Monte Carlo code like MCNP from Los Alamos. NJOY can produce libraries for the MCNP code by using its ACER module.

In this thesis we have adopted the processing sequence for generating the ACE-formatted library suitable for use by the MCNP code shown in Figure (3.6) (*O. Cabellos, 2006 and L. Perot, 2009*). All developments have been made using version NJOY99 (patch up259).

An example of NJOY input file and its detailed explanation are presented in appendix A.

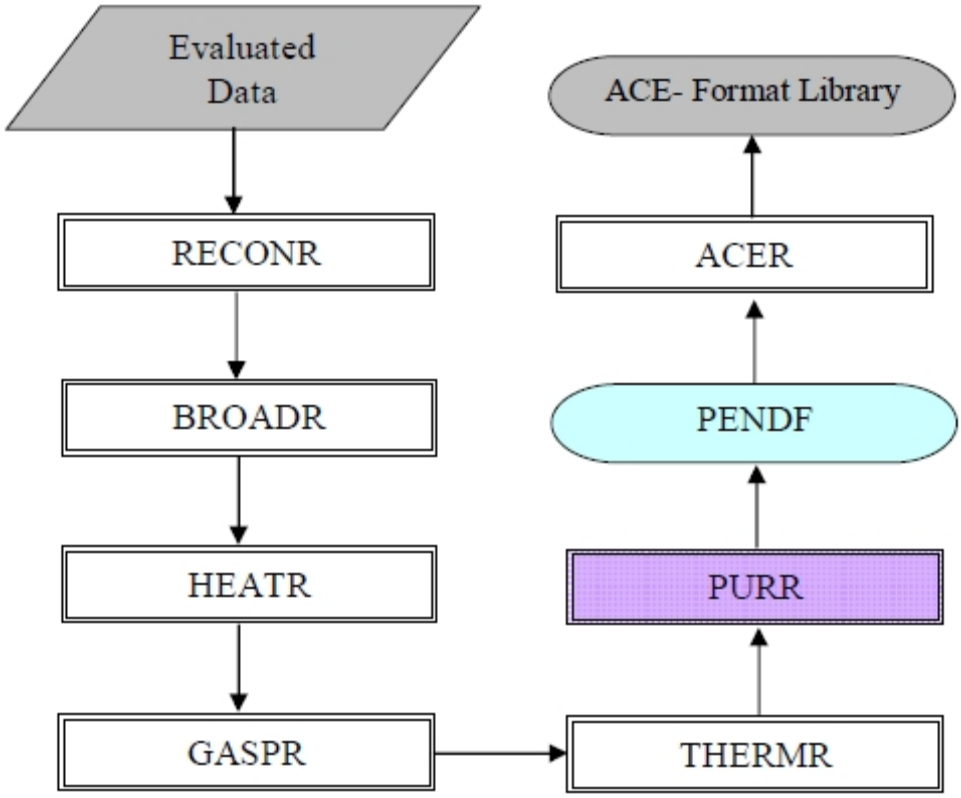

Figure 3.6- NJOY99 processing sequence for an ACE-format neutron library.

4. Benchmark testing of new nuclear data evaluations

In this section we present the results of validation made for the new releases of nuclear data files such as ENDF/B-VII (*M. B. Chadwick, P. Oblozinsky, M. Herman at al., 2006*), ENDF/B-VI.8 (*P. F. Rose, 1991*), JEFF-3.1 (*A. Koning et al., 2006*), JENDL-3.3 (*K. Shibata et al., 2002*), JEF-2.2 (*JEF Collaboration, 2000*) and JEFF-3.0 (*R. Jacqmin, et al., 2002*) processed using NJOY99.259 system and used through this thesis. The study was done by analyzing of some critically predictions and integral parameters for a set of benchmarks that cover the full range of neutron spectrum. Almost all the analyzed benchmarks were taken from the International Handbook of Evaluated Criticality Safety Benchmarks Experiments from OECD (*NEA nuclear science committee, 2003*).

4.1. Characteristics of the analyzed benchmarks

The analyzed benchmarks are characterized by simple compositions and geometries that make them amenable to accurate calculation. These benchmarks are simple experimental problems having a variety of reflector and structural materials and different type of fuels covering the most important fissile isotopes: U-235 and Pu-239 in fast and thermal neutron spectrum

regions. Table (3.2) presents the contribution to the fission rate of neutrons from thermal, intermediate and fast regions of the spectrum for some of the analyzed benchmarks

Table 3.2- Percentage of fissions induced by neutrons in thermal, intermediate and fast neutron energy ranges for some studied benchmarks (*NEA nuclear science committee, 2003*).

Benchmark systems	**Fissions induced by neutrons:**		
	in thermal range (<0.625 ev)	**in intermediate range (0.625 ev - 100 kev)**	**in fast range (>100 kev)**
PU-MET-FAST	0 %	≈ 3%	≈ 97%
HEU-MET-FAST	0 %	≈ 8%	≈ 92%
LEU-COM-THERM	≈ 90%	≈ 6%	≈ 4%
HEU-SOL-THERM	≈ 88%	≈ 11%	≈ 1%

4.1.1. Fast benchmarks

A set of twenty four high enriched uranium benchmarks known as HEU-MET-FAST was studied. It includes GODIVA, TOPSY and FLATTOP. These benchmarks use simple geometry and consist of bare or reflected cores in metallic form. They are qualified as fast because more than 50% of fissions are induced by fast neutrons (*Tab. 3.2*).

For plutonium fast benchmarks we have studied a set of twenty two cases referenced as PU-MET-FAST, such as JEZEBEL-239, JEZEBEL-240, FLATTOP-Pu, THOR, PU-MET-FAST-009, PU-MET-FAST-010, PU-MET-FAST-011 and PU-MET-FAST-018. The benchmarks are simple structures in their geometry and contain metallic plutonium as fissionable material. Different reflectors are used such as water, beryllium, steel, natural uranium, etc.

4.1.2. Thermal benchmarks

Thermal benchmarks are characterized by more than 50% of fissions occurring in the thermal energy range (Table (3.2)). They concern both uranium and plutonium fuel materials. In the case of uranium fuel, two sets of benchmarks were analyzed. They are classified as follow:

- One set of sixteen thermal benchmarks, referenced as LEU-COMP-THERM. Each benchmark consists of a Tank-Critical-Assembly (TCA) type that is a light-water-moderated critical assembly. The TCA cores are composed of low enriched uranium dioxide UO_2 fuel rods arranged in square array and supported by upper and lower

grid plates. Critical sizes were determined by adjusting the water height in the tank. The water to fuel volume ratio in the lattice cells ranged from 1.5 to 3. The main differences between the sixteen benchmarks are lattice pitch, number of rods in the lattice and water level.

- One set of eighteen benchmarks named HEU-SOL-TERM. We find ten cases where we find minimally reflected cylinders of highly enriched solutions of uranyl-nitrate and eight cases formed of water-reflected spheres of uranium-oxyfluoride solutions.

4.2. Generation of cross section libraries

The NJOY99 code has been used to process the evaluated nuclear data files into libraries suitable for use with MCNP5. All the cross sections in the libraries have been processed at 293.6K. For thermal benchmarks, moderators were treated with the S(α,β) thermal scattering approximation. Two different approaches are commonly used: the free gas model, for one isotope, and the molecular treatment, which depends on the chemical binding of atoms within its molecule or lattice.

4.3. Results and discussion

In our benchmark analysis we have used the continuous energy Monte Carlo code MCNP5. All the *keff* values of thermal and fast benchmarks are evaluated using our generated libraries based on ENDF/B-VII, ENDF/B-VI.8, JEF-2.2, JEFF-3.0, JENDL -3.3, and JEFF-3.1, evaluations. Also, we have calculated fission and capture rates for the major elements U-235, U-238 and Pu-239.

The majority of cases studied were run with 2500 cycles of 10.000 neutron histories each. The first 50 cycles were discarded to assure a converged source distribution for a net sum of 24.5 million neutron histories. The resulting 86.5% confidence interval for the eigenvalue is typically between ± 13 and ± 20 pcm. In some illustrations of our results we adopt the following notation:

C: for MCNP calculated reaction rates.

E: for experimental reaction rates published in the literature.

4.3.1. Uranium fast benchmarks

Figure (3.7) represents the variation of ***keff*** for various high enriched uranium benchmark cases. According to this figure, we remark that, for the majority of studied cases, nuclear data libraries based on ENDF/B-VI.8, JEFF-3.1 and JENDL-3.3, give results in good agreement with experiment. JEFF-3.0 and JEF-2.2 underestimate slightly the values of ***keff***. However a good improvement is observed in ***keff*** computation while passing from JEF-2.2 to JEFF-3.0 and from JEFF-3.0 to JEFF-3.1 where the difference to criticality is reduced by about 300 and 250 pcm respectively. Upgrading ENDF/B-VI.8 to ENDF/B-VII increases the disagreement between calculation and experiment by about 230 pcm. The average discrepancies to experimental values are summarized in Table (3.3).

Fission and capture rates were calculated for all studied benchmarks by means of the modified flux estimator feature in MCNP5 code. The corresponding results are presented on Figure (3.8). From this figure, we observe that, all the nuclear data libraries describe well the U-235 average fission and capture rates, except JENDL-3.3 which overestimates with 4.19% the U-235 average capture rate. This, consequently, explains the observed reduction of the discrepancy to criticality in ***keff*** calculation when compared to results deduced from the remaining libraries. The U-238 average fission rate is slightly underestimated when computed by use of ENDF/B-VII, JENDL-3.3 and JEFF-3.1; whereas the other libraries lead to computed values which describe well the behaviour of this fission rate. On the other hand, the U-238 average capture rate is well reproduced by JENDL-3.3 library and slightly overestimated by the remaining nuclear data sets. The evolution from old to newest release for both ENDF and JEFF evaluations increases slightly the discrepancies between calculation and experiment in U-238 fission and capture rates.

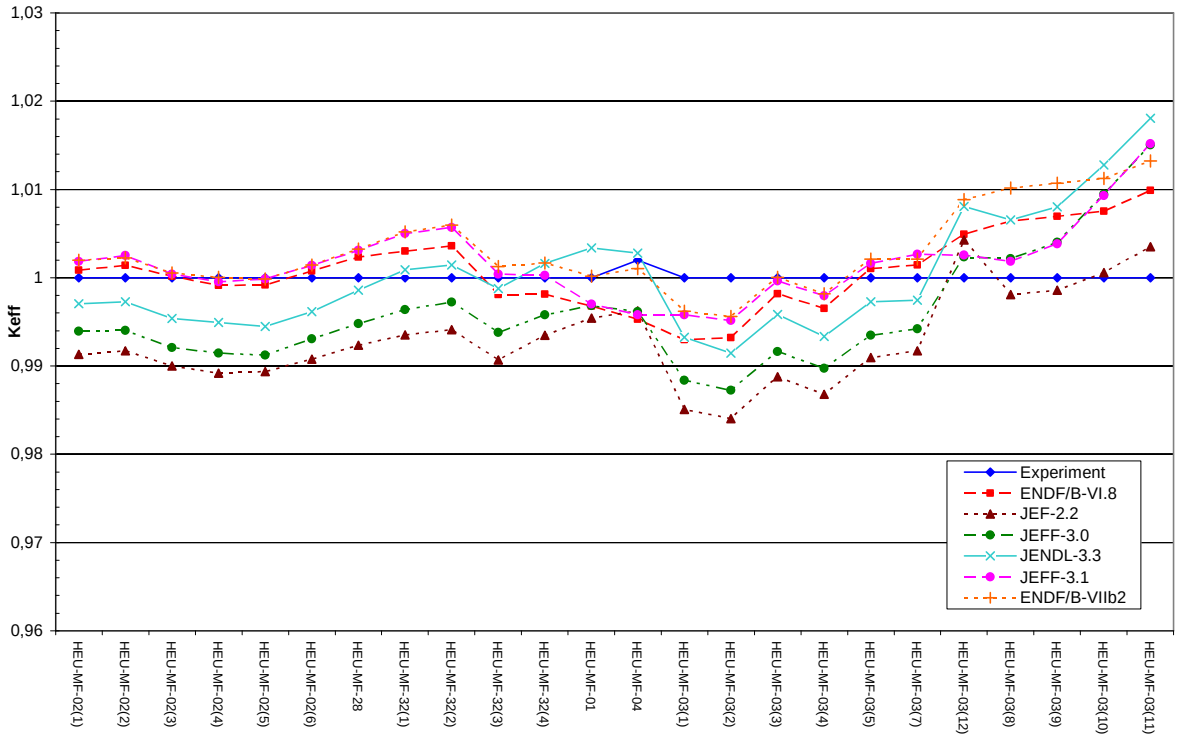

Figure 3.7- Criticality results for high enriched uranium fast benchmarks.

Table 3.3- Discrepancies of computed average *keff* to experiment for high enriched U fast benchmarks.

Neutron cross section data library	**Average *keff***	**discrepancy to experimental value C-E (pcm)**
Experiment	1.00008	-
ENDF/B-VI.8	1.00075	67
ENDF/B-VII	1.00305	296
JEF-2.2	0.99295	-714
JEFF-3.0	0.99602	-406
JEFF-3.1	1.00160	151
JENDL-3.3	1.00021	12

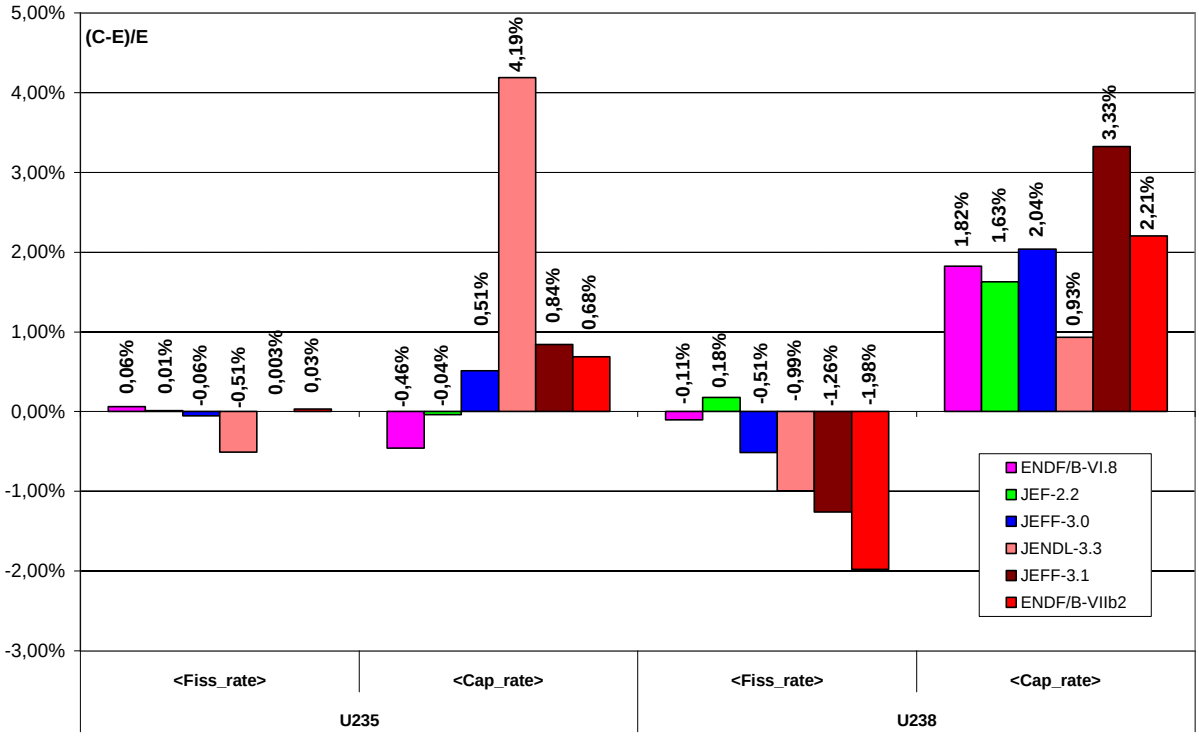

Figure 3.8- (C-E)/E ratio of averaged fission and capture rates for HEU fast benchmarks.

4.3.2. Plutonium fast benchmarks

For Plutonium fast benchmarks the variation of *keff*, represented in Figure (3.9), shows that, generally, the processed libraries based on JEFF-3.0 and JEFF-3.1 describe well the experimental *keff* values, except for beryllium reflected PU-MET-FAST-018 case where JEFF-3.0 overestimates the criticality with roughly 1500 pcm. The study of the neutron cross section data of Be-9, which is used as reflector, shows that JEFF-3.0 evaluation does not take into account the absorption in the energy range bellow 0.7 MeV (*Fig. 3.10*). This means that neutron reflecting efficiency of Be-9 is overestimated in JEFF-3.0. Except for the thorium reflected PU-MET-FAST-008 case; ENDF/B-VII produces good results for all benchmarks. Computation based on libraries deduced from ENDF/B-VI.8, JEF-2.2 and JENDL-3.3 evaluations underestimate the experimental *keff* values and largest discrepancies are seen for JEF-2.2 library. Table (3.4), summarizes the average deviation of calculated values to criticality. We can outline an enhancement while upgrading JEF-2.2 evaluation to JEFF-3.0 and JEFF-3.1. In fact, experiment to calculation discrepancy is reduced by roughly 560 pcm. Furthermore, passing from ENDF/B-VI.8 to ENDF/B-VII enhances the calculated *keff* values and reduces the difference to criticality by 200 pcm.

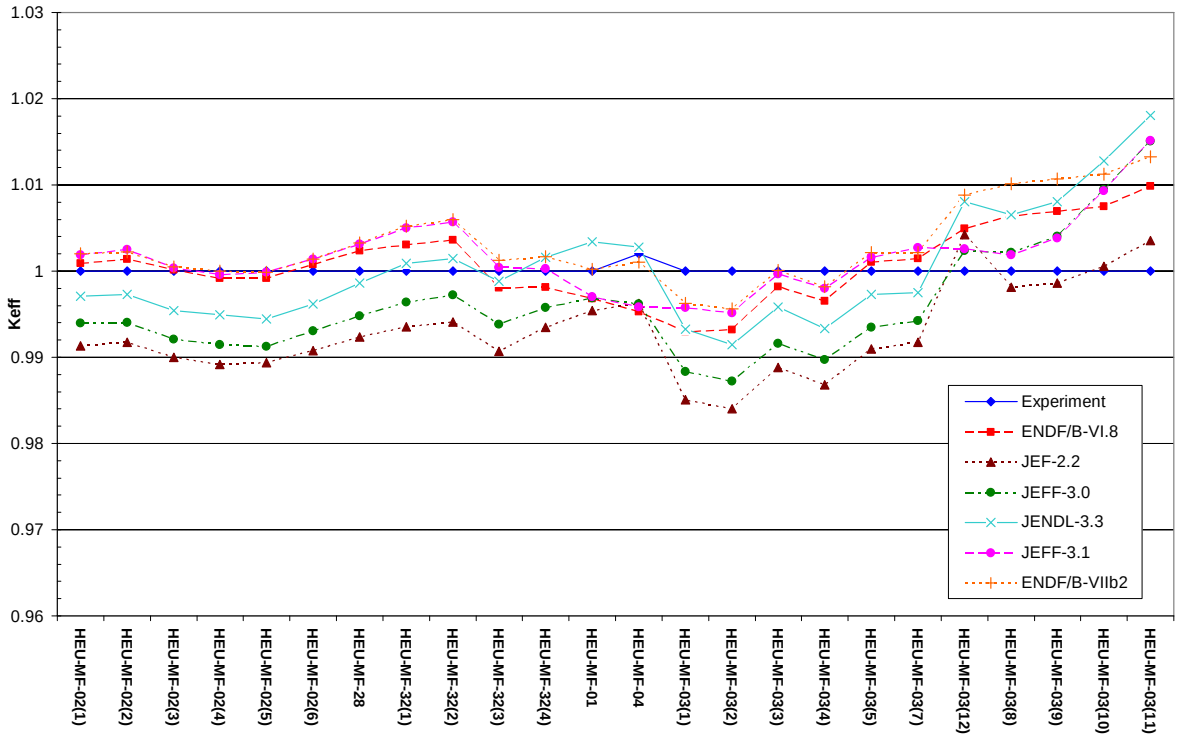

Figure 3.9- *keff* results for Pu-239 fast benchmarks.

Table 3.4- Discrepancies of computed average *keff* to critical experimental value for Pu-239 fast benchmarks.

Neutron cross section data library	Averaged *keff*	discrepancies to critical experimental value C-E (pcm)
Experiment	1.00000	-
ENDF/B-VI.8	0.99694	-306
ENDF/B-VII	0.99896	-104
JEF-2.2	0.99337	-663
JEFF-3.0	0.99899	-101
JEFF-3.1	0.99918	-82
JENDL-3.3	0.99636	-364

From Figure (3.11), we remark that the fission rate of Pu-239 is very well reproduced by all the processed libraries. For the average Pu-239 capture rate, we note a good enhancement when passing from JEF-2.2 to JEFF-3.0, the passage from JEFF-3.0 to the more recent library JEFF-3.1 and from ENDFB-VI.8 to ENDFB-VII did practically not improve the average Pu-

239 capture rate. However, JENDL-3.3 underestimates the average Pu-239 capture rate with 1.81%.

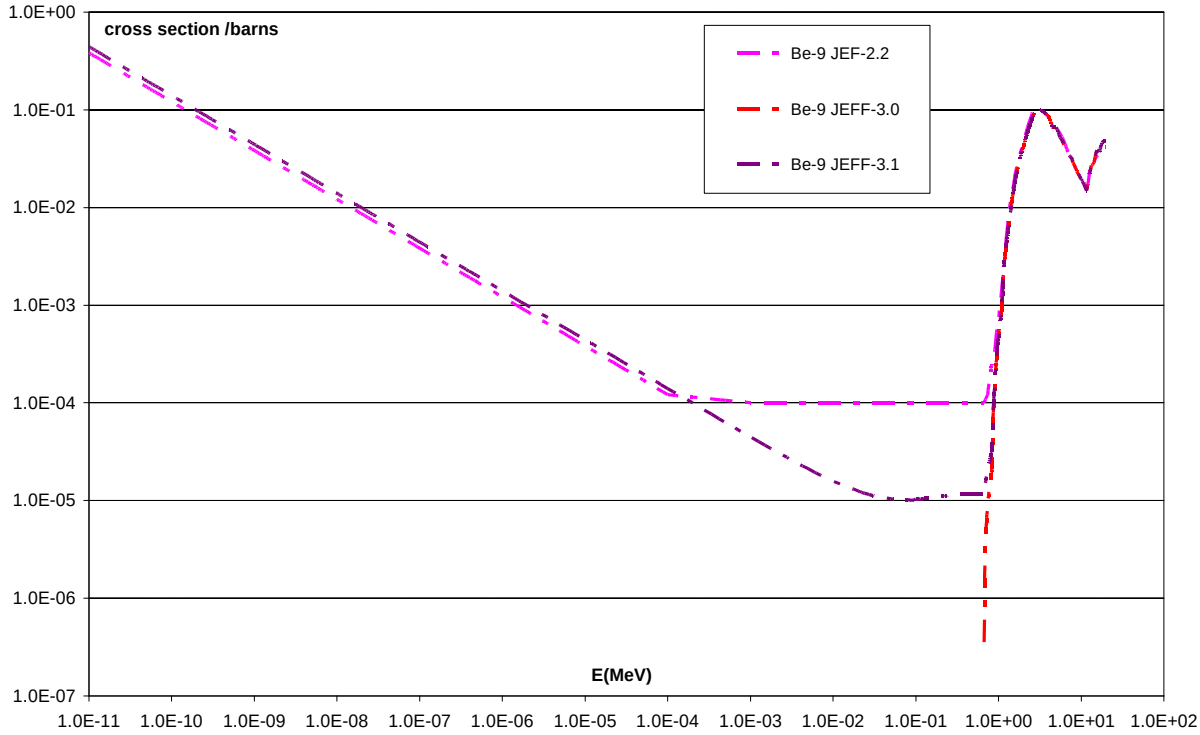

Figure 3.10- Be-9 neutron absorption cross section.

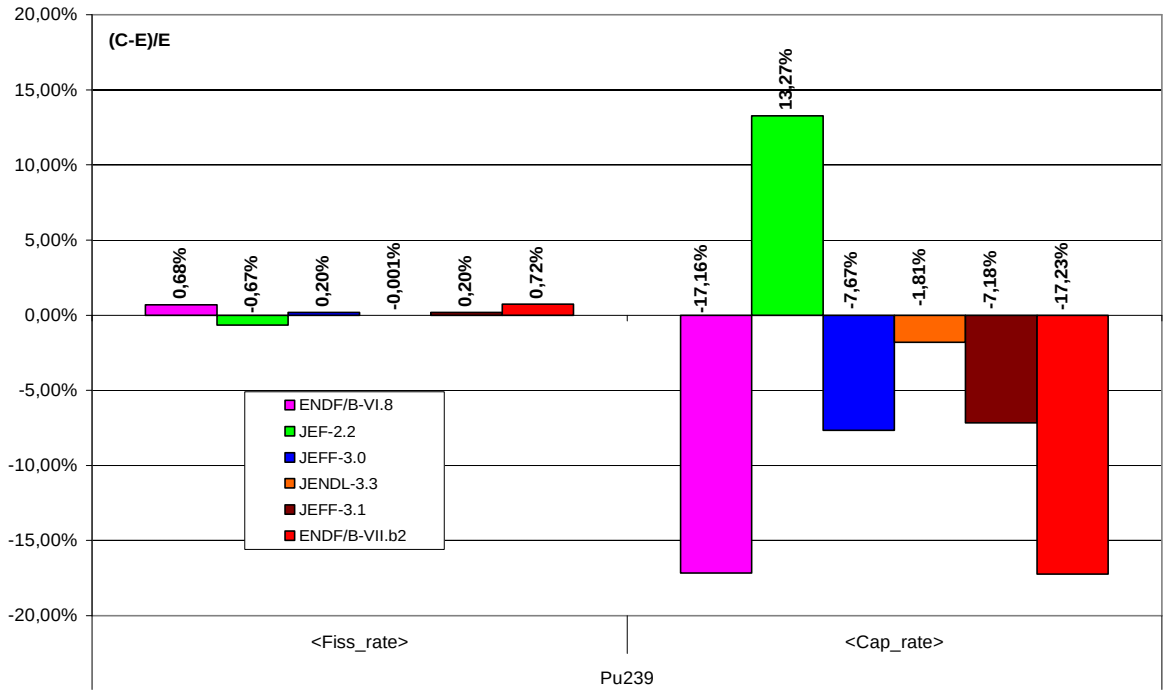

Figure 3.11- (C-E)/E ratio of averaged fission and capture rates for Pu-239 fast benchmarks.

4.3.3. Thermal benchmarks

a) High enriched uranium thermal benchmarks.

The analysis of Figure (3.12) and Table (3.5) shows a slight improvement (36 pcm) when passing from ENDFB-VI.8 to ENDFB-VII, also upgrading JEF-2.2 to JEFF-3.1 improves the results of *keff* with 358 pcm. JENDL-3.3 gives results which are in good agreement with reference criticality values.

Table 3.5- Discrepancies of computed average *keff* to critical value for HEU-SOL-THERM benchmarks.

Neutron cross section data library	**Averaged *keff***	**Discrepancies to critical experimental value C-E (pcm)**
Experiment	1.00000	-
ENDF/B-VI.8	0.99898	-102
ENDF/B-VII	0.99934	-66
JEF-2.2	1.00431	431
JEFF-3.0	0.99997	-3
JEFF-3.1	0.99927	-73
JENDL-3.3	1.00040	40

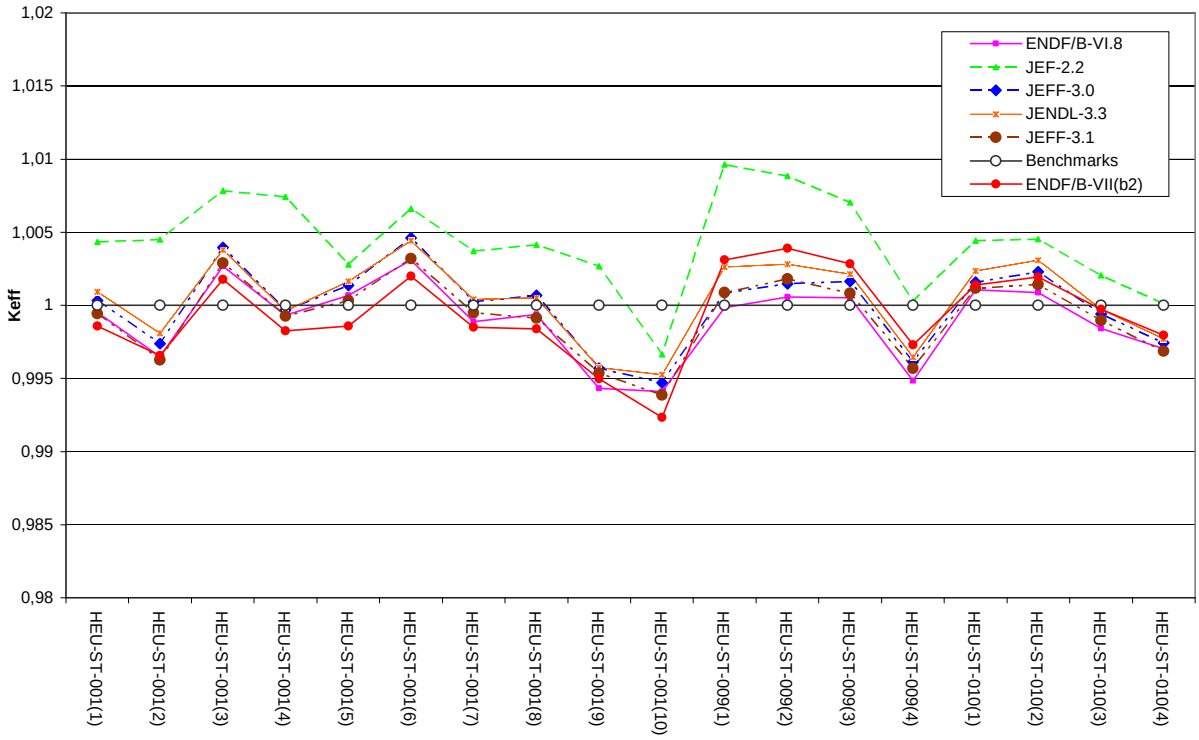

Figure 3.12- *keff* results for HEU-SOL-THERM benchmarks.

Figure (3.13), summarizes the results obtained using our processed nuclear data libraries for the averaged U-235 fission and capture rates. We remark that, the averaged U-235 fission rate is well produced by all the nuclear data libraries. Whereas, except JEF-2.2, all the studied libraries overestimate the published averaged capture rate with roughly 2%.

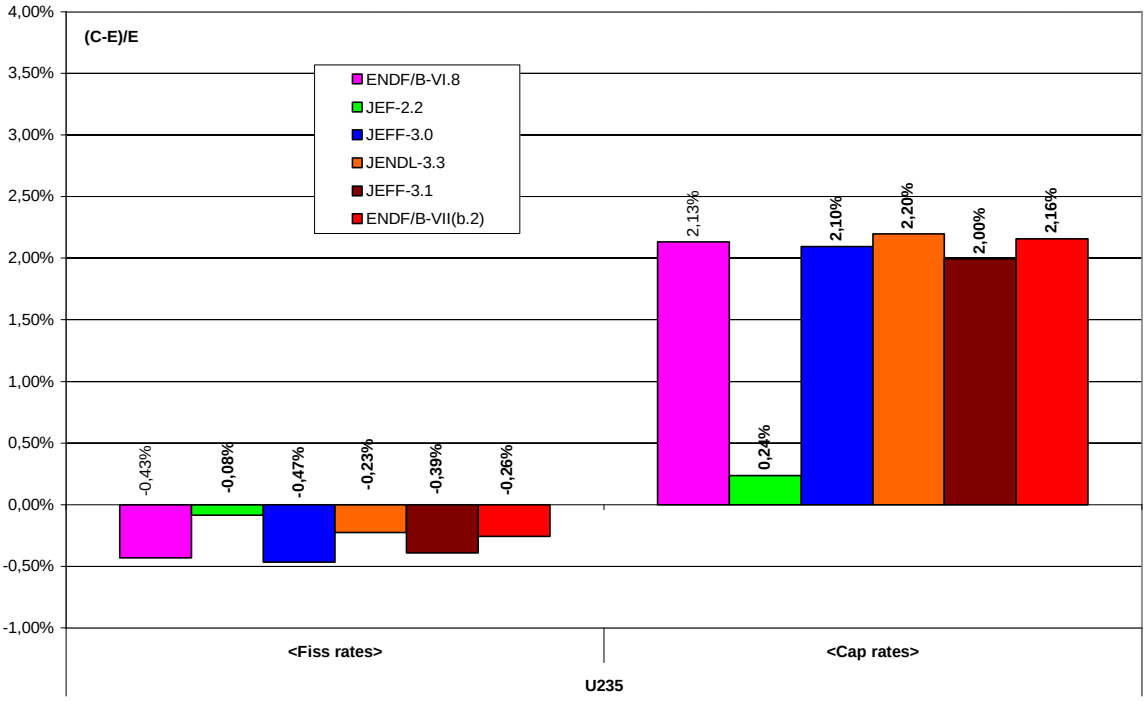

Figure 3.13- (C-E)/E ratio of averaged fission and capture rates for HEU-SOL-THERM benchmarks.

b) Low enriched uranium thermal composed benchmarks.

The analysis of Figure (3.14) and Table (3.6), shows a good enhancement in *keff* calculation when passing from ENDFB-VI.8 to ENDFB-VII. An underestimation of 251 pcm is observed when we passe from JEF-2.2 to JEFF-3.0. However, passing from JEFF-3.0 to JEFF-3.1 improves the results of *keff* with 400 pcm. On the other hand, JENDL-3.3 underestimates the values of *keff* with 270 pcm.

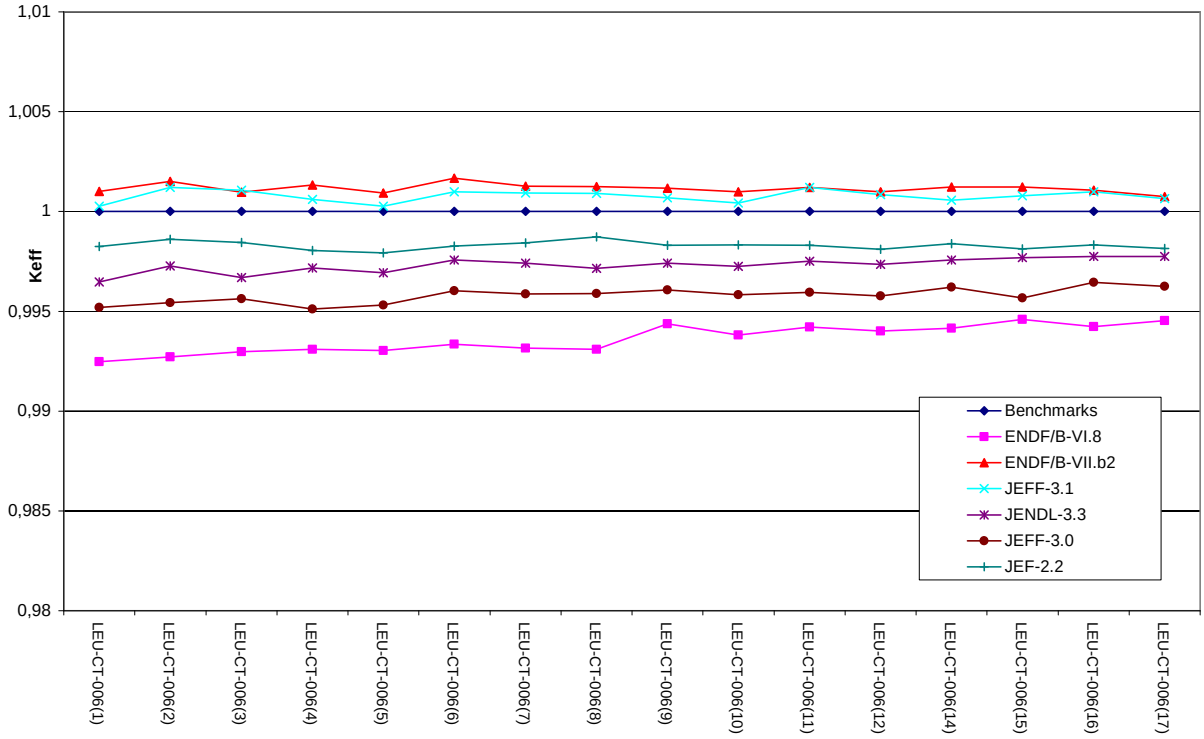

Figure 3.14- The *keff* results for the LEU-COMP-THERM benchmarks.

Table 3.6- Discrepancies of computed average *keff* to critical experimental value for LEU-COMP-THERM benchmarks.

Neutron cross section data library	Averaged *keff*	discrepancies to critical experimental value (pcm)
Experiment	1.00000	-
ENDF/B-VI.8	0.99361	-639
ENDF/B-VII	1.00115	115
JEF-2.2	0.99829	-171
JEFF-3.0	0.99578	-422
JEFF-3.1	1.00077	77
JENDL-3.3	0.99730	-270

From Figure (3.15), we remark that the averaged calculated U-235 and U-238 fission rates agree well with published values. The overestimation of the averaged U-235 capture rate is slightly improved when passing from JEF-2.2 to JEFF-3.1 and from ENDF/B-VI.8 to ENDF/B-VII. In the case of U-238 capture rate, the underestimation obtained when using JEF-2.2 and ENDF/B-VI.8 is increased by use of JEFF-3.1 and ENDF/B-VII respectively.

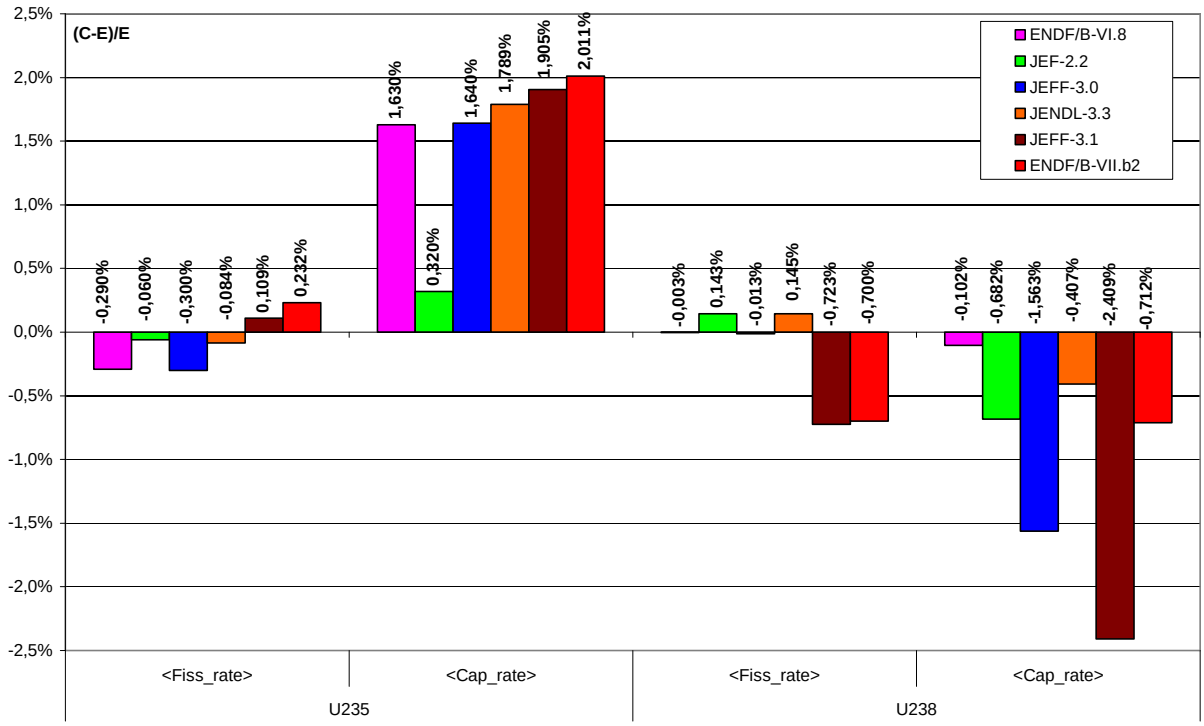

Figure 3.15- (C-E)/E ratio of averaged fission and capture rates for LEU-COMP-THERM benchmarks.

Comparisons of U235, U238, Pu239 and Pu240 fission and capture cross sections as well as the fission and capture reactions rates versus cases from different libraries included in this study are presented in appendix A.

5. Conclusion

New neutron cross section libraries have been processed by means of NJOY99 system and different nuclear data evaluations. The study was focused on U-235 and Pu-239 as the main fissionable materials and aims to assess the performances of the processed libraries through criticality calculations using MCNP5 code and numerous well known critical benchmarks covering both thermal and fast cores. From the analysis of these benchmarks we can deduce the following conclusions:

For uranium cases a significant improvement is observed for updated evaluations in the case of thermal cores. The more recent evaluation releases JEFF-3.1 and JENDL-3.3 describe well

the *keff* multiplication coefficient in both thermal and fast uranium systems. However ENDF/B-VII gives good results for thermal cores only. For all libraries, the averaged U-235 fission rate is well produced in the case of both fast and thermal systems. However, the averaged U-235 capture rate is slightly overestimated with all libraries in thermal region except JEF-2.2 which reproduces well this integral parameter for both thermal and fast benchmarks. Computed averaged U-238 fission rate describes well the thermal region, but it slightly underestimates the fast region when using the newest evaluation releases ENDF/B-VII, JEFF-3.1 and JENDL-3.3. On the other hand, the averaged U-238 capture rate is slightly overestimated for fast systems, but well reproduced in the case of thermal cores except for JEFF-3.0 and JEFF-3.1.

In the case of Pu-239 fast benchmarks, the investigated libraries based on ENDF/B-VII, JEFF-3.0 and JEFF-3.1 evaluations lead to *keff* calculated values in good agreement with experiment. ENDF/B-VI.8, JEF-2.2 and JENDL-3.3 evaluations underestimate the experimental *keff* values. The Pu-239 fission rate is globally well represented, but the capture rate seems to be underestimated by all the libraries except JEF2.2.

From this work we outline the following remarks especially for the more recent evaluations releases:

- In some fast benchmarks, *keff* behaviour cannot be explained by only fission and capture rates of fuel isotopes but some structural materials need to be taken into account in the analysis.
- Compensation between capture and fission is present in some cases and integral results need to be carefully analyzed.
- Fission rate is almost well described for U-235 and Pu-239
- Fast capture data need to be revised for U-238 and Pu-239 in all evaluations and for U-235 in JENDL-3.3
- Thermal capture data need revision for U-235 in all evaluations.

From these results we conclude that our neutron cross section data libraries are well processed and can be used in through this thesis.

4. Development of a new burnup code

This chapter is dedicated to describe the process for the development and validation of a new burnup computer code called «BUCAL1». BUCAL1 is a FORTRAN computer code designed to aid in analysis, prediction, and optimization of fuel burnup performance in nuclear reactors. The code uses output data generated directly by the Monte Carlo neutronics code MCNP to determine the isotopic inventory as a function of time and power density. This allows us to benefit of the full capabilities provided by MCNP and to incorporate them into burnup calculations in the aim to perform more accurate and robust treatment of the problem. The code allows for multiple fueled regions to be analyzed. Neutron transmutation, fission, and radioactive decay are included in the modeling of the production and removal terms for each isotope of interest. For a fueled region, neutron transmutation, fuel depletion, fission-product poisoning, actinide generation, burnable poison loading and depletion effects are included in the calculation.

1. Introduction

Burnup and depletion codes have been developed and used in the nuclear industry since the introduction of digital computing. These codes solve the diffusion equation in one to three dimensions using few neutron energy groups. Only few of the major fission products were included in the calculation. During last years, the enhancement in digital computing capabilities and the amelioration of neutron cross section evaluations have led to the development of more sophisticated numerical techniques, such as Monte Carlo method, to look for system eigenvalues. In burnup codes, the highest fidelity approach uses neutron absorption and fission reaction information generated via neutronics codes to determine the nuclide composition at a desired time step. This kind of model allows the integration of all the neutron flux information into the calculation without post-processing and additional manipulation of neutron flux and cross-sections set (*Parma, 2002*). Neutron absorption and fission reaction rates for individual nuclide are available as output from the Monte Carlo codes like MCNP through the use of tallies. The only requirement is that a pointwise energy-dependent cross section set is available for each nuclide of interest at required temperature.

In this chapter we present a new elaborated burnup computer code called « BUCAL1 ». The code was developed to incorporate the neutron absorption reaction tally information generated directly by MCNP5 code in the calculation of fissioned or neutron-transmuted isotopes for multi-fueled regions. The use of Monte Carlo method and pointwise cross section data characterizing the MCNP code allows an accurate simulation of neutron life cycle in the

reactor and the integration of data on the entire energy spectrum, thus a more accurate estimation of results than deterministic code can do.

The BUCAL1 strategy consists of using the nuclide inventory, MCNP tally information, power density, and other data to determine the new nuclide inventory for a given region of the core at a new time step. Then the new inventories are automatically placed back into MCNP input file and the case run for a new subsequent time step.

2. Code overview

BUCAL1 (*B. El Bakkari et al., 2008 and B. El Bakkari et al. 2009*) is a FORTRAN computer code designed to aid in analysis, prediction and optimization of fuel burnup performance in a nuclear reactor. The code uses output parameters generated by the Monte Carlo neutronics code MCNP to determine the isotopic inventory as a function of time and power density. BUCAL1 differs in comparison to other burnup codes in that it does not use the calculated neutron flux as input to generate the nuclide inventory for the next time step. Instead, BUCAL1 directly uses the neutron absorption reaction tally information generated by MCNP for each nuclide of interest to determine the new nuclide inventory for that region. This allows for the full capabilities of MCNP to be incorporated into the calculation and a more accurate analysis to be performed. Also, the code allows for multi-fueled regions to be analyzed and is designed to perform several modes of burnup calculations: it can do burnup calculation followed by a space of time of cooling, burnup calculation with shuffling fueled regions and burnup calculation with reloading new fresh fuel. BUCAL1 can be used to study the reactivity effects and isotopic inventory as a function of time for a nuclear reactor system. For a fueled region: neutron transmutation, fuel depletion, fission product poisoning, actinide generation and burnable poison loading and depletion effects are included in the calculation. The number of nuclides analyzed is limited only by the neutron cross section availability.

3. Design goals and requirements

The main goal in the development of the BUCAL1 computer code was to construct a burnup code that would use only the neutron absorption tally/reaction information generated by MCNP5 in the calculation of fissioned or neutron-transmuted isotopic compositions for different fuel-loaded regions. Accomplishing this goal would allows for a simple, straightforward and accurate calculation to be performed without having to use the calculated group fluxes in a separate code to perform transmutation analysis. Using the MCNP tally

information directly in the computation allows for the most information to be used in the analysis. Also, using MCNP and the continuous-energy cross sections allows avoiding the cross section manipulations.

In order to accomplish this goal, the following tasks were imposed in the development of the code package. BUCAL code must be able to:

- Read and interpret an MCNP input file such that isotopic concentrations can be identified for different fueled and unfueled regions of a core.
- Read and interpret an MCNP5 output file such that fission and transmutation reaction information can be resolved for each isotope and region of interest.
- Calculate the production and removal of a specific isotope through fission, transmutation and radioactive decay.
- Do burnup calculations for a large variety of nuclear fuels.
- Read, interpret and write to an MCNP input file such that the resultant isotopic concentrations can be inserted automatically into the MCNP input file at their proper locations.

In order to fulfill the above requirements, the code package must be able to read and interpret an MCNP input file correctly. To perform this task for a multi-region problem, the MCNP input file must be structured in such a way that BUCAL code can logically interpret the input information. This requires the use of specific cell numbers, material numbers, keywords and a particular structure and flow in the MCNP input file.

4. Mathematical approach

4. 1. Overview

In routine reactor burnup calculations, the key objective is to determine the time-dependent fuel material compositions as well as the eigenvalues as a function of burnup. Two basic mechanisms of fuel depletion are under consideration: (i) various nuclear reactions such as nuclear fissions, neutron captures, etc. and (ii) the decay of radioactive isotopes. Once material compositions are known, eigenvalues can then be calculated efficiently using MCNP code for specified geometry. Mathematically, the material balance process can be described at any time by the following depletion equations:

$$\frac{dN_i}{dt} = \sum_j g_{ji} s_{f,j} N_j f + \sum_k s_{c,k\to i} N_k f + \sum_l l_{l\to i} N_l - (s_{f,i} N_i f + s_{a,i} N_i f + l_i N_i) \qquad (4.1)$$

and

$$\frac{dN_i}{dt} = \sum_l l_{l\to i} N_l - l_i N_i \qquad (4.2)$$

where,

$\frac{dN_i}{dt}$ = Time rate of change in concentration of isotope i,

$\sum_j g_{ji} s_{f,j} N_j f$ = Production rate per unit volume of isotope i from fission of all fissionable nuclides,

$\sum_k s_{c,k\to i} N_k f$ = Production rate per unit volume of isotope i from neutron transmutation of all isotopes including (n, γ), (n, 2n), etc.,

$\sum_l l_{l\to i} N_l$ = Production rate per unit volume of isotope i from decay of all isotopes including β^-, β^+, α, γ, etc.

$s_{f,i} N_i f$ = Removal rate per unit volume of isotope i by fission,

$s_{a,i} N_i f$ = Removal rate per unit volume of isotope i by neutron absorption (excluding fission),

$l_i N_i$ = Removal rate per unit volume of isotope i by decay.

Eq. (4.1) requires the presence of neutron flux, so it is used by BUCAL1 during reactor operating. However, *Eq. (4.2)* is adopted by BUCAL1 during cooling (or decay) calculations after reactor shutdown. These equations can be solved by using analytical techniques (e. g., Laplace transforms) or by numerical methods (e. g., Rung-Kutta method). Due to the fact that a large number of coupled equations can result, a numerical solution technique is the only practical solution method.

Note that, the neutron flux and isotope concentration are both position and time dependent. Hence, the neutron flux, cross section and concentration should really be defined as

$$f \Rightarrow f(x, y, z, t, E)$$
$$s \Rightarrow s\,(\mathrm{E}), \text{and}$$
$$\mathrm{N_i} \Rightarrow \mathrm{N_i}(x, y, z, t)$$

The energy dependence can be integrated out of the differential equation, since only the flux and cross sections are energy dependent. This lead to write the quantity sNf as shown in *Eq.(4.3*),

$$sNf \Rightarrow N(x, y, z, t)\int_0^\infty s\,(\mathrm{E}) f(x, y, z, t, E)dE \qquad (4.3)$$

4. 2. Solution technique

Eqs. (4.1) and *(4.2)* can be solved by using a variety of numerical solution techniques. In BUCAL1 a solution technique based on the fourth order Rung-Kutta method is proposed. This method allows performing numerical multi-step integrations of differential equations for a system of *n* order with initial conditions. It uses algorithms with separated steps to calculate the N_i density at time t_i, by using just the data of time t_{i-1}. These algorithms thus respect two essential properties of the solution of the differential equations system with the following initial conditions:

- The value of N(t) for $t \geq \tau$, depends only on the value of $N(\tau)$ and not of the above.
- The value of N(t) for $t \leq \theta$, does not depend on the value of $N(\theta)$, nor the following.

Using this method, the solution of *Eq. (4.1)* can be transformed into a system of linear *Eqs. (4.4)* and *(4.5)* those are easy and fast to solve.

$$\begin{cases} N_1^i = N_1^{i-1} + \frac{1}{6}(K_{a,1} + 2K_{b,1} + 2K_{c,1} + K_{d,1}) \\ N_2^i = N_2^{i-1} + \frac{1}{6}(K_{a,2} + 2K_{b,2} + 2K_{c,2} + K_{d,2}) \\ \ldots \\ N_n^i = N_n^{i-1} + \frac{1}{6}(K_{a,n} + 2K_{b,n} + 2K_{c,n} + K_{d,n}) \end{cases} \tag{4.4}$$

where,

$$\begin{aligned} h^i &= t^i - t^{i-1} \\ K_{a,j} &= h^i f_j(t^{i-1}, N_1^{i-1}, N_2^{i-1}, \ldots, N_j^{i-1}, \ldots, N_n^{i-1}) \\ K_{b,j} &= h^i f_j(t^{i-1} + \frac{h^i}{2}, N_1^{i-1} + \frac{K_{a,1}}{2}, N_2^{i-1} + \frac{K_{a,2}}{2}, \ldots, N_j^{i-1} + \frac{K_{a,j}}{2}, \ldots, N_n^{i-1} + \frac{K_{a,n}}{2}) \\ K_{c,j} &= h^i f_j(t^{i-1} + \frac{h^i}{2}, N_1^{i-1} + \frac{K_{b,1}}{2}, N_2^{i-1} + \frac{K_{b,2}}{2}, \ldots, N_j^{i-1} + \frac{K_{b,j}}{2}, \ldots, N_n^{i-1} + \frac{K_{b,n}}{2}) \\ K_{d,j} &= h^i f_j(t^{i-1} + h^i, N_1^{i-1} + K_{c,1}, N_2^{i-1} + K_{c,2}, \ldots, N_j^{i-1} + K_{c,j}, \ldots, N_n^{i-1} + K_{c,n}) \end{aligned} \tag{4.5}$$

with K_a, K_b, K_c and K_d represent the weighting factors, and h^i is the burnup time step.

Numerical verification of the accurateness of the fourth order Rung Kutta method is presented in appendix B.

4. 3. Predictor corrector approach

The depletion algorithm of BUCAL1 assumes that the flux spectrum of reactor is constant during the entire burnup step. This assumption, however, may lead to less accurate results if

one uses too large burnup steps since the spectrum of a reactor changes during such steps. Hence, the reaction rates and the power distribution calculated at the beginning of the step might not adequately account for the changes during the entire burnup step. In this case, BUCAL1 uses a more accurate approach for the depletion calculation known as ‘‘the predictor–corrector depletion approach”. This approach involves the following multistep process:

- A burnup calculation is completed in BUCAL1 to the final time step [ti → tf] (Predictor step).
- Fluxes and reaction rates are recalculated in a steady- state MCNP calculation at the final time step ‘‘tf”.
- Then the recalculated fluxes and reaction rates are used to burn over the full time step [ti → tf] (Corrector step).
- The average atom densities from these two calculations are taken as the end-of-time step material compositions.

This approximation is true only if the flux shape between the two time steps varies linearly; this approach is usually an acceptable approximation. Implementing this approach allows the user to burn a system using fewer burnup steps than if no approximation were made on the average flux behaviour.

4. 4. Total reaction rates calculation

Various reaction rates and the one-group flux in each individual active cell are provided by MCNP flux tallies as:

$$\begin{cases} f_i = \int f_i(E)dE \\ R_{ijk} = \int s_k^j(E) f_i(E)dE \end{cases} \tag{4.6}$$

where

$s_k^j(E)$ = Microscopic cross section of reaction type k for isotope j,

$f_i(E)$ = The region averaged one group flux in cell i,

R_{ijk} = Reaction rates of type k with nuclide j in cell i.

These tallies in MCNP come from track length estimation of cell flux and reaction rates (tally type F4 and FM4 in MCNP).

In the current version of BUCAL1, the two groups of nuclides under consideration are:

- actinides (ACT) that contain heavy metal nuclides with atomic number Z≥90

and their decay daughters;

- fission products (FP) produced by fissions and their decay/capture daughters.

Specifically, the calculated reaction rates identifiers of fission products and actinides are shown on Table (4.1). Only the neutron capture reaction is considered for fission products since the neutron absorption is primarily via (n, γ) reaction. For actinides, four types of reactions are considered including capture, fission, (n, 2n) and (n, 3n) because of their important fission products generating and higher-mass actinides evolving (*Zh. Xu, 2003*).

Table 4.1- MCNP-tallied reactions used in burnup analysis.

	Reaction type	**MCNP reaction identifier**
Actinides	(n, γ)	102
	(n, f)	-6
	(n, 2n)	16
	(n, 3n)	17
Fission products	(n, γ)	102

Note that it is not practical to calculate MCNP reaction rate for all nuclides in BUCAL1 (~ 910 nuclides) due to the excessive CPU time needed and the unavailability of many isotopes cross-sections. Only a limited set of important ones (e.g., strong neutron absorption contributors), typically 45 actinides and 102 fission products are considered in MCNP calculations. Below, we list the most important isotopes adopted in our treatment (*Tab. 4.2*).
For the less capturing nuclides, BUCAL1 uses an approximate model based on *Eq. (4.7)*, to take into account their capture reaction rates (*Tan Dat, 1996*):

$$\overline{s_i^c f} = f_M \left[s_{i,2200}^c \sqrt{\frac{p}{4}} \sqrt{\frac{293}{T}} + rI_i \right] \tag{4.7}$$

where

$\overline{s_i^c f}$ = Microscopic capture rate of isotope i,

f_M = Maxwellien flux,

$s_{i,2200}^c$ = Thermal neutron capture cross section of isotope i at 293K,

T = Temperature of neutrons causing fission,

r = Ratio of epithermal flux per unit of lethargy to the Maxwellien thermal flux,

I_i = Resonance integral capture cross section on isotope i.

Table 4.2- The most important isotopes considered in MCNP calculations.

Fission products				Actinides	
BR-81	RB-85	KR-83	KR-82	TH-232	TH-231
ZR-91	KR-84	Y-89	RB-87	TH-233	PA-231
NB-95	SR-90	ZR-93	ZR-92	PA-233	PA-232
MO-97	ZR-94	ZR-96	MO-95	U-233	U-232
RU-100	MO-96	TC-99	MO-98	U-235	U-234
RH-103	MO-100	RU-102	RU-101	U-236	U-237
PD-105	RU-103	PD-104	RU-104	U-239	U-238
AG-109	RH-105	PD-107	PD-106	NP-236	NP-235
CD-112	PD-108	CD-110	PD-110	NP-238	NP-237
SB-121	CD-111	CD-114	CD-113	NP-239	PU-236
I-129	IN-115	I-127	SB-123	PU-239	PU-238
CS-133	TE-128	XE-132	XE-131	PU-241	PU-240
XE-135	XE-133	CS-134	XE-134	PU-243	PU-242
BA-137	BA-134	XE-136	CS-135	AM-241	CM-246
CE-141	CS-137	LA-139	BA-138	CM-248	CM-247
PR-143	CE-140	CE-142	PR-141	BK-249	CM-249
ND-145	ND-142	CE-144	ND-143	BK-250	CF-249
SM-147	ND-144	ND-147	ND-146	CF-250	CF-251
SM-148	PM-147	$PM148^{M}$	ND-148	CF-252	
SM-150	PM-148	SM-149	PM-149		
SM-153	ND-150	EU-151	SM-151		
GD-154	SM-152	SM-154	EU-153		
GD-156	EU-154	GD-155	EU-155		
DY-160	EU-156	GD-158	GD-157		
ER-166	TB-159	DY-162	DY-161		
ER-167	DY-163				

4. 5. Flux normalization coefficient

MCNP code generates reaction rates to be used for BUCAL1 depletion calculations. These generated reaction rates are normalized to one fission source-neutron, which need to be multiplied by a constant factor to take into account of the entire reactor power. The typical way of calculating this constant factor (CF) as recommended in the MCNP manual (*X-5 Monte Carlo Team, 2003*) is based on the following equation:

$$CF = \frac{P\bar{n}}{Q.keff} \tag{4.8}$$

where

P = Total power of the entire system (watts),

$\bar{u}$ = Average fission neutrons number per fission event,

Q = Average recoverable energy per fission event (J/fission),

keff = Eigenvalue of the system.

MCNP calculates the system-averaged $\bar{u}$ and Q values. The power level used for the constant factor *CF* is the total power of the system and it is a user input. The Q value used in the calculation is an MCNP estimation of the recoverable energy per fission event. BUCAL1 uses the prompt recoverable energy per fission (Q-prompt) multiplied by a constant number (1.111) recommended by the MCNPX2.6 developers (*Hendrichs, 2007*). This factor allows taking into account the delayed fission energy and (n,g) photons contribution.

4. 6. Power fraction calculation

BUCAL1 can do burnup calculations for multi-fuelled regions system where the power fractions for each active cell are calculated by BUCAL1 as follows:

$$f_i = \frac{\sum_{j=1}^{m_i} N_{ij} \left[\int s_{ij,f}(E) f_i(E) dE\right] V_i Q_j}{\sum_{k=1}^{n}\sum_{j=1}^{m_k} N_{kj} \left[\int s_{kj,f}(E) f_k(E) dE\right] V_k Q_j} \tag{4.9}$$

where

N_{ij} = the atom density of actinide j in active cell i,

$s_{ij,f}(E)$ = fission cross section of actinide j in active cell i,

$f_i(E)$ = volume averaged neutron flux in active cell i,

Q_j = recoverable energy for actinide j,

V_i = volume of active cell i,

m_i = total number of actinides in active cell i,

n = total number of cells.

Eq. (4.9) appears complex; however, all quantities involved are transparent and readily available during the neutronic-burnup computational process. Evaluation of *Eq. (4.9)* takes a negligible fraction of CPU time in comparison to MCNP runs. Moreover, this equation is

fully compatible with the BUCAL1 depletion schema. Table (4.3), shows the major actinides used by BUCAL1 and their recoverable energies necessary for the calculation of *Eq. (4.9)*.
The power of each active cell is determined by normalizing the calculated power fraction f_i to the total power of the system. Figure (4.1) shows the simplified flow diagram of BUCAL1.

Table 4.3- Recoverable energies for major actinides used in BUCAL1 for the power fraction calculation.

Actinide	Recoverable energy (MeV)
Th-232	193.42
Pa-233	197.35
U-233	200.98
U-234	201.34
U-235	201.70
U-236	202.06
U-238	202.77
Np-237	206.12
Pu-238	210.23
Pu-239	210.60
Pu-240	211.00
Pu-241	211.34
Pu-242	211.71
Am-241	201.96
Am-242M	202.29

A brief description of the method for the preparation of the BUCAL1 input file, as well as the description of the BUCAL1 outputs files are presented in appendix C.
Appendix D gives some examples of the BUCAL1 input file and the unique structure of the MCNP input file required for burnup calculations using our new elaborated burnup code BUCAL1.

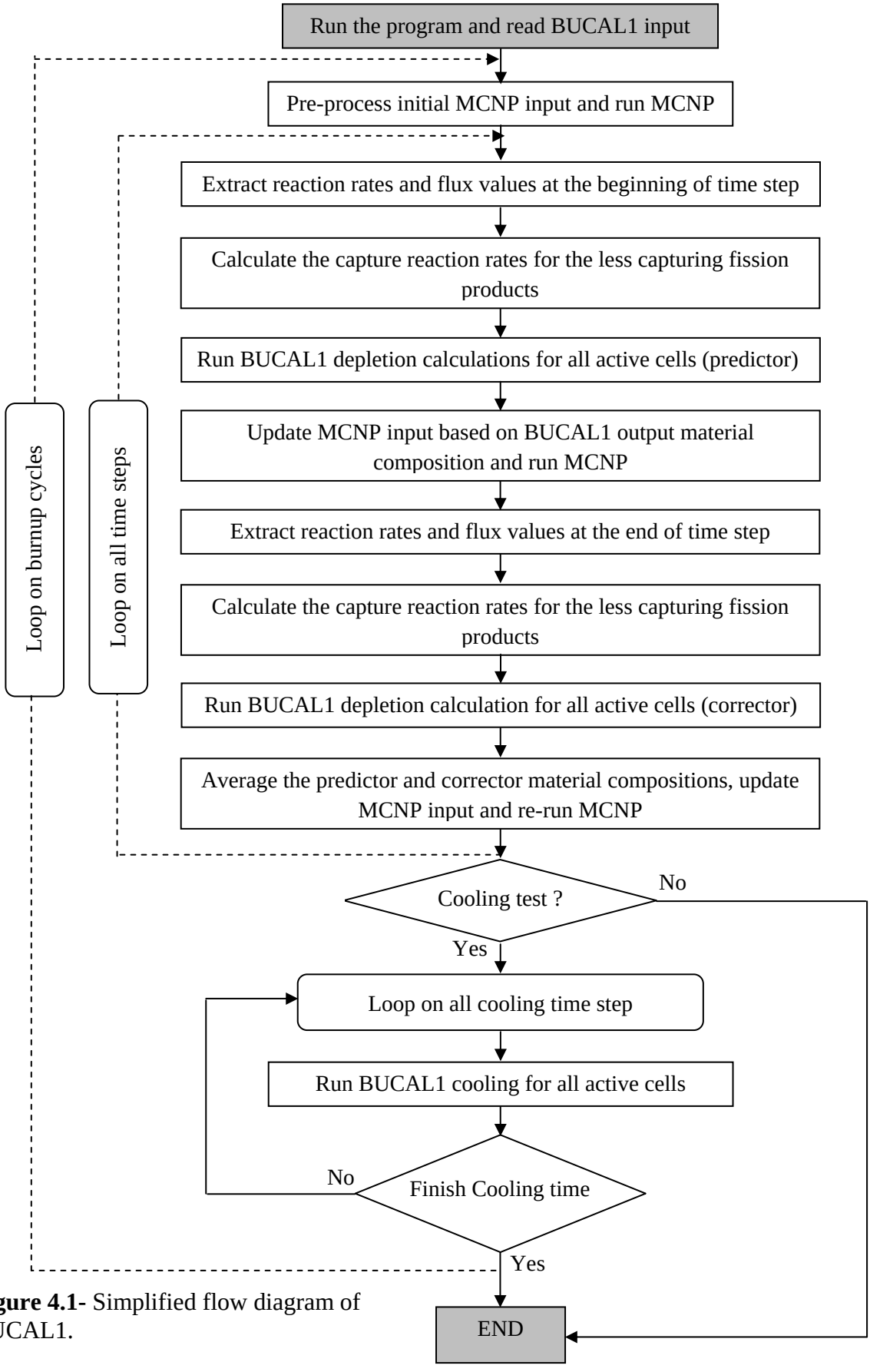

Figure 4.1- Simplified flow diagram of BUCAL1.

5. Validation of BUCAL1 computer code

This section is dedicated to the validation of our new developed burnup code BUCAL1. The validation process was done by code-to-code comparisons. Three kinds of benchmarks were treated in this study. These benchmarks differ each one from the others by nuclear fuel composition, operation conditions, geometry, etc. Results from several burnup codes from the NEA/OCED agency were used in this study (*Zh. Xu, 2003* and *K. D. Weaver et al., 2000*). Appendix E gives a general description of these NEA/OCED burnup codes. In MCNP calculations, we have used the ENDF/B-VII (*M. B. Chadwick et al., 2006*) and JEFF-3.1 (*The JEFF team, 2006*) neutron cross section evaluations. The processing of these evaluations into libraries suitable for use with the MCNP code was done using the modular NJOY99 system (*R. E. MacFarlane, 1999*) with its latest update patch up259 adopting the flow diagram described in chapter 3 of this thesis.

5. 1. Pin-cell benchmarks

5.1.1. Benchmarks description

In this study, two pin-cell benchmark exercises described by (*Zh. Xu, 2003*) and (*K. D. Weaver et al., 2000*) were studied to test for the BUCAL1 code accuracy. These benchmarks use UO2 and ThO2-UO2 as fuel material, respectively. Figure (4.2) shows the pin cell model representing the unit cell of a Westinghouse PWR fuel bundle. Both burnup calculations described in this study are based on this model. The results obtained are benchmarked against CASMO-4 (*Edenius et al., 1995*), MCODE (*Zh. Xu, 2003*) for the first benchmark case and MOCUP (*R.L.Moore et al., 1995*) for the second benchmark case.

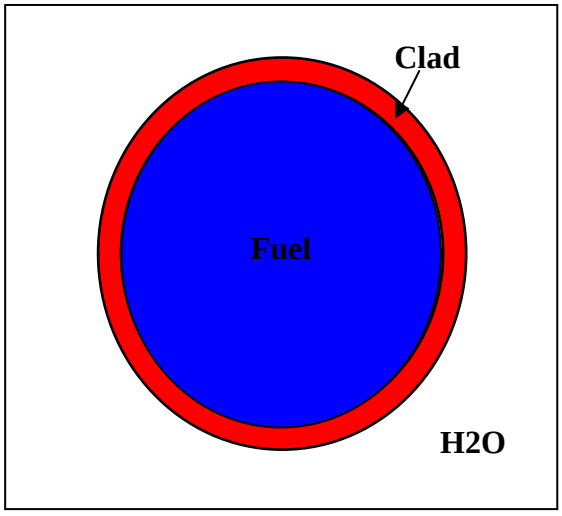

Figure 4.2- Pin-Cell Model.

The first case under study is a 2-D single pin-cell model of a standard Westinghouse 17*17 PWR assembly. Four different regions are considered: the fuel pellet (entire fuel region is taken as one lumped cell), the gap, the cladding and the associated coolant. The fuel is UO2 with very high U-235 enrichment (9.75w/o) which allows achieving high burnup. Boundaries of the cell are set to be reflecting, both in radial and axial directions in MCNP model in order to achieve k_{∞} calculations. The geometrical and operational parameters as well as the initial compositions are presented on Tables [4.4, 4.5].

Table 4.4- UO2 pin-cell model parameters.

Parameters	Values
Fuel pellet radius (cm)	0.4096
Cladding inner radius (cm)	0.4178
Cladding outer radius (cm)	0.4750
Pin pitch (cm)	1.26
Fuel density (g/cm^3)	10.3
Fuel temperature (K)	300
Cladding density (g/cm^3)	6.550
Cladding temperature (K)	300
Coolant density (g/cm^3)	0.997
Coolant temperature (K)	300
Power density (kW/liter core)	104.5
Specific power (W/gU)	34.6679

Table 4.5- Initial compositions (cold conditions at 300 K).

	Nuclide	Weight percent (w/o)	atom density (1/cm^3)
Fuel (9.75 w/o UO2)	U-234	0.0688	1.82239E+19
	U-235	8.5946	2.26826E+21
	U-238	79.4866	2.07128E+22
	O-16	11.8500	4.59686E+22
Cladding	Zircaloy-4	100	4.344182E+22
Coolant	H-1	11.19	6.66295E+22
	O-16	88.81	3.33339E+22

The second case under study involves the analysis of a PWR pin cell excised from a standard 17x17 pin assembly typical of large Westinghouse PWRs. The usual all-UO2 fuel pellets were replaced by a ThO2-UO2 mixture at 94% of theoretical density consisting of 75w/o Th, 25 w/o U on a heavy metal basis, with the later enriched to 19.5 w/o U-235, to give an overall enrichment of 4.869 w/o U-235 in total heavy metal. As in the first case, boundaries of the cell are set to be reflecting, both in radial and axial directions. The benchmark parameters are presented on Tables [4.6, 4.7].

Table 4.6- ThO2-UO2 pin-cell model parameters.

Parameters	Values
Fuel Temperature (K)	900
Power Density (KW/KgHM)	38.1347
Power Density (KW/liter cell)	107.284
Fuel Density (g/cm^3)	9.424
Cladding Temperature (K)	621.1
Cladding Density (g/cm^3)	6.505
Coolant Pressure (bars)	155.13
Coolant Temperature (K)	583.1
Coolant Density (g/cm^3)	0.705
Fuel Pellet Radius (cm)	0.41274
Cladding Inner Radius (cm)	0.41896
Cladding Outer Radius (cm)	0.47609
Pin Pitch (cm)	1.2626

Table 4.7- Initial compositions (at Hot Full Power conditions).

	Nuclide	Weight percent (w/o)	atom density ($1/cm^3$)
Fuel (ThO2- UO2)	Th-232	65.909	1.61215E+22
	U-234	0.034	8.24518E+18
	U-235	4.291	1.03615E+21
	U-238	17.740	4.22957E+21
	O-16	12.026	4.26835E+22
Cladding	Zircaloy-4	100	4.31438E+22
Coolant	H-1	11.19	4.71053E+22
	O-16	88.81	2.35662E+22

MCNP–BUCAL1 calculations are performed on an Intel core 2 Duo Personal Computer with CPU 2.2 GHz and a cache size of 2 MB, under 64-bits Linux system. Each MCNP run is done for 225.000 neutron histories (same neutron histories required as MCODE) that lead to an eigenvalue statistical error of about 130 pcm. The entire MCNP–BUCAL1 calculations take about 15 h for both UO2 and ThO2-UO2 benchmark cases.

5.1.2. UO2 benchmark results and analysis

Figure (4.3) shows the comparison of eigenvalue history obtained by BUCAL1 for UO2 benchmark using two neutron cross section libraries ENDF/B-VII and JEFF-3.1. Results are compared to those provided by CASMO-4 and MCODE codes (*Zh. Xu, 2003*). It can be seen from this figure that between 0 and 40MWd/kg, the benchmark eigenvalues obtained by BUCAL1 using the two cross section libraries are in a very good agreement with those obtained by CASMO and MCODE. From 0 to 90MWd/kg, the system BUCAL1 eigenvalues are closer to MCODE than to CASMO-4. At 100MWd/kg burnup, the eigenvalue difference for BUCAL1 using ENDF/B-VII is about 0.1% from CASMO-4 and -1.6% from MCODE. When using JEFF-3.1 library, the eigenvalue obtained by BUCAL1 differs by -0.1% and -1.7% from CASMO-4 and MCODE, respectively. Several causes may contribute to the eigenvalue difference remarked between the three codes, such as neutronic/burnup algorithms and their coupling, neutron data, statistical error propagation, etc.... The ENDF/B-VII library provides an eigenvalue slightly higher than that obtained when using JEFF-3.1 library.

In addition to the eigenvalue comparison, an isotope composition comparison at 100MWd/kg has been led. The results are presented on Table (4.8). From this table it appears that most of calculated material compositions agree well with CASMO-4 and MCODE. Taking into consideration the high burnup of the system, the obtained differences are acceptable. Table (4.8) also confirms that overall MCOD predicts more fissionable species in burned fuel which explains the high eigenvalues produced by this code. The differences between our code and CASMO-4 are significant for Am and Sm isotopes concentrations, which need further attention.

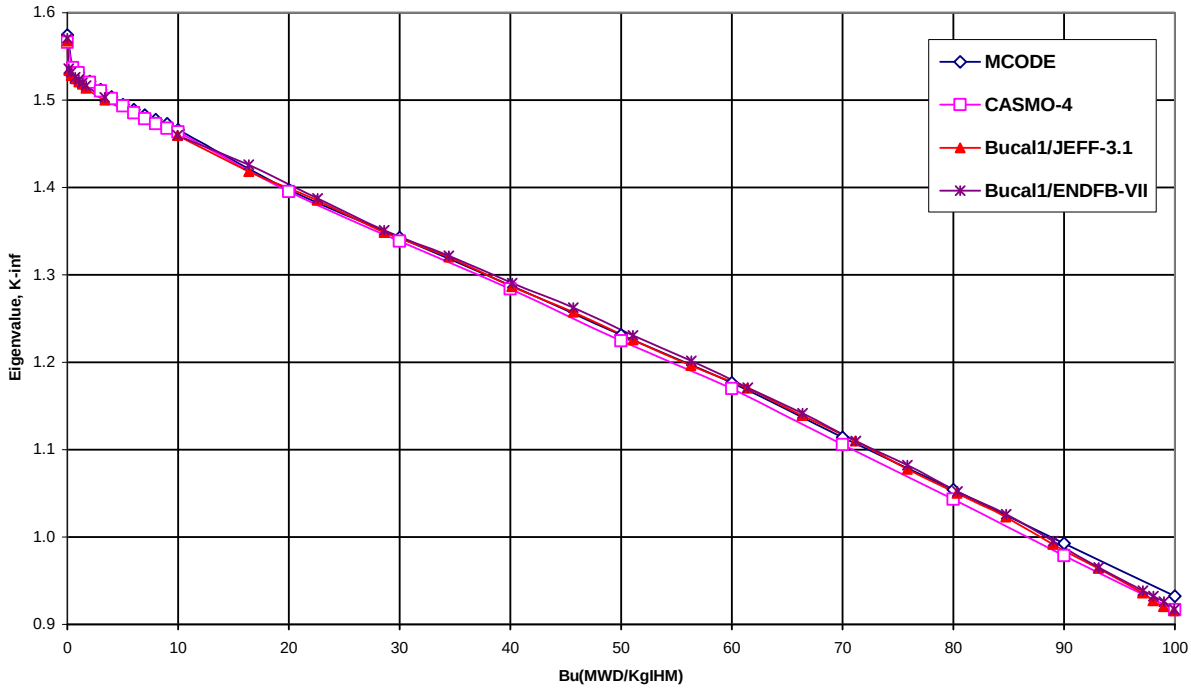

Figure 4.3- Eigenvalue comparison between BUCAL1, MCODE and CASMO-4 for UO2 benchmark.

Table 4.8- Relative difference from CASMO-4 [(a)] in nuclide concentration at 100MWd/kgIHM for UO2 benchmark.

Isotopes	CASMO-4 (at./cc)	MCODE	BUCAL1 ENDFB-VII	BUCAL1 JEFF-3.1
Mo-95	1.2228E+20	-0.002	0.019	0.019
Tc-99	1.1686E+20	0.045	0.006	0.019
Ru-101	1.1927E+20	-0.003	0.004	0.006
Rh-103	4.6015E+19	0.033	0.043	0.057
Ag-109	6.9910E+18	0.146	0.090	0.016
Cs-133	1.1452E+20	0.082	0.068	0.064
Cs-135	6.9820E+19	0.004	0.134	0.119
Nd-143	7.4246E+19	0.003	-0.030	-0.046
Nd-145	7.1091E+19	-0.001	-0.024	-0.005
Sm-147	9.5715E+18	0.141	0.418	0.399
Sm-149	1.2455E+17	-0.058	-0.230	-0.253
Sm-150	2.6757E+19	0.081	-0.006	0.011
Sm-151	7.6817E+17	-0.103	-0.257	-0.238
Sm-152	9.3945E+18	-0.162	-0.175	-0.156
Eu-153	1.1838E+19	-0.114	-0.113	-0.103
U-234	6.7125E+18	0.012	0.075	0.069
U-235	2.5952E+20	0.021	-0.086	-0.082
U-238	1.9672E+22	-0.002	-0.001	-0.001
Np-237	3.4234E+19	-0.089	-0.025	0.016
Pu-238	1.9665E+19	-0.083	-0.006	0.041
Pu-239	1.4767E+20	0.056	-0.005	-0.005
Pu-240	6.3106E+19	0.088	0.055	0.072
Pu-241	4.2801E+19	0.051	-0.033	-0.036
Pu-242	2.6228E+19	-0.031	0.020	0.047
Am-241	2.3505E+18	0.100	0.592	0.427
Am-242m	3.3827E+16	1.030	0.480	0.496
Am-243	6.2320E+18	0.232	0.282	0.210
Total actinides	2.0280E+22	-0.001	-0.002	-0.001
Total fissile	4.9281E+20	0.030	-0.045	-0.042
Total fertile	1.9788E+22	-0.002	-0.001	-0.0003

[a] Relative diff. = (N –NCasmo-4)/NCasmo-4, where N is nuclide concentration (at./cc).

5.1.3. ThO2-UO2 benchmark results and analysis

Figure (4.4) shows the comparison of eigenvalue history provided by CASMO-4, MOCUP and BUCAL1 using ENDF/B-VII and JEFF-3.1 nuclear data libraries. It can be seen that BUCAL1 results obtained for the two neutron libraries are in good agreement with those

obtained by CASMO-4 and MOCUP. Considering that the point of major concern is the burnup value where reactivity reaches 0.03, (which is representative of an n-batch core-average end of cycle value, with allowance of 3% reactivity loss for leakage) (*K. D. Weaver et al., 2000*), this eigenvalue comparison shows almost no difference at that point between BUCAL1/JEFF-3.1, CASMO-4 and MOCUP. Whereas, BUCAL1/ENDFB-VII overestimates the last three sets of results by approximately 0.8%. Generally, this is encouraging because one must achieve better accuracy for thorium fuelled cores than for all-uranium fuelling to achieve equal accuracy in cycle length estimates (*K. D. Weaver et al., 2000*). Up to 40MWd/kgIHM, BUCAL1 results using the two libraries under study are much closer to MOCUP than to CASMO-4. At 60MWd/kgIHM (corresponding to projected end-of-life core-average burnup), BUCAL1/ENDFB-VII produces an eigenvalue difference of about +2% from CASMO-4 and +0.5% from MOCUP. BUCAL1/JEFF-3.1 eigenvalue differs at this burnup value by about +1.2% and -0.05% from CASMO-4 and MOCUP respectively.

The concentrations of the 17 actinides whose information is provided in the benchmark exercise at 60.749MWd/kg (which is the upper limit of discharge burnup if a 3-batch core refuelling scheme is considered) are provided on Table (4.9).

We remark that, the inventory prediction obtained by BUCAL1 for thorium and uranium actinide chains agrees well with CASMO-4 and MOCUP. Only few isotopes concentration differences exceed the 10%, especially Pa-233, U-234, Np-238, and Np-239. Total end-of-life heavy metal destruction is about 2% higher in BUCAL1 using the two libraries ENDF/B-VII and JEFF-3.1. Another point of interest is the large difference in U-234 concentration, which merits further attention, even though this nuclide has a small effect on eigenvalue variations.

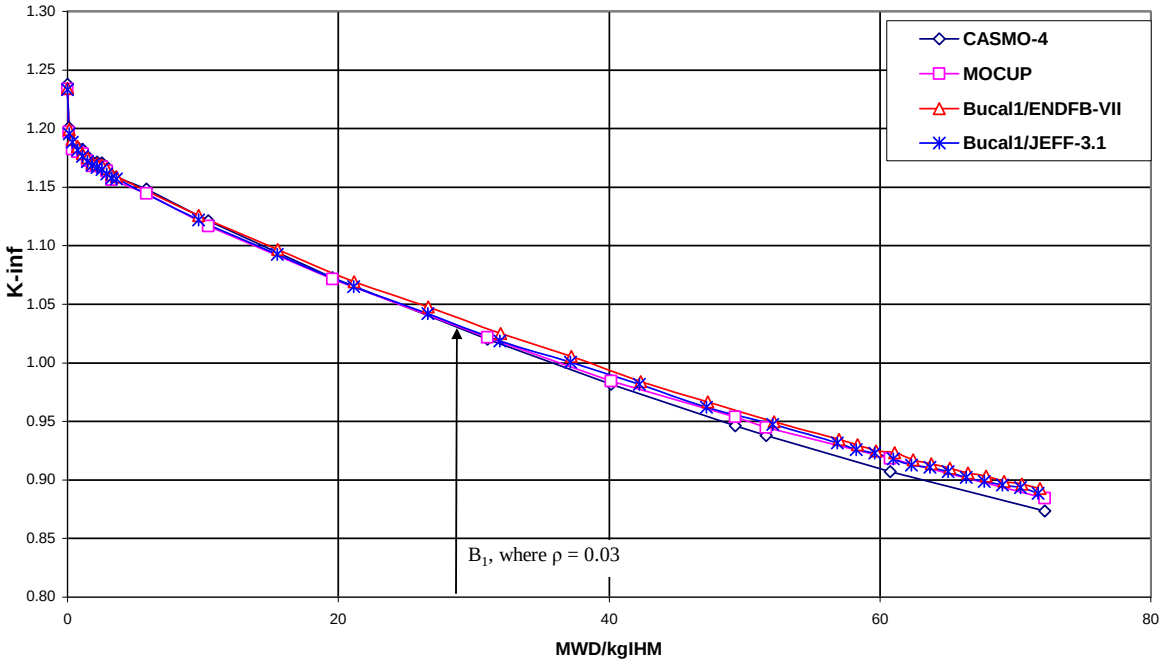

Figure 4.4- Eigenvalue comparison as a function of burnup for ThO2-UO2 benchmark.

Table 4.9- Relative differences from CASMO-4 in isotope concentration at 60.749MWd/kg for ThO2-UO2 benchmark.

Isotopes	CASMO-4 (at./cc)	MOCUP	BUCAL1 ENDFB-VII	BUCAL1 JEFF-3.1
Th-232	1.53769E+22	-0.003	-0.003	-0.003
Pa-231	1.70440E+18	0.048	-0.004	0.107
Pa-233	1.95229E+19	0.035	-0.238	-0.236
U-232	1.56006E+18	0.034	0.057	0.063
U-233	2.74202E+20	0.040	0.061	0.067
U-234	5.15172E+19	0.176	-0.172	-0.188
U-235	1.78104E+20	-0.021	-0.034	-0.031
U-236	1.39420E+20	0.054	0.045	0.035
U-238	3.88419E+21	0.004	0.004	0.005
Np-237	1.82660E+19	-0.058	-0.044	-0.014
Np-238	5.46096E+16	-0.037	-0.338	-0.317
Np-239	7.61806E+17	-0.043	-0.312	-0.316
Pu-238	8.90932E+18	-0.026	-0.059	-0.017
Pu-239	5.37090E+19	-0.071	-0.050	-0.056
Pu-240	1.82233E+19	-0.032	-0.031	-0.030
Pu-241	1.90707E+19	-0.024	-0.052	-0.055
Pu-242	9.96772E+18	-0.036	-0.045	-0.014
Total fissile	7.54683E+20	0.024	-0.002	-0.002
Total Actinide	0.062601217	+0.010	+0.022	+0.020

Depleted[(b)]				
Ratio of Th232 to U238 depletion[(c)]	2.15589	+0.107	+0.109	+0.120

[b] Total Actinide Depleted = $(N_{Actinide,t} - N_{Actinide,0}) / N_{Actinide,0}$, where $N_{Actinide,t}$ is the total amount of actinides at time t; $N_{Actinide,0}$ is the total amount of actinides at time 0.

[c] Ratio = (Th-232 depleted) / (U-238 depleted).

5.2. MOX-lattice benchmark

MCNP-BUCAL1 calculations were performed with 50 cycles of iterations on a nominal source size of 15000 particles per cycle in order to decrease statistical error estimates. Initial 10 cycles were skipped to insure homogeneous neutrons source distribution. The estimated statistical errors (1 s) were reduced below 80 pcm for k_∞ values.

5.2.1. Benchmark specification

The benchmark exercise used for this study is a MOX lattice core, with reflective boundary conditions (*G J O'Connor, 2003*). The benchmark geometry adopted, is a square 17*17 PWR fuel pin assembly with three enrichment zones as shown in Figure (4.5). The initial fresh MOX fuel enrichments for these zones are given in Tables (4.10) to (4.13).

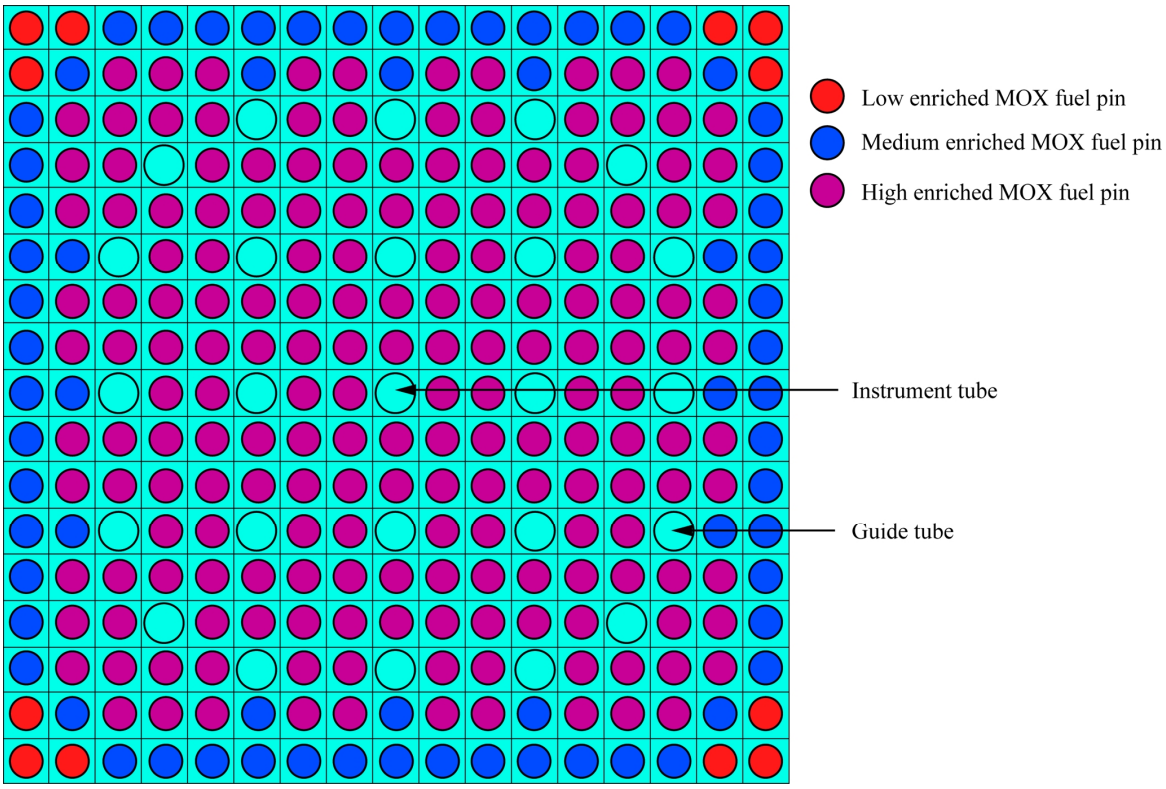

Figure 4.5- The MOX core geometry.

Table 4.10- Plutonium isotopic composition of fresh MOX fuel.

Nuclide	w/o in Pu_{total}
^{238}Pu	2.5
^{239}Pu	54.7
^{240}Pu	26.1
^{241}Pu	9.5
^{242}Pu	7.2

Table 4.11- Uranium isotopic composition of fresh MOX fuel.

Nuclide	w/o in U_{total}
^{234}U	0.00119
^{235}U	0.25000
^{238}U	99.74881

Table 4.12- Initial MOX fuel enrichments.

MOX fuel enrichment zones	MOX fuel plutonium w/o Pu_{total}/[U+Pu]	MOX fuel enrichment, w/o $Pu_{fissile}$/[U+Pu]
High	8.866	5.692
Medium	6.206	3.984
Low	4.894	3.142
Average	8.000	5.136

Table 4.13- Initial MOX fuel composition.

Nuclide	Atoms/barn.cm for given fuel pin (at 900 K)		
	High	Medium	Low
^{234}U	2.5718E-7	2.6436E-7	2.6789E-7
^{235}U	5.3598E-5	5.5300E-5	5.6040E-5
^{238}U	2.1194E-2	2.1786E-2	2.2077E-2
^{238}Pu	5.1677E-5	3.6128E-5	2.8473E-5
^{239}Pu	1.1259E-3	7.8717E-4	6.2038E-4
^{240}Pu	5.3500E-4	3.7403E-4	2.9478E-4
^{241}Pu	1.9392E-4	1.3557E-4	1.0685E-4
^{242}Pu	1.4636E-4	1.0233E-4	8.0644E-5
O	4.6602E-2	4.6553E-2	4.6529E-2

The 24 guide tubes and one instrument tube were modelled as water-filled zircaloy tubes with the following dimensions.

Outer radius = 0.613 cm.

Inner radius = 0.571 cm.

Wall thickness = 0.042 cm.

The non-fissile materials are as follow:

Cladding = zircaloy-2.

Guide tubes/instrument = zircaloy-2.

Coolant/moderator = light water, 600ppm boron.

For the purpose of the benchmark exercise, these materials were modelled as specified in Table (4.14).

Table 4.14- Non-fissile material compositions.

Nuclide	**Atoms/barn.cm**
Zircaloy-2 (5.8736g/cm^3) (at 620 K)	
Zr	3.8657E-2
Fe	1.3345E-4
Cr	6.8254E-5
Coolant/moderator (600 ppm boron, 0.7245g/cm^3) (at 575 K)	
H	4.8414E-2
O	2.4213E-2
^{10}B	4.7896E-6
^{11}B	1.9424E-5

5.2.2. Results and Discussion

One of the main features of BUCAL1 is its ability to do pin-by-pin burnup calculations even for core lattices with high number of fuel elements. To perform an accurate MCNP estimation of eigenvalues, new libraries based on ENDF/B-VII are processed at temperatures 900 K (fuel), 620 K (cladding) and 575 K (borated water).

Figures (4.6), represents the power map of the MOX fresh fuel assembly used in this study and calculated by means of tally F7 of MCNP. From this figure, one can remark that the power fractions corresponding to each of the three enriched zones vary slightly versus pin

locations. Based on this figure, and because of the computer time constraint, burnup calculations with BUCAL1 were done using just three different pin cells that correspond to the three different enriched zones. The pin cells chosen have the following [x, y] indexes in the power map (*Fig. 4.6*): [1, 2], [0, 8] and [8, 7]; these elements were chosen calculating the average power fraction values corresponding to each of the three enriched zones. The average atom density for each isotope was calculated using *Eq. (4.10)*:

$$\overline{N}_i = \sum_{j=1}^{3} vf_j N_{ij} \tag{4.10}$$

where, vf_j is the volume fraction of the enriched zone j, and N_{ij} is the nuclide density of isotope i corresponding to the enriched zone j.

0.77	0.76	0.84	0.83	0.83	0.86	0.84	0.85	0.86	0.84	0.85	0.85	0.84	0.83	0.83	0.75	0.77
0.75	0.85	1.01	1.00	1.06	0.93	1.07	1.06	0.91	1.05	1.07	0.94	1.06	1.01	1.01	0.84	0.76
0.83	1.00	1.01	1.10	1.15	0.00	1.10	1.10	0.00	1.11	1.12	0.00	1.15	1.11	1.03	1.01	0.84
0.83	1.00	1.10	0.00	1.15	1.13	1.04	1.04	1.09	1.04	1.05	1.12	1.17	0.00	1.09	0.99	0.84
0.83	1.06	1.15	1.15	1.11	1.11	1.03	1.04	1.09	1.02	1.02	1.11	1.09	1.15	1.14	1.06	0.83
0.84	0.91	0.00	1.12	1.12	0.00	1.08	1.08	0.00	1.08	1.10	0.00	1.11	1.12	0.00	0.91	0.84
0.86	1.07	1.11	1.03	1.05	1.10	1.02	1.03	1.10	1.02	1.02	1.09	1.03	1.03	1.11	1.06	0.85
0.84	1.06	1.10	1.03	1.02	1.09	1.03	1.02	1.09	1.03	1.03	1.10	1.02	1.03	1.10	1.07	0.85
0.86	0.92	0.00	1.11	1.10	0.00	1.09	1.09	0.00	1.09	1.09	0.00	1.09	1.10	0.00	0.92	0.85
0.85	1.04	1.09	1.04	1.03	1.10	1.02	1.03	1.10	1.02	1.01	1.09	1.03	1.03	1.11	1.05	0.84
0.84	1.05	1.10	1.05	1.02	1.09	1.03	1.03	1.10	1.02	1.03	1.10	1.04	1.04	1.10	1.05	0.84
0.86	0.91	0.00	1.12	1.09	0.00	1.10	1.07	0.00	1.10	1.07	0.00	1.10	1.10	0.00	0.92	0.86
0.83	1.04	1.15	1.16	1.09	1.09	1.04	1.03	1.08	1.02	1.03	1.11	1.09	1.14	1.14	1.05	0.83
0.83	1.00	1.09	0.00	1.15	1.11	1.03	1.02	1.08	1.02	1.03	1.11	1.15	0.00	1.09	1.00	0.83
0.83	1.00	1.02	1.09	1.14	0.00	1.09	1.10	0.00	1.11	1.10	0.00	1.14	1.10	1.02	1.00	0.84
0.76	0.84	1.00	0.99	1.03	0.92	1.07	1.06	0.92	1.07	1.06	0.91	1.06	0.99	1.00	0.84	0.75
0.79	0.75	0.83	0.83	0.83	0.84	0.85	0.85	0.86	0.84	0.85	0.86	0.83	0.83	0.83	0.76	0.78

Figure 4.6- Power map of the MOX fuel assembly.

In order to obtain an efficient comparison of results, the calculations were performed to obtain a constant target burnup for the MOX fuel assembly of 48GWd/teHM. The MOX fuel assembly is irradiated over three operating cycles, as shown below.

- Cycle 1 = 420 days full power, end of cycle (EOC) burnup of MOX =16GWd/teHM.
- First downtime = 30 days.
- Cycle 2 = 420 days full power, EOC burnup of MOX =32GWd/teHM.
- Second downtime = 30 days.
- Cycle 3 = 420 days full power, EOC burnup of MOX =48GWd/teHM.
- Cooling = 0 years, 5 years.

Results from several codes such as: CASLIB, APPOLO/PEPIN2, KENOREST-2001, BOXER/ETOBOX, WIMS8A, MVP-BURN, MONK8A and SAS2D where gathered with those obtained by our BUCAL1 code to perform an objective code-to-code validation study. Description, characteristics of these codes and also the atom densities obtained by all the codes can be found in appendix E. Atom density predictions of some fission products and actinides are not allowed by some codes such as CASLIB, MVP-BURN, and SAS2D. The atom densities of important fission products and actinides used in our code validation are not provided by SAS2D code for cooling time of 5 years.

a) Infinite multiplication factor and reactivity change due to burnup and cooling

Based on the calculation results obtained by different codes, the average (mean) values of infinite multiplication factor (k_{∞}) the average value and the deviations to mean value are summarized in Table (4.15) as a function of burnup and cooling time. The corresponding reactivities are presented in Table (4.16), respectively.

Table 4.15- k_∞ changes due to burnup and cooling.

	k_∞				Relative deviation of k_∞ to the mean value (%)			
Codes	**EOC1**	**EOC2**	**EOC3**	**5y cool.**	**EOC 1**	**EOC 2**	**EOC 3**	**5y cool.**
CASLIB	1.059780	1.007530	0.961000	0.918570	0.16	0.43	0.63	0.66
APPOLO/PEPIN2	1.056240	0.999680	0.948690	0.907150	-0.18	-0.35	-0.66	-0.59
KENOREST-2001	1.059100	0.999090	0.947520	0.903250	0.09	-0.41	-0.79	-1.02
BOXER/ETOBOX	1.060880	1.006180	0.958370	0.918260	0.26	0.30	0.35	0.63
WIMS8A	1.049756	0.996539	0.949737	0.904088	-0.79	-0.67	-0.55	-0.93
MVP-BURN	1.055410	0.997490	0.952920	0.916760	-0.25	-0.57	-0.22	0.46
MONK8A	1.059000	1.004600	0.951000	0.910800	0.08	0.14	-0.42	-0.19
SAS2D	1.062700	1.011700	0.966100	NA	0.43	0.85	1.16	NA
BUCAL1	1.060060	1.006160	0.959890	0.921430	0.18	0.29	0.51	0.97
Average	1.05810	1.00322	0.95503	0.91254				
Stand. dev.	0.00384	0.00521	0.00650	0.00713				
Relative Stand.dev. (%)	0.36	0.52	0.68	0.78				
Ave + SD	1.06194	1.00843	0.96153	0.91967				
Ave - SD	1.05427	0.99801	0.94852	0.90541				
Minimum	1.049756	0.996539	0.947520	0.903250				
Maximum	1.062700	1.011700	0.966100	0.921430				

Table 4.16- Reactivity changes due to burnup and cooling.

	Reactivity change (%)				Relative deviation of reactivity to the mean value (%)			
Codes	**EOC1 to EOC2**	**EOC2 to EOC3**	**5y cool.**	**Total**	**EOC1 to EOC2**	**EOC2 to EOC3**	**5y cool.**	**Total**
CASLIB	-4.9	-4.8	-4.8	-14.5	-5.4	-4.5	1.7	-3.5
APPOLO/PEPIN2	-5.4	-5.4	-4.8	-15.6	3.6	6.8	2.1	3.5
KENOREST-2001	-5.7	-5.4	-5.2	-16.3	9.7	8.3	9.4	8.4
BOXER/ETOBOX	-5.1	-5.0	-4.6	-14.6	-0.9	-1.5	-3.6	-2.6
WIMS8A	-5.1	-4.9	-5.3	-15.3	-1.6	-1.7	12.5	2.1
MVP-BURN	-5.5	-4.7	-4.1	-14.3	6.4	-6.8	-12.4	-4.7
MONK8A	-5.1	-5.6	-4.6	-15.4	-1.1	11.5	-1.8	2.2
SAS2D	-4.7	-4.7	NA	NA	-8.3	-7.3	NA	NA
BUCAL1	-5.1	-4.8	-4.3	-14.2	-2.3	-4.8	-8.0	-5.6
Average	-5.2	-5.0	-4.7	-15.0				
Stand.dev.	0.3	0.4	0.4	0.7				
Relative Stand.dev.(%)	-5.8	-8.0	-8.5	-4.7				
Ave + SD	-4.9	-4.6	-4.3	-14.3				
Ave - SD	-5.5	-5.4	-5.1	-15.7				
Minimum	-5.7	-5.6	-5.3	-16.3				
Maximum	-4.7	-4.7	-4.1	-14.2				

Table (4.15) shows that, at the end of cycle 3, the minimum and maximum k_∞ values obtained are 0.94752 (KENOREST-2001) and 0.96610 (SAS2D), respectively and their corresponding relative deviation to the mean value are -0.79% and 1.16%. Therefore, the spread between the minimum and maximum values of k_∞ at the end of cycle 3 is around 2%. The standard deviation increases as a function of burnup by 0.16% while passing from EOC1 to EOC2 and from EOC2 to EOC3 and by 0.1% after five years cooling (decay).

The k_∞ values at the end of three cycles and after five years cooling obtained using our new elaborated code BUCAL1 are generally in good agreement with the mean values and the results of the remaining codes. After five years cooling, BUCAL1 produces the largest k_∞ value 0.921430 regarding to other, with a relative deviation to mean value of about +1%.

Besides the k_∞ values, there is a strong incentive to investigate the differences on the reactivity changes due to burnup and cooling. It is expected that the effect of different parameters (effective cross sections, half-lives, branching ratios and burnup chains) used in the burnup and cooling calculations would be reflected by these reactivity changes.

Based on Table (4.16), the reactivity swings due to burnup during cycle 3 show minimum and maximum values of -5.6% (MONK8A) and -4.7% (MVP-BURN and SAS2D) respectively. Their relative deviations to the mean value are -7.3% and 11.5% respectively. The reactivity changes due to the five years cooling show minimum and maximum values of -5.3% (WIMS8A) and -4.1% (MVP-BURN) respectively. The corresponding relative deviations to the mean value are -12.4% and 12.5% respectively. The reactivity changes due to burnup and five years cooling obtained using BUCAL1 are -5.1%, -4.8% and -4.3% respectively; that give the higher total reactivity value of -14.2%, which overestimates the mean value by 53%.

b) Total irradiation history

The captures by fission products modify the total macroscopique absorption reaction rate R_{af} of fuel. In order to study the effect of fission products on k_∞ values, we define the poisoning factor (EP) as their contribution to the total macroscopique absorption reaction rate R_{af} .

$$EP = \frac{R_{PF}}{Raf} \tag{4.13}$$

where, R_{PF} designs the total macroscopique absorption reaction rate of fission products.

Figure (4.7), shows the total irradiation history obtained using BUCAL1 (left axis), and the evolution of the EP (%) factor (right axis) for the 17*17 PWR MOX fuel assembly used in this study. At the end of each cycle the eigenvalues obtained by the other codes are shown and compared to our values.

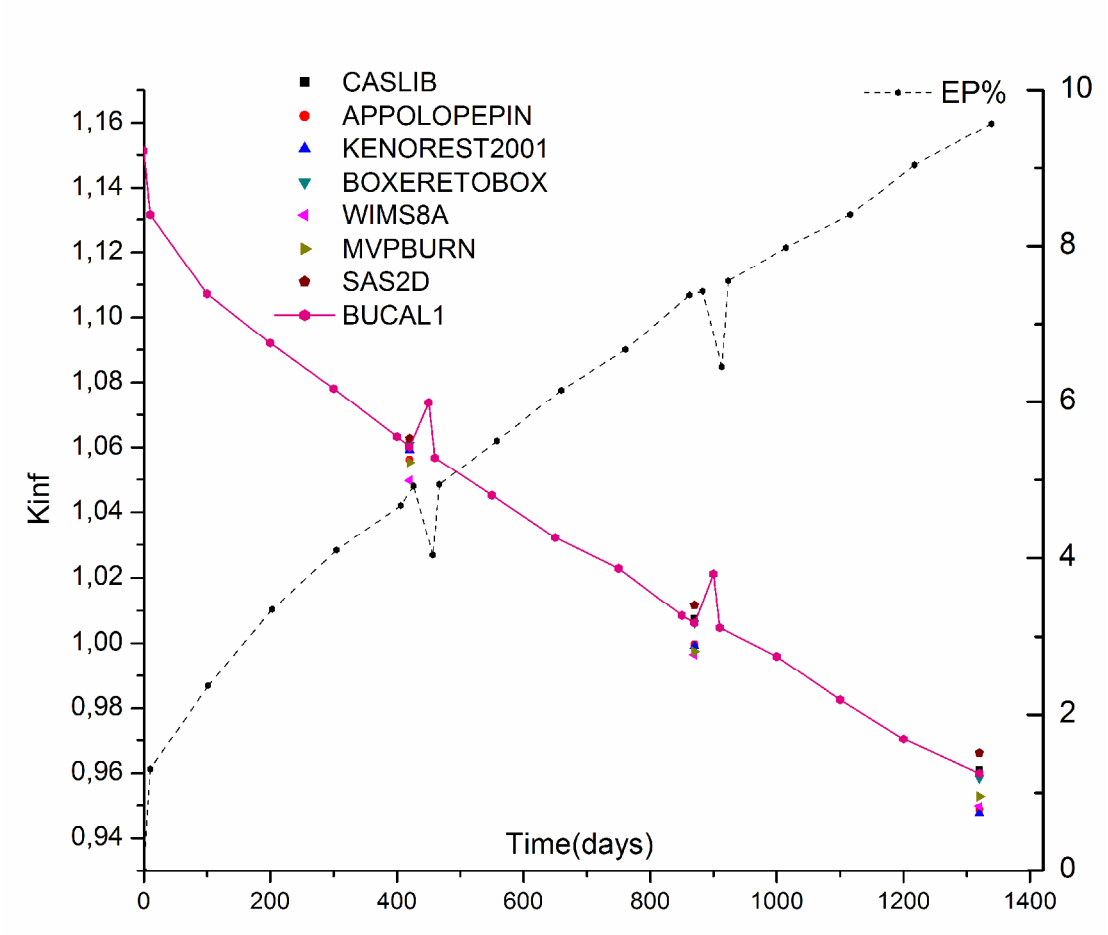

Figure 4.7- Burnup history for the 17*17 PWR MOX fuel assembly obtained using BUCAL1 burnup code.

The loss in reactivity due to the ^{135}Xe and ^{149}Sm equilibrium is about -1711 pcm. This loss is accompanied by an increase of 1.3% in the EP factor value where the ^{135}Xe and ^{149}Sm fission products participate in this increase by 81% and 8%, respectively. The remaining fraction of the increase observed in the EP factor is due to other fission products. The total loss in reactivity during the first cycle is -8594 pcm, which is due to an augmentation of about 5% in the EP factor value. The first downtime produces an excess of reactivity of 1292 pcm and a decrease in the EP factor of 0.88%. At the end of the second cycle the total loss of reactivity produced is -6295 pcm and the corresponding EP factor is increased to 7.42%. The second downtime leads to an excess of reactivity equal to 1491 pcm and a decrease of 0.97% in the EP factor value. At the end of the last cycle, the obtained loss in reactivity is approximately -6000 pcm, however the absorption effect due to fission products increases to 9.57%.

c) Actinide and fission products nuclide densities

The relative deviations of actinides and fission products nuclide densities to the mean value obtained by different codes at the end of cycle 1, cycle 2, cycle 3 and after five years cooling are compared on Figures (4.8) to (4.23).

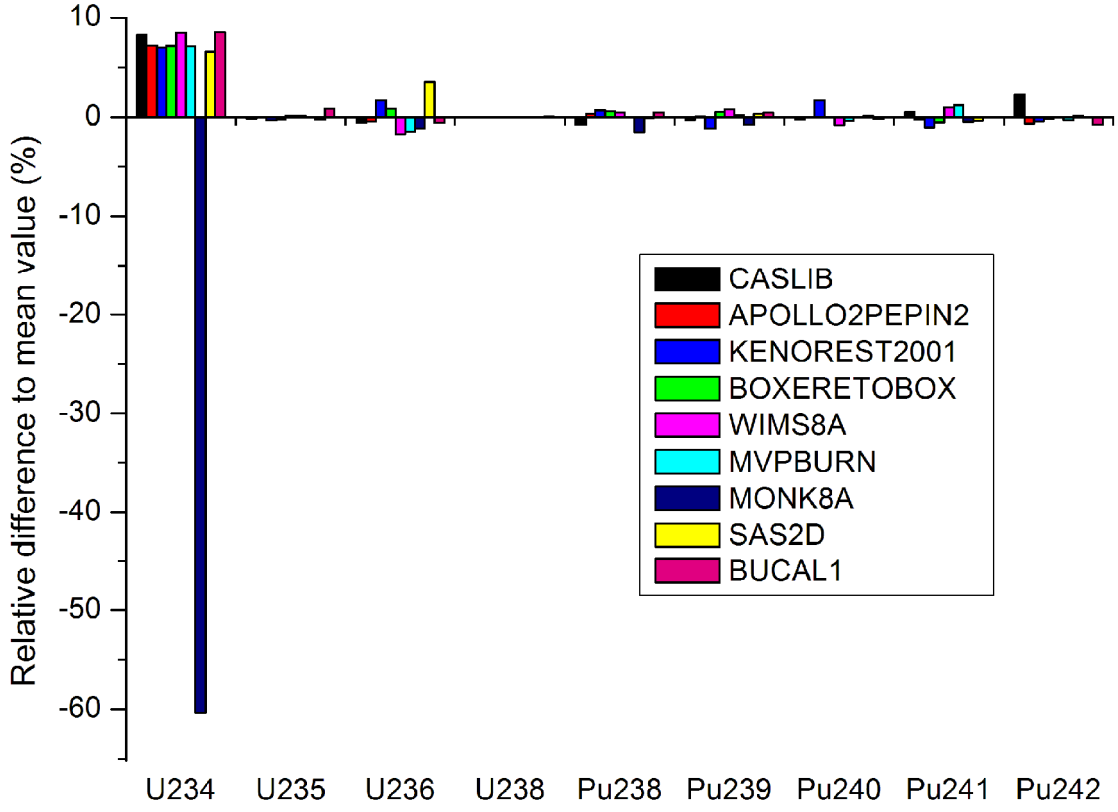

Figure 4.8- Relative difference of major actinide nuclide densities at EOC1.

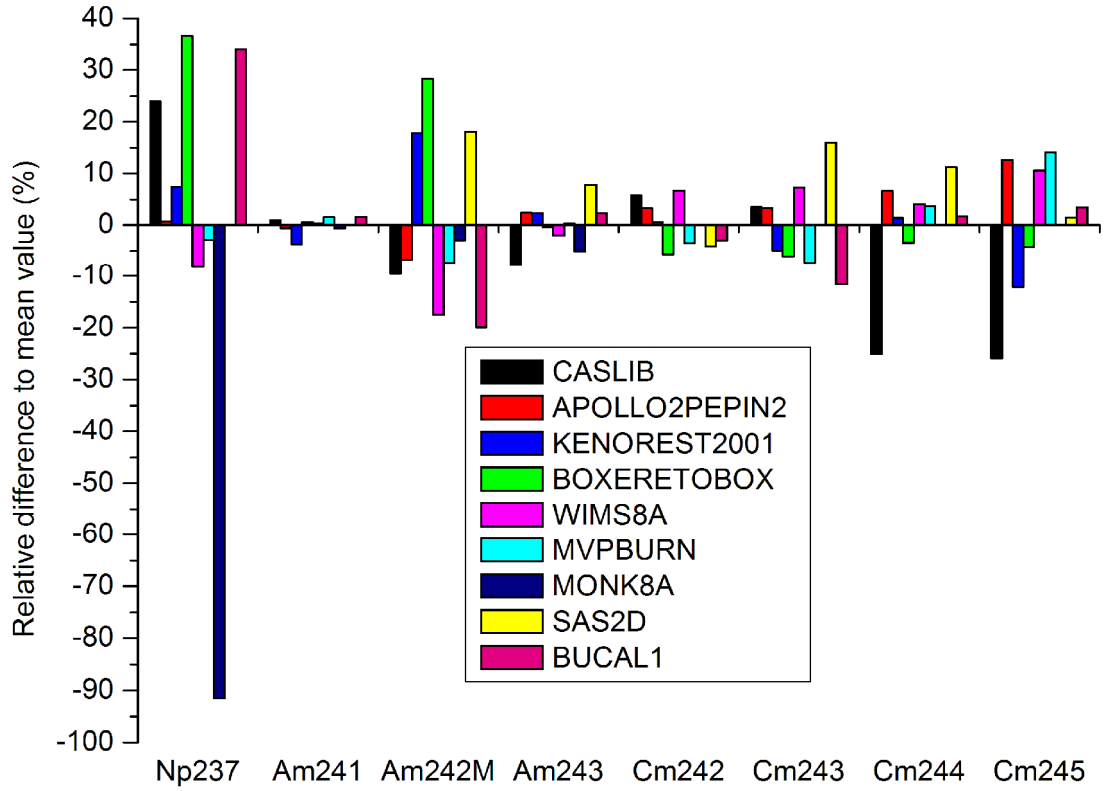

Figure 4.9- Relative difference of minor actinide nuclide densities at EOC1.

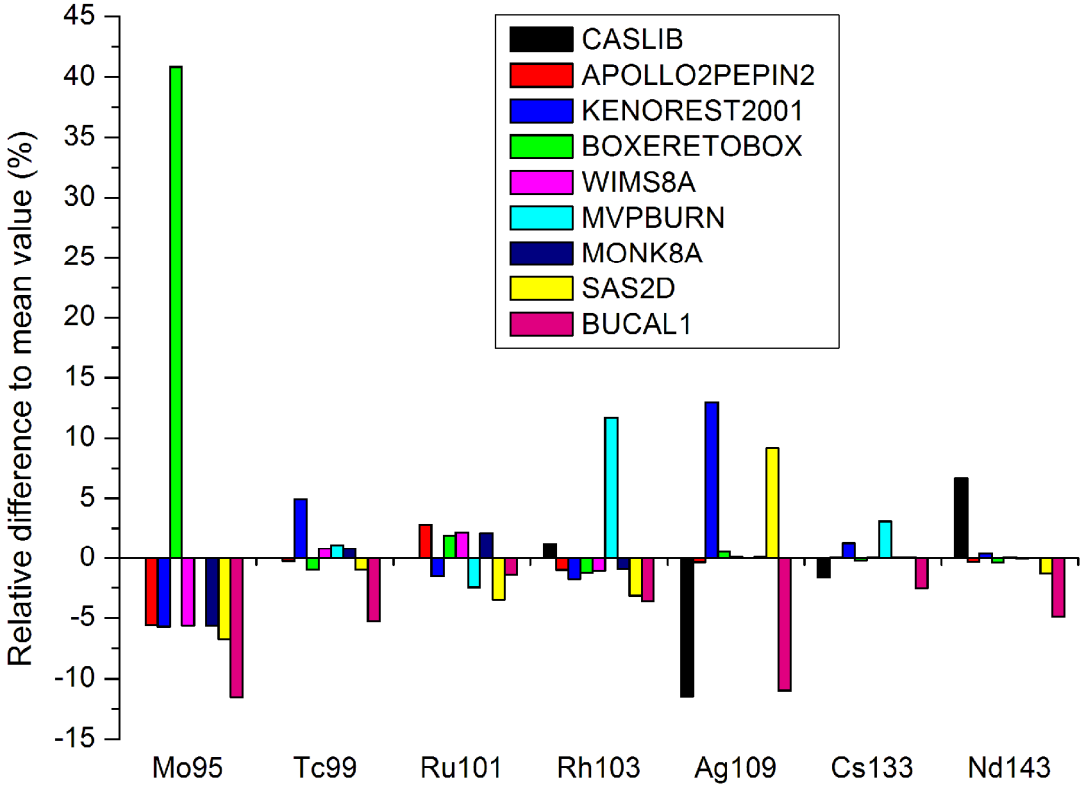

Figure 4.10- Relative difference of fission product nuclide densities at EOC1.

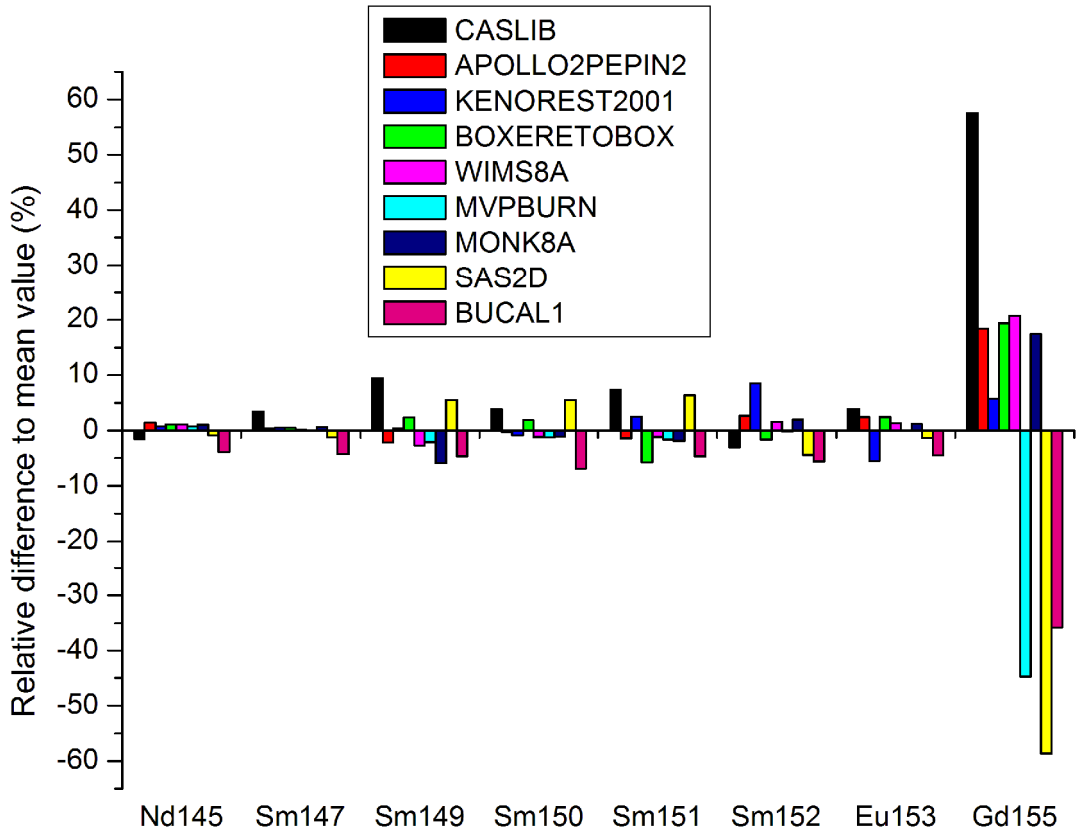

Figure 4.11- Relative difference of fission product nuclide densities at EOC1 (*cont.*).

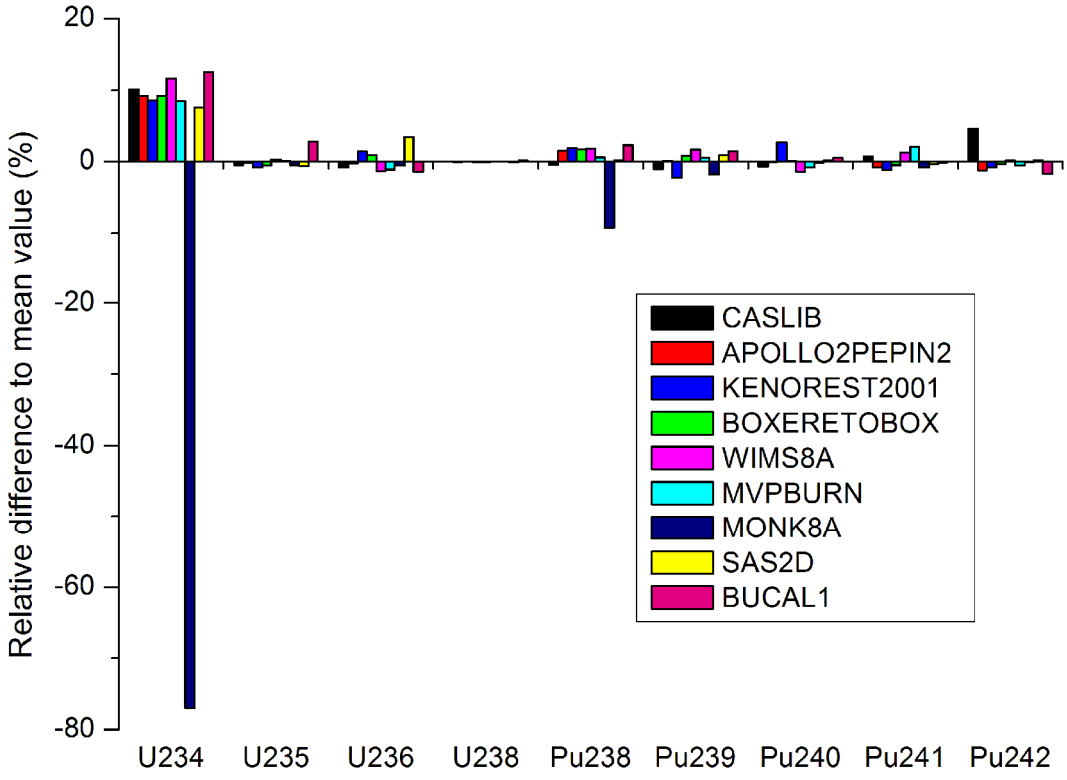

Figure 4.12- Relative difference of major actinide nuclide densities at EOC2.

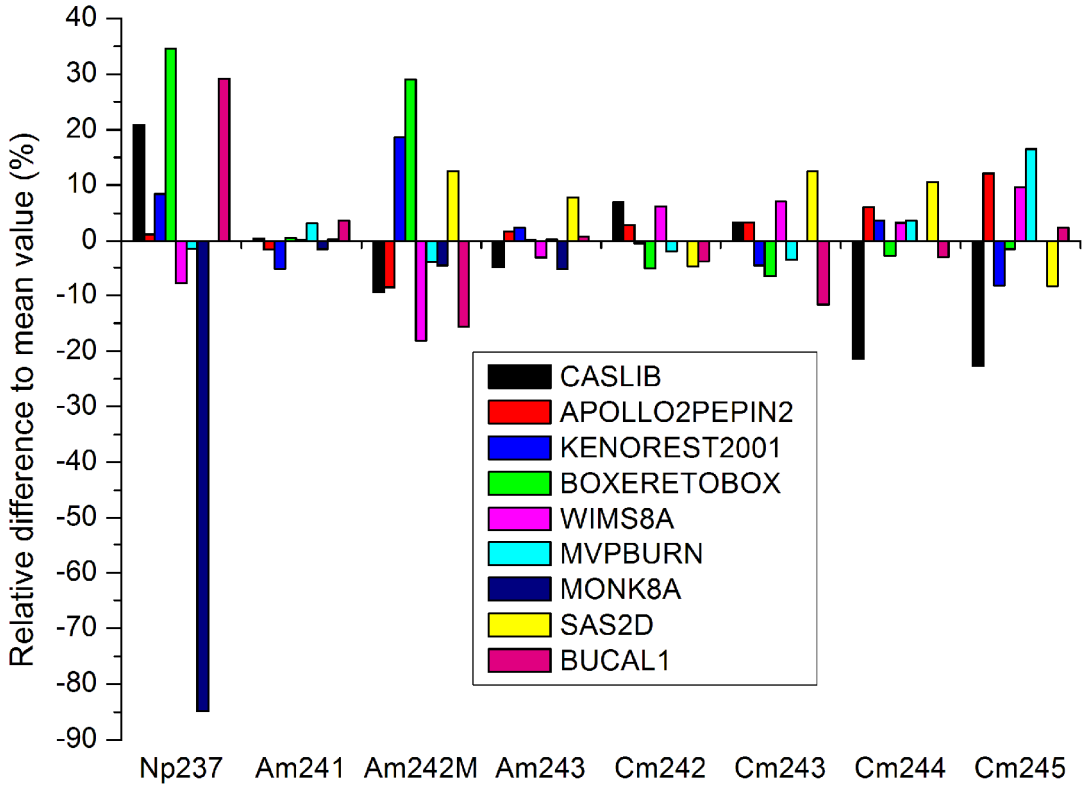

Figure 4.13- Relative difference of minor actinide nuclide densities at EOC2.

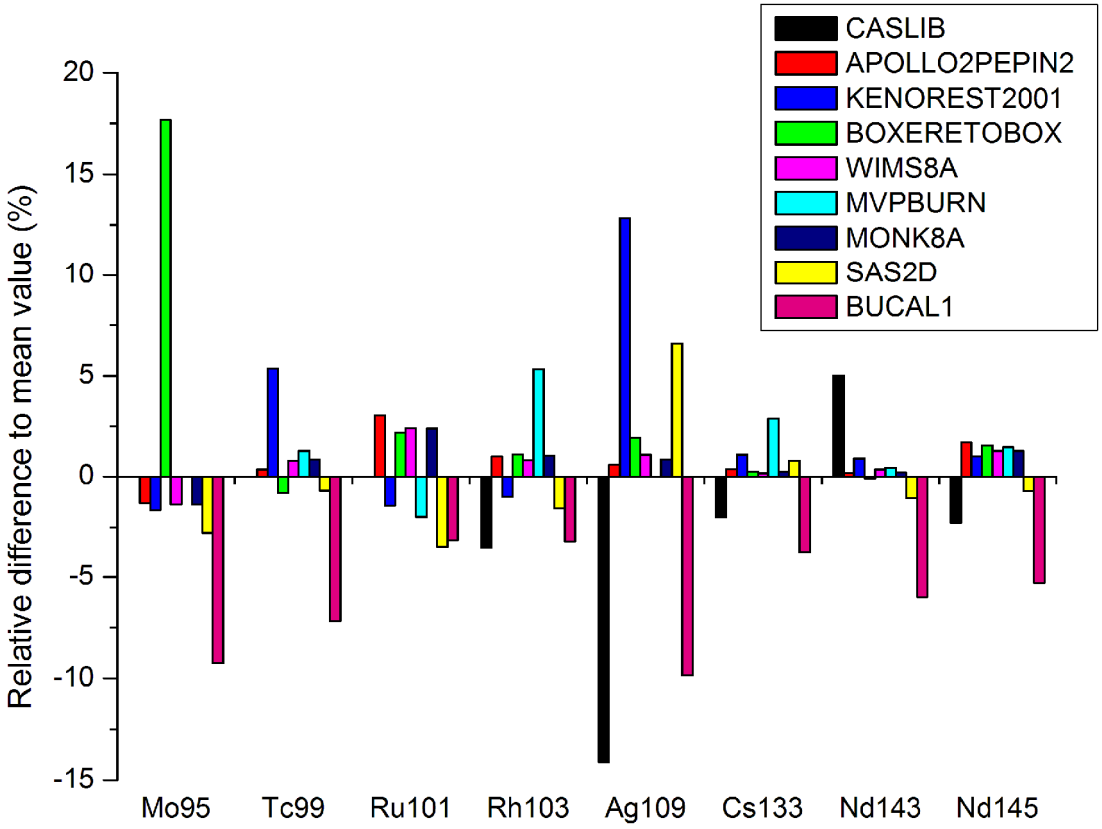

Figure 4.14- Relative difference of fission product nuclide densities at EOC2.

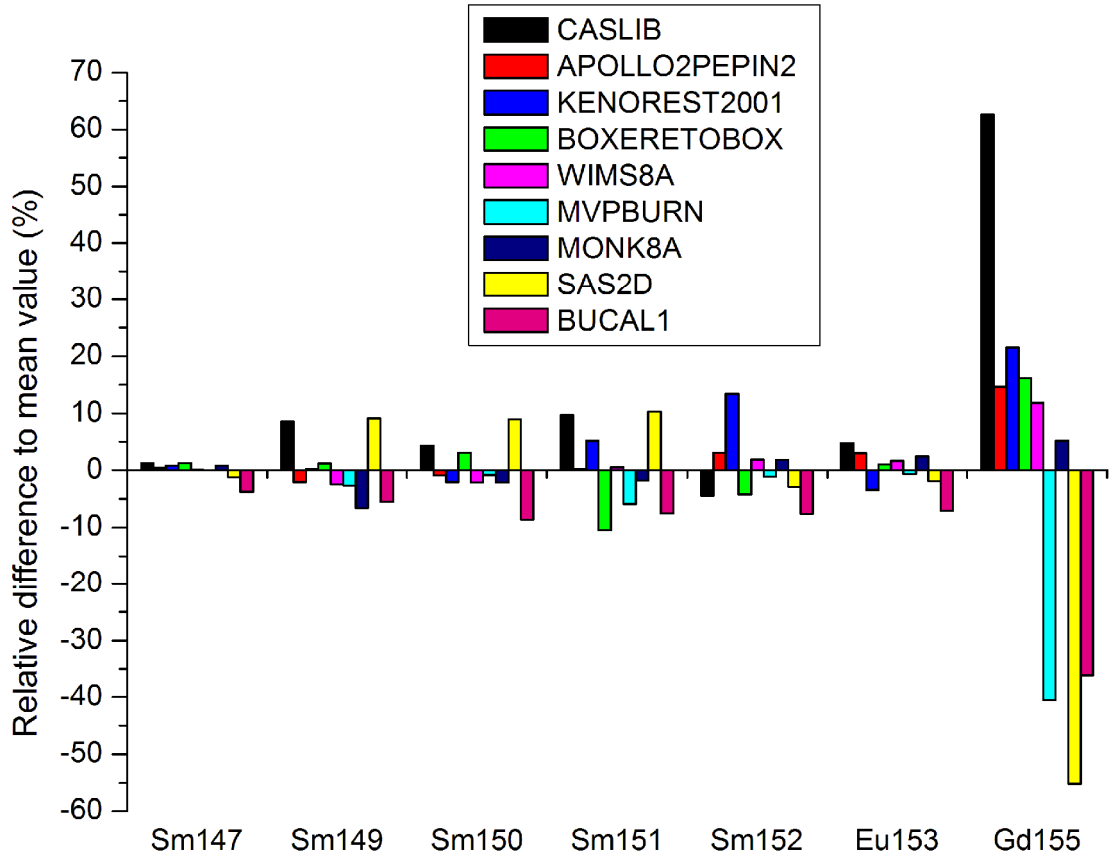

Figure 4.15- Relative difference of fission product nuclide densities at EOC2 (*cont.*).

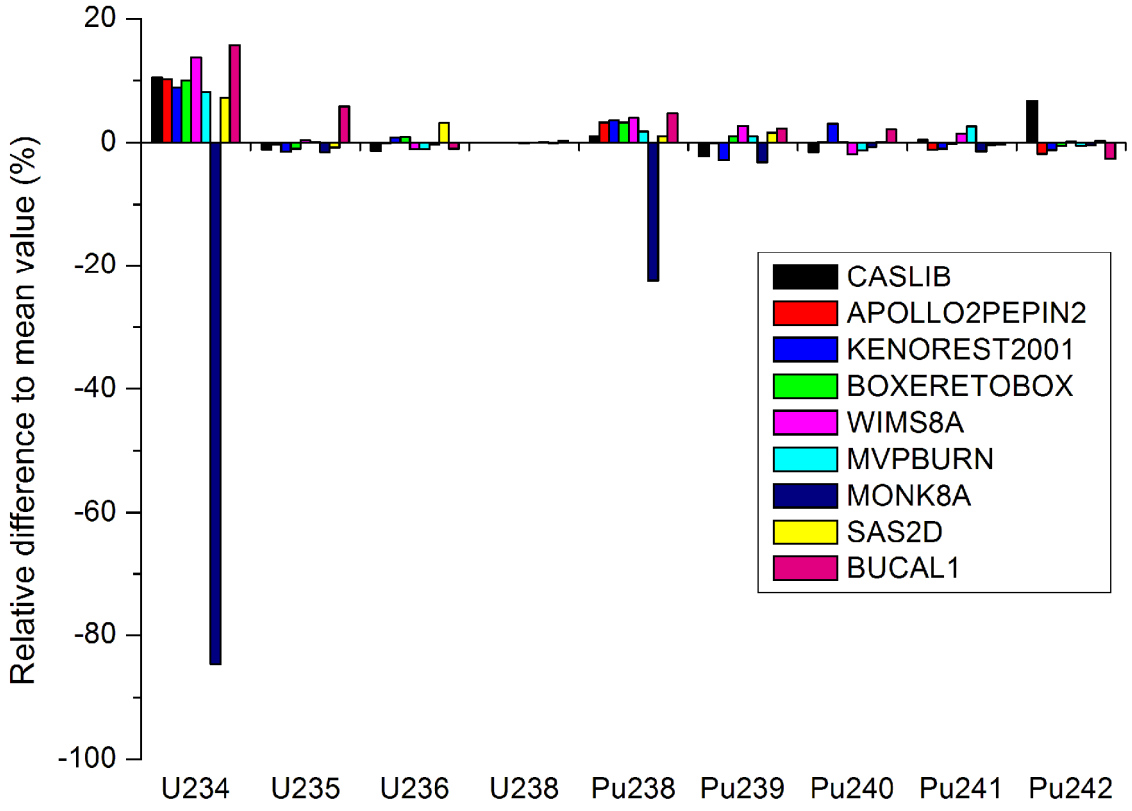

Figure 4.16- Relative difference of major actinide nuclide densities at EOC3.

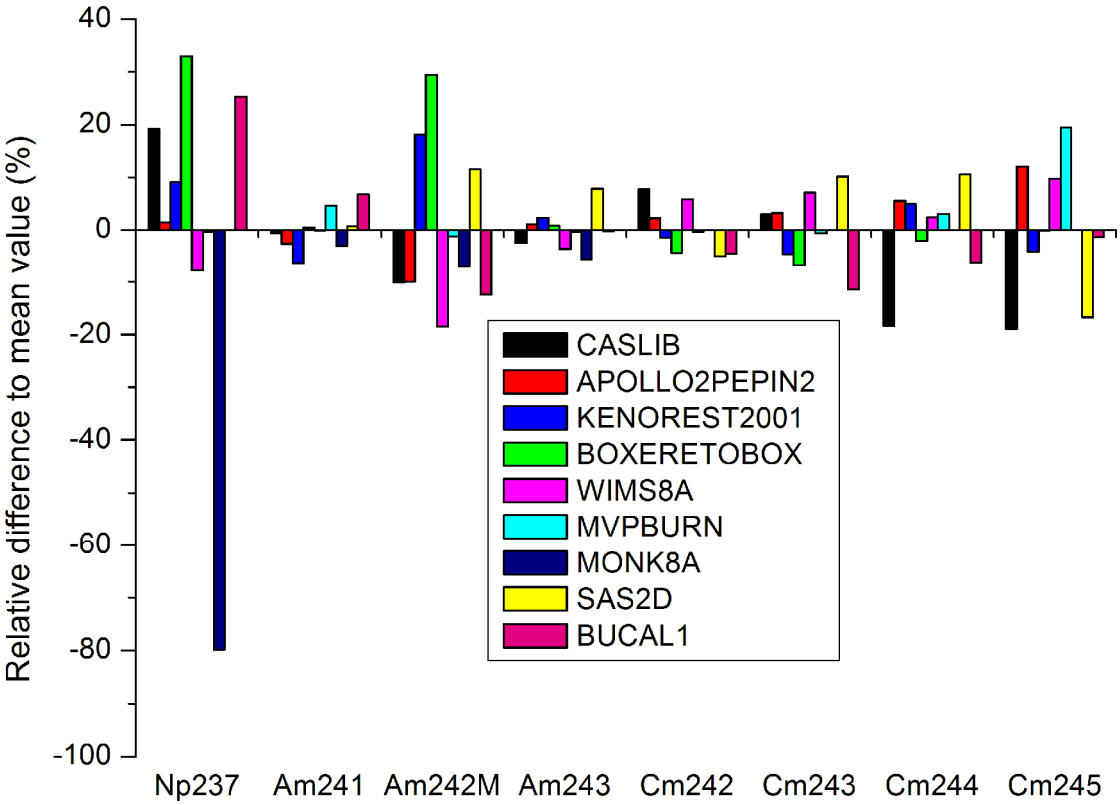

Figure 4.17- Relative difference of minor actinide nuclide densities at EOC3.

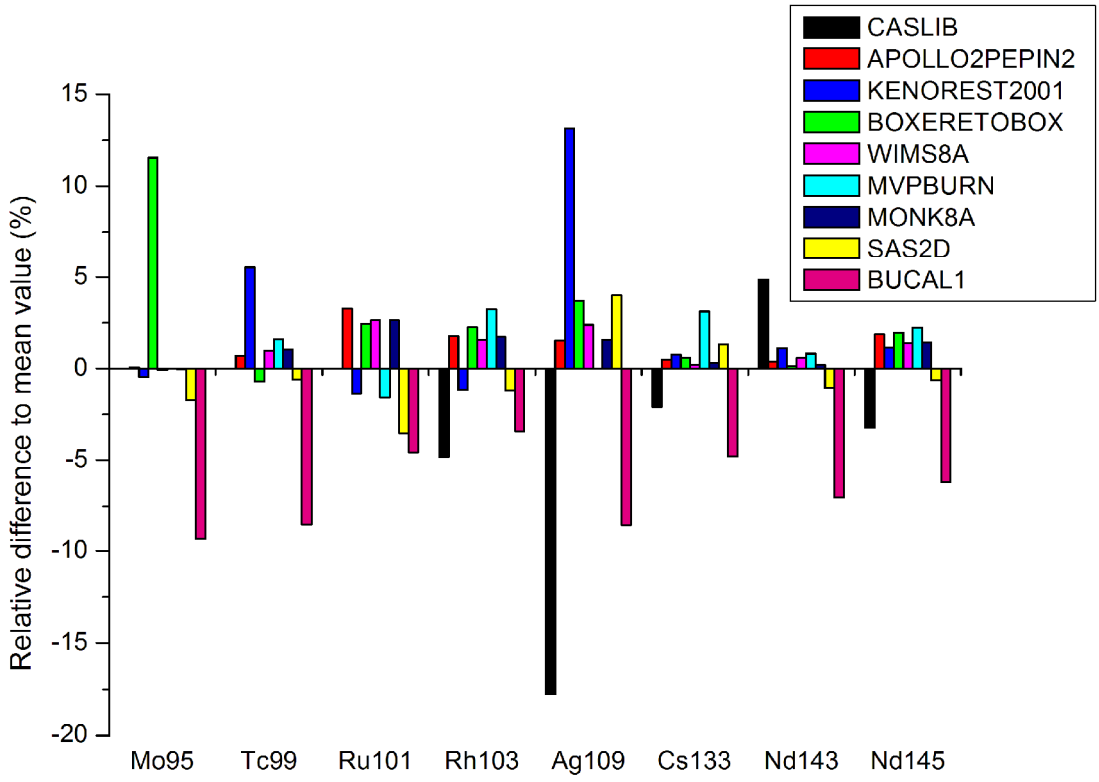

Figure 4.18- Relative difference of fission product nuclide densities at EOC3.

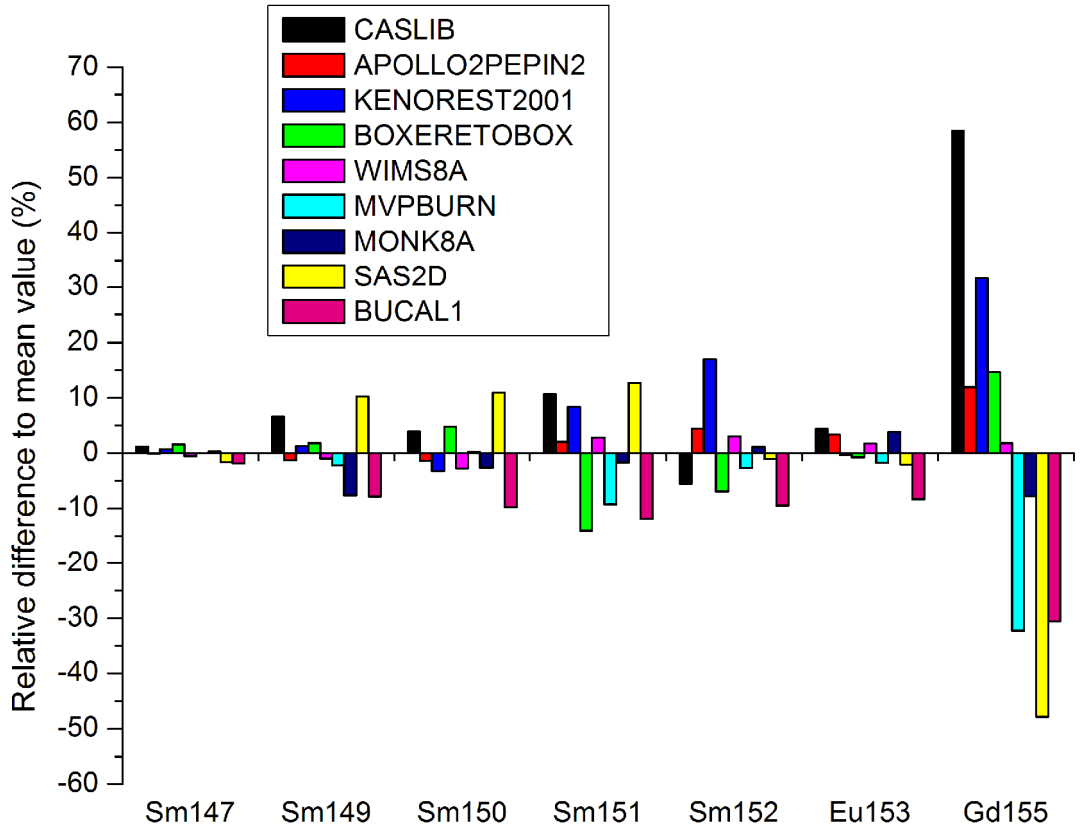

Figure 4.19- Relative difference of fission product nuclide densities at EOC3 (*cont.*).

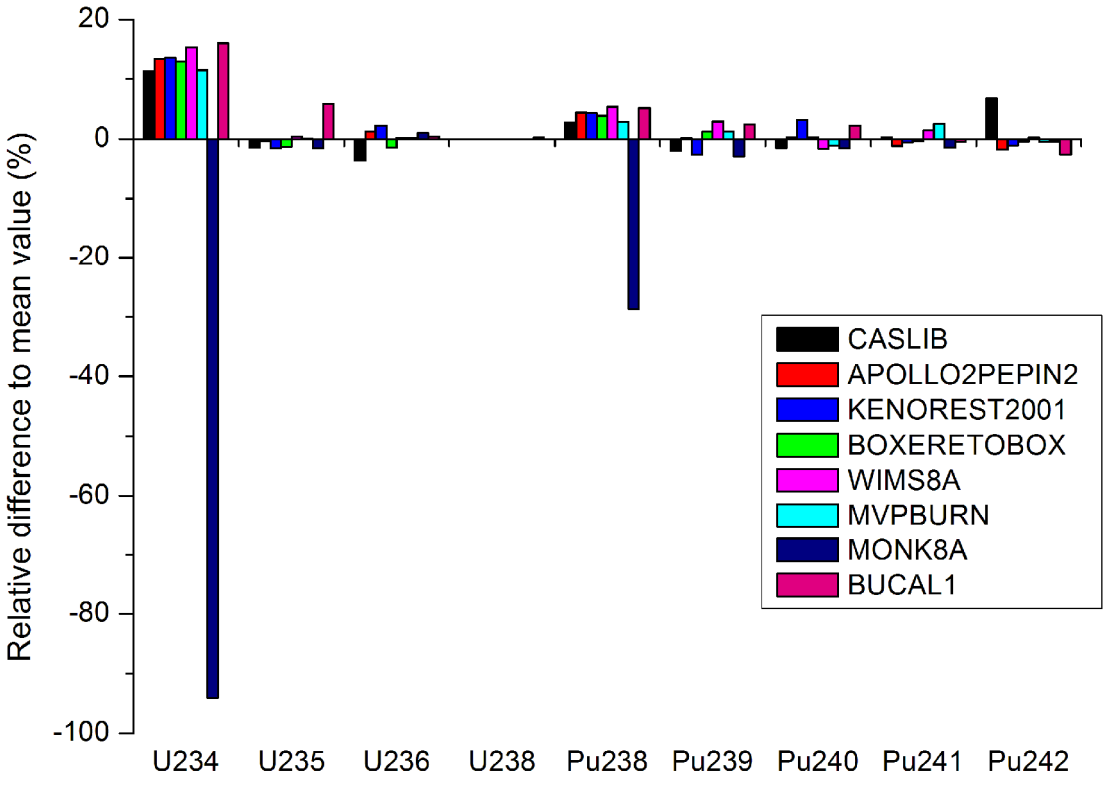

Figure 4.20- Relative difference of major actinide nuclide densities after 5 y cooling.

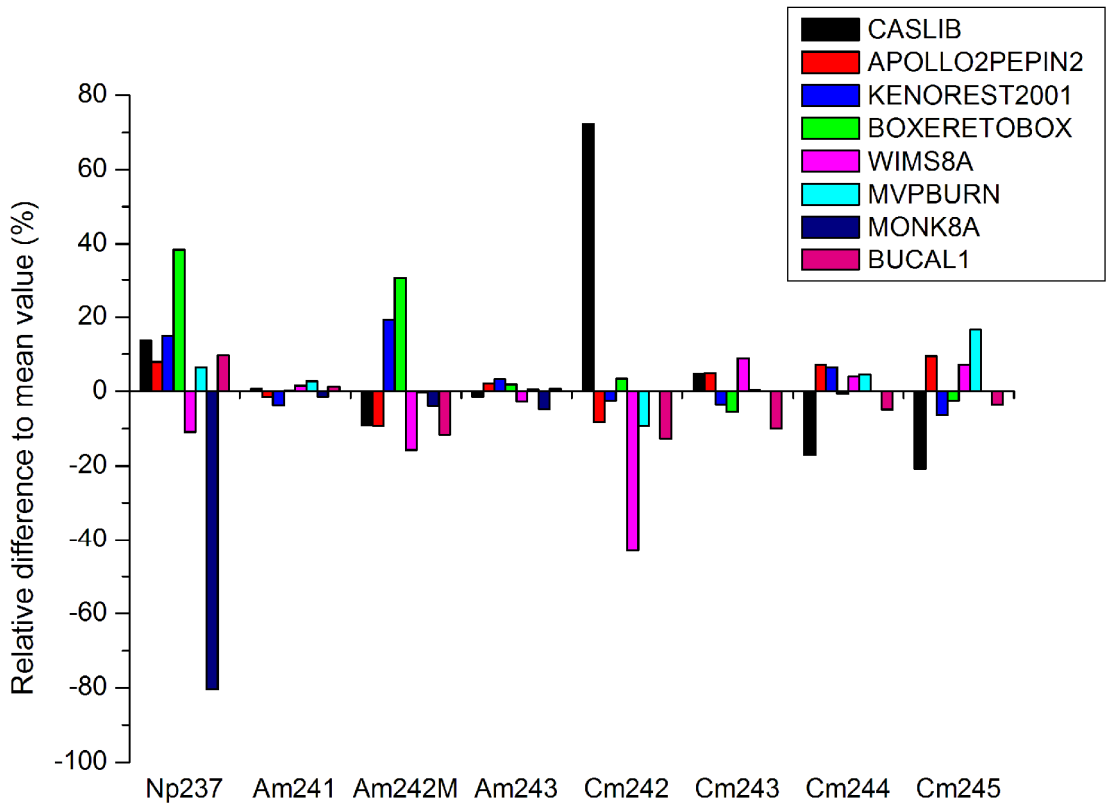

Figure 4.21- Relative difference of minor actinide nuclide densities after 5 y cooling.

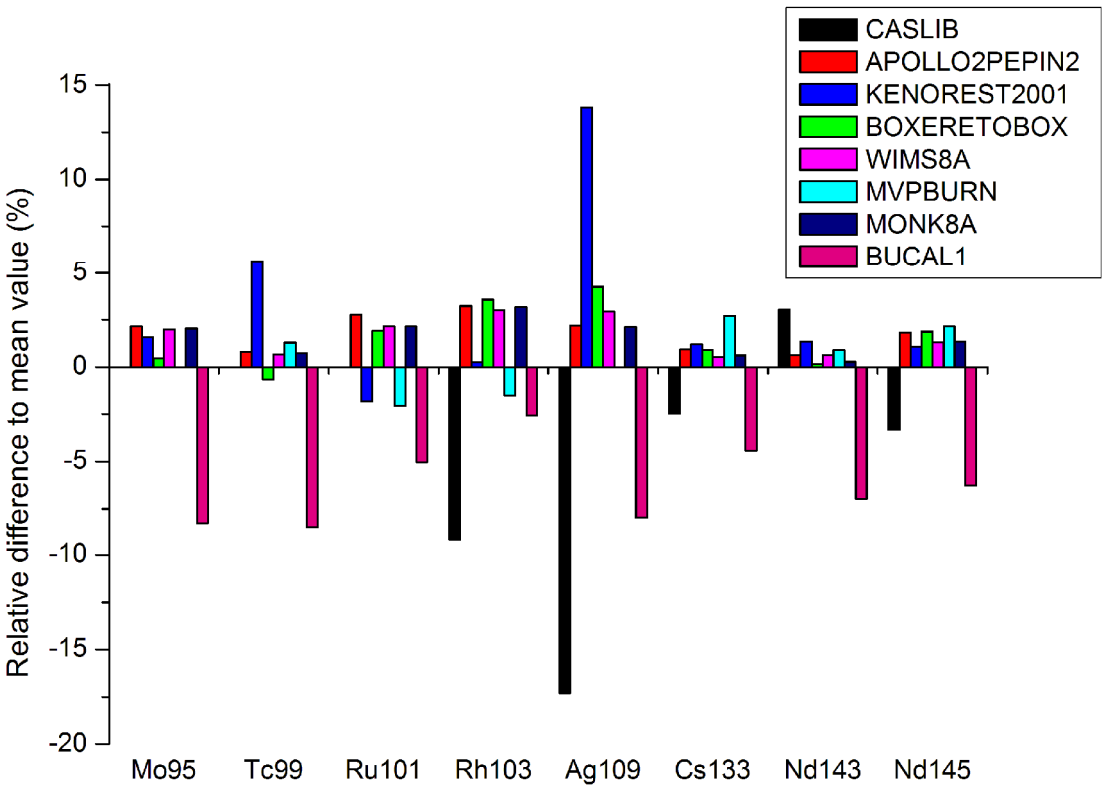

Figure 4.22- Relative difference of fission product nuclide densities after 5 y cooling.

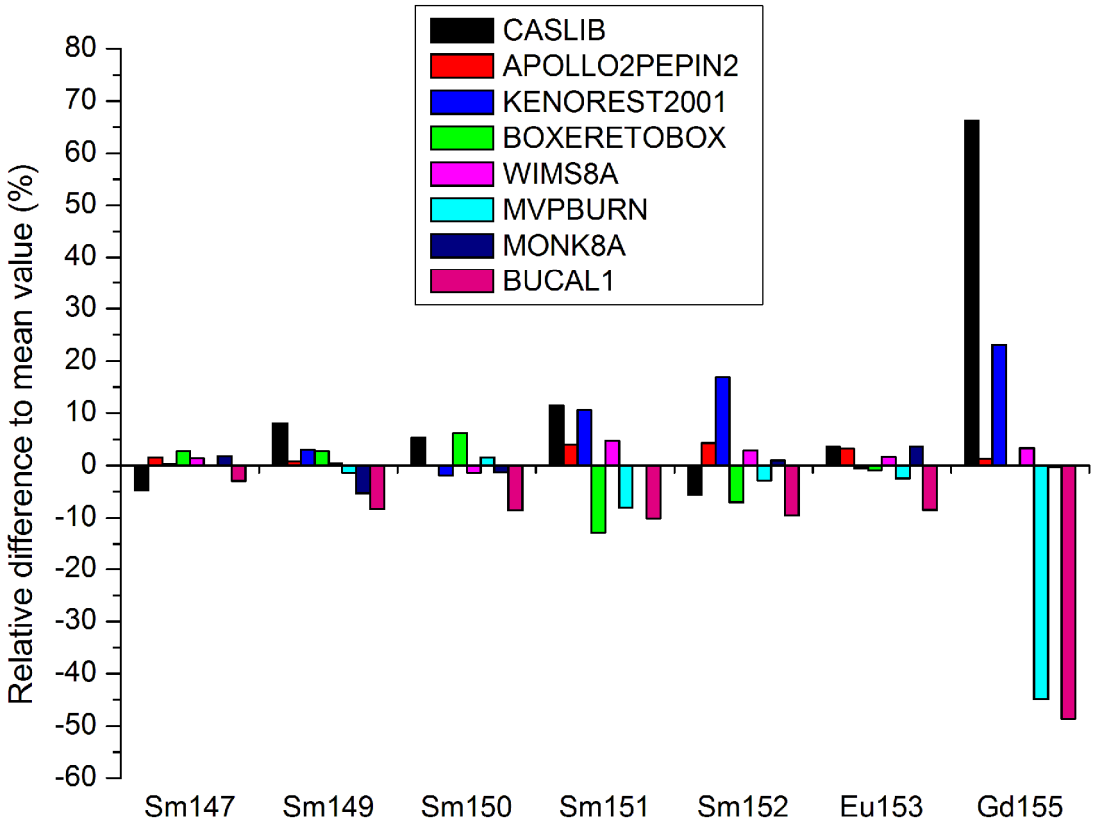

Figure 4.23- Relative difference of fission product nuclide densities after 5 y cooling (*cont.*).

At EOC1, Figure (4.8), for uranium isotopes, a relatively large deviation to the mean value is observed for ^{234}U nuclide density in the case of MONK8A code (about -60%). The other codes, including BUCAL1, produce roughly the same value (about 7.5%). For the remaining uranium isotopes a well agreement between codes is observed, especially for ^{238}U. In the case of plutonium isotopes, very good agreement between codes can be observed. For ^{237}Np, we remark that MONK8A underestimates the mean value by about 91%, whereas CASLIB, BOXER and BUCAL1 produce much higher values: 24%, 36% and 34%, respectively. When excluding MONK8A from the statistical analysis, Figures (4.24) and (4.25), the relative deviation to the mean value decreases, for ^{234}U isotope, from an average value of 7.5% to 1%. For ^{237}Np, the deviation varies from -91% (for MONK8A) and 36% (for BOXER) to -19% (for WIMS8A) and 21% (for BOXER). In the case of minor actinides, the relative deviations among codes results are obtained within ± 30%, this can be due to the differences on the actinides decay chain, reaction types adopted or also to the differences in the cross section libraries between codes. Thus, for fissile isotopes, which contribute significantly to the k_{∞}, a good agreement between codes results is observed.

In the case of important fission products, Figure (4.9), relatively large deviation is observed for ^{155}Gd and ^{95}Mo (40%, BOXER) to the mean value. For the remaining isotopes, all codes produce roughly similar results; the range of relative deviations to the mean values is within ± 12%. All relative deviations to the mean value obtained by BUCAL1 for fission products are underestimated; the maximum value is observed for ^{155}Gd (~ 36%). The other values vary from 1.41% (^{101}Ru) to 11.5% (^{95}Mo). This shows that our results are better compared to that obtained by some other codes.

In the case of EOC2, EOC3 and after five years cooling, Figures (4.10) to (4.23). A small underestimation is observed for ^{238}Pu (about 10%, Figure III-8) at EOC2 by MONK8A, which became much larger at EOC3 (***Fig. 4.12***) and after five years cooling (***Fig. 4.14***): about 23% and 30%, respectively. Also, a relatively large deviation to the mean value, about 73%, is obtained for ^{242}Cm by CASLIB after five years cooling. For the remaining nuclides, roughly the same behaviour as EOC1 is kept by all the codes (including BUCAL1) with small changes in the relative deviations to the mean values.

One other thing to note for BUCAL1, is the small overestimation (6%) observed for ^{235}U isotope after five years cooling (***Fig. 4.15***), this small overestimation can explain the maximum value of k_{∞} obtained between codes after five years cooling (0.921430). The difference in ^{235}U nuclide density remarked for BUCAL1, comparing to other codes, can be due especially to the approximations adopted by the codes concerning the decay chain of actinides. BUCAL1 uses a detailed decay chain, which takes into account the production possibility of ^{235}U through β+ from ^{235}Np, and α from ^{239}Pu. However such codes use just a simplified actinides decay chain supposing that, some isotopes are “stable” and they have no possibilities to come from decay modes of other isotopes, because of this the nuclide densities of some isotopes stay constant between the EOC3 and after five years cooling (*G J O’Connor et al., 2003*), example the ^{235}U nuclide density with CASLIB.

Table 4.17- The atom number densities of important fission products and actinides obtained by BUCAL1.

Isotopes	EOC 1	EOC 2	EOC 3	After 5 years cooling
U234	5.82310E-07	8.49990E-07	1.06960E-06	2.73973E-06
U235	4.42330E-05	3.57785E-05	2.86001E-05	2.86765E-05
U236	2.51583E-06	4.41982E-06	5.86526E-06	6.09067E-06
U238	2.11708E-02	2.09527E-02	2.07362E-02	2.07362E-02
Pu238	4.15453E-05	3.94870E-05	3.99513E-05	4.18975E-05
Pu239	8.09808E-04	6.53891E-04	5.32181E-04	5.33686E-04
Pu240	4.74103E-04	4.53602E-04	4.25087E-04	4.28569E-04
Pu241	2.17543E-04	2.34661E-04	2.33587E-04	1.83405E-04
Pu242	1.33807E-04	1.40732E-04	1.51014E-04	1.51014E-04
Np237	1.62504E-06	3.08335E-06	4.30418E-06	3.95103E-06
Am241	8.87924E-06	1.60462E-05	2.04883E-05	6.97957E-05
Am242M	1.18806E-07	2.96871E-07	4.10694E-07	4.00723E-07
Am243	1.73441E-05	2.95663E-05	3.88837E-05	3.88824E-05
Cm242	8.96539E-07	2.35902E-06	3.58562E-06	2.58454E-09
Cm243	1.10980E-08	5.54730E-08	1.19132E-07	1.06130E-07
Cm244	3.62267E-06	1.14546E-05	2.11620E-05	1.74727E-05
Cm245	1.80028E-07	1.08440E-06	2.66908E-06	2.66795E-06
Mo95	1.10891E-05	2.64486E-05	4.05668E-05	4.55853E-05
Tc99	2.08189E-05	3.91238E-05	5.53328E-05	5.55296E-05
Ru101	2.21098E-05	4.24745E-05	6.13215E-05	6.13227E-05
Rh103	1.95378E-05	3.76117E-05	5.17889E-05	5.47484E-05
Ag109	4.68732E-06	8.50058E-06	1.16987E-05	1.17120E-05
Cs133	2.32589E-05	4.35914E-05	6.11151E-05	6.15833E-05
Nd143	1.47948E-05	2.84710E-05	4.02426E-05	4.09799E-05
Nd145	1.09189E-05	2.06668E-05	2.94471E-05	2.94558E-05
Sm147	7.65794E-07	2.34996E-06	4.01385E-06	1.01316E-05
Sm149	3.82648E-07	3.63491E-07	3.21930E-07	3.63127E-07
Sm150	4.50753E-06	9.51778E-06	1.43637E-05	1.43637E-05
Sm151	1.35717E-06	1.58145E-06	1.57260E-06	1.52348E-06
Sm152	2.74319E-06	4.87771E-06	6.15937E-06	6.15944E-06
Eu153	2.05994E-06	4.85697E-06	7.61329E-06	7.65040E-06
Gd155	6.83426E-09	1.13702E-08	1.85299E-08	3.11375E-07

Table 4.18- Data missing.

	EOC1	EOC2	EOC3	After 5y cool.
CASMO-4		Mo95 Tc99 Ru101		
MVP-BURN		Mo95 Ag109 Sm145		
MONK8A		Cm242 Cm243 Cm244 Cm245		
SAS2D		Np237		No data for all isotopes

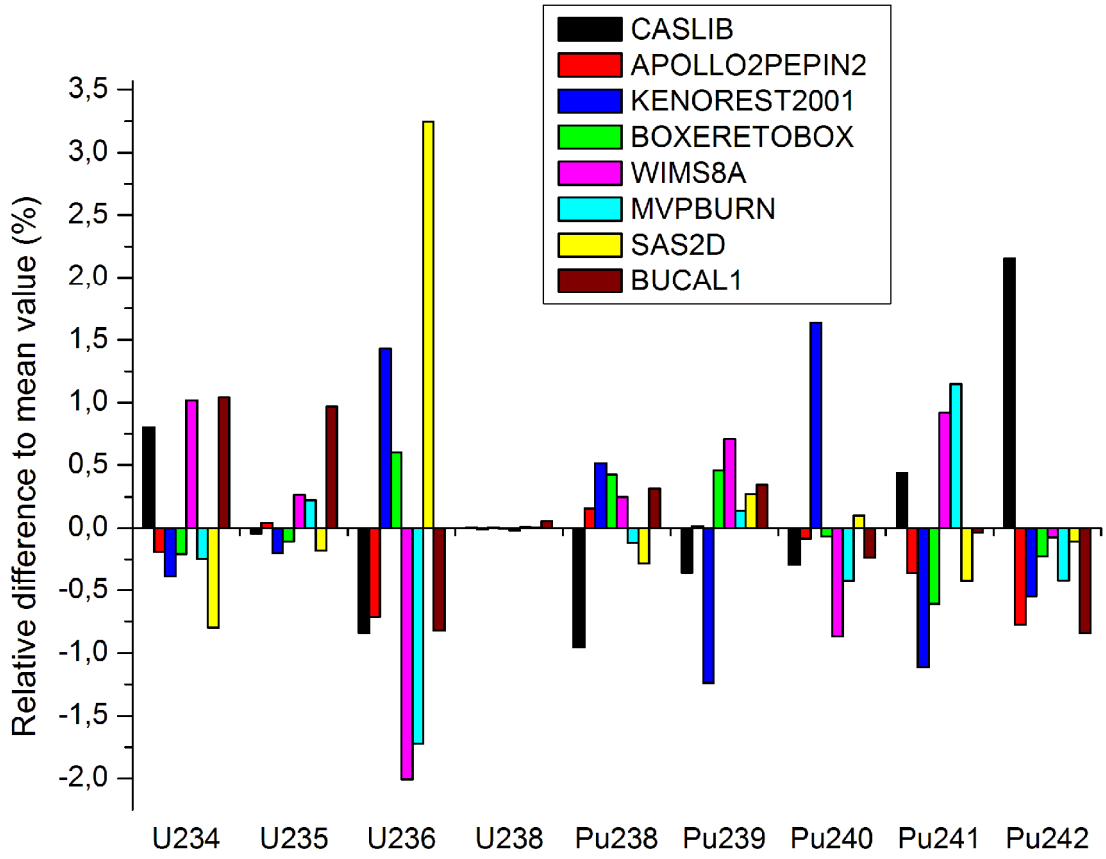

Figure 4.24- Relative difference of major actinide nuclide densities at EOC1 (excluding MONK8A).

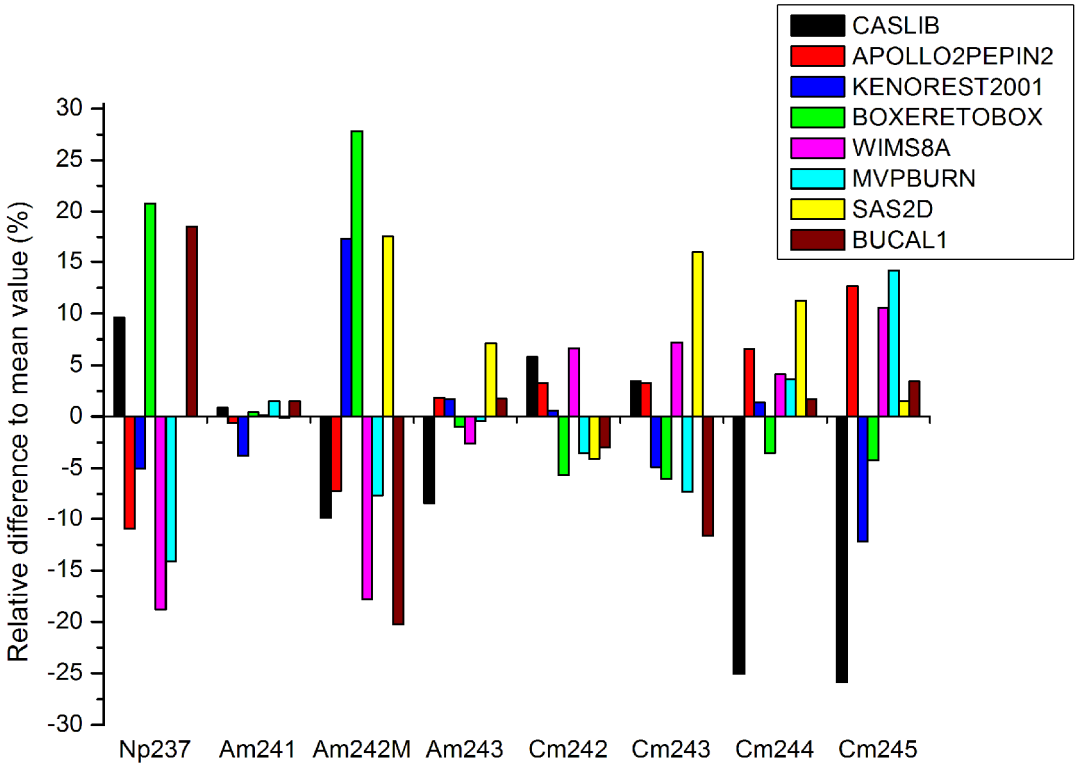

Figure 4.25- Relative difference of major actinide nuclide densities at EOC1 (excluding MONK8A).

6. Conclusion

New burnup code utility called BUCAL1 was developed. The code is different in comparison to other burnup codes primary, because it does not use the calculated neutron flux as input to other computer codes to generate the nuclide inventory for the next time step. Instead, BUCAL1 directly uses the neutron absorption reaction tally information generated by MCNP5 for each nuclide of interest to calculate the new nuclide inventory. This allows the full capabilities of the MCNP code to be incorporated into the calculations and a more direct solution technique to be employed. Secondary, the code is able to do several burnup calculations modes: it can do burnup calculation followed by a space of time of cooling, burnup calculation with shuffling fueled regions, and burnup calculation with reloading new fresh fuel. And, finally, the coupling with the MCNP code for all of these calculations can be done automatically which allows ignoring the propensity to introduce errors.

The validation process of BUCAL1 was done by code to code comparisons using results from several codes from the NEA/OCED. Infinite multiplication factor (k_∞) and important fission products and actinides concentrations were compared and analysed for a large variety of core benchmark exercises.

From the code – vs – code benchmarking of the high burnup UO2 pin–cell under cold conditions, it is concluded that BUCAL1 is suitable and ready to be used in burnup calculations. Even for high burnup cases, the material composition predictions are also acceptable compared to the comprehensive uranium benchmark reported by OECD (*M. D. DeHart, 1996*). Based on the results of the intercomparison done between BUCAL1, CASMO-4 and MOCUP, it appears that BUCAL1 can do also thorium related calculations with an acceptable agreement.

For the MOX–lattice case, the benchmark calculation results obtained by BUCAL1 show good agreement compared to the mean values and results from other codes. After five years cooling the relative deviation from the average value for the infinite multiplication factor (k_∞) using BUCAL1 is lower than 1%. For important fission products and actinides densities, BUCAL1 produces the average value within ± 10%. The relative deviations to the mean values for ^{237}Np and ^{155}Gd are relatively large for the majority of codes used in this study. All–in–all, BUCAL1 is sufficiently accurate and gives consistent results. So it can be used in the study of the time-dependent neutronics parameters of a large variety of nuclear reactors.

5. Neutronics Calculations and burnup of the 2MW TRIGA MARK II Moroccan research reactor

This chapter deals with the neutronic analysis of the current core configuration of the 2MW TRIGA MARK II research reactor at CENM and validation of the results by benchmarking with the experimental, operational and available Final Safety Analysis Report (FSAR) values. The 3-D continuous energy Monte Carlo code MCNP5 was used to develop a versatile and accurate full-core model of the TRIGA reactor. The model represents a very detailed description of all components of the core with literally no physical approximation. All fresh fuel and control elements as well as the vicinity of the core were precisely modelled. Composition and geometry data are almost all deduced from FSAR and as-built data that are available during this study. Continuous energy cross section data from the more recent nuclear data evaluations (ENDF/B-VI.8, ENDF/B-VII.0, JEFF-3.1, and JENDL-3.3) as well as S(α, β) thermal neutron scattering functions distributed with the MCNP5 code were used. The cross section libraries were generated by using the NJOY99 system updated to its more recent patch file "up259". The consistency and accuracy of both Monte Carlo simulation and neutron transport physics were established by benchmarking the TRIGA experiments. The effective multiplication factor, axial and radial peaking factors, reactivity experiments comprising control rod worth, excess of reactivity and shutdown margin were used in the validation process. After validation, the MCNP model of TRIGA was used in the estimation of the life time of the first cycle, calculation of U235 depletion and BOC−EOC axial and radial fluxes of TRIGA reactor using our new elaborated burnup code BUCAL1.

1. Introduction

LESS THAN FIVE years from the date of President Dwight D. Eisenhower's December 1953 "Atoms for Peace" proposal to the United Nations General Assembly, TRIGA a new kind of inherently safe training, research, and isotope-production nuclear research reactor was conceived, built, and operating at the General Atomic Division of General Dynamics Corporation in San Diego, California. Over the years, TRIGA (Training, Research, Isotope production, General Atomic) has evolved into the most widely used research reactor in the world, with operating power levels up to 14 000 kW, designs up to 25 000 kW, and with an installed base of 65 reactors in 24 countries on five continents.

The Moroccan 2MW TRIGA Mark II research reactor at Centre des Etudes Nucléaires de la Maâmora (CENM) achieved initial criticality on *May 2, 2007*. The reactor is designed to effectively implement the various fields of basic nuclear research, manpower training and production of radioisotopes for their use in agriculture, industry and medicine.

For the purpose of modelling of the Moroccan TRIGA MARK II research reactor, the general purpose 3-D Monte Carlo N-Particle transport code MCNP5 release 1.40 (X-5 Monte Carlo Team, 2003) was chosen because of its general modelling capabilities, correct representation of detailed geometry, transport effects and continuous energy cross sections handling. The later is the most significant because it uses eliminate the need for collapsing multigroup cross sections for the reactor modelling and in-core experiments. To reduce possible systematic errors due to inexact geometry simulation, a very thorough 3-D model of the TRIGA reactor was developed. All fresh fuels, control rods, and other in and near core elements were modelled using the maximum details allowed. The repeated structure capability of MCNP was used to create a full three dimensional model of TRIGA reactor. The MCNP input was designed and written in such a way that a very quick setup of any desired core configuration with an adequate position of all control rods is possible.

An essential step of developing and adopting of an accurate reactor physics model is validation. The accuracy of both the neutron transport physics as represented in MCNP code and the user-defined model must be assessed. However, MCNP has been proven to simulate the physical interactions correctly. Since the Monte Carlo method simulates individual particle tracks through a given system, it can provide a very accurate probabilistic transport solution. That does not mean that the model of TRIGA will provide accurate answers. Therefore, to build confidence, all the neutronics parameters including the core excess reactivity, radial and axial power peaking factors as well as the total and integral reactivity rods worth were calculated using the MCNP model of the TRIGA reactor and compared with the experimental and FASR values. Also, in the aim of achieving an exhaustive study of TRIGA reactor core, burnup calculations using our new elaborated code BUCAL1 were done for the estimation of the core life time, U235 depletion and BOC−EOC axial and radial fluxes.

2. TRIGA Mark II research reactor

2.1. Overview

The TRIGA Mark II research reactor in CENM (Centre d'Etudes Nucléaires de la Maâmora) is covered by the Project and Supply Agreement INFCIRC/313, January 1984, between the Kingdom of Morocco, the United States of America and the International Atomic Energy Agency (IAEA). The reactor was designed and constructed by General Atomics (GA) for

2MW thermal power with natural convection cooling, using low enriched uranium fuel (LEU). Figure (5.1) gives a general view of the TRIGA reactor.

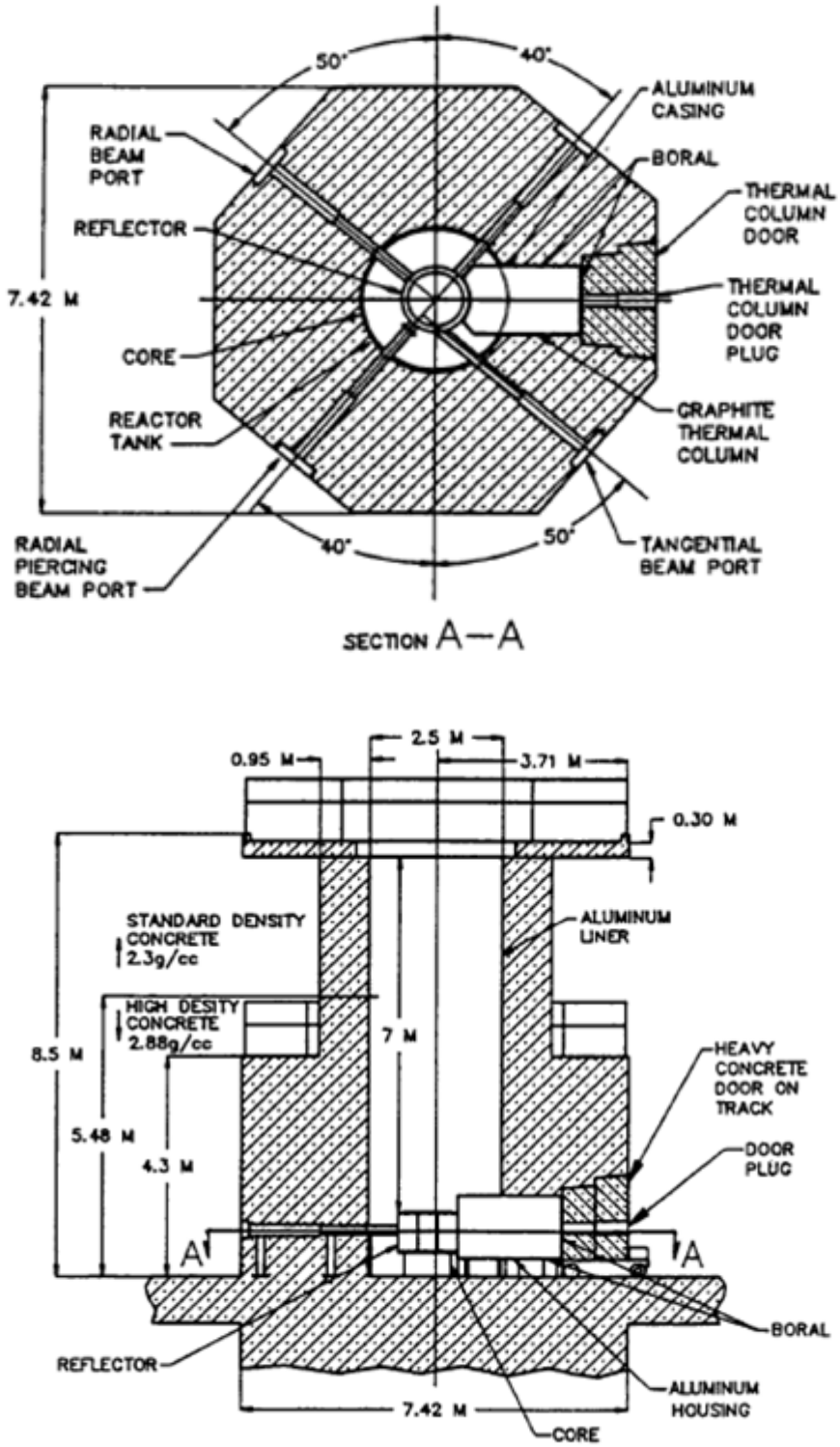

Figure 5.1- Cutaway view of TRIGA reactor – typical dimensions.

2.2. In and near-core elements

In this section, we give a brief description of the in-and-near core elements of TRIGA reactor.

2. 2. 1. Standard Fuel Elements

The TRIGA fuel is a solid, homogeneous mixture of uranium-zirconium hydride alloy containing about 8.5% by weight of uranium enriched to a maximum of 20% U-235. The hydrogen-to-zirconium atom ratio is approximately 1.6. A 6.35-mm diameter hole is drilled through the centre of the active fuel section to facilitate hydriding of the fuel material and zirconium rod inserted in the hole after hydriding is complete. The solidified material is fine machined into cylindrical blocks 36.45-mm diameter and 127-mm long. Three fuel blocks are assembled end to end making an active fuel section 381-mm length. The entire fuel section is encased in a stainless steel cylindrical can 0.05-mm thick wall, having an outside diameter 37.45-mm. Two cylindrical graphite sections are inserted in the can above and below the fuel, which serve as top and bottom reflectors in the core. The top graphite section is 66-mm long, and the bottom section is 94-mm long. A thin molybdenum disc is inserted between the fuel and the bottom graphite. The overall length of the stainless steel casing is approximately 561-mm. Stainless steel fittings are attached to both ends of the canister making the overall length of the fuel element 754-mm. Each of these end fittings is cast with trifluted design that enhances cooling water flow through the grid plates and around the fuel elements. Figure (5.2) shows the standard fuel element.

Figure 5.2- TRIGA standard fuel element.

2. 2. 2. Instrumented Fuel Elements

The instrumented fuel elements, shown in Figure (5.3), are similar to the standard fuel elements in most respects including fuel composition and positioning within the cladding. In addition the instrumented fuel elements are equipped with three Chromel-Alumel thermocouples placed in the active fuel length. The sensing tips of the thermocouples are radially located about 7.6-mm from the vertical centreline of the element. Vertically, one thermocouple is located on the active fuel centreline, with a second thermocouple approximately 25-mm below the active fuel centreline. Each thermocouple consists of two 0.28-mm diameter wires embedded in the magnesium oxide insulation and contained in a 1.5-mm diameter Inconel-600 sheath. The sheathed thermocouples pass through a stainless steel plug in the top fitting. This plug is brazed to the top fitting and the thermocouples sheaths that pass through it to provide a helium-tigh seal.

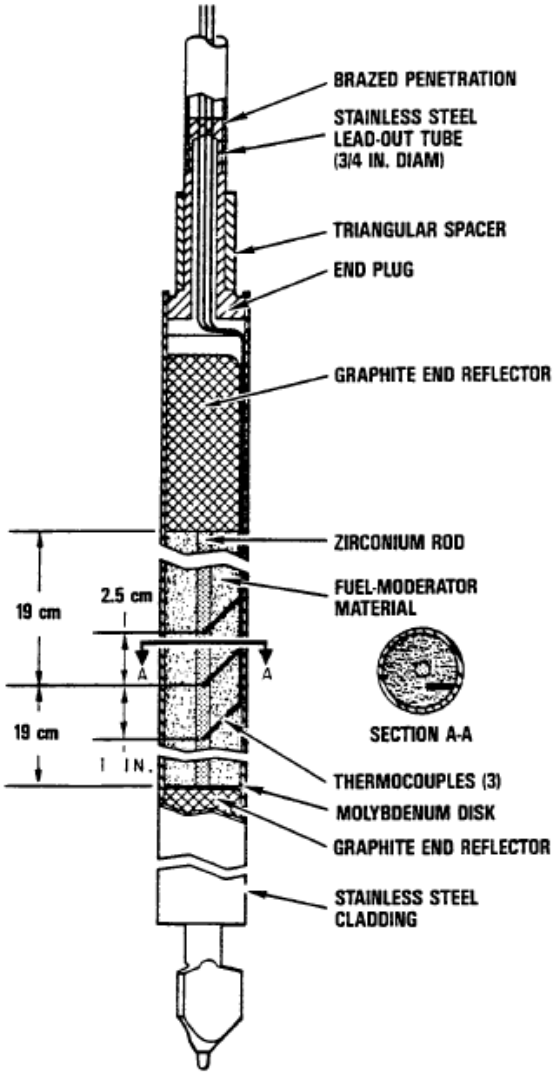

Figure 5.3- Instrumented fuel element.

2. 2. 3. Fuel Follower control rods

Five fuel follower control rods, shown in Figure (5.4), control reactor power during steady-state operation. Each fuel follower control rod consists of a 31.75-mm outside diameter stainless steel tube approximately 1111-mm long closed at either end by top and bottom fittings. At the top of the control rod there is a ~ 150-mm void followed by a 381-mm boron carbide neutron absorber section. Below the absorber section is a standard 381-mm fuel section which is followed by another ~ 150-mm air void. The absorber and fuel sections are separated from each other and held in position by aluminium spacers that are automatically swaged in place. The top end fitting of the control rod has its identification number into it and incorporates a stainless steel male threaded stud that screws into a transition piece. A 2.4-mm diameter pin driven radially through the centre of the transition piece and the control rod top fitting ensures that the control rod will not unscrew accidentally. The top of the transition piece is machined to slide into the connecting rod and is pinned with three 6.3-mm diameter stainless steel pins. The connecting rod is an integral part of the control rod drive mechanism.
The fuel follower control rods pass through and are guided laterally by 38.2-mm diameter holes in the top and bottom grid plates, during the entire stroke of travel. The control rods travel vertically a distance of approximately 381-mm between their fully withdrawn and inserted positions. An aluminium safety plate attached below the bottom grid plate eliminates the possibility of a control rod dropping out of the core if it is accidentally disconnected from its drive.

2. 2. 4. Reflector Elements

The graphite reflector elements are used to fill all grid positions not occupied by standard fuel elements, instrumented fuel elements, fuel follower control rods or other core components. The reflector elements have the same general configurations and physical dimensions as the standard fuel elements, but they have an aluminium alloy cladding and are entirely filled with graphite. The top and bottom fittings do not incorporate triflutes and fit smugly into the grid plate holes, thus preventing coolant flow from bypassing the fuel elements.

2. 2. 5. Top grid plate

The top grid plate is a 31.75-mm thick aluminium plate 552.5-mm diameter, which is machined to tight tolerances in order to provide accurate lateral positioning for the core components. A total of 121 holes, each having a 38.2-mm diameter, are bored in a hexagonal array arround the central hole that accommodates an experimental tube. Edges of the holes are

tapered 20 degrees (top and bottom) to streamline flow through the grid plate and around the core elements; this also reduces coolant flow pressure drop. These holes accommodate:

- 94-standard fuel elements
- 2-instrumented fuel elements
- 5-fuel follower control rods
- 18-reflector elements
- 1-central experiment tube
- 1-terminus pneumatic system

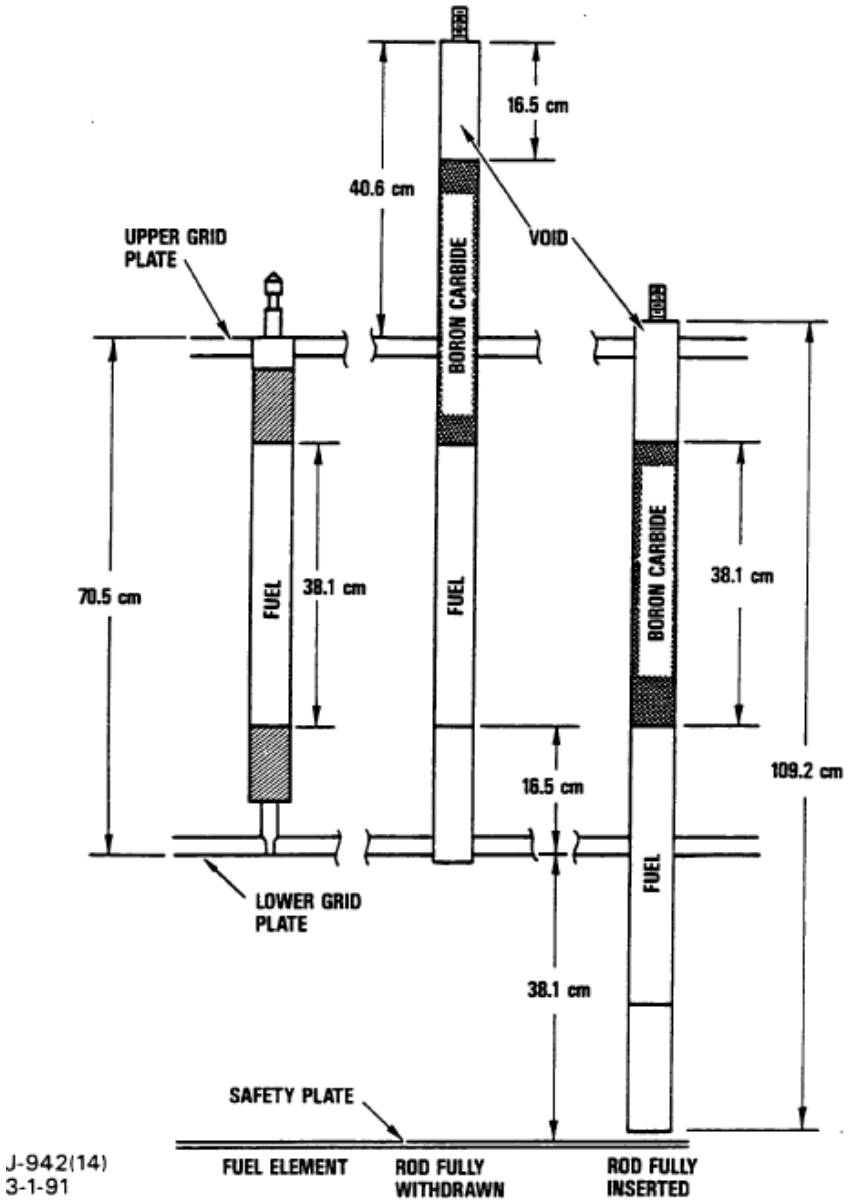

Figure 5.4- Fuel followed control rod.

Six 15.87-mm diameter holes are also bored at the apex of the hexagon array to accommodate neutron source holders.

The top grid plate has a removable hexagonal shaped section encompassing the centre hole and six adjacent holes for insertion of specimens up to 112-diameter into region of highest flux.

The grid plat is made from aluminium alloy plate, anodized to minimize corrosion and wear. The plate is secured in position to the top of the reflector assembly with six 9.52-mm stainless steel bolts.

2. 2. 6. Bottom grid plate

The bottom grid plate is a 31.75-mm thick aluminium plate machined in a hexagonal shape 500-mm across the flats and chamfered on the corners to match the reflector assembly hexagonal inner housing. The bottom grid plate is attached to the inner housing reflector assembly with six 9.25-mm diameter stainless steel bolts that screw into reinforced tapped holes. One hundred and nine holes, 31.73-mm diameter, are aligned with fuel elements holes in the upper grid plate. They are countersunk to receive the adapter end of fuel-moderator elements, graphite dummy elements, and the adapter end of the pneumatic transfer tube. These holes have a 20 degree tapered leading edge (on the underside) to reduce coolant turbulence and pressure drop. The remaining twelve holes are 38-mm in diameter and are counter bored from the bottom of the grid plate with a 41-mm diameter, 25.4-mm deep to accept the top end of the flow tubes. Five of these remaining holes are to accommodate the fuel followed control rods while the remaining seven holes can be used as experiment irradiation locations. The centre hole is typically used to accommodate the central experiment tube, but it can be repositioned in any of the 38-mm holes not occupied by control rods.

The bottom grid plate is made from aluminium alloy plate, anodized to minimize corrosion and wear.

2. 2. 7. Reflector assembly

The reflector, shown in Figure (5.5), is a ring-shaped block of graphite that surrounds the core radially. The graphite is about 210-mm thick radially with an outside diameter of about 940-mm, a height of about 530-mm, and an inside hexagonal configuration with an across flat dimension of about 530-mm. A 63-mm thickness of lead surrounds the graphite to reduce gamma heating in the shield concrete. The lead does not cover the faces of the beam tubes. The graphite and lead are contained within leak-tight welded aluminium housing. The reflector currently accommodates four tangential neutron radiography beam tubes. A graphite thermal column surrounds a portion of the reflector.

Figure (5.6) represents the typical loading diagram of the 2MW TRIGA Mark II research reactor in CENM.

Figure 5.5- Reflector assembly.

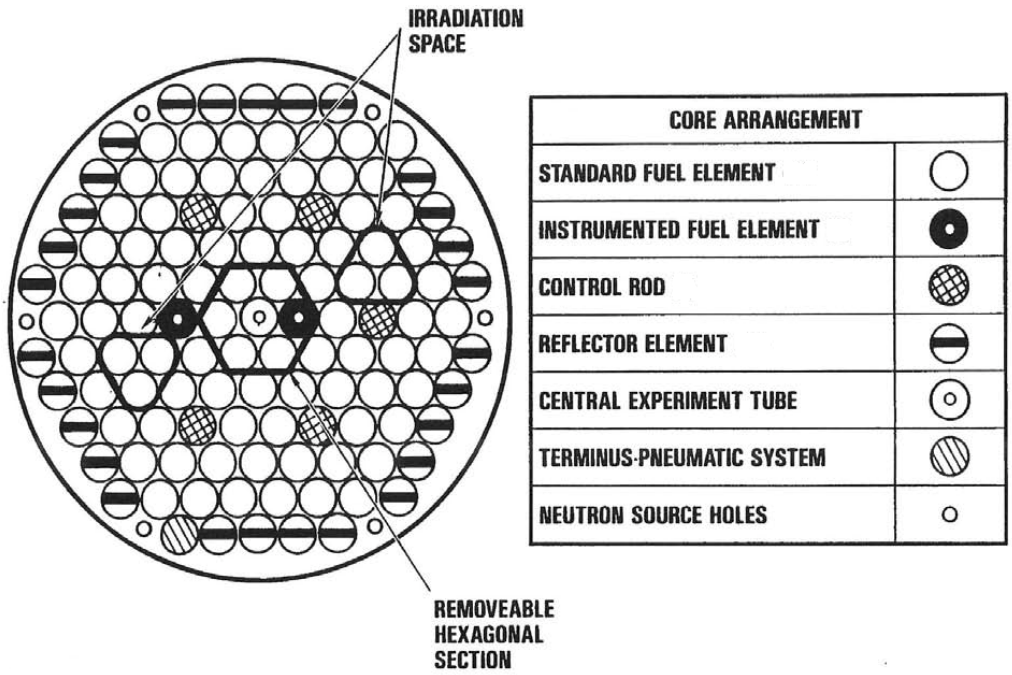

Figure 5.6- Typical 2MW TRIGA MARK II core configuration.

3. Modelling of TRIGA reactor

3.1 History

The first interest by *the Laboratoire de Matière et Rayonnement (LMR) of the faculty of Sciences of Tetuan,* on the modelling of the Moroccan TRIGA reactor, was began in 2004. This work was started by the author of this thesis and Dr. Ossama Meroun in collaboration with Pr. M. Chakir from the faculty of sciences of Kenitra under the supervision of Pr. Tarek El Bardouni. I remember that, in this year Pr. Tarek El Bardouni, with its pragmatic vision, asked us to model the Moroccan TRIGA reactor using data from Ph. D thesis of Dr. A. Htet (*A.Htet, 2001*), Slovenian 250kW TRIGA reactor (*R. Jeraj et al., 2003*) and the 3MW TRIGA reactor of Bangladesh (*M. Q. Hauda et al., 2004*). Directly after the proposition of Dr. Tarek, we started working hardly for the elaboration of our first MCNP model of our TRIGA reactor. In 2006, two new Ph. D students Chafik El Younoussi and Yassin Boulaich joined the LMR staff and participated seriously in this work. Hence, the first MCNP model of the Moroccan TRIGA reactor was finished in 2006 and the fruits of this work were presented by Pr. M. Chakir in the National Conference on Nuclear Physics, organized at the faculty of sciences of Kenitra, 2007. After, the MCNP model was used by LMR in the development of new research areas such as Prompt Gamma Neutron Activation Analysis and Boron Neutron Capture Therapy studies. During 2009, and after establishing a scientific collaboration between the Reactor Operating Unit (ROU or UCR) of CNESTEN and LMR, there was a very hard work under the supervision of Pr. Tarek El Bardouni and Mr. Nacir Bouzekri the Chief of UCR on the refining of the MCNP model using the new data from the manufacturer General Atomics of USA. The final results of this work are presented in this chapter.

3.2. MCNP modelling of TRIGA reactor

The Triga reactor is a light water cooled, graphite-reflected one, designed for operating at a steady state thermal power level of 2000 kW. An outstanding feature of the TRIGA reactor is its proven intrinsic safety, which stems from the large instantaneous negative temperature coefficient of reactivity of its U-ZrH fuel moderator-material. The TRIGA core consists of 101 fuel elements, 17 graphite elements, central thimble and a pneumatic transfer tube. The cross-sectional view of the present core configuration of the reactor is show on Figure (5.7) which was achieved on June 2007 during reactor start-up at full power operation. Elements are arranged in seven concentric rings in hexagonal geometry and the spaces between the rods are filled with water that acts as coolant and moderator.

The reactor was modelled in full 3-D details to minimize geometry approximations. The repeated structure capability of MCNP was used to create a full core 3-D model of TRIGA.

The TRIGA lattice can be represented as a hexagonal prism with eight faces. The fuel elements were modelled explicitly specifying the detailed structure of the rod to eliminate any homogenisation effects. The tapered end fixtures of stainless steel were also modelled with a very little approximation. The power level of the reactor is controlled with five control rods: a regulating rod and four shim safety rods. The control rods were explicitly modelled along the active length containing three vertical sections of boron carbide, fuel follower and void region. The central thimble was considered to be filled with water and the pneumatic tube was considered to be void. The graphite dummy elements are of the same general dimensions and construction as the fuel-moderator elements, except these elements are made of aluminium alloy and filled entirely with graphite.

The model was extended up radially containing the graphite reflector and lead shield. An annular well on the inside diameter in the top of the graphite reflector that provides for the rotary specimen rack was also modelled along with the radial and tangential beam ports that serve for experimentations around the TRIGA core. To complete the modelling of all reactor facilities the thermal column, which is a squared graphite assembly located in the side of the reactor shield structure, is also modelled. It is located between beam ports NB1 and NB4 and the reactor tank that consists of an aluminium vessel installed in the reactor shield structure, this facility serves for the irradiation of large experimental specimens.

All the geometric and material data were taken from the fabrication shipment documentation provided by the reactor manufacturer General Atomics of USA.

Figures (5.8) and (5.9) represent the radial and axial view of MCNP5 model of the 2MW TRIGA MARK II research reactor of CENM.

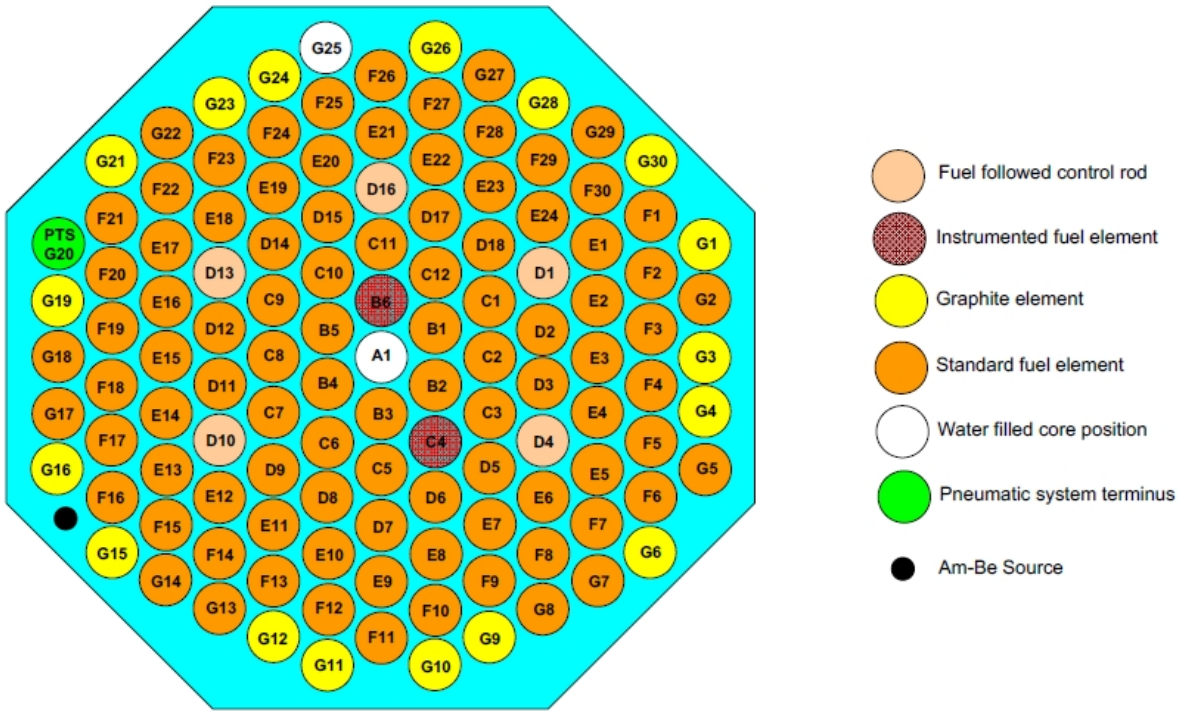

Figure 5.7- Present core configuration of the TRIGA reactor.

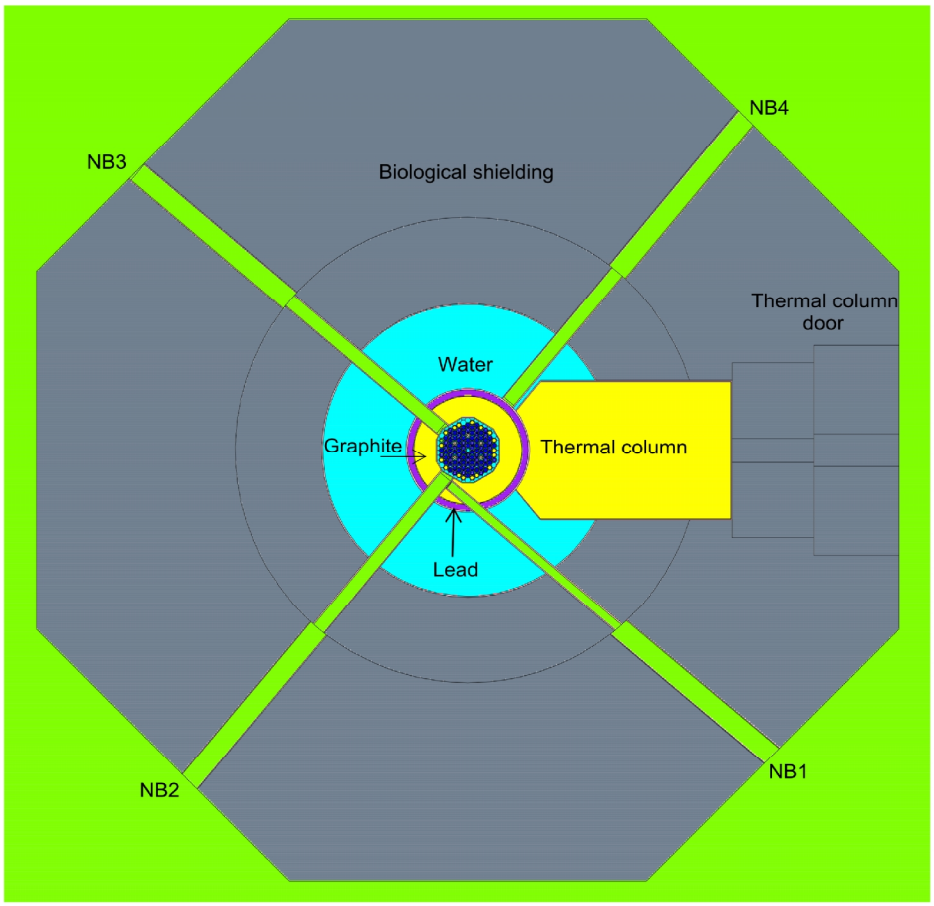

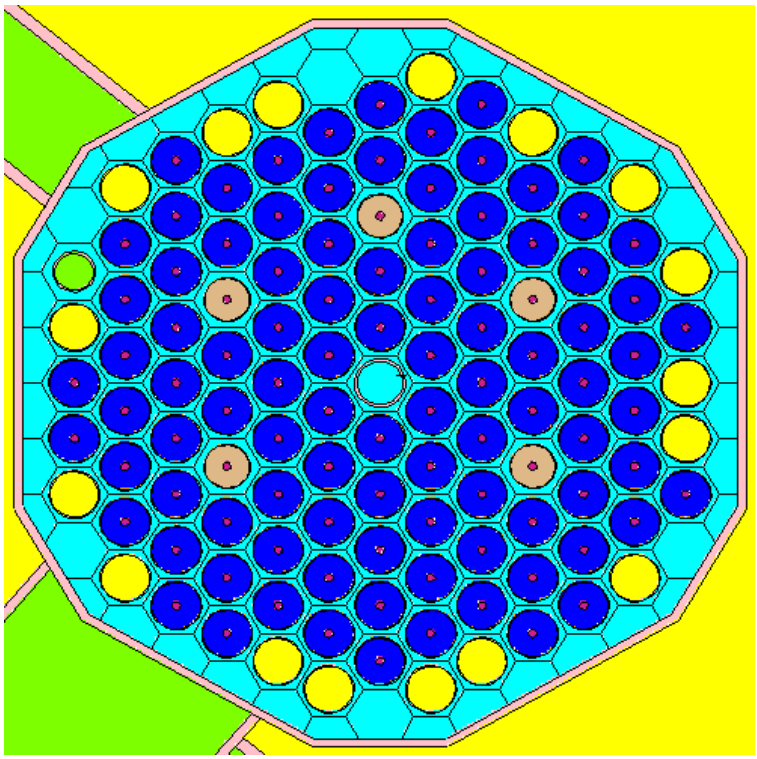

Figure 5.8- The radial view of the MCNP model of TRIGA reactor.

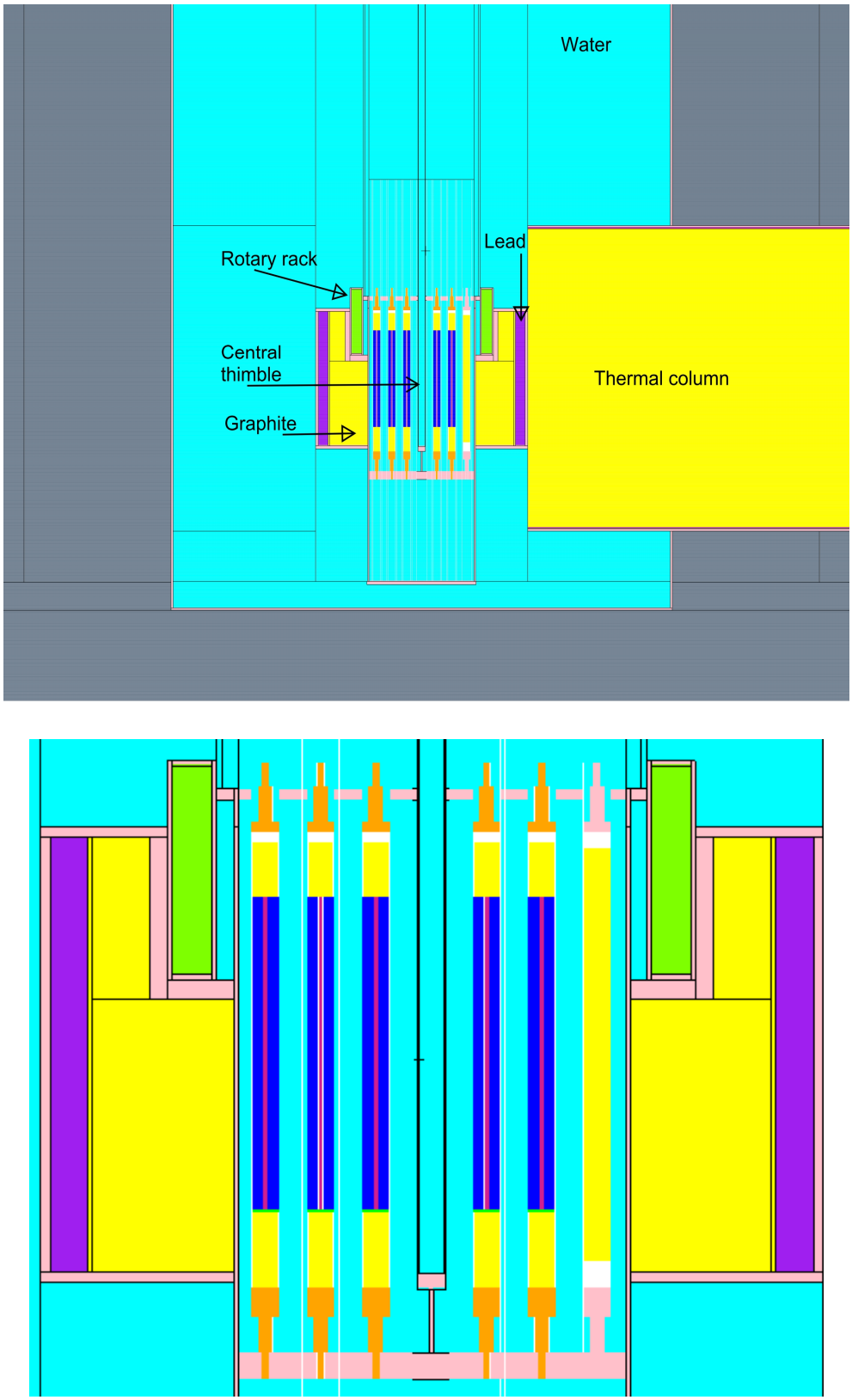

Figure 5.9- The axial view of the MCNP model of TRIGA reactor.

4. Neutronics parameters and burnup of TRIGA reactor

The calculations of the effective multiplication factor (***keff***) in the eigenvalue problems were performed with the "KCODE" option in the MCNP5 code. The initial source distribution for the ***keff*** calculations was given on the fuel meat points. The calculations were performed with 60000 cycles of iterations on a nominal source size of 60000 particles per cycle in order to decrease statistical error estimates. Initial 100 cycles were skipped to insure homogeneous neutrons source distribution. The estimated statistical errors ($1\,s$) were reduced below 10 pcm for ***keff*** values and below 0.3 % for fission rates and neutron spectra calculations.

4. 1. Core excess reactivity

Nuclear criticality, the ability to sustain a chain reaction by fission neutrons, is characterized by the effective multiplication factor (***keff***), wich is the eigenvalue of the neutron transport equation. Calculations of ***keff*** for the fresh core were performed with control rods completely in withdrawn positions. This was done because the core multiplication factor is an integral quantity and a criticality calculation is easy to perform. Also, any gross errors in the modelling should have been immediately apparent. The combined average of the absorption/collision/track-length estimators are quoted as the ***keff*** value in MCNP. Since we cannot determine the value of ***keff*** experimentally, the calculated ***keff*** values obtained by MCNP were converted to reactivity values using the following equation:

$$r = \frac{keff - 1}{keff} \Big/ b_{eff} \tag{5.1}$$

where, r is the reactivity value in units of dollar ($) and, b_{eff} is the fraction of effective delayed neutrons (b_{eff} =0.007 for TRIGA fuel types (*Gh. Negut et al., 2006 and M. T. Simnad, 1981*)).

Experimentally, fuel elements are increased stepwise in number from the initially critical minimum volume to maximum volume core. At each step, measurement is made of the increased core reactivity brought by the added fuel elements. By this method, the first criticality of the core was reached with 71 fuel elements and the maximum core excess reactivity was found to be 10.28$ with 101 fuel elements. The comparison between the MCNP calculated core excess reactivity values and the experimental one is shown in Table (5.1).

The MCNP calculated values were found to be underestimating the experimental core excess reactivity by 1.3%, 2.3% and 2.5% using ENDF/B-VI.8, JEFF-3.1 and JENDL-3.3 data libraries, respectively. However, an overestimated value of 2.7% was observed using ENDF/B-VII.0 data library.

Table 5.1- Comparison between the calculated and experimental core excess reactivity.

	Reactivity value ($)	**C/E**
Experiment	10.27	–
ENDF/B-VII	10.55 ± 0.01	1.027
ENDF/B-VI.8	10.14 ± 0.01	0.987
JEFF-3.1	10.03 ± 0.01	0.977
JENDL-3.3	10.02 ± 0.01	0.975

4. 2. Control rod worth

The calculation of the control rods worth simulated explicitly the experiment which was carried out by the positive period method (*T. MATSUMOTO et al., 2000*). Using this method, the worth of one control rod was measured in the presence of other rods used for compensating the excess reactivity. We started the simulation with the control rods critically positioned calculating the $keff_0$ of the core. Then one of the control rods was withdrawn at a certain position "*i*", calculating the new $keff_i$ value. The control rod worth represented by reactivity r for that position was determined by comparing $keff_i$ and $keff_0$ as denoted by *Eq. (5.2)*. The propagated error is deduced from *Eq. (5.3)* (*Hugo M. Dalle et al., 2002*):

$$r = r_0 - r_1 \tag{5.2}$$

$$= (1 - \frac{1}{keff_0}) - (1 - \frac{1}{keff_i}) = \frac{1}{keff_i} - \frac{1}{keff_0}$$

$$\Delta r = \left(\left(\frac{\Delta keff_i}{keff_i} \right)^2 + \left(\frac{\Delta keff_0}{keff_0} \right)^2 \right)^{1/2} \tag{5.3}$$

Figures (5.10) to (5.14) show the MCNP calculated integral reactivity curves for Shim I, Shim II, Shim III, Shim IV and Regulating rod, respectively.

From these curves it can be observed that the MCNP calculated integral reactivity worth of control rods Shim I, Shim II and Shim III are consistent. The measured reactivity worth of

Shim IV and Regulating rod are slightly superior to the calculated results. Nevertless, this small disagreement remains acceptable regarding the published results of some other TRIGA reactors (*M. Q. Huda et al. 2004, and Hugo M. Dalle et al., 2002*). Also, it can be seen that, for all control rods the largest differences between measured and calculated reactivity worth occurred when the rods supposed fully withdrawn. The calculated and measured reactivity worth due to the withdrawing of the rods from 90% to 100% is less than 0.1$ and around 0.5$ when withdrawing from 40% to 50%. Table (5.2) shows a comparison of the total reactivity worth of all the control rods. It can be seen that, the maximum differences obtained are 2% for Shim I with ENDF/B-VI.8, 8% for Shim II with ENDF/B-VI.8, 4% for Shim III with JEFF-3.1, 8% for Shim IV using JENDL-3.3 and 6% for Regulating rod with JEFF-3.1.

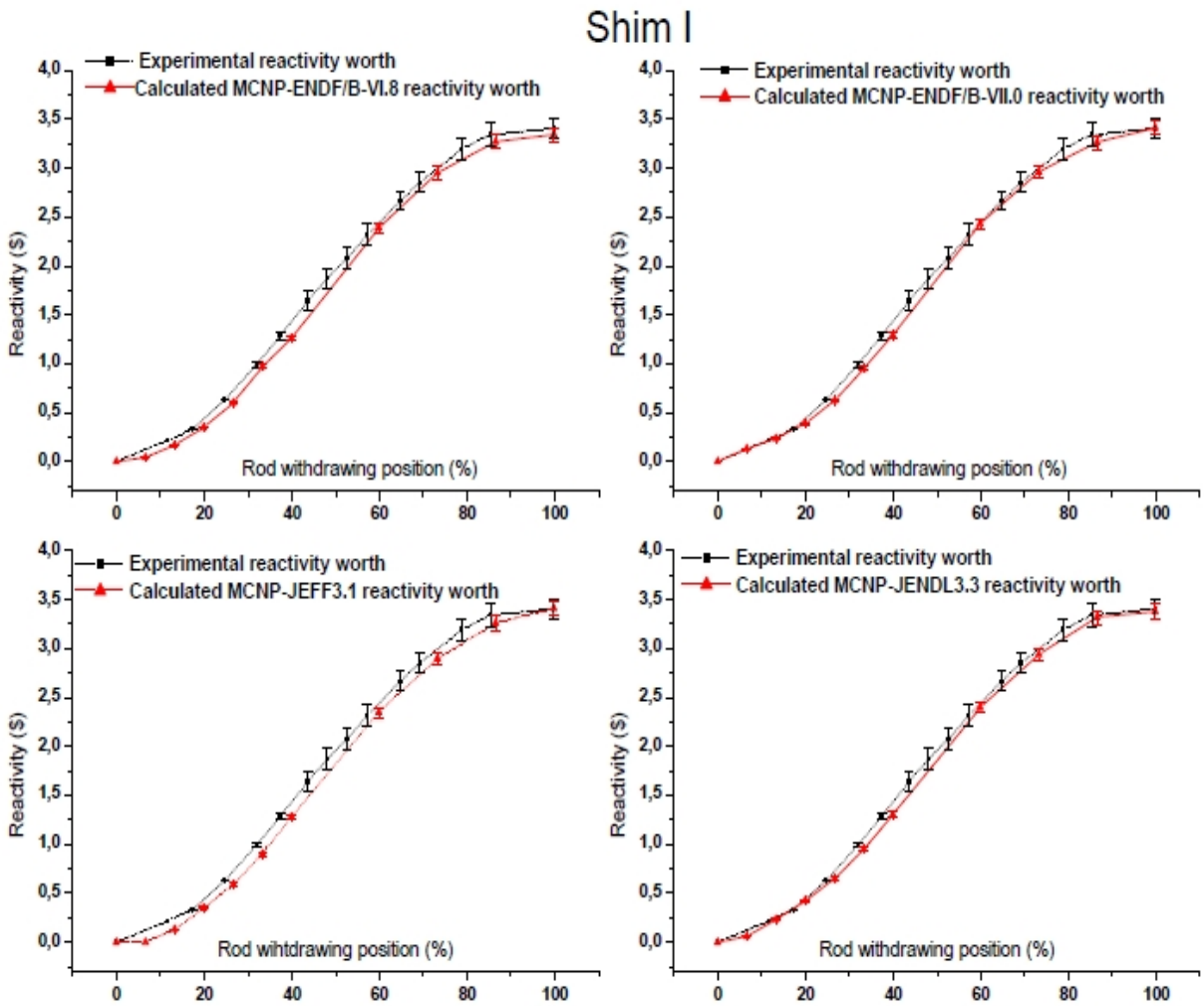

Figure 5.10- MCNP calculations and experimental integral rod worth for Shim I.

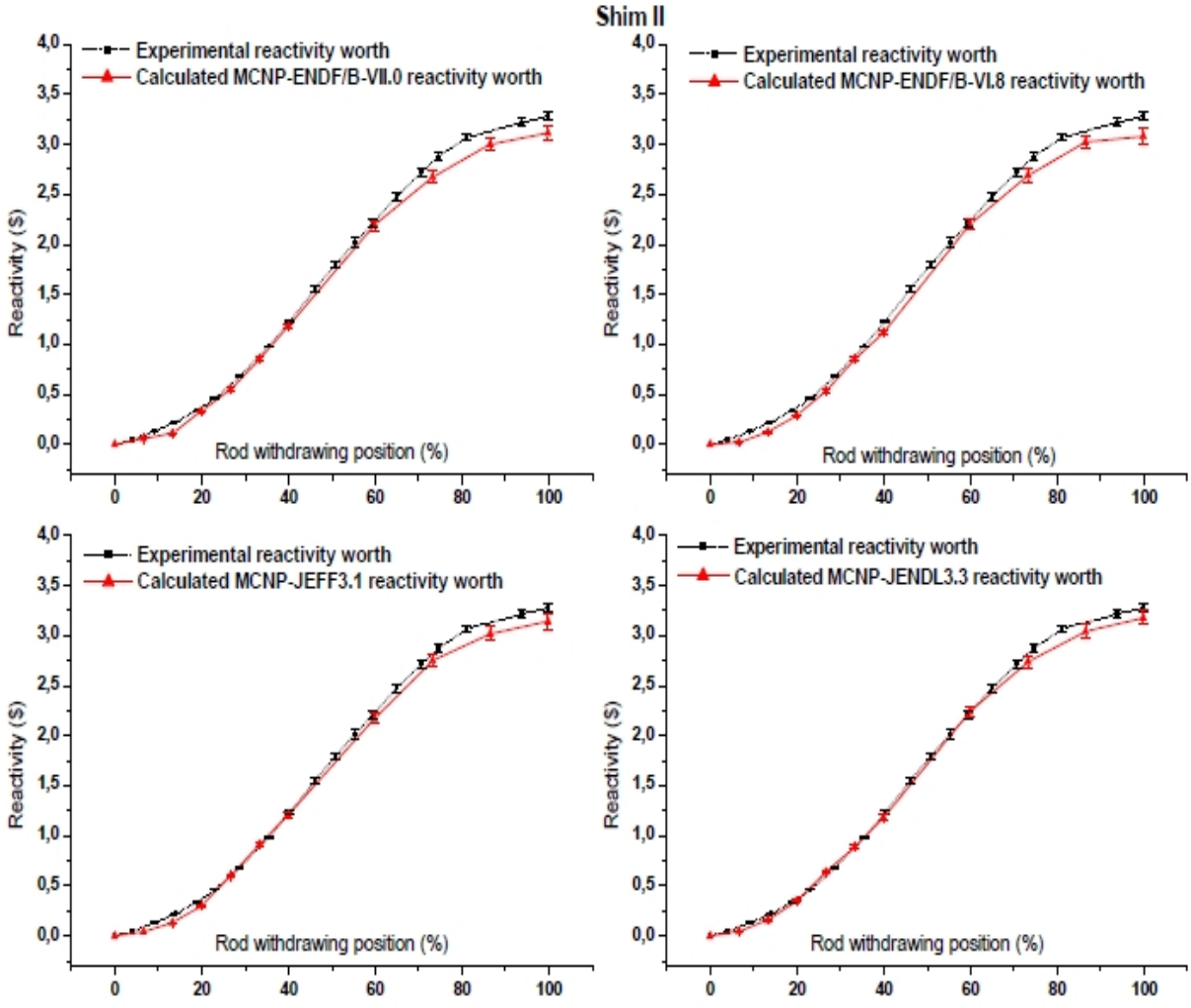

Figure 5.11- MCNP calculations and experimental integral rod worth for Shim II.

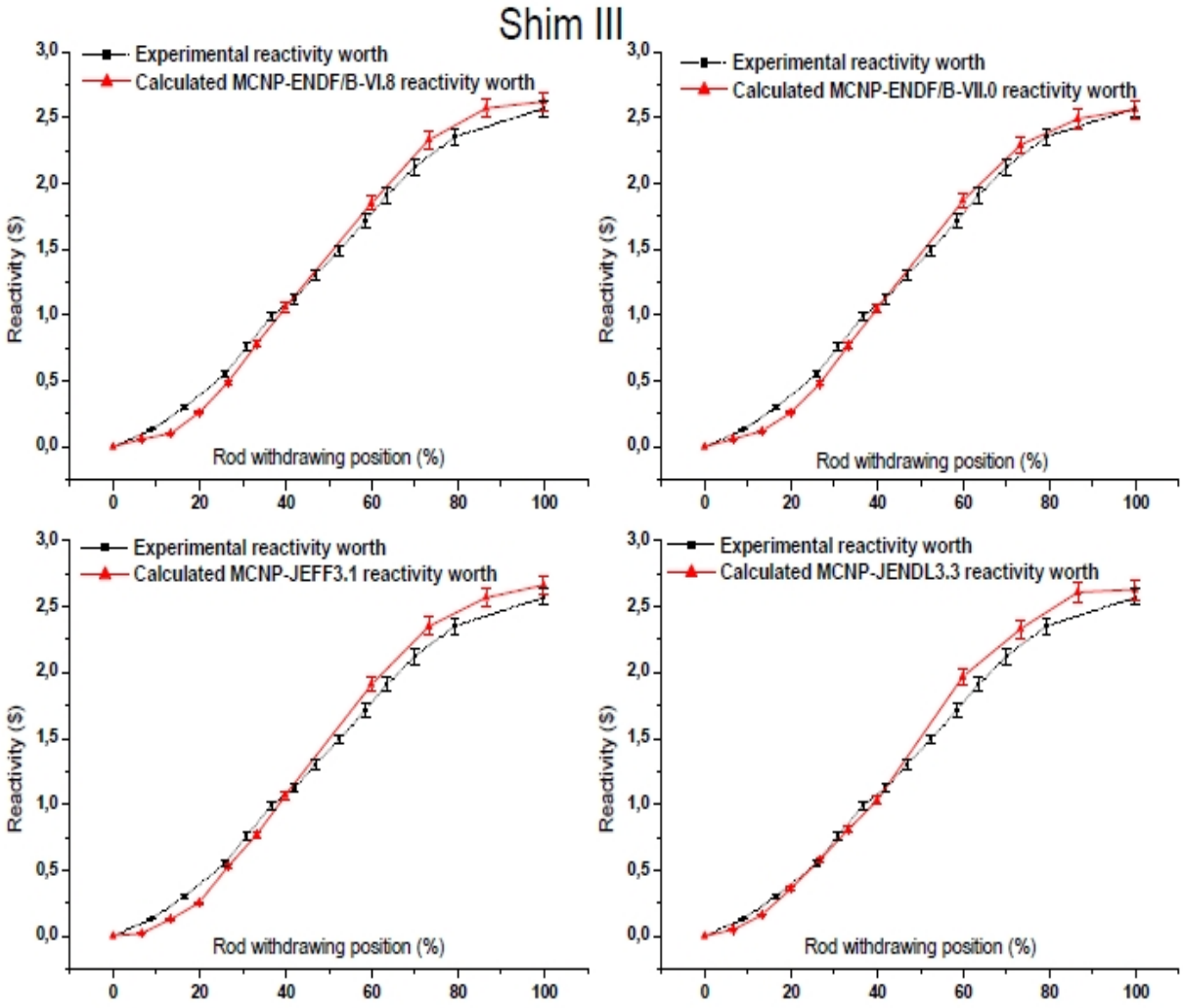

Figure 5.12- MCNP calculations and experimental integral rod worth for Shim III.

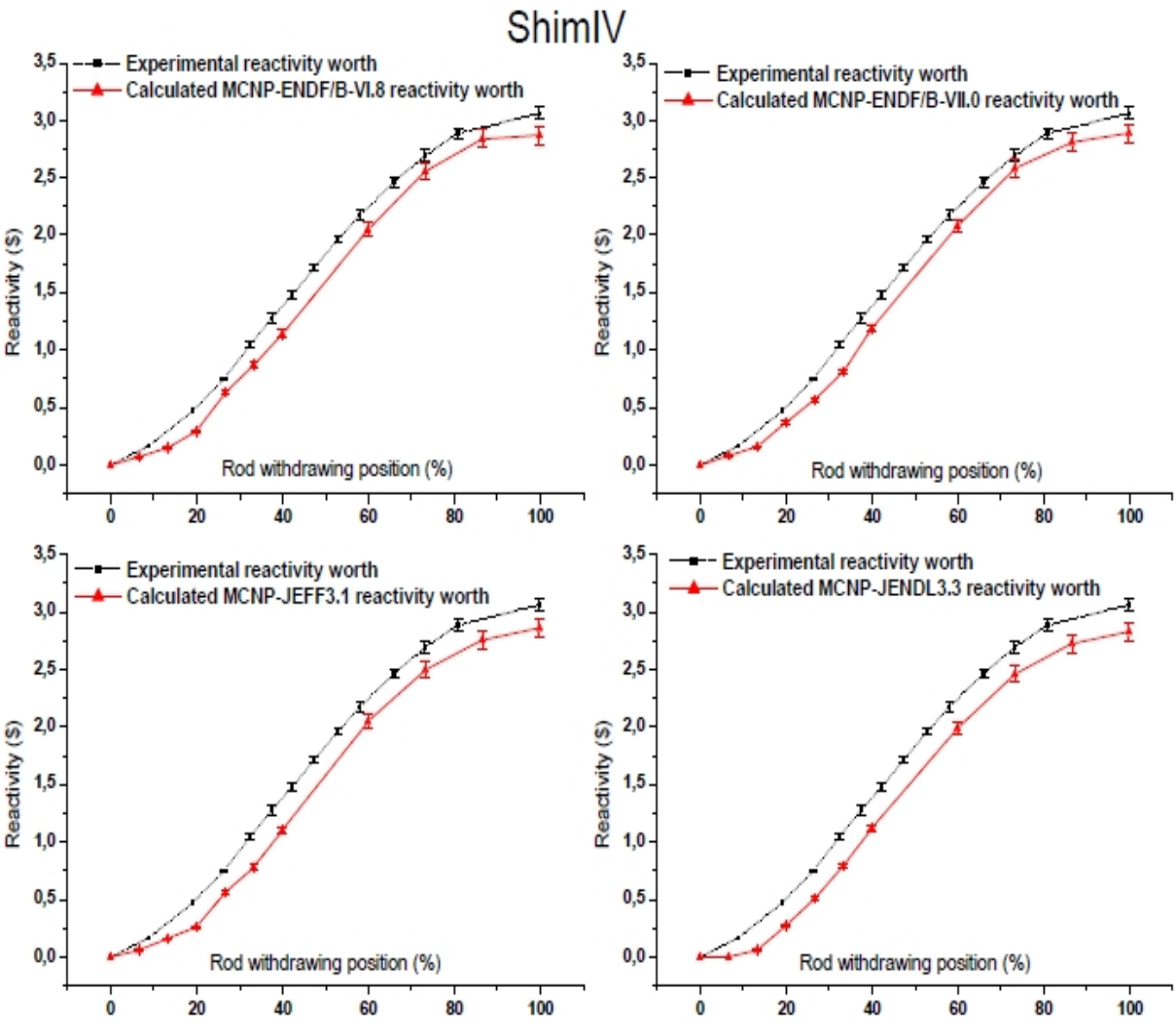

Figure 5.13- MCNP calculations and experimental integral rod worth for Shim IV.

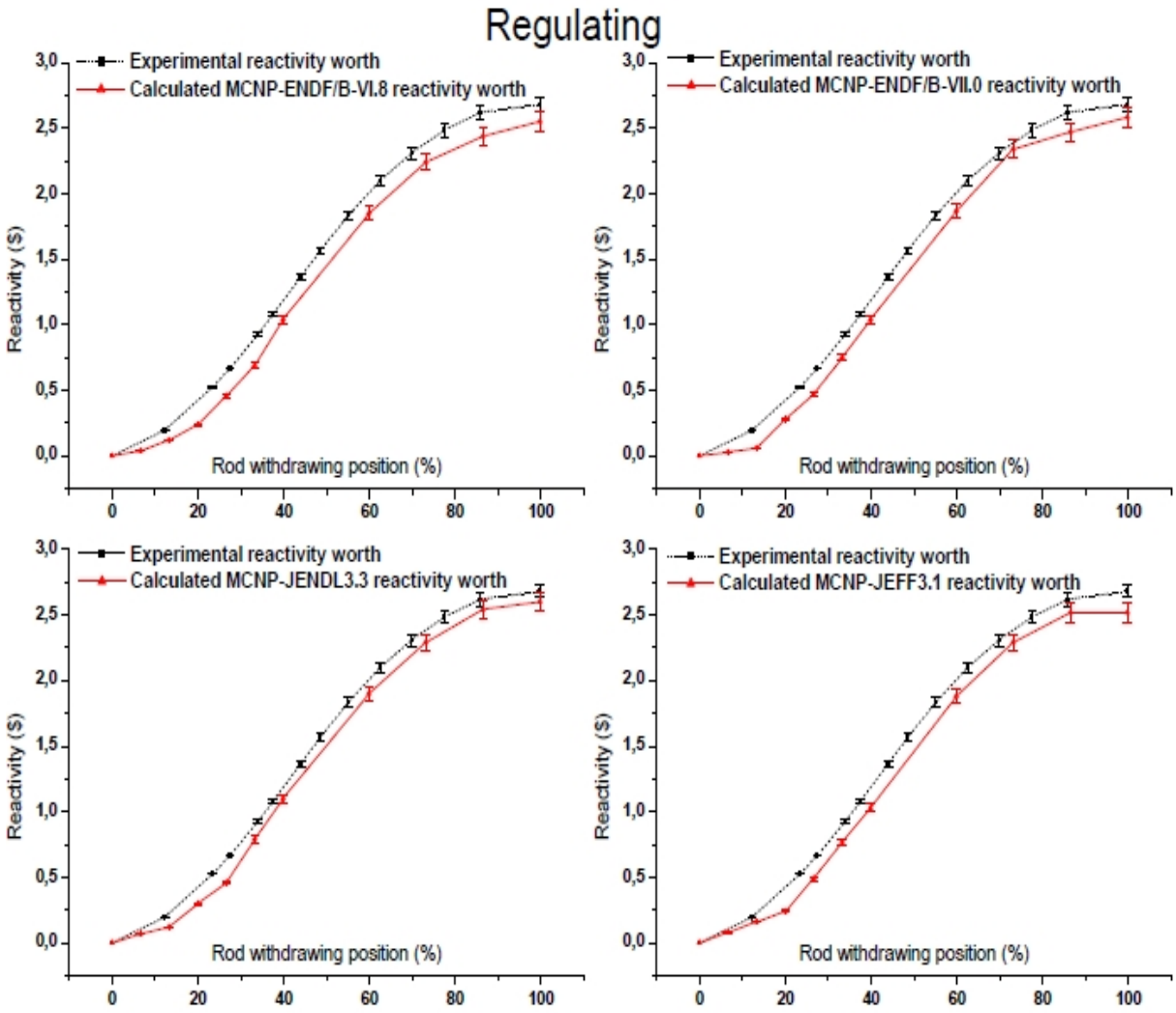

Figure 5.14- MCNP calculations and experimental integral rod worth for Regulating rod.

Table 5.2- Comparison between the MCNP calculated and measured total reactivity worth of TRIGA reactor control rods.

	C/E			
Control rod	**ENDF/B-VII**	**ENDF/B-VI.8**	**JEFF-3.1**	**JENDL-3.3**
Shim I	1.00	0.98	1.00	0.99
Shim II	0.93	0.92	0.94	0.95
Shim III	1.02	1.02	1.04	1.02
Shim IV	0.94	0.94	0.93	0.92
Regulating	0.96	0.95	0.94	0.97

4. 4. Power peaking factors

As a first application of the elaborated MCNP model of the TRIGA reactor, it was used for the calculation of three power peaking parameters.

1. Hot rod power peaking factor f_{HR}.
2. Axial power peaking factor f_Z.
3. Radial power peaking factor f_R.

These three factors are important for steady state operations; they determine the maximum total power released by one fuel element as well as its axial and radial peaking values which are used as input parameters in thermal-hydraulic analysis (maximum fuel temperature calculation, fuel and cladding temperature distribution, departure from nucleate boiling ratio calculation, etc …).

The calculated power peaking factors can be defined as follows (*Luka Sonj et al., 2008*):

The hot rod power peaking factor is considered as the ratio between the maximum power released by one fuel rod $(P_{Rod})_{\max}$ and the average power per element in the core $\overline{P}_{Core}$,

$$f_{HR} = \frac{(P_{Rod})_{\max}}{\overline{P}_{Core}} \tag{5.4}$$

and

$$\overline{P}_{Core} = \frac{P}{N_{EL}} \tag{5.5}$$

where, P is the total power, which is 2MW in our case. The term N_{EL} is the number of fuel elements, which is considered to be 101 (96 fuel elements + 5 fuel follower control rods).

The axial power peaking factor f_Z is defined as peak-to-average axial power density $p(z)$ in the fuel element.

$$f_Z = \frac{p(z)_{\max}}{\overline{p}_Z} \tag{5.6}$$

The radial power peaking factor f_R is defined as peak-to-average radial power density $p(r)$ in the fuel element.

$$f_R = \frac{p(r)_{\max}}{\overline{p}_R} \tag{5.7}$$

In our calculations, we assumed that the power density is directly proportional to the fission density. In MCNP, this is done by the use of tally F6. Thus, the hot rod power peaking factor f_{HR} was deduced by calculating the fission density integrated over the entire volume of the

fuel meat in every fuel rod (*Luka Sonj et al., 2008*) and searched for the fuel rod with maximum integral fission density. Then we calculated the average fission density of all the rods and calculated the peaking factor according to *Eq. (5.4)*. The axial power peaking factor f_Z was calculated by dividing axially the hot rod fuel element into several volumes (*Luka Sonj et al., 2008*) and calculating the fission density integrated over each of the volumes then the axial power peaking factor was calculated by dividing the maximum axial fission density to the average axial fission density according to *Eq. (5.6)*. For the radial power peaking factor f_R, calculation was done by dividing the hot rod fuel element radially into several volumes (*Luka sonj et al., 2008*) and following the same way as in the case of f_Z.

Figure (5.15) gives the total power distribution calculated by MCNP within fuel and fuel follower elements. The fuel and fuel follower elements numbering is such that numbers from 1 to 6 represent the B ring of fuel elements arrangement (*Fig 5.7*), and similarly from 7 to 18 represent the C ring, from 19 to 36 represent the D ring, from 37 to 60 represent the E ring, from 61 to 90 represent the F ring and from 91 to 101 represent the G ring.

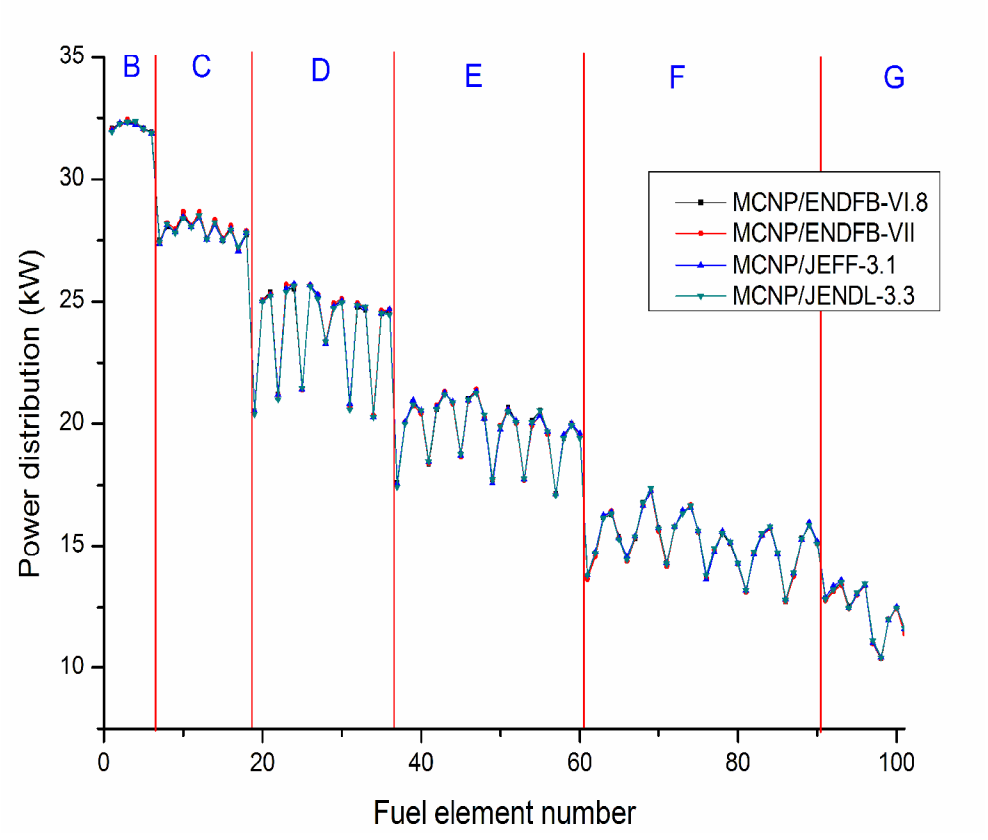

Figure 5.15- Power distribution within the fuel and fuel – follower elements of the TRIGA reactor core at 2MW operation.

The maximum power produced in the hottest fuel element is found to be 32.42kW in B3 fuel element with ENDF/B-VII, 32.32kW in B2 fuel element with ENDF/B-VI.8, 32.30kW in B2

fuel element with JEFF-3.1 and 32.36kW in B3 fuel element with JENDL-3.3. Based on these results, the calculated hot rod power peaking factors are found to be 1.62 for ENDF/B-VI.8, ENDF/B-VII, JENDL-3.3 and 1.61 for JEFF-3.1.

Figure (5.16) shows the axial power distribution within the fuel meat of the hottest fuel elements calculated by MCNP. This figure shows an almost analytical chopped cosine shape of axial power distribution with a peak-to-average value of 1.28 obtained by all the libraries at the middle point of the fuel elements which is equivalent also to the axial mid-

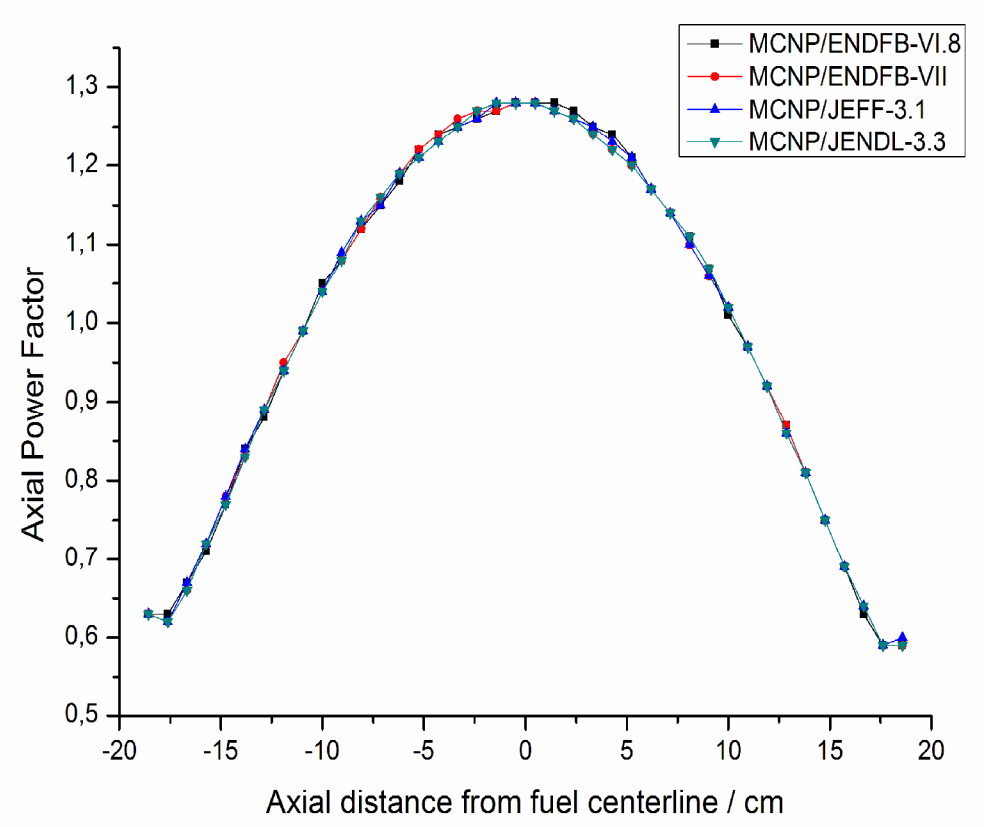

Figure 5.16- Hot channel fuel axial power factor profiles.

plane of the core. One other thing to note is that the small increments shown on the left and the right sides of the axial power profiles are principally due to the lower and upper graphite reflectors of TRIGA fuel element (*Fig. 5.3*).

Figure (5.17) gives the radial power distribution within the fuel meat of the hottest fuel element calculated using MCNP code. The power density is approximately proportional to the thermal flux distribution, which reaches its maximum in water around the element and decreases in the fuel element due to much higher absorption in fuel than in water (*S. I. Bhuiyan, et al., 1992*). The radial power peaking factor obtained is 1.91 by all data libraries.

On the basis of thermal-hydraulic analysis it was concluded that maximum hot rod power peaking factor ranging between 1.6 and 1.7, an axial power peaking of 1.3 and a radial power

peaking factor ranging from 1.7 to 2 are acceptable for 2MW operation according to the Final Safety Analysis Report (FSAR) and (*M. Ravnik, 1995*). This indicates that our calculated hot rod, axial and radial power peaking results present a good agreement with the recommended values.

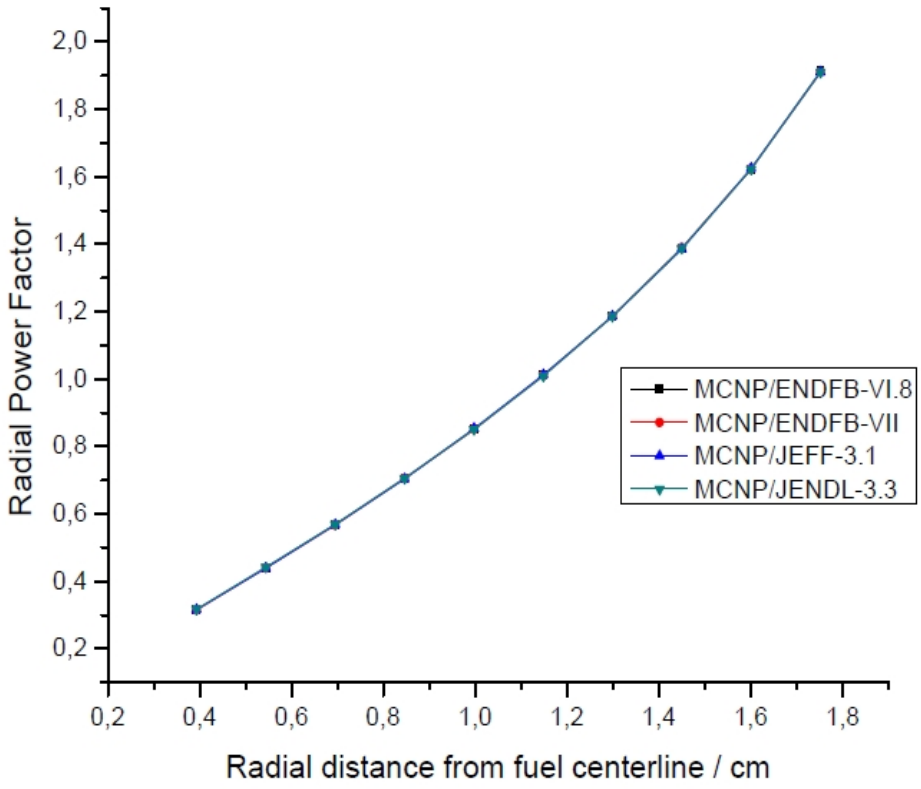

Figure 5.17- Hot channel fuel radial power factor profiles.

5. Effet of temperature on neutron spectrum

5. 1. Temperature coefficient of reactivity

TRIGA fuel was developed around the concept of inherent safety. A core composition was sought which had a large prompt negative temperature coefficient reactivity (a) such that if all the available excess reactivity were suddenly inserted into the core, the resulting fuel temperature increase would automatically cause power excursion to terminate before any induced core damage resulted. Experiments demonstrated that zirconium hybrid possesses a basic mechanism to produce the desired characteristic (M. T. Simnad, 1981).

The Moroccan TRIGA MARK II research reactor has a prompt negative temperature coefficient reactivity (*Eq. (5.7)*) value of -0.01% ($dk/k/°C$) (FSAR). In this section, we studied the evolution of the core excess reactivity due to two different operating conditions. Cold condition means that the reactor temperature is 300 K and hot condition, reached for full

power operating conditions. Table (5.3) gives the prompt negative temperature coefficient reactivity calculated by MCNP using the four libraries for our TRIGA model.

In this purpose we have prepared our cross section libraries at the desired temperatures for the fuel meat, cladding and water around the fuel elements. The thermal scattering S(α, β) tables were determined. The effect of thermal expansion of water is taken into account whereas it is supposed to be negligible for the fuel meat and cladding material (*Ch. Tippayakul et al., 2008*).

$$a = \left[\left(\frac{1}{k_{eff,Cold}} \right) - \left(\frac{1}{k_{eff,Hot}} \right) \right] / (T_{Hot} - T_{Cold}) \qquad (5.7)$$

where, $k_{eff,Hot}$ is the effective multiplication factor at hot conditions, $k_{eff,Cold}$ is the effective multiplication factor at cold conditions, T_{Hot} is the fuel temperature at hot conditions and T_{Cold} is the fuel temperature at cold conditions.

Table 5.3- The prompt negative temperature coefficient reactivity calculated by MCNP for our TRIGA model.

	ENDF/B-VI.8	**ENDF/B-VII**	**JEFF-3.1**	**JENDL-3.3**
$a\ (dk/k/°C)$	-0.0085	-0.0085	-0.0085	-0.0086

As it can be shown in Table (5.3), all the libraries produces results which are slightly underestimated in comparison with the recommended FSAR value -0.01% ($dk/k/°C$), which can be due to the fact that the thermal expansion phenomenon for the fuel meat and cladding material were considered with no effect.

5. 2. Effect of temperature on neutron spectrum

As our MCNP model of TRIGA reactor reproduces very well neutronics parameters of the core both at cold and hot conditions, we performed in this section, spectra calculation for the TRIGA fuel meat located in B ring by means of tally (F4). The neutron energy range was divided to 35 bins, the maximum standard deviation value was found to be less than 0.11% for 24000000 neutron histories. Results for each of the libraries used in this study are shown in Figure (5.18).

So from these spectra, it can be noticed that the dependent energy fluence in the thermal range changes noticeably with of the average fuel temperature while the spectrum in the fast and epithermal ranges remains almost the same when the average fuel temperature increases. It is evident from the close-up plots of Figure (5.19) that the up-scattering rate by the bounded H

in ZrH increases as the average fuel temperature increases. Increase in fuel temperature results in shift and deformation of the Maxwellian spectrum in fuel while the spectrum in water is slightly affected, because the water temperature remains almost constant. Consequently, the fuel reaction rate is decreased, while it remains constant in a non-fission part of the unit cell (the water and cladding). So the ratio between fission and the absorption reaction rate is reduced on the average over the entire unit cell. The multiplication factor is thus reduced, and the spectrum hardening effect is negative (*S. I. Bhuiyan et al., 1991*). This phenomenon causes the decreasing of the TRIGA core reactivity as observed by the calculations (*Tab. 5.3*). Although the up-scattering by the bounded H in ZrH is the major effect that decreases the core excess reactivity in TRIGA core, the Doppler broadening has also an impact on the change in the excess reactivity because, the absorption rate in the fuel meat increases with increasing average fuel temperature due to the Doppler broadening (*Ch. Tippayakul et al., 2008*). The excess reactivity generally decreases with the increasing absorption rate. Therefore, it is clear that Doppler effect is another phenomenon which decreases the excess reactivity of TRIGA reactor.

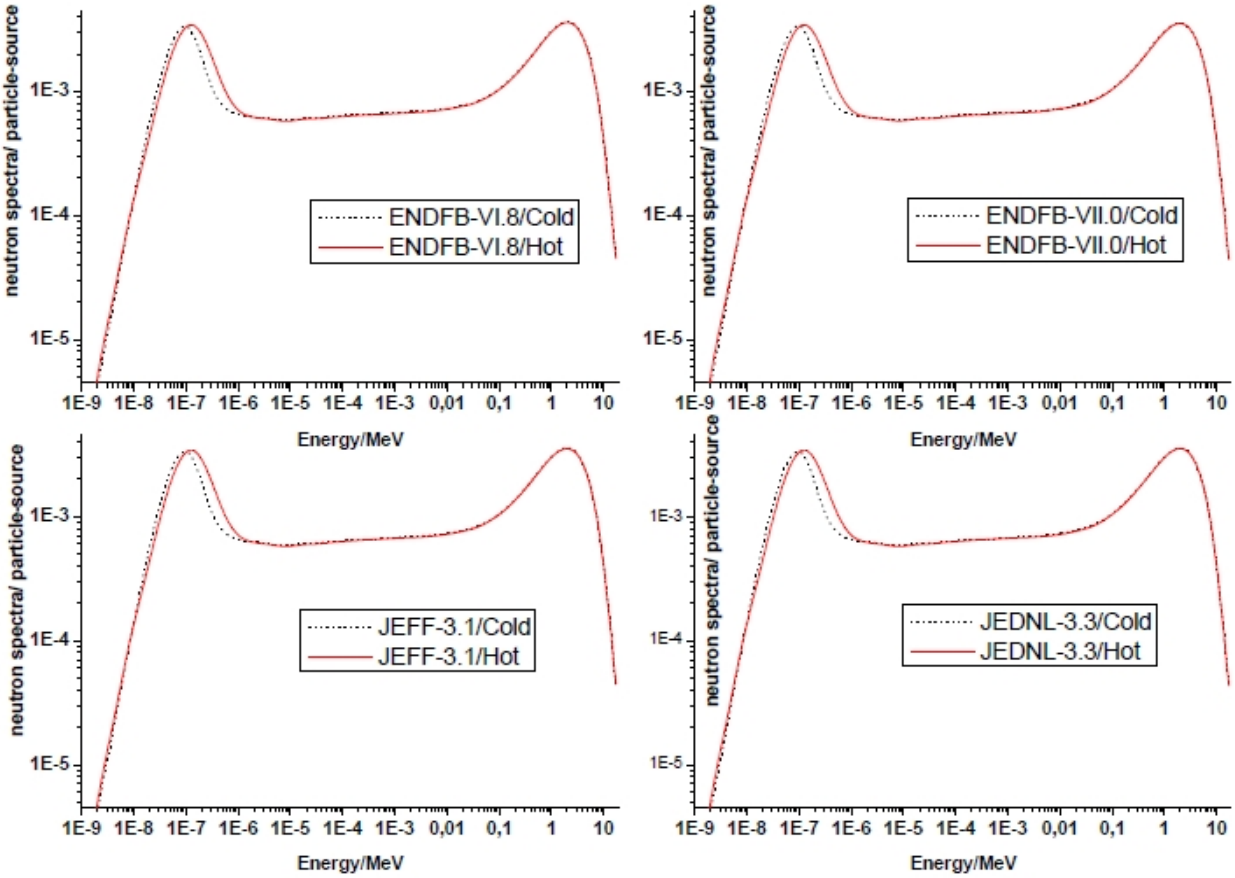

Figure 5.18- Neutron energy spectrum for the TRIGA fuel element located in B ring calculated by MCNP.

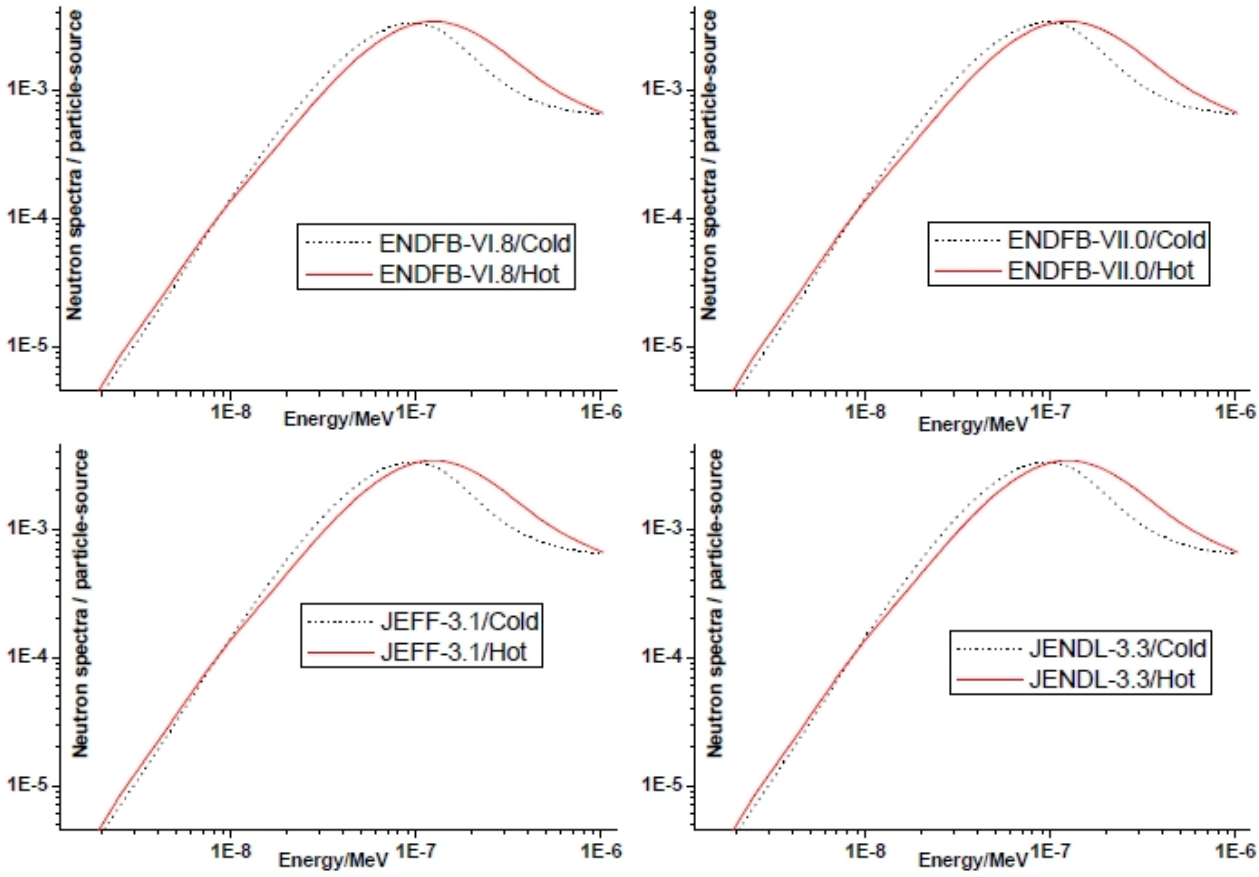

Figure 5.19- Close – up plots in thermal range.

6. Burnup calculation of the TRIGA reactor

The principal thrust of this section is on the burnup calculation of the 2MW TRIGA MARK II research reactor at CENM. By burnup we mean the following changes in the core: 1) depletion of U235, 2) fission products build-up, 3) spectral changes of flux, 4) negligible plutonium and 5) depletion of burnable poison.

6. 1. Description of the burnup calculation

The criticality calculation gave confidence to perform a set of burnup calculations for the core loaded with fresh LEU fuel. Burnup calculations were performed for realistic operating conditions at full power using our new elaborated burnup code BUCAL1 (*B. El Bakkari et al., 2008; B. El Bakkari et al. 2009*) and the latest nuclear data library ENDF/B-VII. The initial burnup steps in the calculation were taken smaller to consider the Xe and Sm build-up poisoning. The calculations were done using 2850000 neutrons histories and the standard deviation on *keff* values was found to be ± 45pcm.

In order to optimize the MCNP calculation time, the 101 fuel elements in the TRIGA core were grouped into 7 different groups taken into account their power level distribution deduced from Figure (5.15) and represented by Figure (5.20). Then burnup calculations were done for just 7 separate fuel elements instead of 101 fuel elements. Each of the seven fuel elements represents one different group. Figure (5-20) shows the 7 different groups of fuel elements.

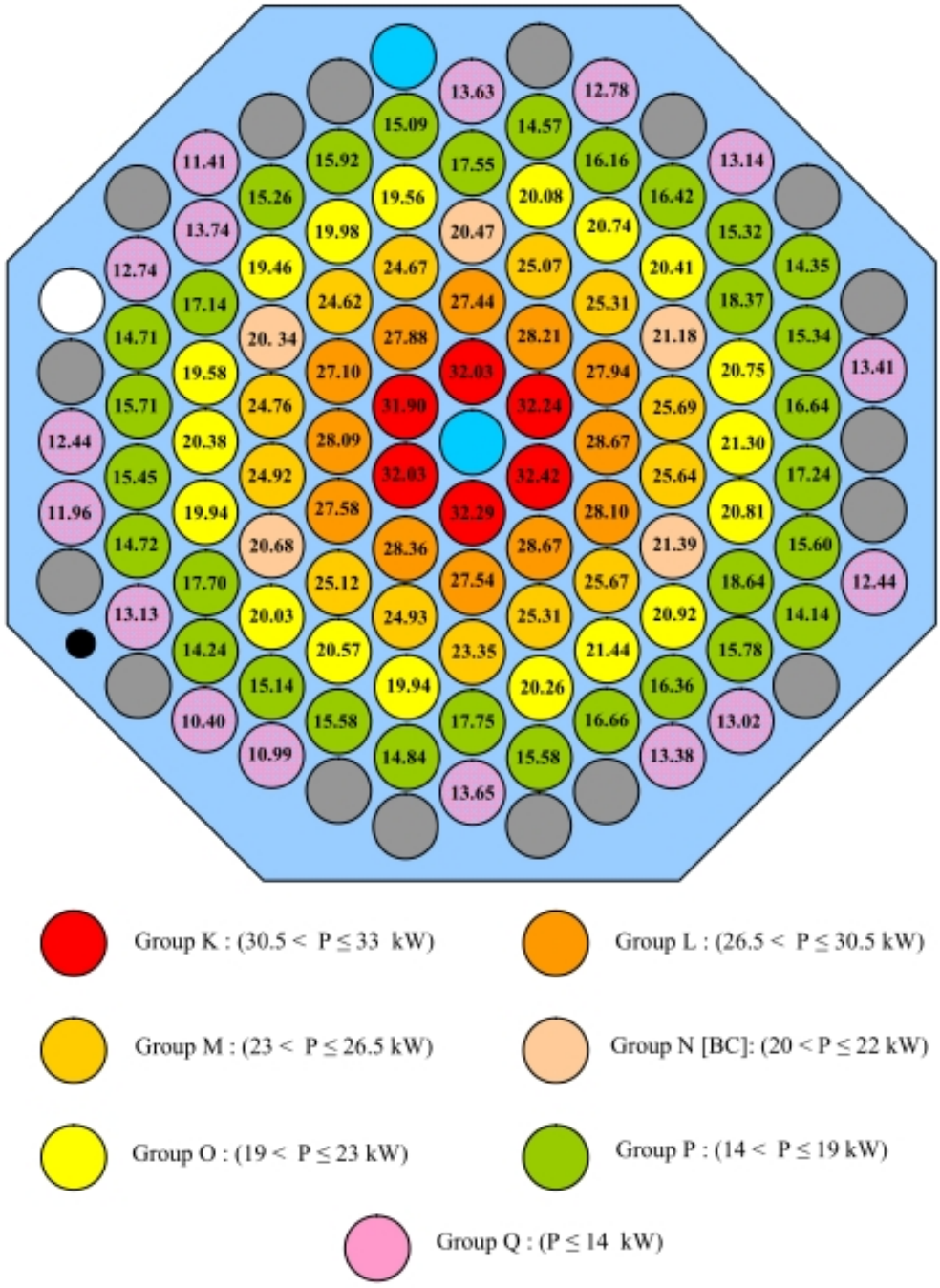

Figure 5.20- Fuel elements distribution for burnup calculation.

6. 2. TRIGA core life time estimation

The calculation of the *keff* and its relationship with core burnup is of primary importance to determine the core life time. First the excess reactivity for the beginning of the core life was calculated by MCNP at 2 MW reactor power and was found to be 6.77$ (*keff* = 1.04975). Then burnup calculation was performed for the TRIGA core without changing the loading pattern to determine the core life of the primary fuel cycle and for the primary core configuration. The variation of *keff* as a function of total thermal power produced in the core is presented on Figure (5.21).

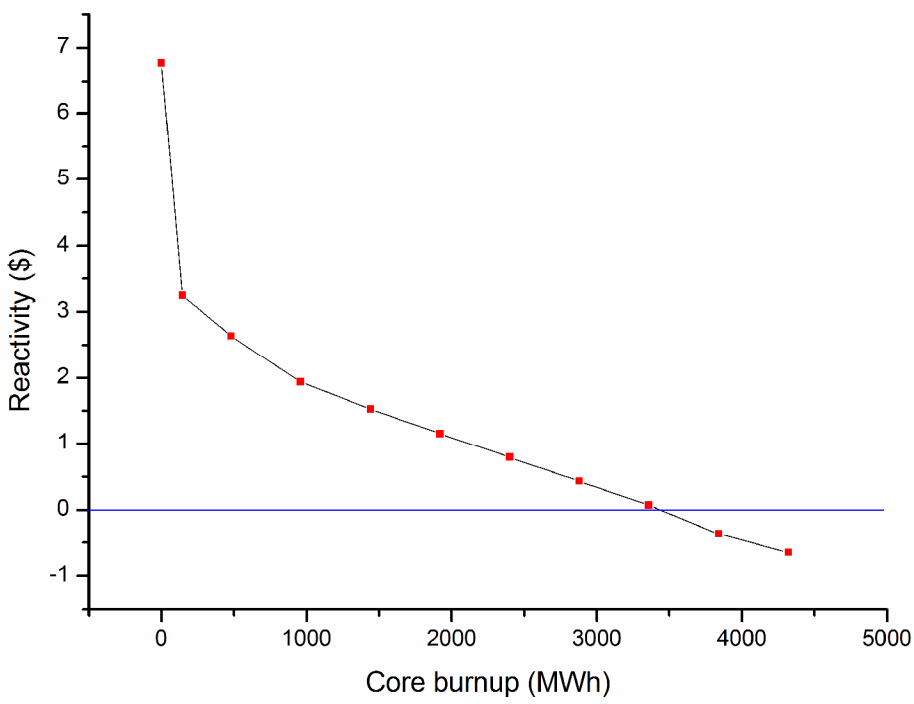

Figure 5.21- Excess of reactivity ($) for TRIGA reactor as a function of burnup (MWh).

At the initial burnup time a sharp loss of reactivity of 3.52$ is observed which is particularly due to the build-up of ^{135}Xe and ^{149}Sm. The concentration of these fission products poisons influence strongly the reactivity and eventually reaches equilibrium at about 150MWh and 1500MWh for Xe and Sm respectively (*Figs. 5.22 and 5.23*). The excess reactivity becomes zero at 3360 MWh of reactor operating history which correspond to 73 days of continuous operating at full power which represents the life time of primary fuel cycle for the actual core configuration.

The individual burnup (% ^{235}U depletion) of fuel and fuel-follower elements is calculated for each of the seven groups during the core life time (*Fig. 5.20*). The results are shown in Figure (5.24). The maximum value (~ 7 %) of ^{235}U depletion is observed for group K which

corresponds to the hottest fuel elements of B ring (*Fig. 5.7*). Then the ^{235}U depletion decreases when passing from the core centre to the core periphery until it reaches its minimal value of 2.8 % for fuel elements of Q group. The core average burnup is found to be 4.54 %.

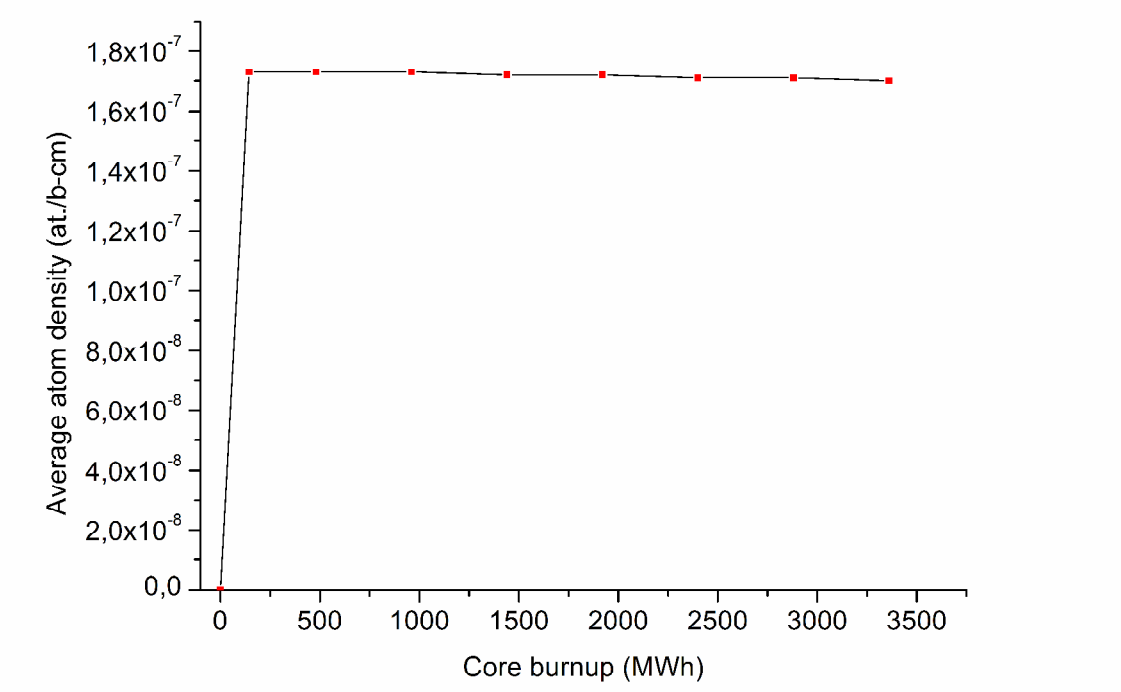

Figure 5.22- ^{135}Xe build-up as a function of core burnup.

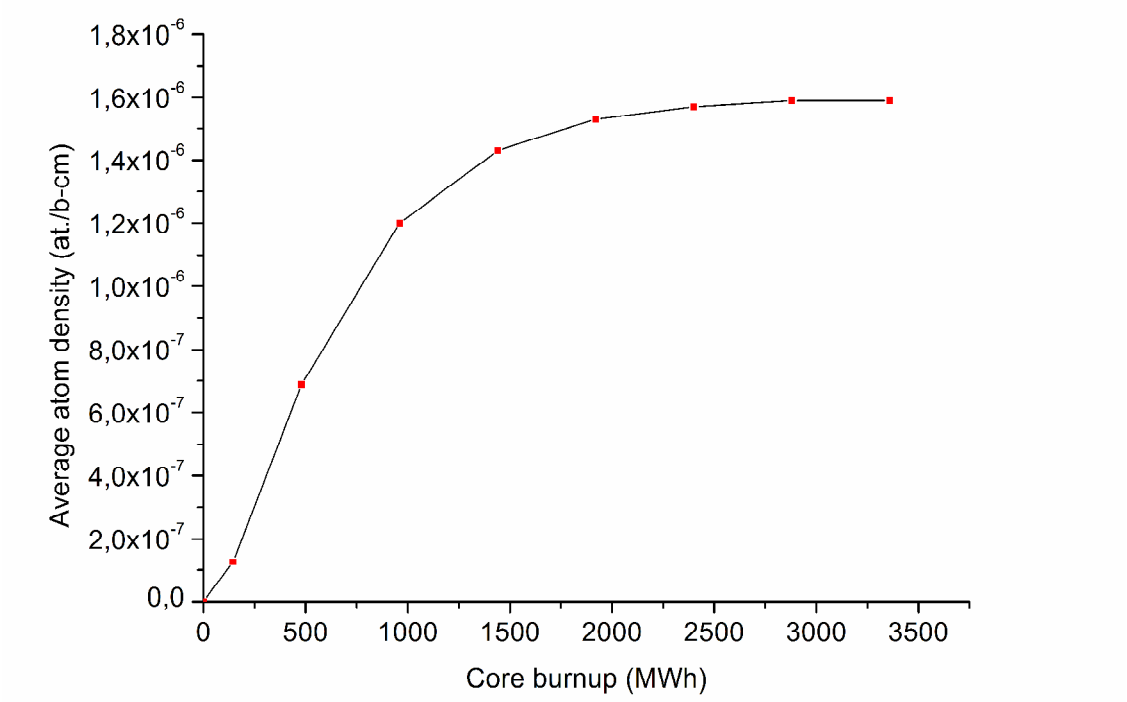

Figure 5.23- ^{149}Sm build-up as a function of core burnup.

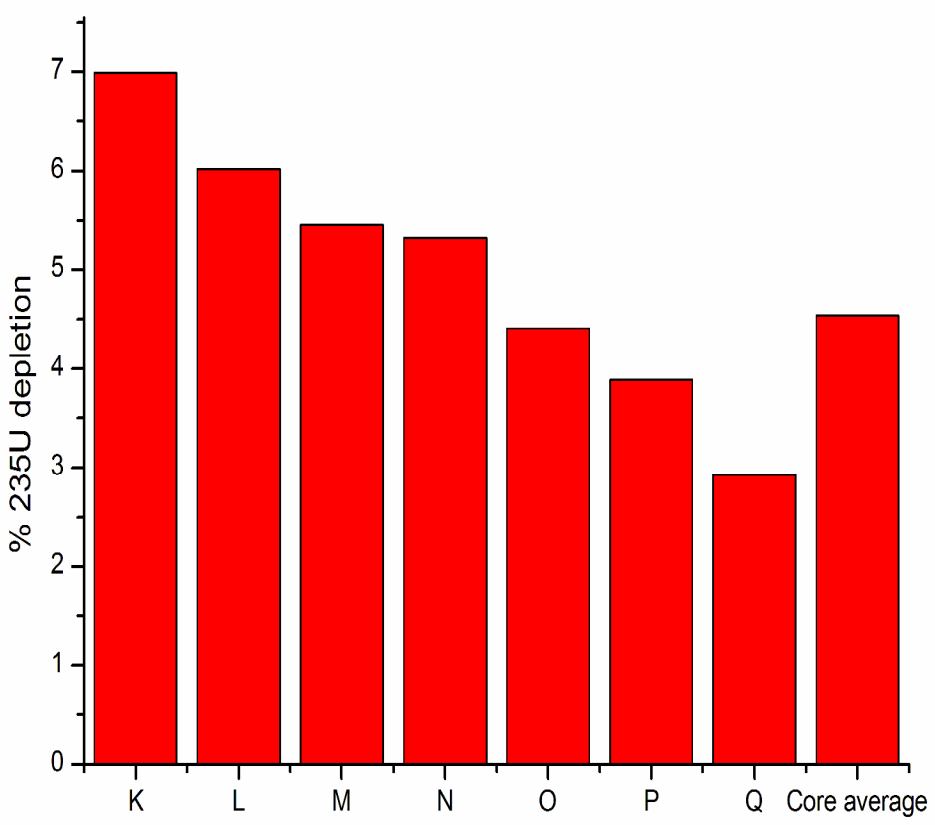

Figure 5.24- % ^{235}U depletion as a function of fuel groups.

6. 3. Axial and radial in-core flux distributions

Typical three-energy groups average neutron axial and radial flux distributions at the beginning of life (BOL) and end of life (EOL) of the core for 2 MW operating power were calculated and plotted in Figures (5.25) and (5.26), respectively.

For radial flux distribution, it is shown that, the thermal flux peaks in the central thimble which is considered to be filled with water. This distribution falls sharply to ~40% of its initial value in B-ring. The fall continues down to G-ring. In the graphite reflector, the thermal flux falls down with ~70% of its G-ring value. Epithermal and fast fluxes peak in B-ring and fall down to the outer region.

Axially, the three-group average neutron fluxes peak at the axial mid-plane of the TRIGA core and fall down gradually as a cosine function.

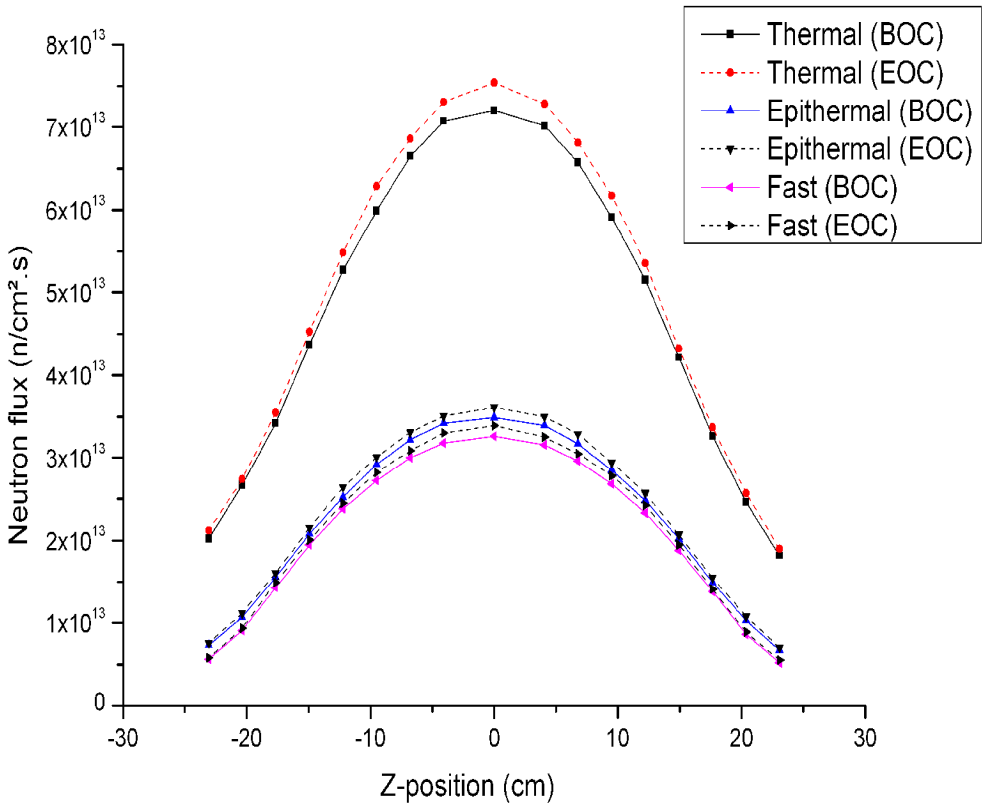

Figure 5.25- In-core axial flux distribution.

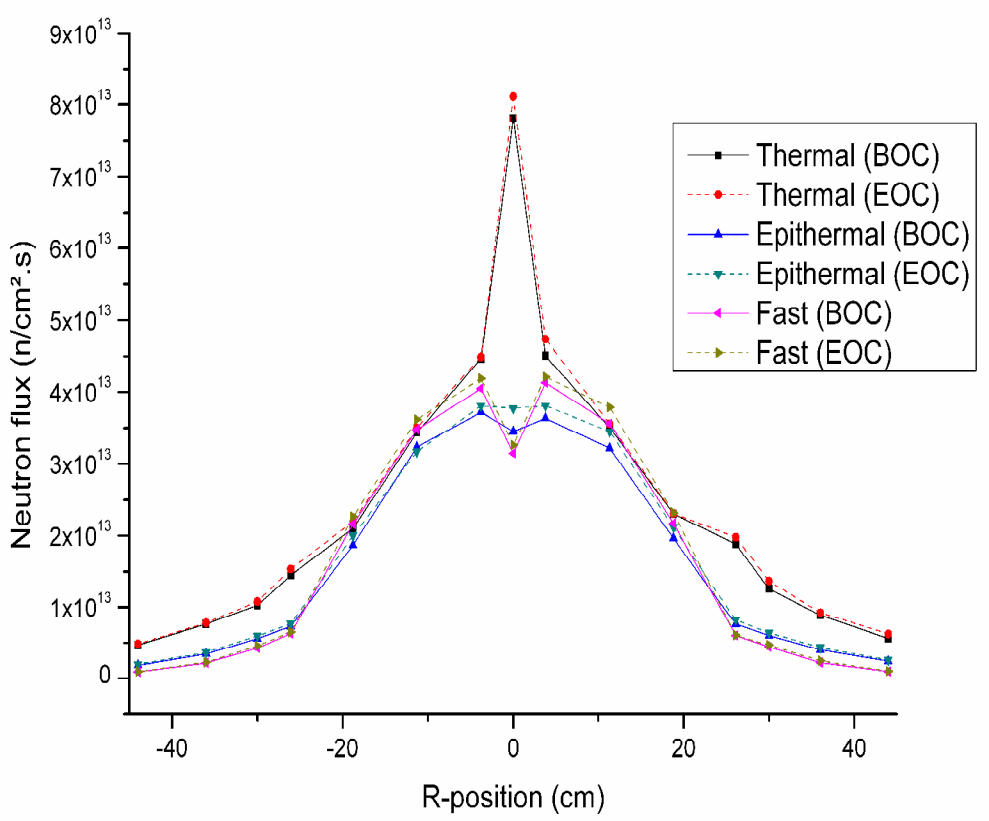

Figure 5.26- In-core Radial flux distribution.

7. Conclusion

The complete and detailed 3D MCNP model of the Moroccan TRIGA MARK II research reactor is presented. ENDF/B-VI.8, ENDF/B-VII, JEFF-3.1 and JENDL-3.3 neutron cross section evaluations were used for this study. Several continuous cross sections at various temperatures were processed for the MCNP code using the updated NJOY99 system. The consistency and accuracy of the MCNP model was established by comparing calculations to the experimental results of the benchmark experiments. Most of the steady – state experiments were simulated in the validation process of the physical model; effective multiplication factors, power distribution within the core, the power peaking factors, total and integral rods worth and the prompt negative temperature coefficient were performed and analysed. The MCNP calculated values were found to be in very good agreement with the experimental and the FSAR data within the estimated error of 8%. The burnup calculations realised by means of our new elaborated burnup code BUCAL1 show that the averaged life time of the present core configuration is 3360MWh and the core average burnup is found to be 4.54%.

Conclusion

In the frame of this thesis, a new burnup computer code called “BUCAL1” was elaborated. The code directly uses the neutron absorption tally/reaction information generated by MCNP5 for each nuclide of interest to calculate the new nuclide inventory. This allows the full capabilities of the MCNP code to be incorporated into the calculations and a more direct solution technique to be employed.

BUCAL1 uses the fourth order Rung Kutta method coupled with the predictor corrector approach in the resolution of the depletion equation. The code strategy consists of using the nuclide inventory, MCNP tally information, power density, and other data to determine the new nuclide inventory for a given region of the core at a given time step. Then the new inventories are automatically placed back into MCNP input file and the case run for a new subsequent time step.

Validation of BUCAL1 was processed by code-to-code comparisons for a large variety of benchmarks such as: UO2 and ThO2-UO2 PWR pin-cell benchmarks and a MOX 17*17 PWR benchmark assembly. Infinite multiplication factor (k_∞) and important fission products and actinides densities were used in this study. The Validation study was done using published results from several of well-known burnup computer codes (e.g, CASMO-4, MCODE, MOCUP, ...). Analysis of the results shows that for UO2 benchmark fuel type BUCAL1 is sufficiently accurate. Even for high burnup cases, the material composition predictions are very acceptable compared to the comprehensive uranium benchmark reported by OECD. For ThO2-UO2 benchmark fuel type, BUCAL1 showed its big ability to simulate the evolution of related thorium and uranium chains with a very good agreement. For MOX benchmark fuel assembly, BUCAL1 reproduced with a very good agreement the multi-cycles burnup calculations. After five years cooling the relative deviation from the average value for the infinite multiplication factor (k_∞) using BUCAL1 is lower than 1%. For important fission products and actinides densities the deviation to the average values for BUCAL1 are within the range of 10%.

In the second part of this thesis, BUCAL1 was used to study the burnup and time-dependent neutronic parameters of the 2MW TRIGA MARK II Moroccan research reactor. In the aim of this study a full model of the TRIGA MII reactor was elaborated based on the data

provided by its constructor General Atomics of USA, using the 3-D continuous energy Monte Carlo code MCNP5. The validation of the 3-D MCNP model was processed by benchmarking the TRIGA experiments. The results obtained showed that the elaborated MCNP model of TRIGA reactor is precise enough to reproduce reactivity experiments, flux measurements, dose mapping and fuel management studies. Thus, burnup calculations made by use of our new elaborated burnup code BUCAL1 show that the averaged life time of the present core configuration is 3360MWh and the core average burnup is found to be 4.54%. This last value shows that the core average life time can be increased by shuffling of fuel elements.

References

[1] Akio YAMAMOTO, Tadashi IKEHARA, Takuya ITO and Etsuro SAJI, « *Benchmark Problem Suite for Reactor Physics Study of LWR Next Generation Fuels* », Journal of NUCLEAR SCIENCE and TECHNOLOGY, Vol. 39, No. 8, p. 900–912 (August 2002).

[2] A. Koning, R. Forrest, M. Kellett, R. Mills, H. Henriksson and Y. Rugama « The JEFF-3.1 Nuclear Data Library » JEFF Report 21, 2006.

[3] Alberto Talamo, Wei Ji, Jerzy Cetnar, Waclaw Gudowski, « Comparison of MCB and MONTEBURNS Monte Carlo burnup codes on a one-pass deep burn », Annals of Nuclear Energy 33 (2006) 1176–1188.

[4] A. Htet, « Constitution et qualification de nouvelles bibliothèques de sections efficaces multigroupes pour les calculs neutroniques: application à la mise à jour de la bibliothèque du code de transport WIMSD », Thèse de doctorat, Faculté de Sciences de Rabat, Septembre 2001.

[5] B. EL Bakkari et al., « Development of an MCNP-tally based burnup code and validation through PWR benchmark exercises », Annals of Nuclear Energy 36 (2009) p. 626-633.

[6] B. EL Bakkari et al., « Validation of a new continuous Monte Carlo burnup code using a MOX fuel assembly », Nuclear Engineering and Design 239 (2009) p. 1828–1838.

[7] B. EL Bakkari et al., « The Development of an MCNP-Tally based burnup code », Int. J. Nuclear Energy Science and Technology, Vol. 4, No. 3, 2009.

[8] B. EL Bakkari et al., « Neutronic Analysis of the 2 MW TRIGA MARK II Moroccan research reactor », submitted to Annals of Nuclear Energy on Octobre 2009.

[9] B. EL Bakkari et al., « Benchmark analysis of the 2MW TRIGA MARK II Moroccan research reactor using the MCNP5 code and the latest nuclear data libraires », IAEA Technical meeting in collaboration with NEA on Specific Applications of Research Reactors: Provision of Nuclear Data, International Atomic Energy Agency, Vienna, Austeria, 12 – 16 October 2009.

[10] C. Behr, R. Bijttger, H. Klein, P. von Neumann-Cose, A. Richter, D. Schmidt, K. Schweda, S. Strauch, « Calculation of neutron response functions in complex geometries with the MCNP code », Nuclear Instruments and Methods in Physics Research A 411 (1998) 430-436.

[11] Ch. Tippayakul et al., “Development of a practical Monte Carlo based fuel management system for the Penn State University Breazeale Research Reactor (PSBR)”, Annals of Nuclear Energy 35 (2008) 539-551.

[12] Christophe Demazière, « Reactor physics calculations on MOX fuel in boiling water reactors (BWRs) », Chalmers University of Technology Department of Reactor Physics SE-412 96 Gothenburg Sweden.

[13] Daniel L. Aldama, Andrej Tarkov, « Analysis of the Burnup Credit Benchmark with an updated WIMS-D library », Annals of Nuclear Energy 27 (2000) 169-174.

[14] Deng Li, Xie Zhongsheng and Li Shu, « Monte Carlo transport and burnup calculation », Annals of Nuclear Energy 30 (2003) 127–132.

[15] Ed J Parma « BURNCAL: A Nuclear Reactor Burnup code Using MCNP Tallies » Sandia National Laboratories, SAND2002-3868 (November 2002).

[16] Edenius, M. and Forssen, B.: "CASMO-4, A Fuel Assembly Burnup Program, User's Manual", Studsvik/SOA-95/1, Studsvik Energiteknik (1995).

[17] F. RAHNEMA and H. N. M . GHEORGHIU, « ENDF/B-VI Benchmark Calculations for the Doppler Coefficient of reactivity », Annals of Nuclear Energy Vol. 23. No. 12, pp. 1011-1019, 1996.

[18] Gregory J. O'Connor « Burn-up Credit Criticality Benchmark - PHASE IV-A: Reactivity Prediction Calculations for Infinite Arrays of PWR MOX Fuel Pin Cells », Radioactive Materials Transport Division (RMTD) Department for Transport (DfT) United Kingdom, NEA/NSC/DOC(2003)3.

[19] G J O'Connor, P H liem « Phase IV- B: Results and analusis of MOX Fuel Depletion Calculations » Nuclear Science NEA/NSC/DOC (2003)4, OECD 2003.

[20] H Tan Dat « Mise au point de la bibliothèque physique et développement du système PEPABAC (PROGICIEL FAKIR) à l'aide des codes PEPIN et APOLLO1 », thèse du doctorat CEA Saclay – Note CEA-N-2815 (December 1996).

[21] I.J.HASTINGS and RD. MACDONALD, « High burnup performance of nuclear UO2 fuel with inter-pellet graphite discs», Journal of Nuclear Materials 126 (1984) 177-180.

[22] Jacques DI SALVO, « Contribution à l'étude des incertitudes des paramètres neutroniques d'un cœur compact et hétérogène : le réacteur d'irradiation Jules Horowitz », RAPPORT CEA- R-60 7 5 (2003).

[23] Jh S. Hendricks, Gregg W. McKinney, Michael L. Fensin, Michael R. James, Russell C. Johns, Joe W. Durkee, Joshua P. Finch, Denise B. Pelowitz, Laurie S. Waters and Franz X. Gallmeier, « MCNPX, VERSION 26D », Los Alamos National Laboratory (USA), LA-UR-07-4137, JUNE 20, 2007.

[24] Jh S, Hendrichs, Gr W Mckinney « MCNPX, Version 26E », LA-UR-07-6632, Los Alamos National Laboratory (November 17, 2007).

[25] Jinn-Jer Peir, Tien-Ko Wang, Chao-Chin Liu, « TRIGA fuel enrichment verification based on the measurement of short-lived fission products », Applied Radiation and Isotopes 50 (1999) 1085-1096.

[26] Joe D. Hoffman, « Numerical Methods for Engineers and Scientists » second edition, Department of Mechanical Engineering Purdue University West Lafayette, Indiana (New York Basel, 1992).

[27] K. Shibata, T. Kawano, T. Nakagawa, O. Iwamoto, J. Katakura, T. Fukahori, S. Chiba, A. Hasegawa, T. Murata, H. Matsunobu, T. Ohsawa, Y. Nakajima, T. Yoshida, A. Zukeran, M. Kawai, M. Baba, M. Ishikawa, T. Asami, T. Watanabe, Y. Watanabe, M. Igashira, N. Yamamuro, H. Kitazawa, N. Yamano and H. Takano, 2002. « Japanese Evaluated Nuclear Data Library Version 3 Revision-3: JENDL-3.3 » J. Nucl. Sci. Technol. 39, 1125.

[28] K. D. Weaver et al., 2000 « A PWR Thorium Pin Cell Burnup Benchmark», Advances in Reactor Physics and Mathematics and Computation into the Next Millennium (PHYSOR 2000), INEEL/CON-2000-00227.

[29] Makoto Takano, Michaele C. Brady, « Burnup credit criticality benchmark part 1 simple PWR spent fuel cell» NEACRP-L-337 (Revision-1, Jan. '92), JAERI-M 94-003.

[30] M B Chadwick et al., « ENDF/B-VII.0: Next generation evaluated uclear data library for nuclear science and technology » Nuclear data Sheets, vol. 107, pp. 2931–3060, 2006. [Online]. Available: http://www.nndc.bnl.gov/exfor7/endf00.htm.

[31] M D DeHart, M C Brady, C V Parks, « OECD/NEA Burnup Credit Calculational Criticality Benchmark Phase 1-B Results » ORNL-6901, Oak Ridge National Laboratory, June 1996.

[32] M. Herman, « ENDF-102 ENDF-6 data formats and procedures for the evaluated nuclear data file ENDF-VII », Informal Report BNL-NCS-44945-01/04-Rev.

[33] Michael PLASCHY, Fabian JATUFF, Peter GRIMM, Filippo TANI, Roland JACOT-GUILLARMOD, Flavio GIUST, Jan KROUTHEN and Rakesh CHAWLA, « Comparisons of Deterministic Neutronic Calculations with Monte Carlo Results for an Advanced BWR Fuel Assembly with Hafnium Control Blades », Journal of NUCLEAR SCIENCE and TECHNOLOGY, Vol. 43, No. 11, p. 1298–1310 (2006).

[34] M. Q. Huda, M. Rahman, M. M. Sarker, S. I. Bhuiyan, « Benchmark analysis of the TRIGA MARK II research reactor using Monte Carlo techniques ». Annals of Nuclea Energy 31 p. 1299-1313, 2004.

[35] M. Ravnik « TRIGA Reactor Power Upgrading Analysis. Nuclear Society of Slovenia », 2nd Regional Meeting: Nuclear Energy in Central Europe Portoroz, SLOVENIA, 11 – 14 Spetember 1995.

[36] M.T. SIMNAD, « THE U-ZRHx ALLOY: ITS PROPERTIES AND USE IN TRIGA FUEL », Nuclear Engineering and Design 64 (1981) 403-422.

[37] Nu. Ga. Herranz, Os. Cabellos « APPLICABILITY OF THE MCNP-ACAB SYSTEM TO INVENTORY PREDICTION IN HIGH-BURNUP FUELS: SENSITIVITY/UNCERTAINTY ESTIMATES », Mathematics and Computation, Supercomputing, Reactor physics and Nuclear and biological Applications, Avignon, France (September 12-15-2005).

[38] O. Merroun, A. Al Mers, M.A. Veloso, T. El Bardouni, B. El Bakkari, E. Chakir, « Experimental validation of the thermal-hydraulic code SACATRI », Nuclear Engineering and Design (2009), Article in press.

[39] O. Merroun, A. Almers, T. El Bardouni, B. El Bakkari, E. Chakir, « Analytical benchmarks for verification of thermal-hydraulic codes based on sub-channel approach », Nuclear Engineering and Design 239 (2009) p.735–748.

[40] P. F. Rose (Comp. and Ed.) « ENDF-201, ENDF/B-VI Summary Documentation » BNL-NCS-17541, 4th Edition (1991).

[41] P. Mohanakrishnan, « Development and validation of a fast reactor core burnup code – FARCOB », Annals of Nuclear Energy, ref.

[42] R. E. MacFarlane, (2002), NJOY-99 Nuclear Data Processing System. [Online]. Available: http://t2.lanl.gov/codes/njoy99/index.html (update web site).

[43] R. L. Moore, B.G. Schnitzler, C.A. Wemple, « MOCUP, MCNP/ORIGEN Coupling Utility Programs, User's Manual», Idaho National Engineering Laboratory, INEL-95/0523, September 1995.

[44] R. Jacqmin, M Kellett and A. Nouri, «The JEFF3-0 Nuclear Data Library», PHYSOR 2002, Seoul Korea.

[45] R. Jeraj et al., «TRIGA MARK II REACTOR: U(20)-Zirconium hybride fuel rods in water graphite reflector – IEU-COMP-THERM-003», NEA/NSC/DOC/(95)03/III, 2003.

[46] Safety Comity « Final Safety Analysis report for the 2MW TRIGA MARK II research reactor (FSAR) at CENM » Rabat, Morocco, 2007.

[47] Tetsuo Matsumoto and Nobuhiro Hayakawa « Benchmark Analysis of TRIGA MARK II Reactivity Experiment Using a Continuous Energy Monte Carlo Code MCNP ». Journal of Nuclear Science and Technology, vol. 37, No. 12, p 1082 – 1087, 2000.

[48] The JEFF Team, « The JEFF-3.1 library », JEFF Report 21, NEA/OECD No. 6190, 2006, ISBN92-64-02314-3. Available:http://www.nea.fr/html/dbdata/projects/nds_jef.htm.

[49] X-5 Monte Carlo Team « MCNP- A General Monte Carlo N-Particle Transport Code », Version5- Los Alamos National Laboratory (April 24, 2003).

[50] Yang-Hyun Koo, Byung-Ho Lee, Dong-Seong Sohn, « COSMOS: a computer code to analyze LWR UO2 and MOX fuel up to high burnup », Annals of Nuclear Energy 26 (1999) 47~57.

[51] Yoichiro SHIMAZU, « Simplest Simulation Model for Three-Dimensional Xenon Oscillations in Large PWRs », Journal of NUCLEAR SCIENCE and TECHNOLOGY, Vol. 41, No. 10, p. 959–965 (October 2004).

[52] Zh Xu « Design Strategies for optimizing High Burnup Fuel in Pressurized Water Reactors » Doctor thesis, MASSACHUSETTS INSTITUTE OF TECHNOLOGY (January 2003).

Appendix A. NJOY input file and cross sections comparisons

I- Data flow in NJOY

The modules of NJOY99 can be linked in a number of different ways to prepare libraries for various nuclear applications. We will briefly describe here only a basic input structure to create an ACE file for MCNP. Next, we find a typical input file (235U at 600 Kelvin) needed to run NJOY and we will comment it:

The word tape is used, by convention, for each module; the input and output file are named **tapeXX** (*tape20, tape21* …).

All modules parameters are clearly described in the NJOY99 user manual and summary here just few comments about the NJOY99 input used through this thesis.

- **moder** reads the ENDF file (*tape 20*) which contains the material (for ^{235}U the material number is 9228), extracts it and put the ENDF file in binary mode (negative sign) in *tape 21*. **moder** is usallay used at the beginning of an NJOY99 run to convert ENDF library files into binary for calculation efficiency. It can also (it is the case here and in every instance) be used to extract desired materials from a multi-material library.
- **reconr** module reconstructs point-wise cross-sections: read *tape21*, extract material 9228 and reconstruct cross-section at 0 Kelvin with a reconstruction tolerance of 0.001 and a resonance integral check tolerance of 0.003. The resulting point-wise cross-sections are written in a PENDF (for Point-ENDF) *tape22* for future use.
- **broadr** module reads tape22 and Doppler-broadens at 600 Kelvin (only one temperature) the data using the accurate point-kernel method for material 9228. The union grid allows all resonance reactions to be broadened simultaneously, resulting in a great savings of processing time. After broadening and thinning with a tolerance of 0.001 and with an integral criterion tolerance of 0.003, the summation cross-sections are reconstructed from their parts. Doppler broadening was forced up to the upper energy limit of the resolved resonance range, but never above 2MeV. **broadr** needs in input the ENDF file (*tape21*) and the PENDF file (*tape22*). The results are written out in a new PENDF tape23 for future use.
- **heart** module compute energy-balance heating and damage energy for material 9228 for the 600 Kelvin temperature. Input files are *tape21* (ENDF file) and *tape23*. Line (302 303 304 402 442 444) are associated to the partial KERMA for reactions which must be added. Output file is *tape24* which is for the results for all the added processes.

- **Gaspr** adds gas production reactions (mt203-207) to the PENDF tape. Any old gas sections on the input tape are deleted. Input tape: *tape21* is the ENDF file in binary mode, tape24 is the PENDF tape; Output tape is *tape25* (PENDF tape).
- **thermr** generates neutron scattering cross-sections and point-to-point scattering kernels in the thermal range. Input file is only *tape25*, which is the previous PENDF file, output file is *tape41*. The generation of neutron scattering cross-sections is done for material 9228 with 8 equi-probable angles at one temperature (600K), parameter for inelastic options 1 (compute as free gas). Next parameter is 0 for the elastic options (no elastic cross-sections in the thermal range). In this case, we consider only 1 principal atom. The **mt** value for inelastic reaction is 221. A tolerance of 0.001 is chosen and the maximum energy for thermal treatment is 1 eV.
- **purr** calculate probability tables for treating unresolved-resonance self-shielding for Monte-Carlo codes (see NJOY99 user manual). Input: *tape21* and *tape41*, PENDF output: *tape26*. The calculation is done for material 9228 for one temperature (600K) with sigma0 (1E10, 1E5, 1E4, 1000, 100, 10,1). A study was done with MCNP for different value of sigma0: choosing value 1 didn't give the correct results for the self-shielding effect; 1E10 is more representative but can be not adaptated for all material; only a table from 1 up to 1E10 gives systematically the good results. M. Mac Farlane from Los Alamos says that it is dependent of the considered material (i.e. the cross section). One has chosen 20 probability bins and 16 resonance ladders. It can be noticed that the ENDF file must contain some definition of probability tables for treating unresolved resonance, if it is not the case, NJOY99 don't crash but just write a warning message. Here is the answer (*taken from L. Perrot and O. Méplan, 2009*) of Mr Mac Farlane concerning the purr module and chosen parameters:

> "***The background cross-section is important for multigroup methods, but it is not needed for Monte Carlo. It can be convenient just to judge how important self shielding might be for a given material in a particular energy range. The purr module takes a lot of time to do its calculation, and that time is determined by nladr. If you can afford it, values on the order of 16 to 32 should be OK. Look at how closely the average over the ladders matches the infinitely dilute cross section to get an idea if you are getting sufficient convergence. I haven't done many studies on the optimum size for nbin-I juste use 20. A problem here is with the occasional very small cross-section in interference minima. It is hard to get enough samples into the minima. As a result, the accuracy may begin to suffer for deep penetration, which is equivalent to very low sigma zero values. Examples might be very thick depleted uranium or thick iron with strong flux in the 200 keV***

range. Anyway, there is always doubt about such low cross-sections between resonances because they are hard to measure and because single-level Breit-Wigner theory doesn't represent them well" (Mr MacFarlane).

- The first call to **acer** module prepares a data library for MCNP (in ACII). Input file are *tape21* (ENDF file) and *tape26* (binary PENDF), output file are *tape27* (the ACE file) and *tape28* (the line will be copy in the XSDIR file of MCNP). These data are designed by fast data (value 1), with a minimal printed info (next value 0) in output file of ***njoy***. The ACE output type for the file (*tape27* in ACII) is defined by the value 1, with the id suffix for ZAID. 06 (default in NJOY is .00). The material to process is 9228 at 600K.
- The second call to **acer** module reads *tape27* (ASCII ACE file) and prepares new *tape29* (ACE file) and tape30 (XSDIR file).

```
moder /
1 -21
'PENDF tape for ENDFB-VI.8 92235(0)'/
20 9228
0/
reconr /
-21 -22
'PENDF tape for ENDFB-VI.8 92235(0)'/
9228 1 0 /
0.001 0. 0.003 /
'92235(0) from ENDFB-VI.8'/
'Processed by NJOY-99.9-up259 Apr2008'/
0/
broadr /
-21 -22 -23
9228 1 0 0 0./
0.001 2.0e6 0.003 1.e-12 /
600./
0/
heatr /
-21 -23 -24/
9228 6 0 1 0 2/
302 303 304 402 443 444/
gaspr /
-21 -24 -25
thermr /
0 -25 -41
0 9228 8 1 1 0 1 221 2/
600./
0.001 1.0/
purr /
-21 -41 -26
9228 1 7 20 16/
600./
1.e10 1.e5 1.e4 1000 100 10 1./
0/
acer /
-21 -26 0 27 28
1 0 1 .06/
'92235(0) from ENDFB-VI.8'/
9228 600./ matd tempb
/
/
acer /
0 27 0 29 30
7 1 2 .06/
/
```

Fig. A-1. NJOY99 input used to generate an ACE library for 235U at 600 Kelvin.

II- Fission and capture reaction rates

II-1 HEU-MET-FAST Benchmarks

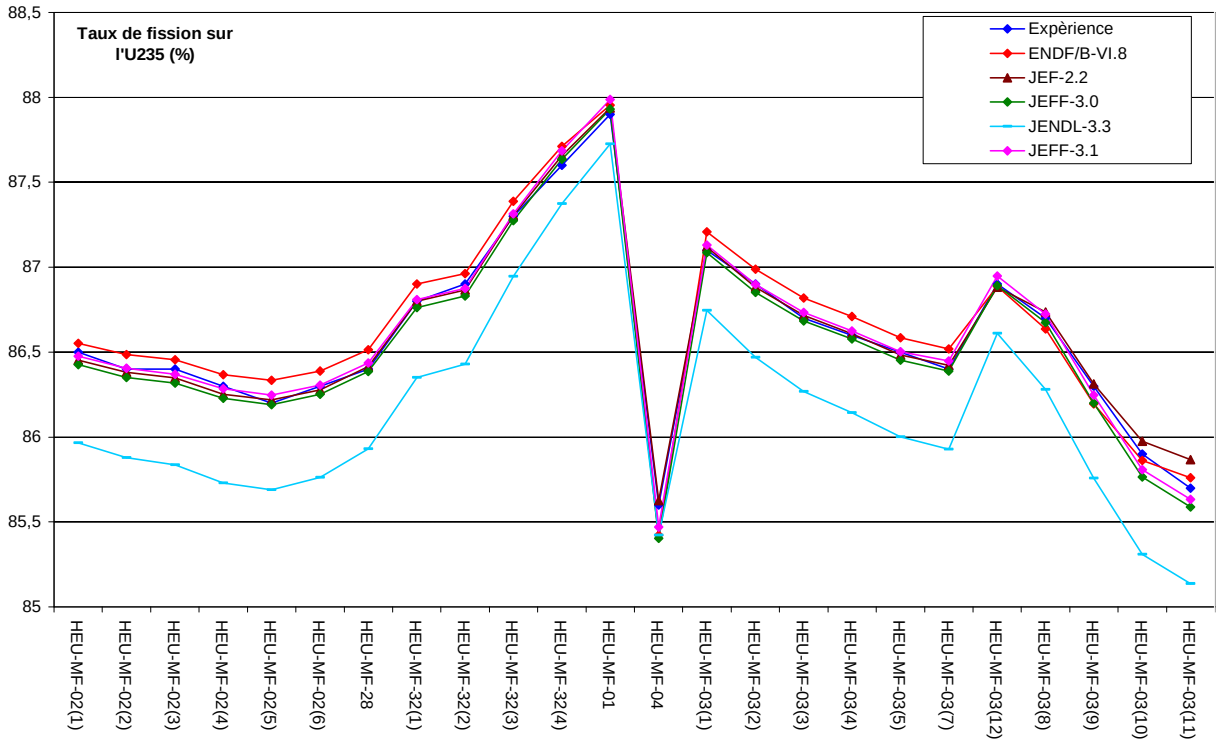

Fig. A-2. U235 fission rates for HEU-MET-FAST.

Fig. A-3. U235 capture rates for HEU-MET-FAST.

II-2 Pu-MET-FAST Benchmarks

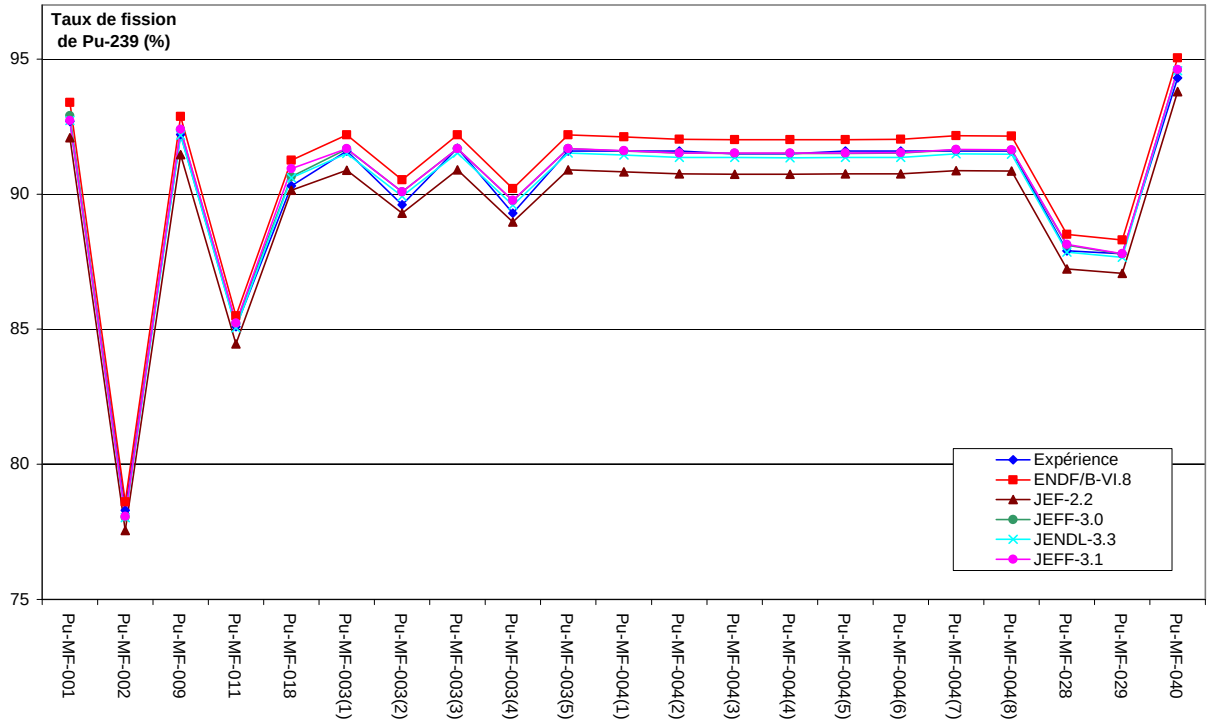

Fig. A-4. Pu239 fission rates for Pu-MET-FAST.

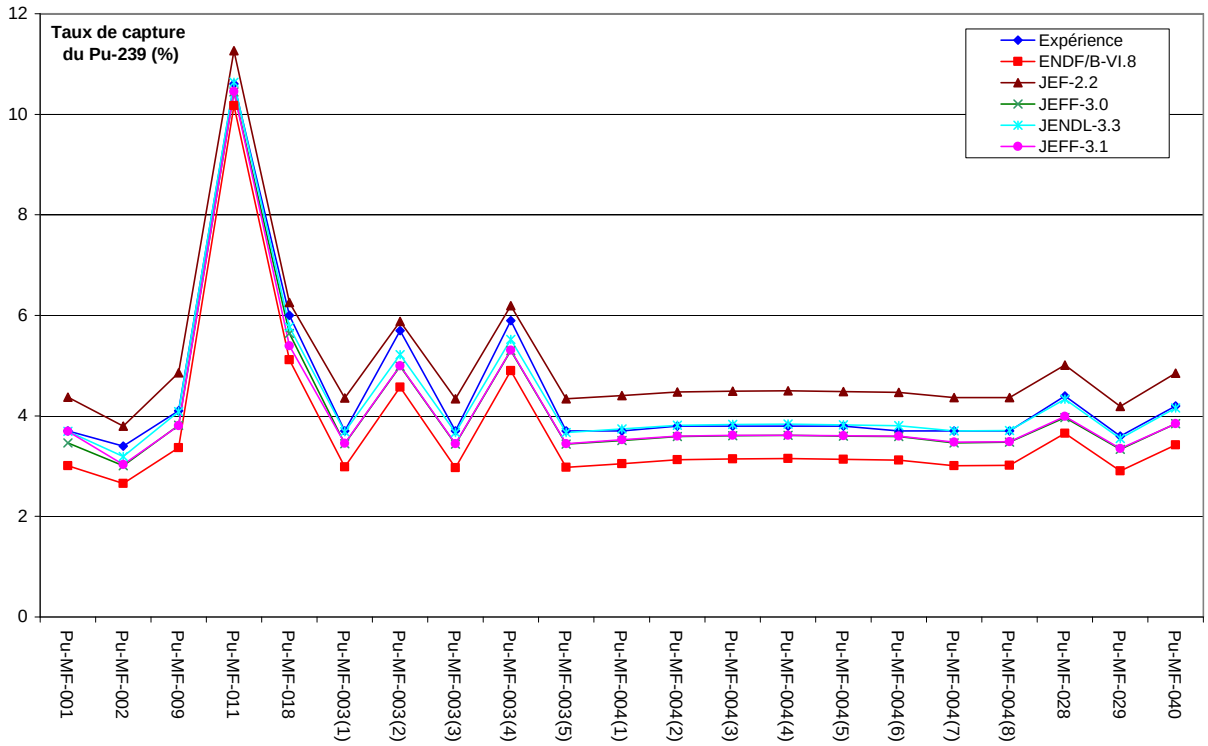

Fig. A-5. Pu239capture rates for Pu-MET-FAST.

Fig. A-6. U235 fission rates for HEU-SOL-THERM.

Fig. A-7. U235 capture rates for HEU-SOL-THERM.

III- Comparison between different libraries of fission and capture cross sections

III-1 U235 Fission cross section

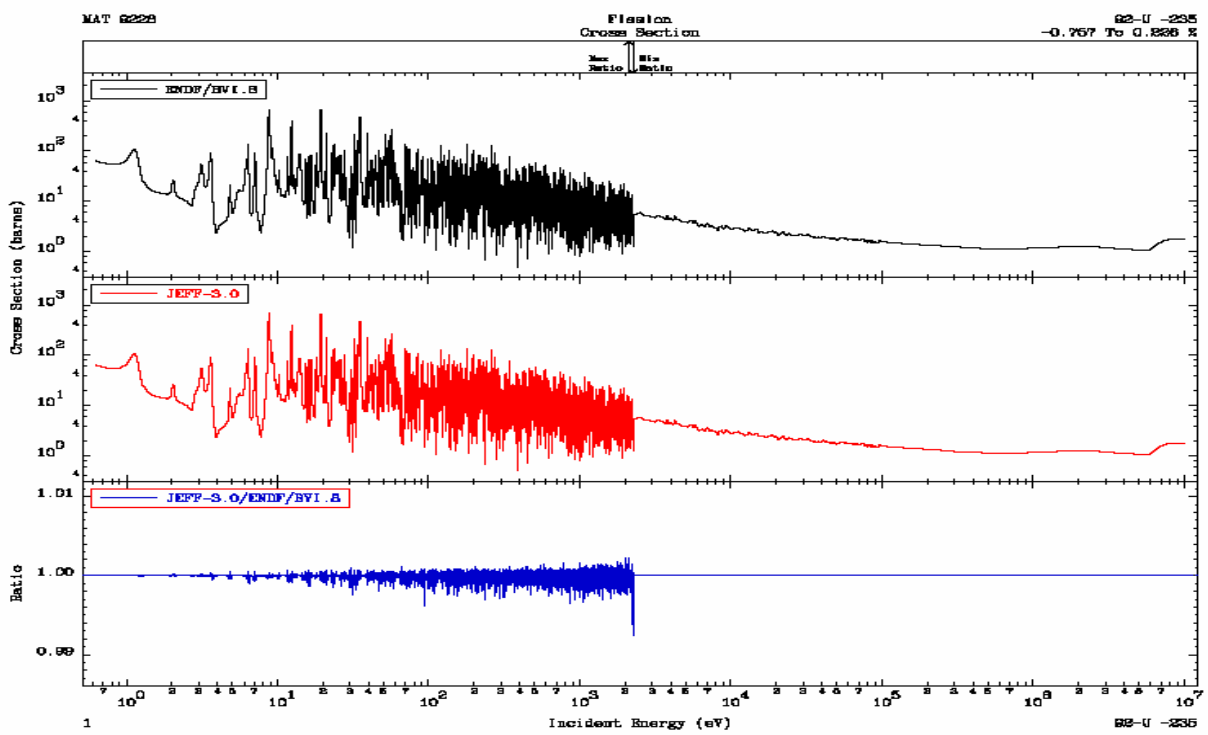

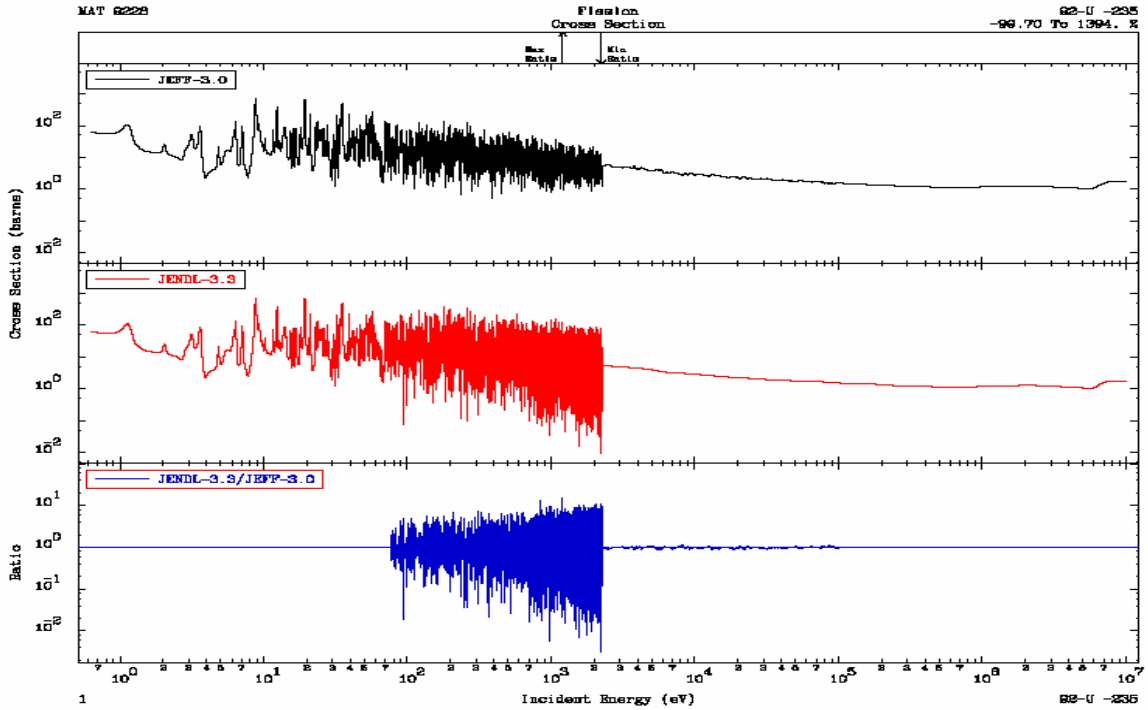

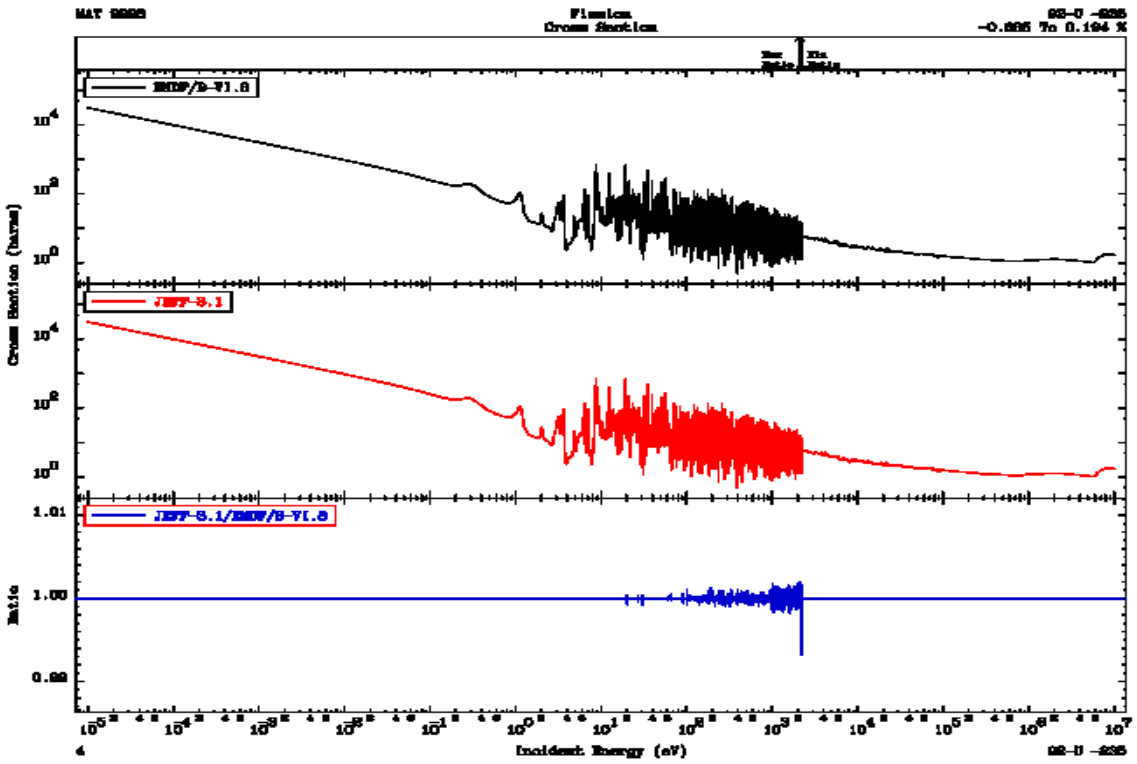

III-2 U235 Capture cross section

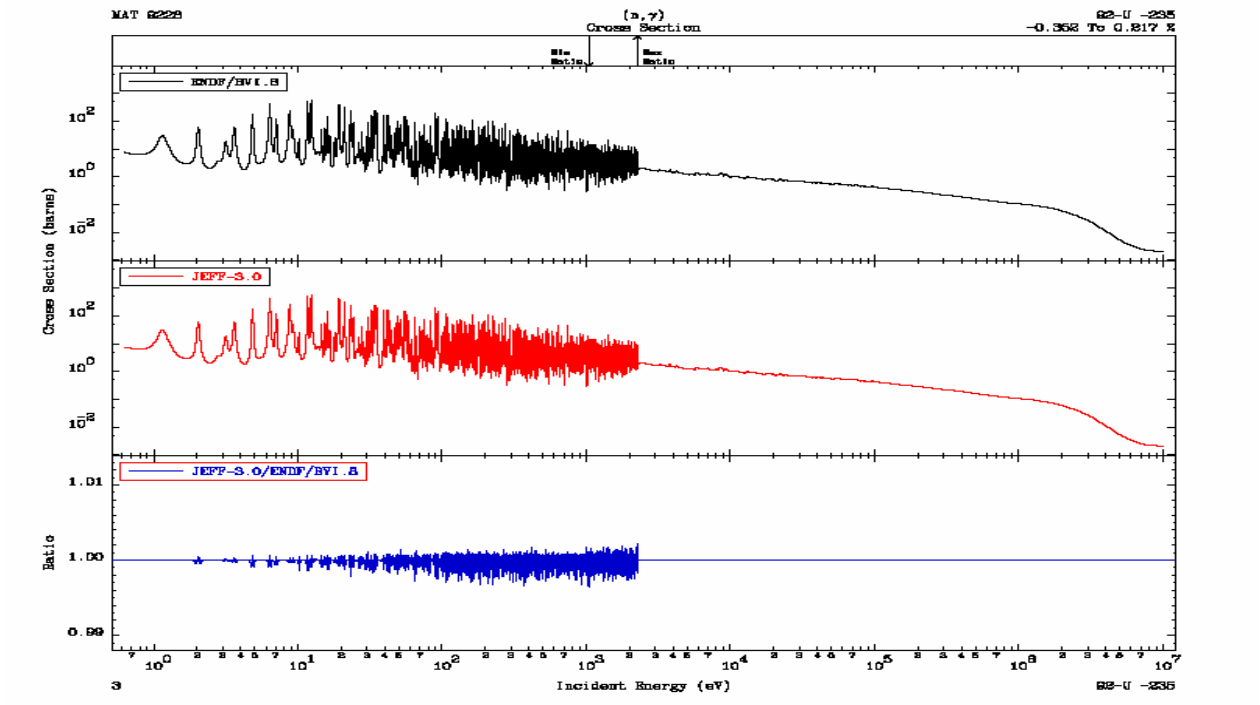

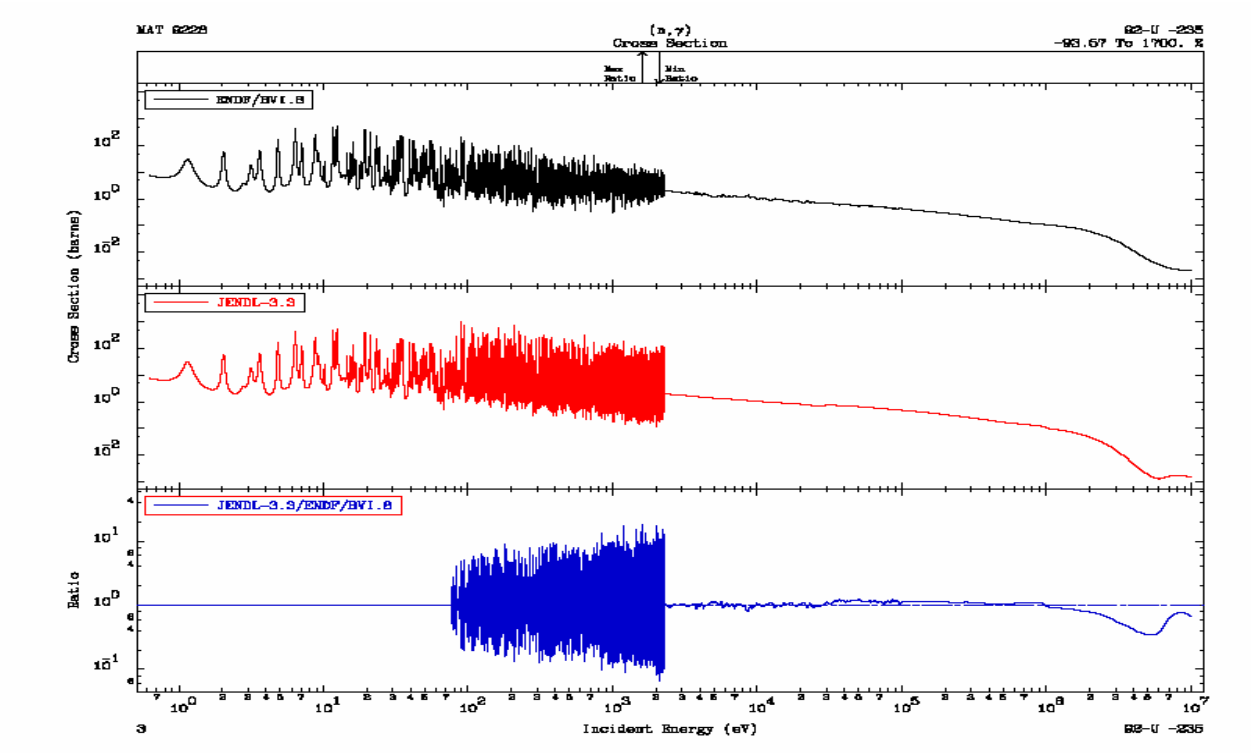

III- 3 U238 Fission cross section

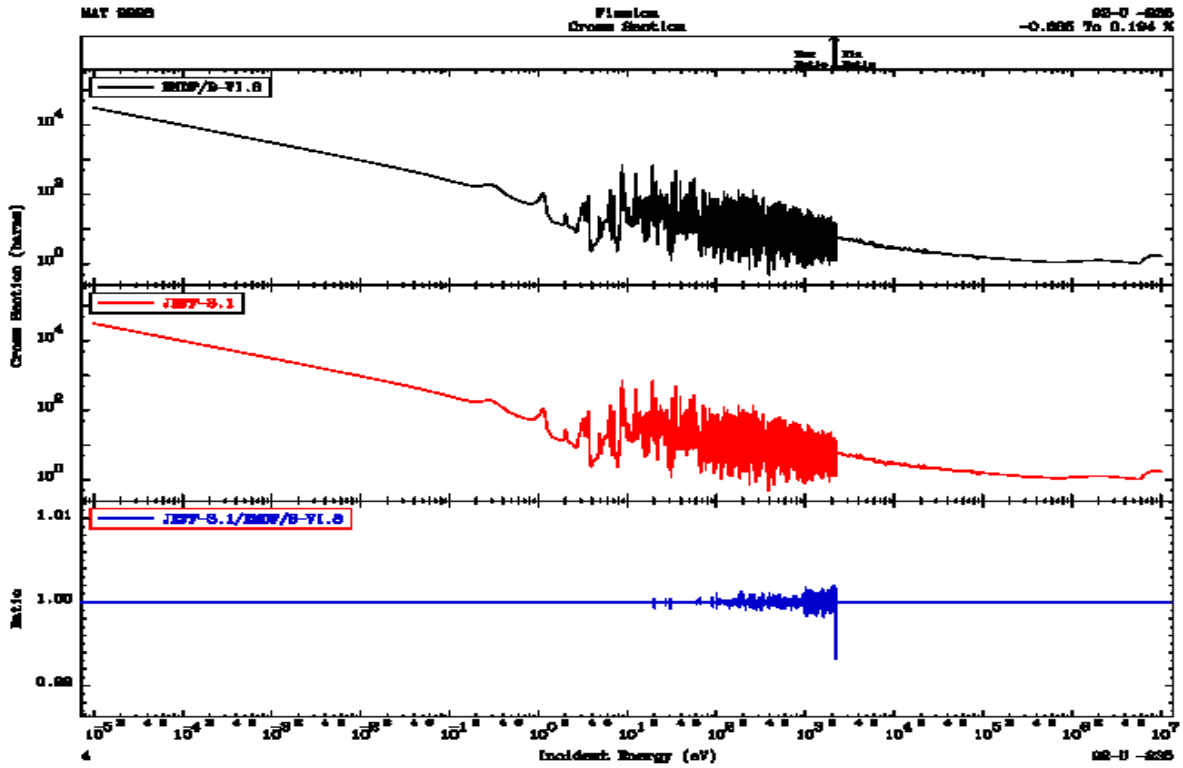

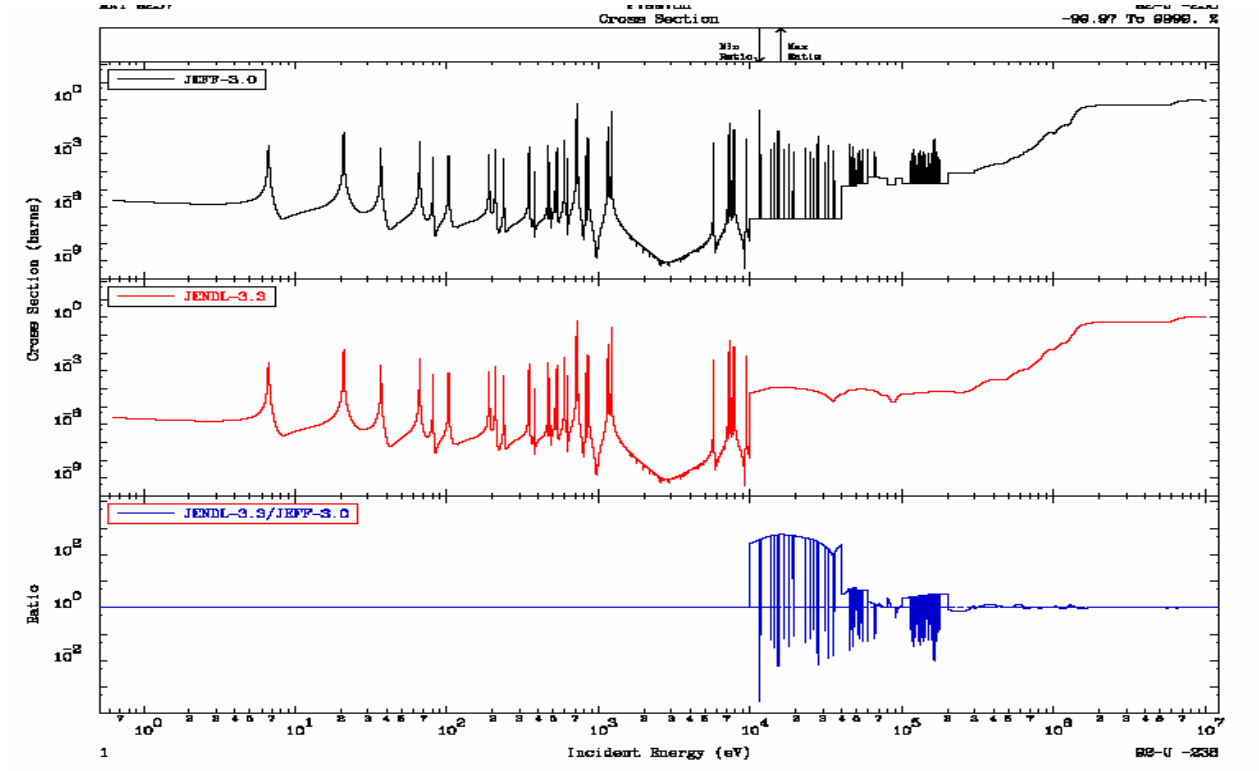
Fission
Cross Section
-99.97 To 9999. %
Min Ratio
Max Ratio
JEFF-3.0
JENDL-3.3
JENDL-3.3/JEFF-3.0
Cross Section (barns)
Ratio
Incident Energy (eV)
92-U -238

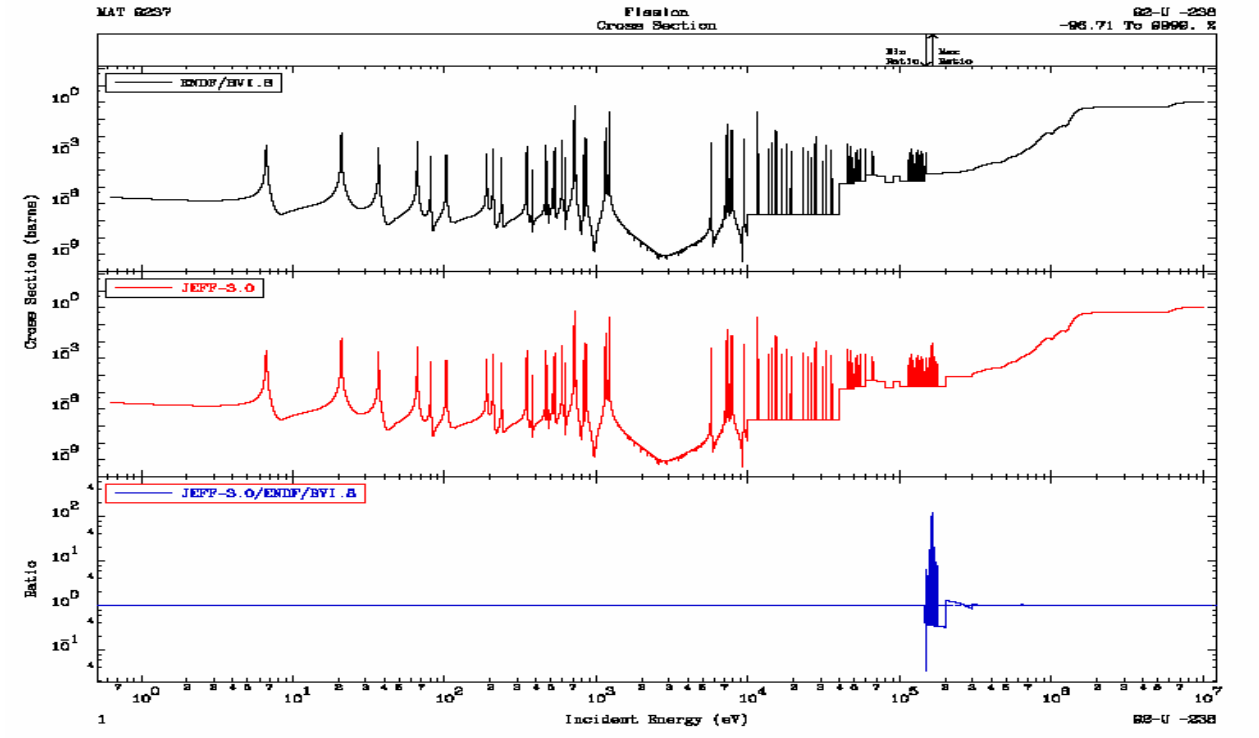
MAT 9237
Fission
Cross Section
92-U -238
-96.71 To 9999. %
Min Ratio
Max Ratio
ENDF/BVI.8
JEFF-3.0
JEFF-3.0/ENDF/BVI.8
Cross Section (barns)
Ratio
Incident Energy (eV)
92-U -238

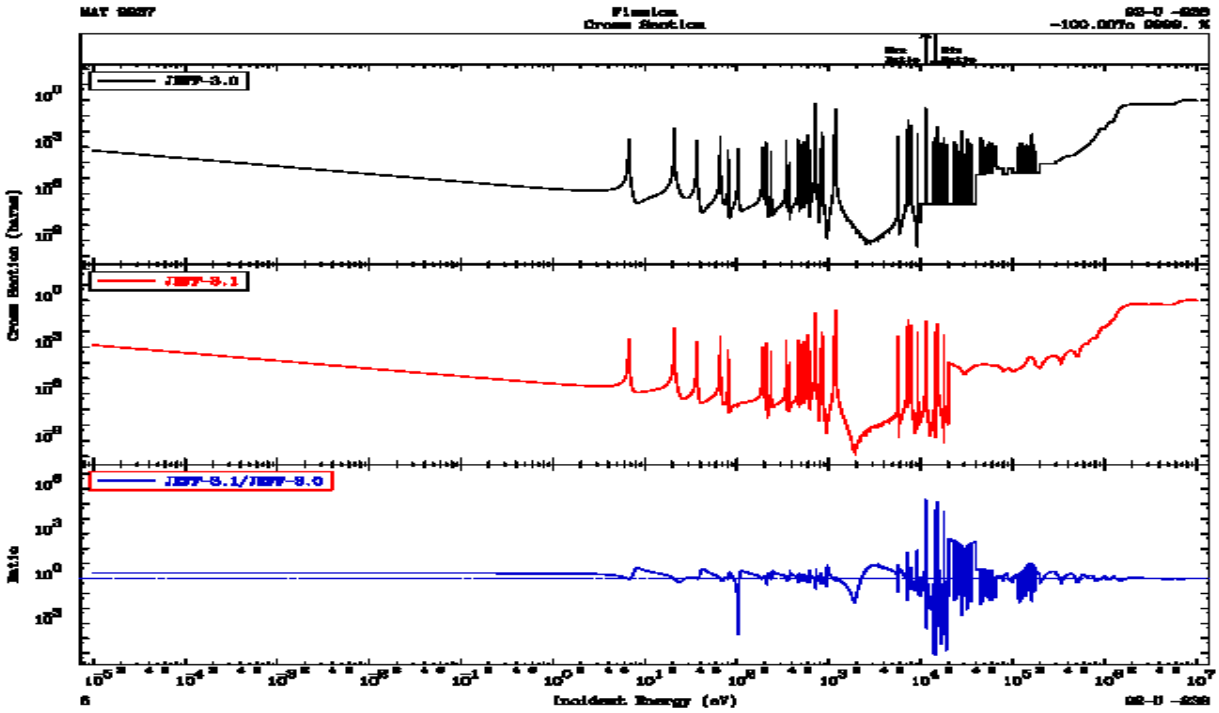

III-4 U238 Capture cross section

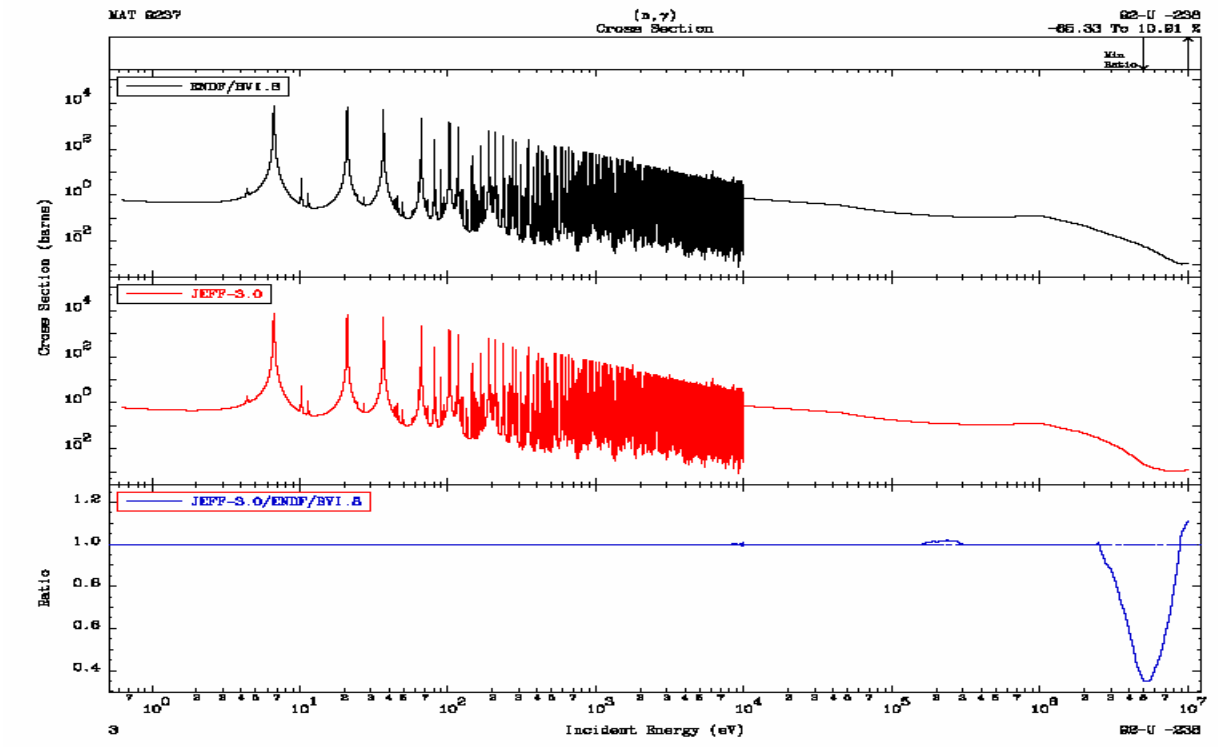

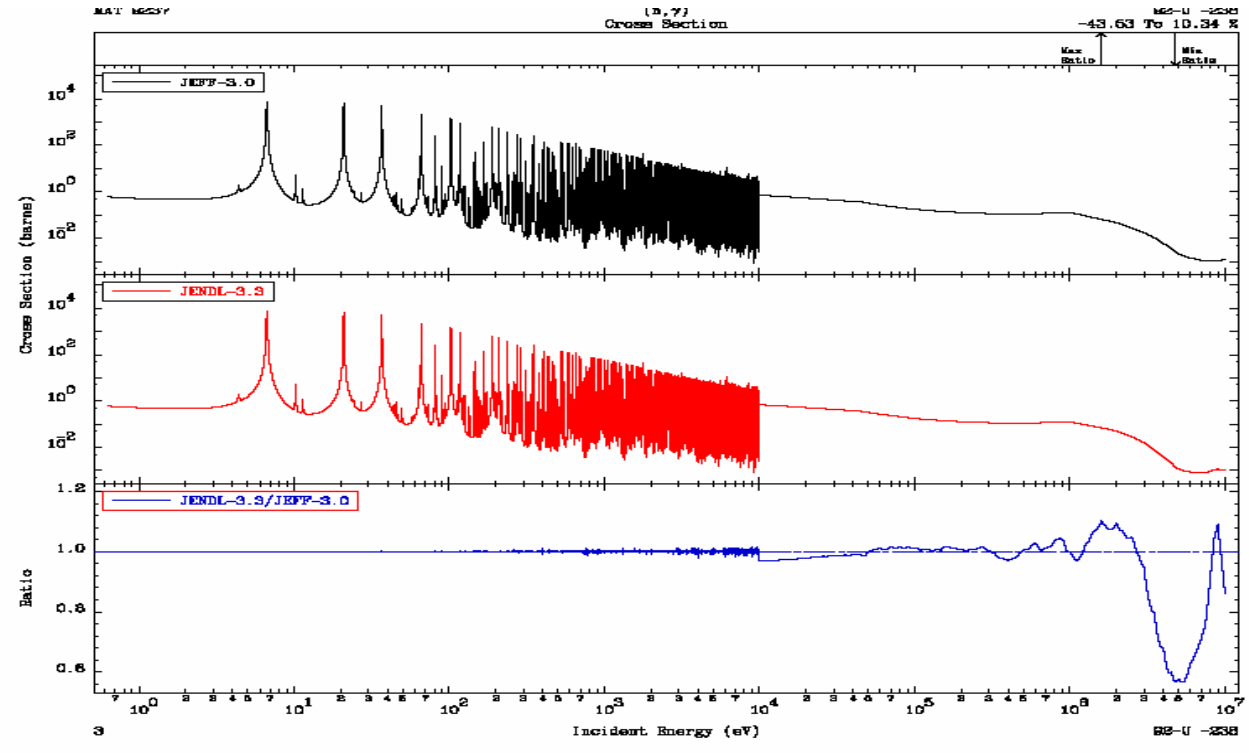
(n,γ)
Cross Section
-43.63 To 10.34 %
JEFF-3.0
JENDL-3.3
JENDL-3.3/JEFF-3.0
Cross Section (barns)
Ratio
Incident Energy (eV)

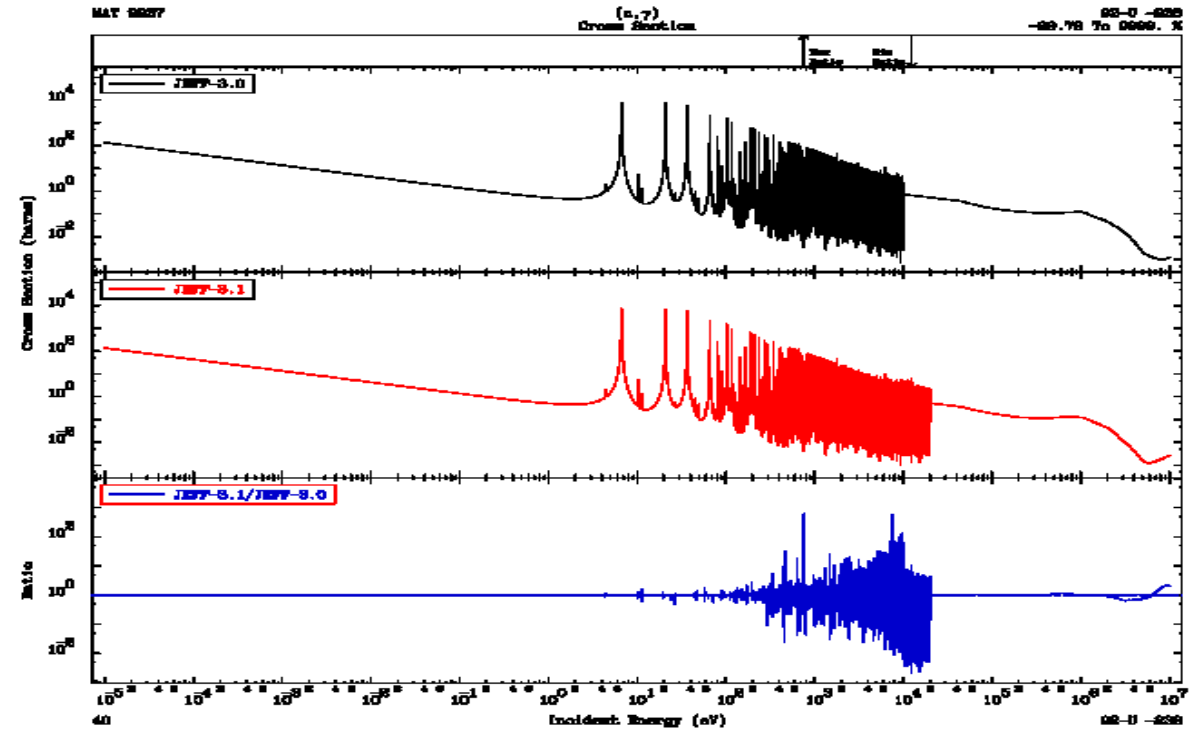
(n,γ)
Cross Section
JEFF-3.0
JEFF-3.1
JEFF-3.1/JEFF-3.0
Cross Section (barns)
Ratio
Incident Energy (eV)

III-5 Pu239 Fission cross section

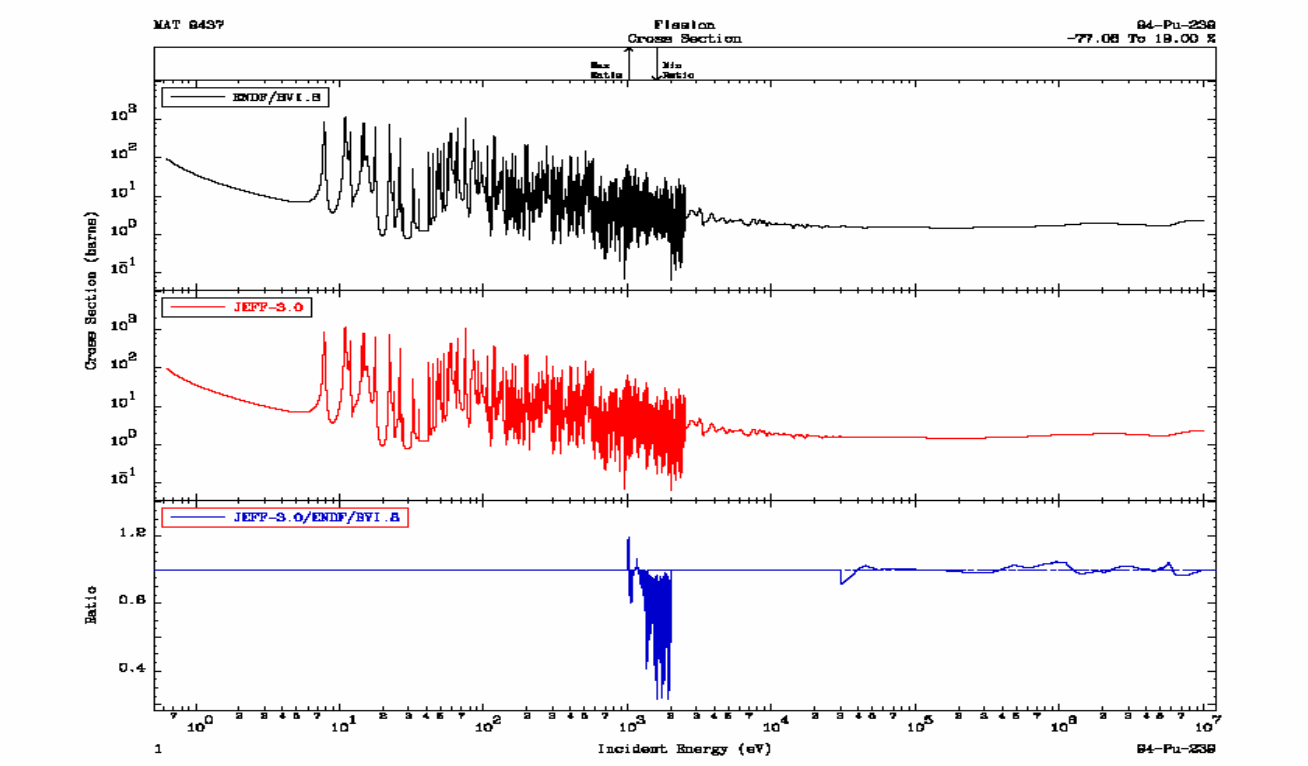

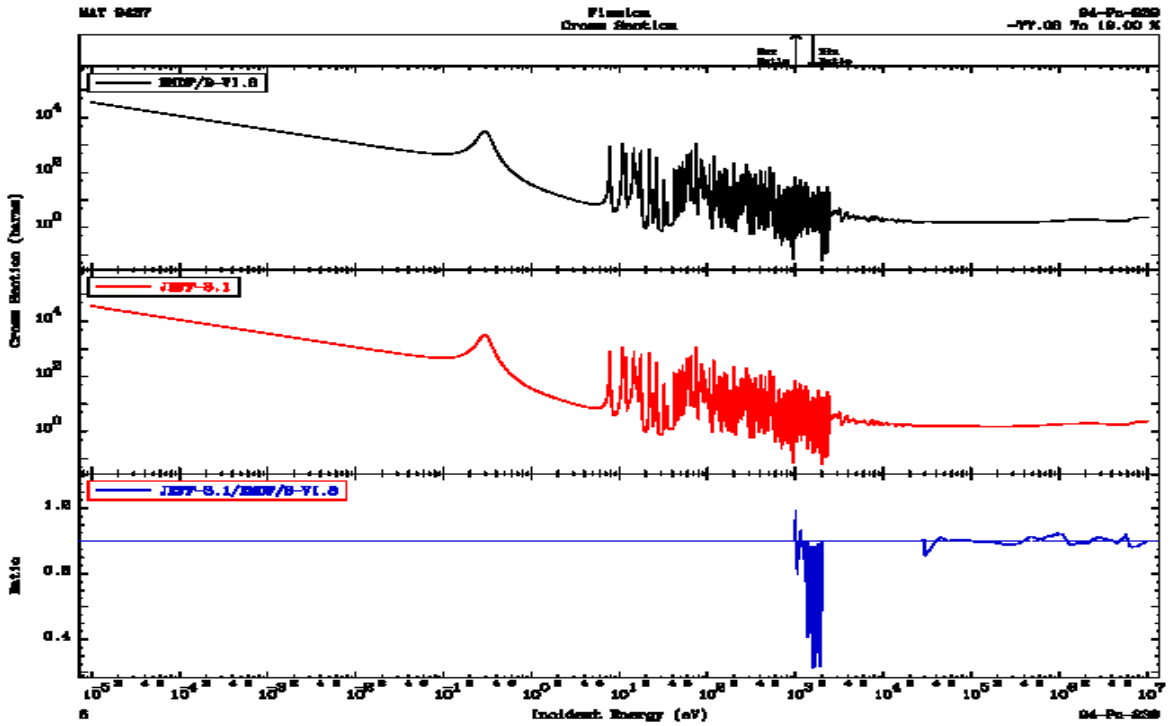

III-6 Pu239 Capture cross section

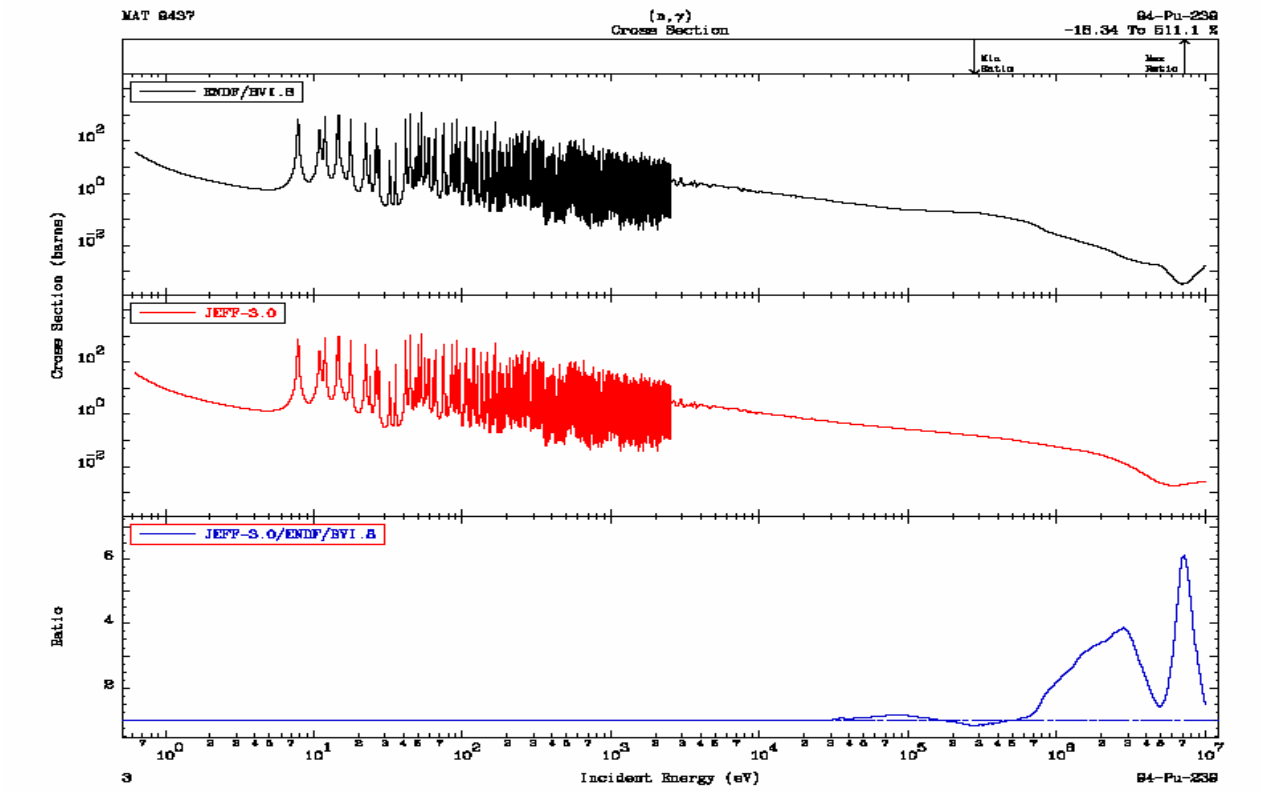

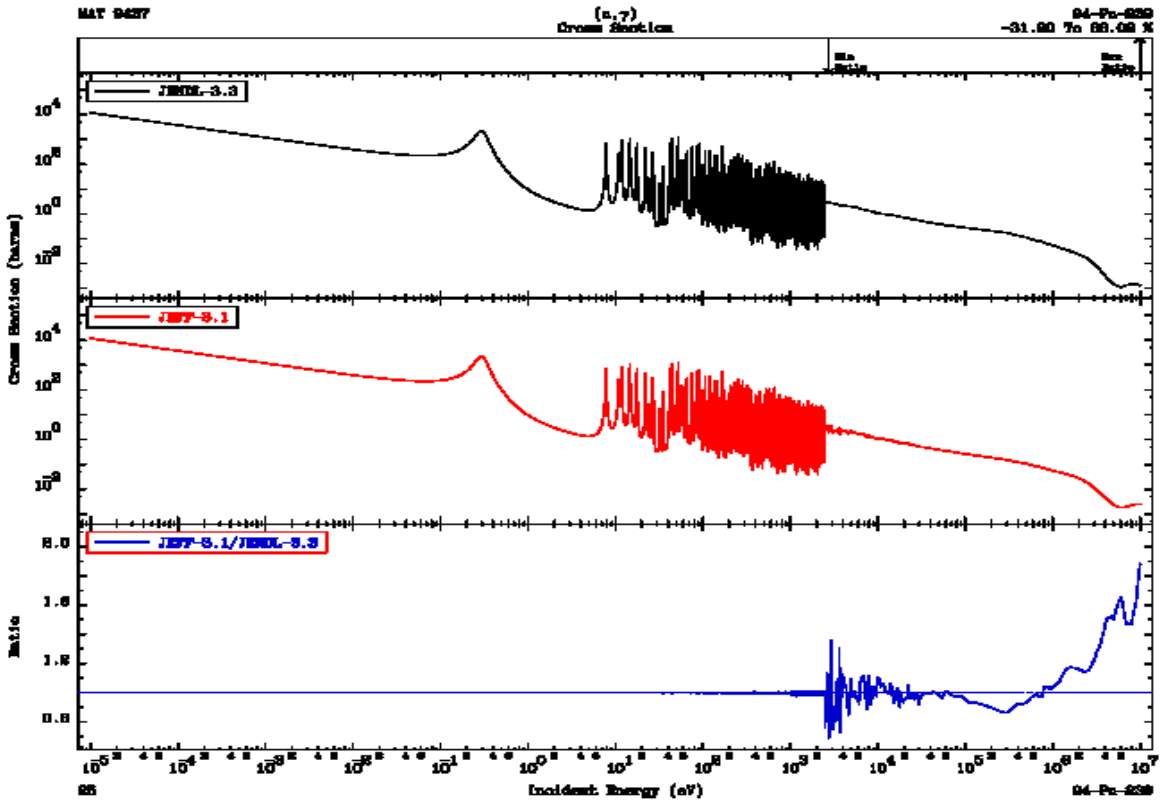

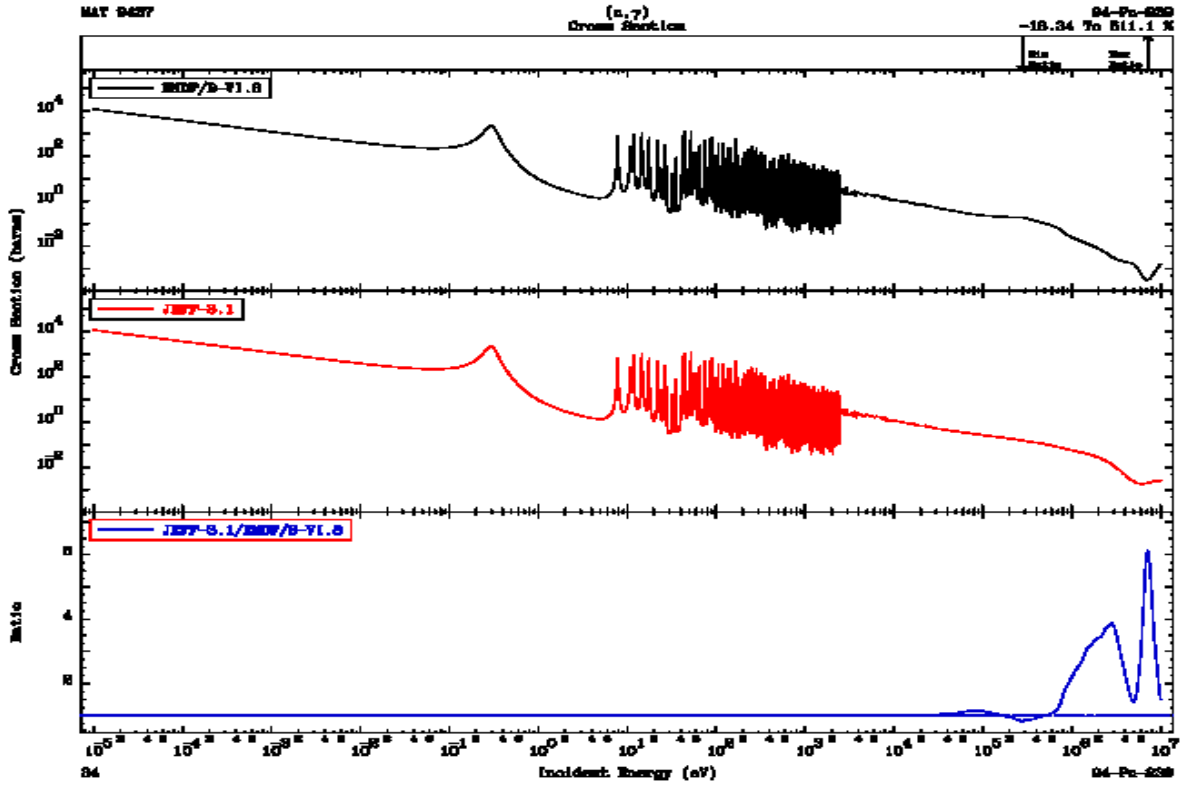

III-7 Pu240 Fission cross section

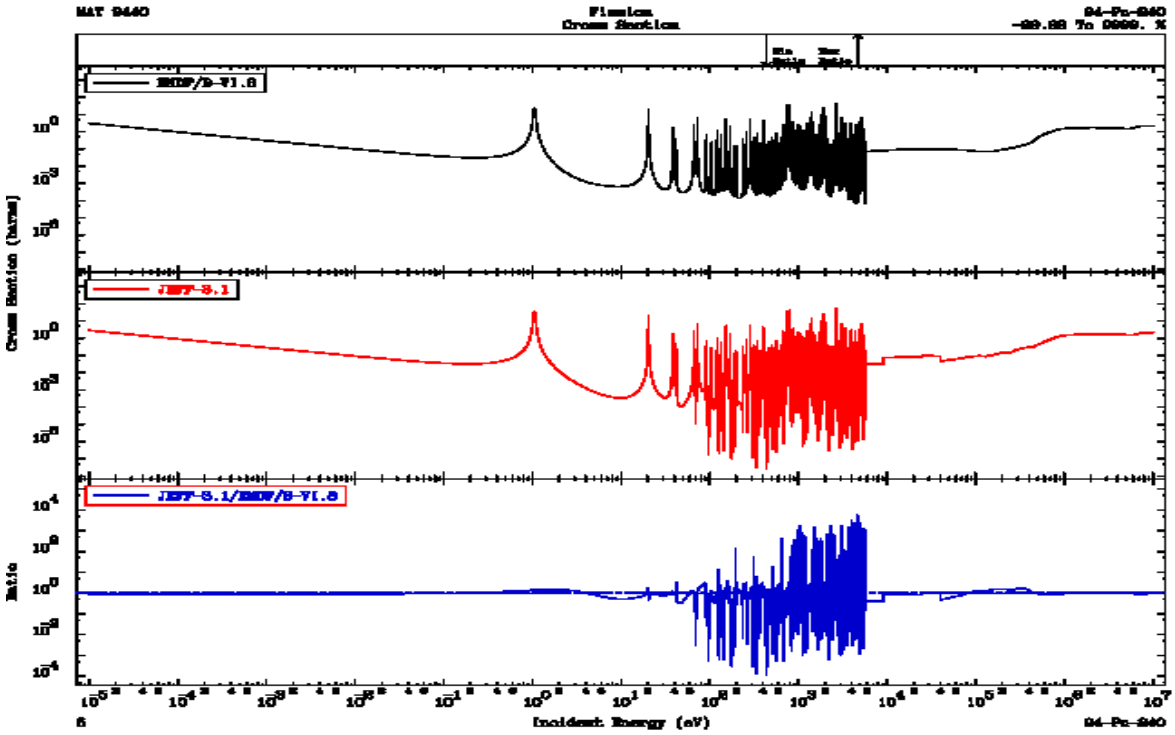

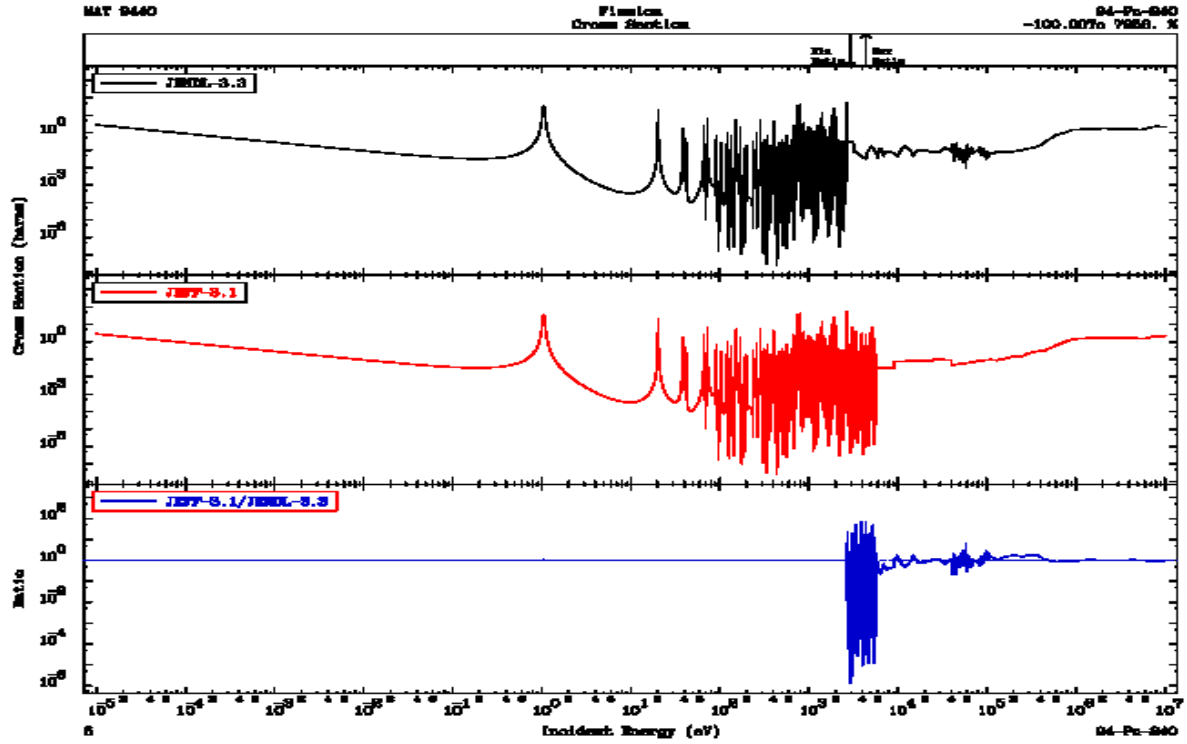

III-8 Pu240 Capture cross section

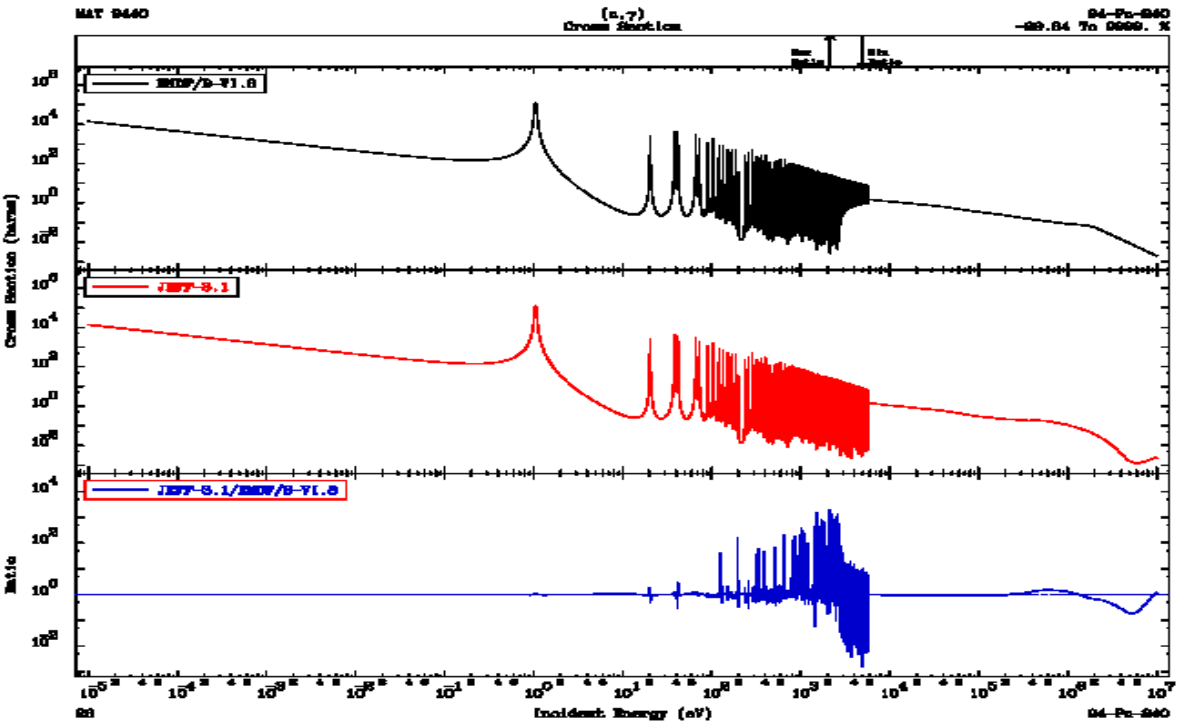

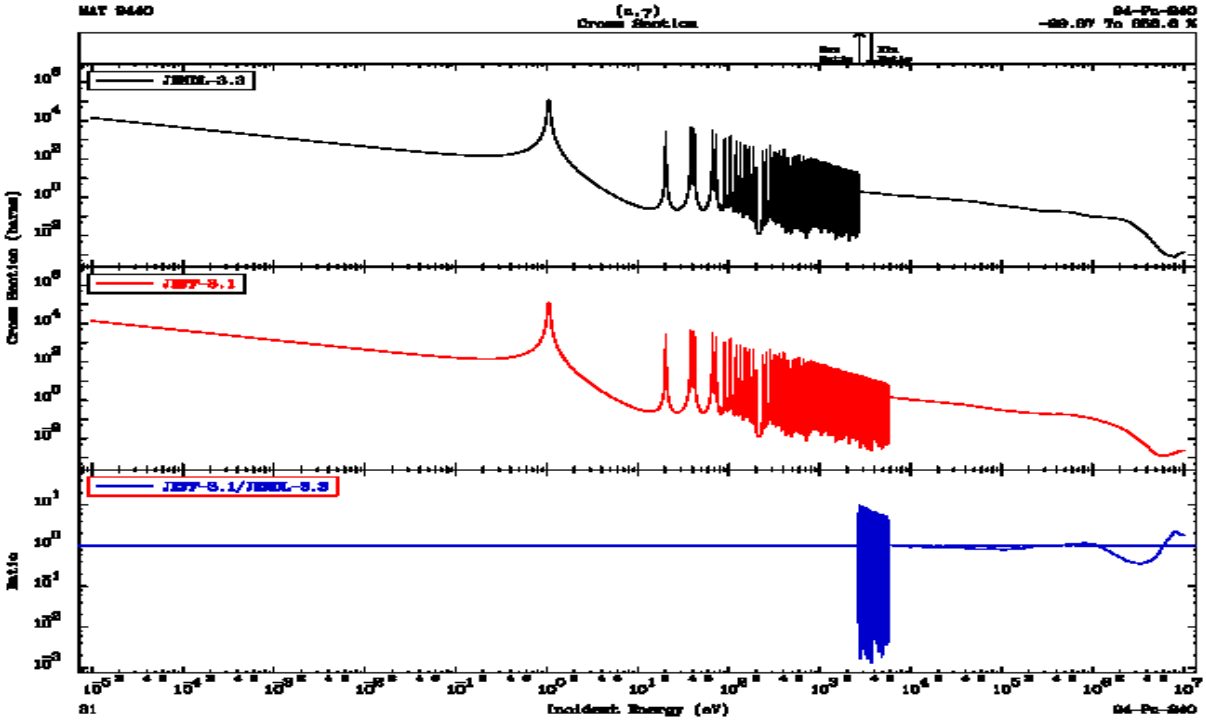
MAT 9440
(n,γ)
Cross Section
94-Pu-240
JENDL-3.3
JEFF-3.1
JEFF-3.1/JENDL-3.3
Cross Section (barns)
Ratio
Incident Energy (eV)
94-Pu-240

Appendix B. Verification of the fourth order Rung Kutta method

I- Verification of the fourth order Rung Kutta algorithm

The verification of the numerical solution method chosen by computer codes (including burnup computer codes) needs to be given special attention. It is a key issue for codes which ultimately determines the quality of the results.

In order to illustrate the accurateness of the fourth order Rung Kutta (*RK4*) method used in our burnup computer code, numerical example is first examined.

The example is to study the decay of atomic concentrations of 27 major actinides, for an UOX nuclear spent fuel. Concentrations at the end of irradiation are from a nuclear fuel enriched to 4.0% on uranium, irradiated to 45.000 MW.d / tIHM.

For these calculations, we adopted the decay chain of actinides shown in *Fig. B-1*. While the codes EVA, REFACTN and PEPABAC use the decay chain shown in *Fig. B-2*.

Table (*B-1)* gives the initial atomic concentrations of the 27 major actinides used in this study.

Tables (*B-2*) and (*B-3*) represent the results of calculations obtained for the 27 major actinides using the codes EVA, REFACTN and PEPABAC as well as those obtained with our chosen algorithm (*RK4*), after one day and after one year of cooling, respectively.

Based on Tables (*B-2)* and (*B-3)*, we can see that the algorithm (*RK4*) chosen for our burnup calculation code BUCAL1, gives results that are in very good agreement with those obtained by the codes EVA, REFACTN and PEPABAC. The only difference exist is for the concentration of Np239 after a year of cooling (*Tab. B-3*), we can see that for codes EVA, REFACTN and PEPABAC the concentration of Np239 is almost negligible, whereas it is not the case for our algorithm (*RK4*), which is due to the fact that the codes EVA, REFACTN and PEPABAC do not take into account the production of Np239 from the alpha decay (α) of Am243 because they use just a simplified decay chain (*Fig. B-2*).

Table B-1. Initial Concentrations of the major actinides (1.0E+21 At./tU).

Nuclides	Initial Concentrations (1.0E+21 At./tU)
U232	7.7400E-3
U233	0.0000E+00
U234	5.3236E+00
U235	2.0549E+04
U236	1.3222E+04
U237	0.0000E+00
U238	2.3483E+06
U239	1.3555E+00
Np236	0.0000E+00
Np237	1.9526E+02
Np238	0.0000E+00
Np239	1.9526E+02
Pu236	1.9730E-02
Pu238	7.5259E+02
Pu239	1.4934E+04
Pu240	6.5723E+03
Pu241	4.0280E+03
Pu242	1.9450E+03
Pu243	0.0000E+00
Am241	2.2839E+02
Am242(M)	3.3378E+00
Am242	0.0000E+00
Am243	4.3643E+02
Am244	0.0000E+00
Cm242	7.0723E+01
Cm243	3.2056E+01
Cm244	1.6616E+02

Table B-2. Atomic Concentrations calculated after one day of cooling.

Nuclides	EVA	REFACTN	PEPABAC	RK4
U232	7.7529E-03	7.7530E-03	7.7529E-03	7.7528E-03
U233	1.5011E-06	-	1.5011E-06	-
U234	5.3399E+00	5.3990E+00	5.3399E+00	5.3397E+00
U235	2.0549E+04	2.0549E+04	2.05499E+04	2.0549E+00
U236	1.3222E+04	1.3222E+04	1.3222E+04	1.3222E+04
U237	-	-	-	4.8980E-03
U238	2.3483E+06	2.3483E+06	2.3483E+06	2.3483E+06
U239	5.1974E-19	5.1917E-19	5.1974E-19	4.9334E-19
Np236	-	-	-	0.0000E+00
Np237	1.6934E+03	1.6934E+03	1.6934E+03	1.6934E+03
Np238	-	-	-	0.0000E+00
Np239	1.4649E+02	1.4648E+02	1.4649E+02	1.4658E+02
Pu236	1.9717E-02	1.9717E-02	1.9717E-02	1.9717E-02
Pu238	7.5287E+02	7.5287E+02	7.5287E+02	7.5287E+02
Pu239	1.4934E+04	1.4934E+04	1.4934E+04	1.4984E+04
Pu240	6.5723E+03	6.5723E+03	6.5723E+03	6.5723E+03
Pu241	4.0275E+03	4.0275E+03	4.0275E+03	4.0275E+03
Pu242	1.9450E+03	1.9450E+03	1.9450E+03	1.9450E+03
Pu243	-	-	-	0.0000E+00
Am241	2.2891E+02	2.2891E+02	2.2891E+02	2.2890E+02
Am242(M)	3.3378E+00	3.3377E+00	3.3378E+00	3.3378E+00
Am242	2.7823E-05	4.3068E-05	2.7823E-05	2.7950E-05
Am243	4.3643E+02	4.3643E+02	4.3643E+02	4.3643E+02
Am244	-	-	-	0.0000E+00
Cm242	7.0423E+01	7.0423E+01	7.0423E+01	7.0423E+01
Cm243	3.2054E+00	3.2054E+00	3.2054E+00	3.2054E+00
Cm244	1.6614E+02	1.6614E+02	1.6614E+02	1.6614E+02

Table B-3. Atomic Concentrations calculated after one year of cooling.

Nuclides	EVA	REFACTN	PEPABAC	RK4
U232	1.1898E-02	1.1898E-02	1.1898E-02	1.1900E-02
U233	5.4799E-04	-	5.4799E-04	-
U234	1.1515E+01	1.1515E+01	1.1515E+01	1.1520E+01
U235	2.0549E+04	2.0550E+04	2.0549E+04	2.0549E+04
U236	1.3223E+04	1.3223E+04	1.3223E+04	1.3223E+04
U237	-	-	-	4.8401E-02
U238	2.3483E+06	2.3483E+06	2.3483E+06	2.3483E+06
U239	0.0000E+00	0.0000E+00	0.0000E+00	0.0000E+00
Np236	-	-	-	0.0000E+00
Np237	1.6939E+03	1.6939E+03	1.6939E+03	1.6957E+03
Np238	-	-	-	0.0000E+00
Np239	**4.2039E-45**	**0.0000E+00**	**0.0000E+00**	**3.8233E-04**
Pu236	1.5474E-02	1.5474E-02	1.5474E-02	1.5472E-02
Pu238	8.0216E+02	8.0215E+02	8.0216E+02	8.0217E+02
Pu239	1.4934E+04	1.4934E+04	1.5130E+04	1.5130E+04
Pu240	6.5778E+03	6.5778E+03	6.5778E+03	6.5778E+03
Pu241	3.8426E+03	3.8426E+03	3.8426E+03	3.8425E+03
Pu242	1.9450E+03	1.9450E+03	1.9450E+03	1.9450E+03
Pu243	-	-	-	0.0000E+00
Am241	4.1325E+02	4.1326E+02	4.1325E+02	4.1154E+02
Am242(M)	3.3214E+00	3.3214E+00	3.3214E+00	3.3214E+00
Am242	4.2858E-05	4.2857E-05	4.2858E-05	4.3026E-05
Am243	4.3639E+02	4.3639E+02	4.3639E+02	4.3639E+02
Am244	-	-	-	0.0000E+00
Cm242	1.4980E+01	1.4980E+01	1.4980E+01	1.4957E+01
Cm243	3.1286E+00	3.1286E+00	3.1286E+00	3.1286E+00
Cm244	1.5992E+02	1.5992E+02	1.5992E+02	1.5992E+02

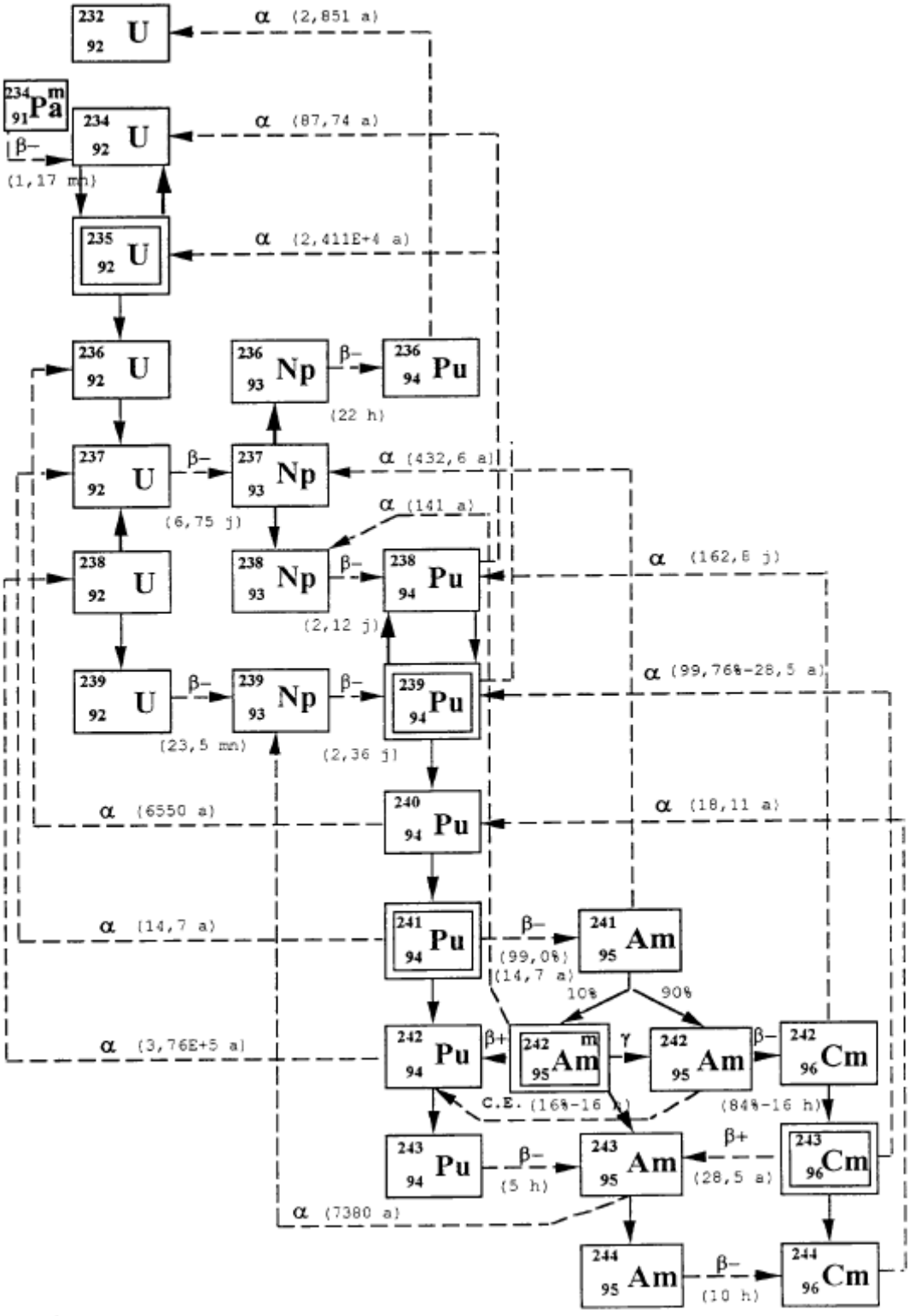

Fig. B-1. Uranium decay chain used for (RK4) verification.

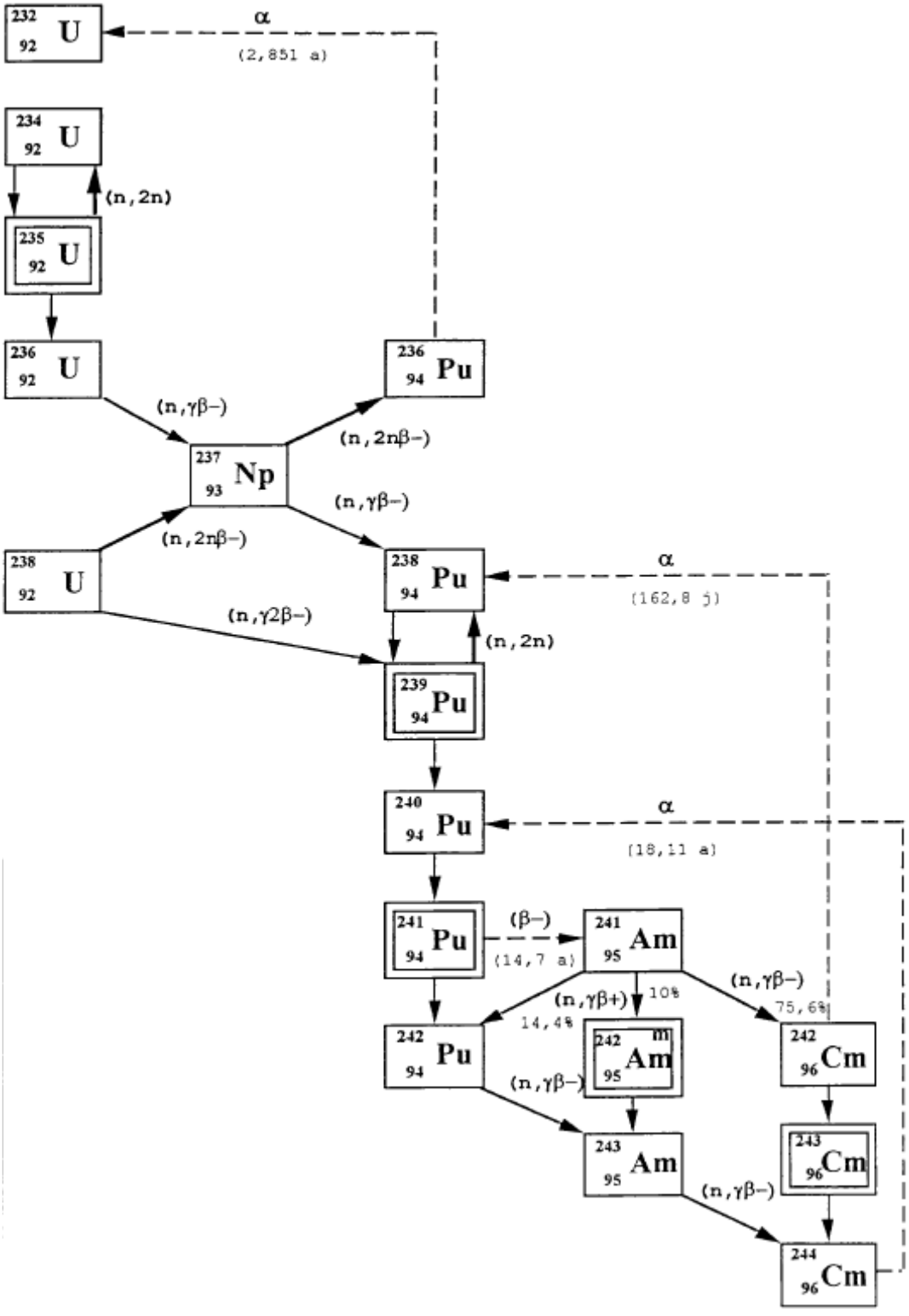

Fig. B-2. Uranium decay chain used by EVA, REFACTN and PEPABAC.

Appendix C. BUCALl1 input and outputs description

I. Code description

A general description of the BUCAL1 code package is presented in this section. The code modules, input, outputs, and library files required to perform a burnup analysis are also presented along with a flow diagram.

I-1 BUCAL1 code description

BUCAL1 is a Fortran 90/95 program that can be run under Windows or Linux systems, the code is made up of a number of subprograms that perform the necessary data interpretation requirements, calculate the new nuclide inventory, and insert the new data into the MCNP file, the script file controls the overall flow of the code package and runs BUCAL1 at every iteration in the burnup analysis. The main subprograms and their function are as follows:

- ***Main program***: Controls overall flow in the code and determines when the last iteration is reached.
- ***Burinp***: read and interpret the BUCAL1 input file.
- ***Multiplication_factor***: extract the necessary data from the MCNP output file, and calculate the conversion factor CF.
- ***MCNPOUT***: read the MCNP output file and extract the average one group capture, fission, absorption, (n, 2n), and (n, 3n) reaction rates and the three groups energy neutron flux.
- ***Conversion***: convert the average one group reaction rates and the three energy groups of neutron flux from the MCNP units "reactions/cm^3-source-neutron" to reel units, and organise the data into a suitable format to be used by the "***Evo***" subprogram.
- ***Evo***: calculate the new nuclide inventory (atom/b-cm) by using the BUCAL1 data bases, initial and final time steps, reaction rates and flux for both predictor and corrector steps.
- ***MCNPINPUT***: this subprogram is used to read and write into the MCNP input file, that allows updating the MCNP input automatically and without user interventions.
- ***Data_edit***: write the calculated data even by the MCNP code such as *keff*, or by BUCAL1 such as the nuclide inventories for each region, as a function of time in the output files.
- ***Refresh***: this subprogram is used to do cooling (or decay) calculations in case after reactor shutdown. This subprogram is optional and depends on the user demand.

- ***Shuffling***: this subprogram is used for shuffling and reloading of fuel elements, and it is used for fuel management studies. Also note that, this subprogram is optional and depends on the user demand.

The rest of subprograms are used for the treatment of data and to ensure a correct exchange of data between the principal subprograms.

I-2 BUCAL1 code database

BUCAL1 uses mainly five database files which are “cap_br”, “decay”, “ffy”, “thfy”, “fp_xs”, these files contain the necessary information about the isotopes included in the burnup chains of BUCAL1 code (approximately 900 isotopes), such as, fast and thermal fission products yields, half-lives, branching ratios, etc… . The code is designed to handle isotopes in both metastable and ground states simultaneously. For this version of BUCAL1, there are 6 decay modes that are taken into account such as: b^-, gamma, b^+, electronique capture *CE*, alpha, and (b,n). Also, in this version of BUCLA1 there are 11 actinides that are considered as fissile isotopes such as, *Th232*, *Pa231*, *U233*, *U235*, *U238*, *Pu239*, *Pu240*, *Pu241*, *Pu242*, *Am241*, and *Am242M*, that allows doing burnup calculations for a large variety of nuclear fuels such as, *UO2*, *ThO2-UO2*, *MOX*, *U-ZrH*, etc…. The fission product yields of these fissile isotopes as well as decay data were taken from the ENDF/B-VI.8 and JEFF3-1 decay libraries.

I-3 BUCAL1 input description

The BUCAL1 input file is identified as “burinp.dat”, the file is a user-supplied file that allows the user to specify the number of burnup iterations to be performed, the time increment for solving the burnup equations, the power density, the number of burnable materials, the isotopic composition of burnable materials, the temperature of burnable materials, etc. Although, the BUCAL1 input file is required to be structured and formatted in such a way as to allow the BUCAL1 code to correctly read and extract the information, the intent in developing the code was to minimize the requirements as much as possible.

Figure C-1, represents a general description of “burinp.dat” input file, the main structure and the formatting requirements for the BUCAL1 input file.

```
                ****************************************
                !                                      !
                        !!!!!!! BUCAL1 input file !!!!!!!
                !                                      !
                 ****************************************
* Power
    Pow      SPow
* Number of active cells
    N_cell
* Number of cells similar to active cells
  N_sc(i)  (i =1, N_cell)
* Volume (cc) and density (g/cc)
    Vol(i)     Dens(i)  (i =1, N_cell)
* Number of Burnable elements (in each active cell)
    N_BU(i)   (i = 1, N_cell)
* Material composition in each active cell
* Active cell (i)     , (i =1, N_cell)
    MAT(i)    N_0(i)  (i = 1, N_BU)
* Temperatures (Kelvin)
  Temp(i)   (i = 1, N_cell)
* Number of cycles
  N_cycle
* Number of Time steps per cycle
  N_TS
* Time
+ T_Cylce (i)    ( i = 1, N_cycle)
  T_cy(i)    (i = 1, N_TS)
* Micro time steps per cycle
+ MTS_Cylce (i)    ( i = 1, N_cycle)
  M_TS(i)  (i = 1, N_TS-1)
* Refreshment
+ R_Cylce (i)  ( i = 1, N_cycle)
  TR(i)
* Shuffling
  Yes/No
* MCNP name file (maximum 8 characters)
  Name file
* Isotope importance
  Mat1     1/0
  Mat2     1/0
    ……        …….        ……
```

Fig. C-1. Standard format of “burinp.dat” BUCAL1 input file.

The BUCAL1 input file defined as "Burinp.dat" consists of 15 cards, these cards contain the data required to do burnup calculations for a wide variety of nuclear systems ranging from unit cell benchmarks to nuclear reactors using very complicated physical and geometrical data.

The significance of these cards is as follows:

- **Power:**

  Pow: The total power of the system (Watts).

  SPow: The power density of the system (W/gIHM). (IHM = Initial heavy metal).

- **Number of active cells:** The total number of active cells (fueled regions) to be considered for burnup calculations.
- **Number of cells similar to active cells:** For benchmarks using several fuel elements we can reduce the time of burnup calculations by reducing the number of active cells, because of the symmetrical distribution of neutron flux in these fuel elements.

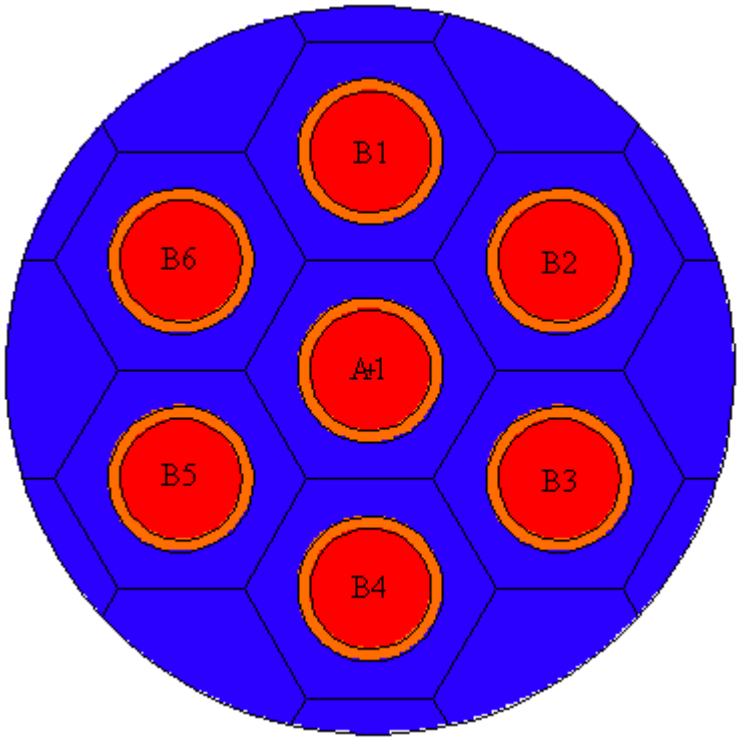

Fig. C-2. Benchmark with 7 fuel elements.

For example, Figure C-2 represents a benchmark with 7 fuel elements. So, due to the symmetry of the neutron flux for the cells of ring B, one can choose just one cell of this ring (B1, for example) to do burnup calculations. In this case, there will be 2 as total active cells,

which are A1 and B1, and for the card "***Number of cells similar to active cells***" one should write 1 and 6, respectively. The number 6 represents the total number of cells similar to B1 cell.

- **Volume and density:**

  Vol (i): The volumes of active cells chosen by the user for burnup calculations.

  Dens (i): The densities of active cells chosen by the user for burnup calculations.

- **Number of burnable elements:** The total number of element in each active cell chosen by the user to be as burnable elements.
- **Material composition:** The user must specifies the material balance, material identifier (Z*1000 + A) and the initial atom density (at./b-cm), of burnable elements chosen by the user in each active cell.
- **Temperature:** The user must specify the temperatures in unite of Kelvin for each fuel region.
- **Number of cycles:** The user must specify the number of fuel cycles considered for each burnup calculation. Note that, a fuel cycle is considered as a period of burnup under neutron flux (or irradiation).
- **Number of time steps per cycle:** The total number of time steps per cycle used for burnup calculations.
- **Time:** The set of time steps used for burnup calculations. The maximum number of burnup points allowed by BUCAL1 is 100. And one should use smaller time step size in the beginning of irradiation.
- **Micro-time steps per cycle:** Specifies the number of micro – burnup time steps between two successive burnup points.

  The MTS numbers should be one less than the number of time steps (Tcy).

- **Refreshment:** The number of time steps used for cooling (or decay) calculations after reactor shutdown.
- **Shuffling:** The user must specify if he wants to do shuffling of fuel elements after a period of burnup or not. If the "Yes" option is selected than the user must fill a small shuffling input file that contains the necessary information for shuffling, such as, the times of shuffling and the fuel elements to be shuffled, etc … .

- **MCNP input file:** Specify the MCNP source file. The MCNP source file must have a maximum of 8 characters.
- **Isotope importance:** This card allows the user to choose from the important isotopes ones that he wants to take into account in his burnup study. Defaults, all the important isotopes are included. “0” means that the selected isotope is excluded from the burnup study.

I-4 MCNP input description

The MCNP input file is required to be structured and formatted in such a way as to allow BUCAL1 code to properly resolve the information and update the isotopic inventory automatically within the MCNP input. The user will find that the basic format for typical ***keff***-type calculations exists with the ability to include lattices and universe. The main structure and formatting requirements include proper identification of cell cards and material cards to be analyzed, the use of “print” card as an end identifier, correct column formatting for cells and materials cards, isotope concentration in density (atom/b-cm) format, addition of keywords and Tally comment card (FC) to identify the start and the end of materials for tally identifiers, the addition of “vol” card, and the proper use of the tally multiplier cards. The cross sections used in the analysis, the amount of detail in the geometry, and the number of neutrons and histories used in the analysis are user specified.

I-5 MCNP-BUCAL1 outputs

The MCNP-BUCAL1 output consists of many neutronic parameters data allow a real burnup study. These parameters are distributed into the following output files, “burnup_history”, “density.edit”, “mass.edit”, “flux.edit”, “actrates.edit”, “activity.edit”, and “errorhistory”.

The description of the content of each of these files is as follows:

- ***Burnup_history***: this file contains the average system eigenvalues, such as, keff (and its standard deviation error), nubar ($\bar{u}$), the average fission energy *Q*(Mev), burnup (MW.d/KgIHM), and power (MW) variations as a function of time.

A simple example of this file is presented in ***Fig.*** C-3.

Time(d)	*Keff*	*Err*	*Power(MW)*	*Bu(MW.d/KgU)*	*Nubar*	*Q(MeV)*
Cycle number ::	*1*					
0.00000E+00	1.56835	0.13200E-02	0.66362E-03	0.00000E+00	0.24541E+01	0.20098E+03
0.30000E+01	1.53385	0.13000E-02	0.66362E-03	0.10400E+00	0.24545E+01	0.20098E+03
0.10000E+02	1.52811	0.13500E-02	0.66362E-03	0.34668E+00	0.24552E+01	0.20099E+03
0.20000E+02	1.52363	0.13800E-02	0.66362E-03	0.69336E+00	0.24562E+01	0.20101E+03
0.30000E+02	1.51702	0.13600E-02	0.66362E-03	0.10400E+01	0.24571E+01	0.20104E+03
0.40000E+02	1.51691	0.12300E-02	0.66362E-03	0.13867E+01	0.24582E+01	0.20106E+03
0.50000E+02	1.51243	0.12600E-02	0.66362E-03	0.17334E+01	0.24591E+01	0.20108E+03
……..						

Fig. C-3. A simple example of Burnup_history output file.

- ***Density.edit***: this file gives the nuclide densities (atom/b-cm) for the most important isotopes used by MCNP for burnup calculation as a function of time and for all the regions (or cells) considered as burnable by the user. This file can also contain the nuclide density of isotopes during the time of cooling (or decay). A simple example of this file is presented in *Fig. C-4.*
- ***Mass.edit***: this file gives the masses (kg) for the most important isotopes used by MCNP for burnup calculation as a function of time and for all the regions (or cells) considered as burnable by the user. A simple example of this file is presented in *Fig. C-5.*
- ***Flux.edit***: this file gives the neutron flux information as a function of time and for all the regions (or cells) considered as burnable by the user, for three groups of energy: thermal (from 0 to 0.625 eV), epithermal (from 0.625eV to 100 keV), and fast from (100keV to 20MeV).

A simple example of this file is presented in *Fig. C-6.*

```
============================================================
 Isotopes densities(at/b-cm) for each active cell and at each burnup time step
============================================================
 =====> Cycle number    ::          1
 =====> Time step (day) ::   3.00
 ncell ::          1
   35081      0.49698E-08    54134      0.18933E-06    66162      0.98949E-12
   36082      0.11758E-11    55134      0.15542E-11    66163      0.37178E-12
   36083      0.12307E-07    56134      0.90990E-15    68166      0.72994E-14
   36084      0.21571E-07    54135      0.17212E-07    68167      0.46303E-13
   37085      0.22507E-07    55135      0.72083E-07    90231      0.80410E-14
   37087      0.58817E-07    54136      0.15711E-06    90232      0.79281E-16
   39089      0.21974E-08    55137      0.15243E-06    90233      0.64716E-22
   38090      0.13891E-06    56137      0.16968E-10    91231      0.10233E-13
   40091      0.70495E-09    56138      0.16395E-06    91232      0.42866E-17
   40092      0.12815E-06    57139      0.15423E-06    91233      0.57330E-18
   40093      0.91380E-07    58140      0.37122E-08    92232      0.68543E-14
   40094      0.15635E-06    58141      0.13035E-06    92233      0.84100E-12
   41095      0.24743E-08    59141      0.38561E-08    92234      0.18210E-04
   42095      0.49170E-10    58142      0.13807E-06    92235      0.22652E-02
   40096      0.15551E-06    60142      0.19677E-13    92236      0.60445E-06
   42096      0.74640E-11    59143      0.66121E-07    92237      0.40366E-08
   42097      0.92927E-07    60143      0.37735E-08    92238      0.20712E-01
   42098      0.14313E-06    58144      0.13417E-06    92239      0.53706E-08
   43099      0.36999E-07    60144      0.48756E-09    93235      0.14200E-19
   42100      0.15754E-06    60145      0.85196E-07    93236      0.10737E-16
   44100      0.47303E-11    60146      0.74150E-07    93237      0.64568E-09
   44101      0.12879E-06    60147      0.50769E-07    93238      0.21395E-12
   44102      0.10908E-06    61147      0.48938E-08    93239      0.45274E-06
   44103      0.78026E-07    62147      0.35570E-11    94236      0.19905E-22
   45103      0.19818E-08    60148      0.42278E-07    94238      0.64385E-13
   44104      0.50905E-07    61148      0.17703E-11    94239      0.22662E-06
   46104      0.83279E-12    61148      0.18444E-11    94240      0.11611E-09
   45105      0.14490E-07    62148      0.20420E-12    94241      0.25924E-12
   46105      0.11218E-07    61149      0.17333E-07    94242      0.48632E-16
   46106      0.33281E-09    62149      0.85938E-08    94243      0.45482E-20
   46107      0.58549E-08    60150      0.17143E-07    95241      0.20801E-16
    …….. (Not Finished) ……
xxxxxxxxxxxxxxxxxxxxxxxxxxxxxxxxxxxxxxxxxxxxxxxxxxxxxxxxxxxxxxxxxxxxxxxxxxx
```

Fig. C-4. Example of “Density.edit” file.

```
=====================================================
 Mass(Kg) for important isotopes
=====================================================
 ====> Cycle number    ::         1
 ====> Time step (day) ::   3.00
 ncell ::         1
   35081      0.14078E-08   54134   0.88755E-07   66162   0.56093E-12
   36082      0.33718E-12   55134   0.72860E-12   66163   0.21206E-12
   36083      0.35725E-08   56134   0.42655E-15   68166   0.42914E-14
   36084      0.63368E-08   54135   0.81290E-08   68167   0.27060E-13
   37085      0.66906E-08   55135   0.34044E-07   90231   0.65039E-14
   37087      0.17896E-07   54136   0.74753E-07   90232   0.64404E-16
   39089      0.68396E-09   55137   0.73060E-07   90233   0.52799E-22
   38090      0.43722E-07   56137   0.81326E-11   91231   0.82769E-14
   40091      0.22435E-09   56138   0.79155E-07   91232   0.34822E-17
   40092      0.41233E-07   57139   0.75002E-07   91233   0.46773E-18
   40093      0.29722E-07   58140   0.18182E-08   92232   0.55681E-14
   40094      0.51401E-07   58141   0.64301E-07   92233   0.68614E-12
   41095      0.82212E-09   59141   0.19023E-08   92234   0.14921E-04
   42095      0.16337E-10   58142   0.68596E-07   92235   0.18640E-02
   40096      0.52215E-07   60142   0.97755E-14   92236   0.49951E-06
   42096      0.25061E-11   59143   0.33082E-07   92237   0.33500E-08
   42097      0.31526E-07   60143   0.18879E-08   92238   0.17261E-01
   42098      0.49060E-07   58144   0.67597E-07   92239   0.44947E-08
   43099      0.12812E-07   60144   0.24564E-09   93235   0.11685E-19
   42100      0.55102E-07   60145   0.43222E-07   93236   0.88727E-17
   44100      0.16544E-11   60146   0.37878E-07   93237   0.53584E-09
   44101      0.45497E-07   60147   0.26113E-07   93238   0.17831E-12
   44102      0.38914E-07   61147   0.25171E-08   93239   0.37890E-06
   44103      0.28110E-07   62147   0.18295E-11   94236   0.16449E-22
   45103      0.71398E-09   60148   0.21893E-07   94238   0.53658E-13
   44104      0.18517E-07   61148   0.91675E-12   94239   0.18966E-06
   46104      0.30293E-12   61148   0.95513E-12   94240   0.97576E-10
   45105      0.53218E-08   62148   0.10574E-12   94241   0.21878E-12
   46105      0.41199E-08   61149   0.90367E-08   94242   0.41212E-16
   46106      0.12339E-09   62149   0.44804E-08   94243   0.38702E-20
   46107      0.21913E-08   60150   0.89979E-08   95241   0.17555E-16
…….. ( Not Finished) ……
xxxxxxxxxxxxxxxxxxxxxxxxxxxxxxxxxxxxxxxxxxxxxxxxxxxxxxxxxxxxxxxxxxxxxxx
```

Fig.C-5. Example of “Mass.edit” file.

```
Cycle number ::          1
 Time (days)  ::  0.00
   1  0.34162E+00    0.62690E+00    0.40297E+01
 Cell / Energy Groups(MeV):
      0.62500E-06  0.10000E-03  0.20000E+02
==========================================
 Cycle number ::          1
 Time (days)  ::   3.00
   1  0.33592E+00    0.62398E+00    0.40274E+01
 Cell / Energy Groups(MeV):
      0.62500E-06  0.10000E-03  0.20000E+02
==========================================
 Cycle number ::          1
 Time (days)  ::   10.00
   1  0.33233E+00   0.62860E+00   0.40222E+01
 Cell / Energy Groups(MeV):
      0.62500E-06  0.10000E-03  0.20000E+02
…….…… (Not Finished) …….....
```

Fig. C-6. Example of "Flux.edit" file.

- ***Activity.edit***: this file contains the activity (Bq) for some of important isotopes; this file is available only in case of cooling (or decay) after reactor shutdown.

A simple example of this file is presented in *Fig.C-7*. This figure shows also the isotopes selected in this option.

- ***Actrates.edit***: This file gives the one group microscopic fission, capture, and absorption reaction rates for all the actinides used by MCNP for burnup calculations as a function of time and for all the regions (or cells) considered as burnable by the user. Note that, the values in this file are in ($n.s^{-1}$).

A simple example of this file is presented in *Fig.C-8*.

- ***Errorhistory***: this file allows the user to follow the code history under running and to identify easily the program errors if occurred.

```
================================================================
 Isotopes activities in Bq for each active cell and at each burnup time step
================================================================
 =====> Time step (day) =   10.00
 Ncell =          1
 Total activity in Bq =  2.780616951964347E+043

 37087  0.79810E+31  60144  0.28823E+27  92233  0.47670E+31  95241  0.22087E+40
 38090  0.27420E+41  60147  0.48959E+42  92234  0.24659E+36  95242  0.91697E+38
 40093  0.68398E+36  61147  0.19915E+42  92235  0.62593E+34  95242  0.10581E+39
 41095  0.19925E+43  62147  0.81817E+30  92236  0.11068E+35  95243  0.24972E+39
 43099  0.10197E+38  61148  0.65289E+41  92237  0.96835E+41  95244  0.66201E+35
 44103  0.24881E+43  61148  0.50199E+41  92238  0.47497E+36  96242  0.20887E+42
 45105  0.24506E+41  62148  0.15399E+26  92239  0.49155-141   96243  0.41866E+38
 46107  0.19376E+36  61149  0.29030E+41  93235  0.20656E+34  96244  0.22220E+41
 48113  0.63459E+24  62149  0.21401E+26  93236  0.70385E+31  96245  0.24576E+37
 49115  0.28098E+26  62151  0.15543E+40  93237  0.79560E+35  96246  0.75906E+35
 53129  0.25956E+35  62153  0.12047E+41  93238  0.18031E+40  96247  0.15507E+30
 54133  0.98413E+42  63154  0.40210E+40  93239  0.12427E+43  96248  0.16209E+30
 55134  0.56409E+41  63155  0.43637E+40  94236  0.60512E+36  96249  0.52130E+33
 54135  0.11795E+36  63156  0.10143E+42  94238  0.47453E+41  97249  0.63703E+32
 55135  0.79592E+36  68167  0.00000E+00  94239  0.33525E+40  97250  0.19404E+10
 55137  0.79803E+41  90232  0.35610E+24  94240  0.72278E+40  98249  0.16824E+29
 58141  0.18425E+43  91231  0.26510E+23  94241  0.15362E+43  98250  0.33007E+30
 59143  0.13082E+43  91233  0.71985E+35  94242  0.35785E+38  98251  0.10478E+28
 58144  0.11219E+43  92232  0.39388E+34  94243  0.16225E+30  98252  0.24142E+29
xxxxxxxxxxxxxxxxxxxxxxxxxxxxxxxxxxxxxxxxxxxxxxxxxxxxxxxxxxxxxxxxxxxxxxxxxxxxxxx
```

Fig. C-7. Example of “Activity.edit” file.

Cycle number :: 1

Time (days) :: 0.00
cell number :: 1

90231	0.38236E-03	0.45509E-03	0.72418E-04
90232	0.36836E-04	0.37305E-04	0.38853E-06
90233	0.77472E-03	0.81368E-03	0.38574E-04
91231	0.53634E-03	0.54237E-03	0.59740E-05
91232	0.39302E-03	0.13640E-02	0.97085E-03
91233	0.31977E-03	0.32223E-03	0.24367E-05
92232	0.13295E-03	0.33125E-03	0.19826E-03
92233	0.70942E-04	0.59570E-03	0.52473E-03
92234	0.24682E-03	0.25475E-03	0.79217E-05
92235	0.88508E-04	0.44492E-03	0.35635E-03
92236	0.12050E-03	0.12528E-03	0.47380E-05
92237	0.32855E-03	0.33702E-03	0.83478E-05
92238	0.10930E-04	0.12594E-04	0.15898E-05
92239	0.32990E-03	0.33368E-03	0.34333E-05
93235	0.89628E-03	0.90463E-03	0.83280E-05
93236	0.70063E-04	0.19733E-02	0.19032E-02
93237	0.38766E-03	0.39566E-03	0.79835E-05
93238	0.70062E-04	0.16393E-02	0.15692E-02
93239	0.20038E-03	0.20968E-03	0.92810E-05
94236	0.11356E-03	0.53228E-03	0.41872E-03
94238	0.26870E-03	0.29749E-03	0.28766E-04
94239	0.48018E-03	0.13362E-02	0.85599E-03
94240	0.28239E-02	0.28331E-02	0.91875E-05
94241	0.30578E-03	0.11807E-02	0.87481E-03
94242	0.46822E-03	0.47497E-03	0.67170E-05
94243	0.13283E-03	0.40692E-03	0.27381E-03
95241	0.10635E-02	0.10775E-02	0.13996E-04
95242	0.85207E-03	0.53493E-02	0.44972E-02

…… (*Not Finished*) ……

Capture Absorption Fission

xxxxxxxxxxxxxxxxxxxxxxxxxxxxxxxxxxxxxxxxxxxxxxxxxxxxxx

Fig. C-8. Example of “Actrates.edit” file.

II- Recommendations on Choosing Number of Neutron Histories

In the MCNP kcode calculation, users usually need to determine how to allocate the number of neutrons per cycle and total number of cycles. The total number of neutron histories determines the accurateness of results, which depends on the available computational resources. But it is up to the user to specify number of neutrons per cycle and number of

cycles. On a single-CPU machine, one can typically specify ~2000 neutrons/cycle for a simple-geometry problem (such as a unit cell) and ~5000 neutrons/cycle for a complicated problem (such as a fuel assembly). The rule of thumb is to ensure that there are fission neutron sources in each individual fuel region. Then it is straightforward to decide the number of cycles.

On a cluster-type machine (parallel computing), one needs to select a certain number of nodes to do an MCNP calculation. Once that is determined, say 10 nodes, the user then needs to adjust the pattern of allocation of the number of neutrons per cycle and the total number of cycles. Generally speaking it is more computationally efficient to increase number of neutrons per cycle than increasing the number of cycles. Thus, it is worthwhile to increase the number of neutrons by ~50% while reducing the number of cycles by ~50% compared to cases running on a single-CPU machine.

III- Running BUCAL1

To run burnup calculation with BUCAL1 code, first of all, the user must create a directory for its calculation. In this directory, he must put the directory "data_code" which contains all the necessary databases for BUCAL1 code, the executable program of BUCAL1 code "bucal1.64S" (actually version), the MCNP input file prepared in a format readable by the BUCAL1 code, "burinp.dat" file which contains the data required for BUCAL1 for doing burnup calculations, and the "xsdir" file for MCNP code which contains data on the neutron cross sections used: temperature, size of files, cross sections file paths, etc. Once this is done!. The user must enter to his directory through the "***Konsole***", for Linux systems, and execute the command" **./bucal1.64S &** "and then calculation will run automatically.

Appendix D. BUCAL1 inputs and outputs examples

```
c ========================================================
c            MCNP5 input file for UO2 Benchmark
c ========================================================
c     Created on: Thursday, February 15, 2007 at 23:12
c     the power of the system = 663.616 W
c     the specfic power = 34.6679 W/gU
     1      1  6.8967884e-2 -1 4 -5 vol=2.1083 tmp=2.5851e-8
     2      2  3.76622e-005  1 -2 4 -5 vol=8.5259e-2 tmp=2.5851e-8
     3      3  4.34418e-2    2 -3 4 -5 vol=6.4174e-1 tmp=2.5851e-8
     4      4  9.99634e-2    3 -6 7 -8 9 4 -5 vol=3.5151 tmp=2.5851e-8
     5      0         6 :-7 :8 :-9 :-4 :5 tmp=2.53e-8

     1         cz 0.4096
     2         cz 0.4178
     3         cz 0.475
    *4         pz -2
    *5         pz 2
    *6         px 0.63
    *7         px -0.63
    *8         py 0.63
    *9         py -0.63

mode  n
kcode 1500 1.000000 5 500
ksrc  0.000000 0.000000 -1.000000
      0.000000 0.000000 0.000000
      0.000000 0.000000 1.000000
C Start burnup
C Fuel material number:01
m1      8016.70c   0.0459686
C burnable elements
  35081.55c  1.00000E-48  55133.66c  1.00000E-48  66160.20c  1.00000E-48
  36082.59c  1.00000E-48  54134.66c  1.00000E-48  66161.20c  1.00000E-48
  36083.59c  1.00000E-48  55134.60c  1.00000E-48  66162.20c  1.00000E-48
  36084.59c  1.00000E-48  56134.70c  1.00000E-48  66163.20c  1.00000E-48
  37085.55c  1.00000E-48  54135.50c  1.00000E-48  68166.20c  1.00000E-48
  37087.55c  1.00000E-48  55135.70c  1.00000E-48  68167.20c  1.00000E-48
  39089.35c  1.00000E-48  54136.66c  1.00000E-48  90232.66c  1.00000E-48
  38090.70c  1.00000E-48  55137.60c  1.00000E-48  91231.66c  1.00000E-48
  40091.66c  1.00000E-48  56137.70c  1.00000E-48  91233.66c  1.00000E-48
  40092.66c  1.00000E-48  56138.66c  1.00000E-48  92232.66c  1.00000E-48
  40093.50c  1.00000E-48  57139.70c  1.00000E-48  92233.66c  1.00000E-48
  40094.66c  1.00000E-48  58140.70c  1.00000E-48  92234.66c  1.82239E-05
  41095.70c  1.00000E-48  58141.70c  1.00000E-48  92235.66c  2.26826E-03
  42095.50c  1.00000E-48  59141.50c  1.00000E-48  92236.66c  1.00000E-48
  40096.66c  1.00000E-48  58142.70c  1.00000E-48  92237.66c  1.00000E-48
  42096.70c  1.00000E-48  60142.20c  1.00000E-48  92238.66c  2.07128E-02
  42097.70c  1.00000E-48  59143.70c  1.00000E-48  92239.70c  1.00000E-48
  42098.70c  1.00000E-48  60143.50c  1.00000E-48  93235.42c  1.00000E-48
  43099.66c  1.00000E-48  58144.70c  1.00000E-48  93236.70c  1.00000E-48
  42100.70c  1.00000E-48  60144.20c  1.00000E-48  93237.66c  1.00000E-48
  44100.70c  1.00000E-48  60145.50c  1.00000E-48  93238.70c  1.00000E-48
  44101.50c  1.00000E-48  60146.20c  1.00000E-48  93239.66c  1.00000E-48
  44102.70c  1.00000E-48  60147.50c  1.00000E-48  94236.66c  1.00000E-48
  44103.50c  1.00000E-48  61147.50c  1.00000E-48  94238.66c  1.00000E-48
  45103.66c  1.00000E-48  62147.66c  1.00000E-48  94239.66c  1.00000E-48
  44104.70c  1.00000E-48  60148.50c  1.00000E-48  94240.66c  1.00000E-48
  46104.66c  1.00000E-48  61148.80c  1.00000E-48  94241.66c  1.00000E-48
  45105.50c  1.00000E-48  61148.50c  1.00000E-48  94242.66c  1.00000E-48
  46105.66c  1.00000E-48  62148.20c  1.00000E-48  94243.66c  1.00000E-48
  46106.66c  1.00000E-48  61149.50c  1.00000E-48  95241.66c  1.00000E-48
```

```
  46107.70c  1.00000E-48  62149.66c  1.00000E-48  95242.80c  1.00000E-48
  46108.66c  1.00000E-48  60150.20c  1.00000E-48  95242.66c  1.00000E-48
  47109.66c  1.00000E-48  62150.50c  1.00000E-48  95243.66c  1.00000E-48
  46110.66c  1.00000E-48  62151.50c  1.00000E-48  95244.70c  1.00000E-48
  48110.66c  1.00000E-48  63151.66c  1.00000E-48  96242.66c  1.00000E-48
  48111.66c  1.00000E-48  62152.50c  1.00000E-48  96243.66c  1.00000E-48
  48112.66c  1.00000E-48  62153.20c  1.00000E-48  96244.66c  1.00000E-48
  48113.66c  1.00000E-48  63153.66c  1.00000E-48  96245.66c  1.00000E-48
  48114.66c  1.00000E-48  62154.20c  1.00000E-48  96246.66c  1.00000E-48
  49115.70c  1.00000E-48  63154.66c  1.00000E-48  96247.66c  1.00000E-48
  51121.70c  1.00000E-48  64154.66c  1.00000E-48  96248.66c  1.00000E-48
  51123.70c  1.00000E-48  63155.66c  1.00000E-48  96249.70c  1.00000E-48
  53127.66c  1.00000E-48  64155.66c  1.00000E-48  97249.66c  1.00000E-48
  52128.70c  1.00000E-48  63156.70c  1.00000E-48  97250.70c  1.00000E-48
  53129.60c  1.00000E-48  64156.66c  1.00000E-48  98249.66c  1.00000E-48
  54131.66c  1.00000E-48  64157.66c  1.00000E-48  98250.66c  1.00000E-48
  54132.66c  1.00000E-48  64158.66c  1.00000E-48  98251.66c  1.00000E-48
  54133.70c  1.00000E-48  65159.70c  1.00000E-48  98252.66c  1.00000E-48
C END Burnup
m2    8016.70c   3.76622e-005  $MAT
c
c Zircaloy-4 (6.550g/cc)
m3    8016.70c  -0.00125  $ O
      24000.50c -0.001 26000.55c -0.0021 40000.60c -0.98115
      50000.42c -0.00145
c
c H2O (15.5MPa at 300K) (0.997g/cc)
m4    8016.70c  0.0333339  $MAT
      1001.70c 6.66295e-2
mt4 lwtr.60t
imp:n             1 3r                        0  $ 1, 5
c
=============================================================================
=
c   importances, neutron mode only and keff calculation
c
=============================================================================
=
c Fission products <=========================<
m856  35081.55c             1  $
m857  36082.59c             1  $
m858  36083.59c             1  $
m859  36084.59c             1  $
m860  37085.55c             1  $
m861  37087.55c             1  $
m862  39089.35c             1  $
m863  38090.70c             1  $
m864  40091.66c             1  $
m865  40092.66c             1  $
m866  40093.50c             1  $
m867  40094.66c             1  $
m868  41095.70c             1  $
m869  42095.50c             1  $
m870  40096.66c             1  $
m871  42096.70c             1  $
m872  42097.70c             1  $
m873  42098.70c             1  $
m874  43099.66c             1  $
m875  42100.70c             1  $
m876  44100.70c             1  $
m877  44101.50c             1  $
```

```
m878   44102.70c                1   $
m879   44103.50c                1   $
m880   45103.66c                1   $
m881   44104.70c                1   $
m882   46104.66c                1   $
m883   45105.50c                1   $
m884   46105.66c                1   $
m885   46106.66c                1   $
m886   46107.70c                1   $
m887   46108.66c                1   $
m888   47109.66c                1   $
m889   46110.66c                1   $
m890   48110.66c                1   $
m891   48111.66c                1   $
m892   48112.66c                1   $
m893   48113.66c                1   $
m894   48114.66c                1   $
m895   49115.70c                1   $
m896   51121.70c                1   $
m897   51123.70c                1   $
m898   53127.66c                1   $
m899   52128.70c                1   $
m900   53129.60c                1   $
m901   54131.66c                1   $
m902   54132.66c                1   $
m903   54133.70c                1   $
m904   55133.66c                1   $
m905   54134.66c                1   $
m906   55134.60c                1   $
m907   56134.70c                1   $
m908   54135.50c                1   $
m909   55135.70c                1   $
m910   54136.66c                1   $
m911   55137.60c                1   $
m912   56137.70c                1   $
m913   56138.66c                1   $
m914   57139.70c                1   $
m915   58140.70c                1   $
m916   58141.70c                1   $
m917   59141.50c                1   $
m918   58142.70c                1   $
m919   60142.20c                1   $
m920   59143.70c                1   $
m921   60143.50c                1   $
m922   58144.70c                1   $
m923   60144.20c                1   $
m924   60145.50c                1   $
m925   60146.20c                1   $
m926   60147.50c                1   $
m927   61147.50c                1   $
m928   62147.66c                1   $
m929   60148.50c                1   $
m930   61148.80c                1   $
m931   61148.50c                1   $
m932   62148.20c                1   $
m933   61149.50c                1   $
m934   62149.66c                1   $
m935   60150.20c                1   $
m936   62150.50c                1   $
m937   62151.50c                1   $
m938   63151.66c                1   $
```

```
m939   62152.50c                1   $
m940   62153.20c                1   $
m941   63153.66c                1   $
m942   62154.20c                1   $
m943   63154.66c                1   $
m944   64154.66c                1   $
m945   63155.66c                1   $
m946   64155.66c                1   $
m947   63156.70c                1   $
m948   64156.66c                1   $
m949   64157.66c                1   $
m950   64158.66c                1   $
m951   65159.70c                1   $
m952   66160.20c                1   $
m953   66161.20c                1   $
m954   66162.20c                1   $
m955   66163.20c                1   $
m956   68166.20c                1   $
m957   68167.20c                1   $
c Actinides <======================
m958   90232.66c              1
m959   91231.66c              1
m960   91233.66c              1
m961   92232.66c              1
m962   92233.66c              1   $
m963   92234.66c              1   $
m964   92235.66c              1   $
m965   92236.66c              1   $
m966   92237.66c              1   $
m967   92238.66c              1   $
m968   92239.70c              1   $
m969   93235.42c              1   $
m970   93236.70c              1   $
m971   93237.66c              1   $
m972   93238.70c              1   $
m973   93239.66c              1   $
m974   94236.66c              1   $
m975   94238.66c              1   $
m976   94239.66c              1   $
m977   94240.66c              1   $
m978   94241.66c              1   $
m979   94242.66c              1   $
m980   94243.66c              1   $
m981   95241.66c              1   $
m982   95242.80c              1   $
m983   95242.66c              1   $
m984   95243.66c              1   $
m985   95244.70c              1   $
m986   96242.66c              1   $
m987   96243.66c              1   $
m988   96244.66c              1   $
m989   96245.66c              1
m990   96246.66c              1
m991   96247.66c              1
m992   96248.66c              1
m993   96249.70c              1
m994   97249.66c              1
m995   97250.70c              1
m996   98249.66c              1
m997   98250.66c              1
m998   98251.66c              1
```

```
m999  98252.66c            1
C
xxxxxxxxxxxxxxxxxxxxxxxxxxxxxxxxxxxxxxxxxxxxxxxxxxxxxxxxxxxxxxxxxxxxxxxxxxxxxxx
C                             Burnup
C
xxxxxxxxxxxxxxxxxxxxxxxxxxxxxxxxxxxxxxxxxxxxxxxxxxxxxxxxxxxxxxxxxxxxxxxxxxxxxxxx
C
@@@@@@@@@@@@@@@@@@@@@@@@@@@@@@@@@@@@@@@@@@@@@@@@@@@@@@@@@@@@@@@@@@@@@@@@@@@@@@@
FC4 Capture rates
C
@@@@@@@@@@@@@@@@@@@@@@@@@@@@@@@@@@@@@@@@@@@@@@@@@@@@@@@@@@@@@@@@@@@@@@@@@@@@@@@
F4:n 1
FM4  (1  856  102) (1  857  102) (1  858  102) (1  859  102) (1  860  102)
     (1  861  102) (1  862  102) (1  863  102) (1  864  102) (1  865  102)
     (1  866  102) (1  867  102) (1  868  102) (1  869  102) (1  870  102)
     (1  871  102) (1  872  102) (1  873  102) (1  874  102) (1  875  102)
     (1  876  102) (1  877  102) (1  878  102) (1  879  102) (1  880  102)
     (1  881  102) (1  882  102) (1  883  102) (1  884  102) (1  885  102)
     (1  886  102) (1  887  102) (1  888  102) (1  889  102) (1  890  102)
     (1  891  102) (1  892  102) (1  893  102) (1  894  102) (1  895  102)
     (1  896  102) (1  897  102) (1  898  102) (1  899  102) (1  900  102)
     (1  901  102) (1  902  102) (1  903  102) (1  904  102) (1  905  102)
     (1  906  102) (1  907  102) (1  908  102) (1  909  102) (1  910  102)
     (1  911  102) (1  912  102) (1  913  102) (1  914  102) (1  915  102)
     (1  916  102) (1  917  102) (1  918  102) (1  919  102) (1  920  102)
     (1  921  102) (1  922  102) (1  923  102) (1  924  102) (1  925  102)
     (1  926  102) (1  927  102) (1  928  102) (1  929  102) (1  930  102)
     (1  931  102) (1  932  102) (1  933  102) (1  934  102) (1  935  102)
     (1  936  102) (1  937  102) (1  938  102) (1  939  102) (1  940  102)
     (1  941  102) (1  942  102) (1  943  102) (1  944  102) (1  945  102)
     (1  946  102) (1  947  102) (1  948  102) (1  949  102) (1  950  102)
     (1  951  102) (1  952  102) (1  953  102) (1  954  102) (1  955  102)
     (1  956  102) (1  957  102) (1  958  102) (1  959  102) (1  960  102)
     (1  961  102) (1  962  102) (1  963  102) (1  964  102) (1  965  102)
     (1  966  102) (1  967  102) (1  968  102) (1  969  102) (1  970  102)
     (1  971  102) (1  972  102) (1  973  102) (1  974  102) (1  975  102)
     (1  976  102) (1  977  102) (1  978  102) (1  979  102) (1  980  102)
     (1  981  102) (1  982  102) (1  983  102) (1  984  102) (1  985  102)
     (1  986  102) (1  987  102) (1  988  102) (1  989  102) (1  990  102)
     (1  991  102) (1  992  102) (1  993  102) (1  994  102) (1  995  102)
     (1  996  102) (1  997  102) (1  998  102) (1  999  102)
C
@@@@@@@@@@@@@@@@@@@@@@@@@@@@@@@@@@@@@@@@@@@@@@@@@@@@@@@@@@@@@@@@@@@@@@@@@@@@@@@
FC14  n2n rates for Actinides
C
@@@@@@@@@@@@@@@@@@@@@@@@@@@@@@@@@@@@@@@@@@@@@@@@@@@@@@@@@@@@@@@@@@@@@@@@@@@@@@@
F14:n 1
FM14 (1  958  16) (1  959  16) (1  960  16) (1  961  16) (1  962  16)
     (1  963  16) (1  964  16) (1  965  16) (1  966  16) (1  967  16)
     (1  968  16) (1  969  16) (1  970  16) (1  971  16) (1  972  16)
     (1  973  16) (1  974  16) (1  975  16) (1  976  16) (1  977  16)
     (1  978  16) (1  979  16) (1  980  16) (1  981  16) (1  982  16)
     (1  983  16) (1  984  16) (1  985  16) (1  986  16) (1  987  16)
     (1  988  16) (1  989  16) (1  990  16) (1  991  16) (1  992  16)
     (1  993  16) (1  994  16) (1  995  16) (1  996  16) (1  997  16)
     (1  998  16) (1  999  16)
C
@@@@@@@@@@@@@@@@@@@@@@@@@@@@@@@@@@@@@@@@@@@@@@@@@@@@@@@@@@@@@@@@@@@@@@@@@@@@@@@
FC24  n3n rates for Actinides
C
@@@@@@@@@@@@@@@@@@@@@@@@@@@@@@@@@@@@@@@@@@@@@@@@@@@@@@@@@@@@@@@@@@@@@@@@@@@@@@@
```

```
F24:n 1
FM24 (1  958  17) (1  959  17) (1  960  17) (1  961  17) (1  962  17)
     (1  963  17) (1  964  17) (1  965  17) (1  966  17) (1  967  17)
     (1  968  17) (1  969  17) (1  970  17) (1  971  17) (1  972  17)
     (1  973  17) (1  974  17) (1  975  17) (1  976  17) (1  977  17)
     (1  978  17) (1  979  17) (1  980  17) (1  981  17) (1  982  17)
     (1  983  17) (1  984  17) (1  985  17) (1  986  17) (1  987  17)
     (1  988  17) (1  989  17) (1  990  17) (1  991  17) (1  992  17)
     (1  993  17) (1  994  17) (1  995  17) (1  996  17) (1  997  17)
     (1  998  17) (1  999  17)
C
@@@@@@@@@@@@@@@@@@@@@@@@@@@@@@@@@@@@@@@@@@@@@@@@@@@@@@@@@@@@@@@@@@@@@@@@@@@@@@@@@
FC34 Fissin rates
C
@@@@@@@@@@@@@@@@@@@@@@@@@@@@@@@@@@@@@@@@@@@@@@@@@@@@@@@@@@@@@@@@@@@@@@@@@@@@@@@@@
F34:n 1
FM34 (1  958  -6) (1  959  -6) (1  960  -6) (1  961  -6) (1  962  -6)
     (1  963  -6) (1  964  -6) (1  965  -6) (1  966  -6) (1  967  -6)
     (1  968  -6) (1  969  -6) (1  970  -6) (1  971  -6) (1  972  -6)
     (1  973  -6) (1  974  -6) (1  975  -6) (1  976  -6) (1  977  -6)
     (1  978  -6) (1  979  -6) (1  980  -6) (1  981  -6) (1  982  -6)
     (1  983  -6) (1  984  -6) (1  985  -6) (1  986  -6) (1  987  -6)
     (1  988  -6) (1  989  -6) (1  990  -6) (1  991  -6) (1  992  -6)
     (1  993  -6) (1  994  -6) (1  995  -6) (1  996  -6) (1  997  -6)
     (1  998  -6) (1  999  -6)
e34 0.625e-6 20
C
@@@@@@@@@@@@@@@@@@@@@@@@@@@@@@@@@@@@@@@@@@@@@@@@@@@@@@@@@@@@@@@@@@@@@@@@@@@@@@@@@
FC44 Average fission energy(MeV) & nubar
C
@@@@@@@@@@@@@@@@@@@@@@@@@@@@@@@@@@@@@@@@@@@@@@@@@@@@@@@@@@@@@@@@@@@@@@@@@@@@@@@@@
F44:n  1   $ fuel cell number
FM44:n (-1  1 -6 ) (-1  1 -6 -7) (-1  1 -6 -8)
prdmp 150 150 150
print -30 -60 -85 -130 -140
```

```
c ================================================
c BUCAL1 input file for UO2 benchmark
c ================================================
* Power
  663.616  34.6679
* Number of active cells
  1
* Number of cells look like active cells
  1
* Volume(cc) and density(g/cc)
  2.1083  10.3
* Number of Burnable elements (in each active cell)
  3
* Material composition in each active cell
* Active cell 01
  92234  1.82239e-05
  92235  2.26826e-03
  92238  2.07128e-02
* Number of Time steps
  5
* Time
  0
  3
  10
  100
  3900
* Macro time steps
  3
  7
  10
  100
* MCNP name file (maximum 8 characters)
  pin1
* Isotope importance
   35081  1  45103  1  55133  1  62147  1  66160  1  94239  1
   36082  1  44104  1  54134  1  60148  1  66161  1  94240  1
   36083  1  46104  1  55134  1  61148  1  66162  1  94241  1
   36084  1  45105  1  56134  1  61148  1  66163  1  94242  1
   37085  1  46105  1  54135  1  62148  1  68166  1  94243  1
   37087  1  46106  1  55135  1  61149  1  68167  1  95241  1
   39089  1  46107  1  54136  1  62149  1  90232  1  95242  1
   38090  1  46108  1  55137  1  60150  1  91231  1  95242  1
   40091  1  47109  1  56137  1  62150  1  91233  1  95243  1
   40092  1  46110  1  56138  1  62151  1  92232  1  95244  1
   40093  1  48110  1  57139  1  63151  1  92233  1  96242  1
   40094  1  48111  1  58140  1  62152  1  92234  1  96243  1
   41095  1  48112  1  58141  1  62153  1  92235  1  96244  1
   42095  1  48113  1  59141  1  63153  1  92236  1  96245  1
   40096  1  48114  1  58142  1  62154  1  92237  1  96246  1
   42096  1  49115  1  60142  1  63154  1  92238  1  96247  1
   42097  1  51121  1  59143  1  64154  1  92239  1  96248  1
   42098  1  51123  1  60143  1  63155  1  93235  1  96249  1
   43099  1  53127  1  58144  1  64155  1  93236  1  97249  1
   42100  1  52128  1  60144  1  63156  1  93237  1  97250  1
   44100  1  53129  1  60145  1  64156  1  93238  1  98249  1
   44101  1  54131  1  60146  1  64157  1  93239  1  98250  1
   44102  1  54132  1  60147  1  64158  1  94236  1  98251  1
   44103  1  54133  1  61147  1  65159  1  94238  1  98252  1
```

```
c ============================================================
c         MCNP input file for ThO2-UO2 benchmark
c ============================================================
c     Created on: samedi, mai 10, 2008 at 14:24
     1   1  -9.424         -1 -8 9             imp:n=1
     2   0         1 -2 -8 9                   imp:n=1
     3   2  -6.505         2 -3 -8 9           imp:n=1
     4   3  -0.705         3 -8 9 -5 4 -7 6    imp:n=1
     5   0         8 :-9 :5 :-4 :7 :-6         imp:n=0

     1        cz  0.41274
     2        cz  0.41896
     3        cz  0.47609
    *4        px -0.6313
    *5        px  0.6313
    *6        py -0.6313
    *7        py  0.6313
    *8        pz  50
    *9        pz -50

mode n
C Start burnup
C Fuel material number:01
m1     8016.90c 4.26835e-02
C burnable elements
   35081.90c  1.00000E-48  55133.90c  1.00000E-48  66160.90c  1.00000E-48
   36082.90c  1.00000E-48  54134.90c  1.00000E-48  66161.90c  1.00000E-48
   36083.90c  1.00000E-48  55134.90c  1.00000E-48  66162.90c  1.00000E-48
   36084.90c  1.00000E-48  56134.90c  1.00000E-48  66163.90c  1.00000E-48
   37085.90c  1.00000E-48  54135.90c  1.00000E-48  68166.90c  1.00000E-48
   37087.90c  1.00000E-48  55135.90c  1.00000E-48  68167.90c  1.00000E-48
   39089.90c  1.00000E-48  54136.90c  1.00000E-48  90232.90c  1.61215e-02
   38090.90c  1.00000E-48  55137.90c  1.00000E-48  91231.90c  1.00000E-48
   40091.90c  1.00000E-48  56137.90c  1.00000E-48  91233.90c  1.00000E-48
   40092.90c  1.00000E-48  56138.90c  1.00000E-48  92232.90c  1.00000E-48
   40093.90c  1.00000E-48  57139.90c  1.00000E-48  92233.90c  1.00000E-48
   40094.90c  1.00000E-48  58140.90c  1.00000E-48  92234.90c  8.24518e-06
   41095.90c  1.00000E-48  58141.90c  1.00000E-48  92235.90c  1.03615e-03
   42095.90c  1.00000E-48  59141.90c  1.00000E-48  92236.90c  1.00000E-48
   40096.90c  1.00000E-48  58142.90c  1.00000E-48  92237.90c  1.00000E-48
   42096.90c  1.00000E-48  60142.90c  1.00000E-48  92238.90c  4.22957e-03
   42097.90c  1.00000E-48  59143.90c  1.00000E-48  92239.90c  1.00000E-48
   42098.90c  1.00000E-48  60143.90c  1.00000E-48  93235.90c  1.00000E-48
   43099.90c  1.00000E-48  58144.90c  1.00000E-48  93236.90c  1.00000E-48
   42100.90c  1.00000E-48  60144.90c  1.00000E-48  93237.90c  1.00000E-48
   44100.90c  1.00000E-48  60145.90c  1.00000E-48  93238.90c  1.00000E-48
   44101.90c  1.00000E-48  60146.90c  1.00000E-48  93239.90c  1.00000E-48
   44102.90c  1.00000E-48  60147.90c  1.00000E-48  94236.90c  1.00000E-48
   44103.90c  1.00000E-48  61147.90c  1.00000E-48  94238.90c  1.00000E-48
   45103.90c  1.00000E-48  62147.90c  1.00000E-48  94239.90c  1.00000E-48
   44104.90c  1.00000E-48  60148.90c  1.00000E-48  94240.90c  1.00000E-48
   46104.90c  1.00000E-48  61148.91c  1.00000E-48  94241.90c  1.00000E-48
   45105.90c  1.00000E-48  61148.90c  1.00000E-48  94242.90c  1.00000E-48
   46105.90c  1.00000E-48  62148.90c  1.00000E-48  94243.90c  1.00000E-48
   46106.90c  1.00000E-48  61149.90c  1.00000E-48  95241.90c  1.00000E-48
   46107.90c  1.00000E-48  62149.90c  1.00000E-48  95242.91c  1.00000E-48
   46108.90c  1.00000E-48  60150.90c  1.00000E-48  95242.90c  1.00000E-48
   47109.90c  1.00000E-48  62150.90c  1.00000E-48  95243.90c  1.00000E-48
   46110.90c  1.00000E-48  62151.90c  1.00000E-48  95244.90c  1.00000E-48
   48110.90c  1.00000E-48  63151.90c  1.00000E-48  96242.90c  1.00000E-48
   48111.90c  1.00000E-48  62152.90c  1.00000E-48  96243.90c  1.00000E-48
```

```
   48112.90c  1.00000E-48  62153.90c  1.00000E-48  96244.90c  1.00000E-48
   48113.90c  1.00000E-48  63153.90c  1.00000E-48  96245.90c  1.00000E-48
   48114.90c  1.00000E-48  62154.90c  1.00000E-48  96246.90c  1.00000E-48
   49115.90c  1.00000E-48  63154.90c  1.00000E-48  96247.90c  1.00000E-48
   51121.90c  1.00000E-48  64154.90c  1.00000E-48  96248.90c  1.00000E-48
   51123.90c  1.00000E-48  63155.90c  1.00000E-48  96249.90c  1.00000E-48
   53127.90c  1.00000E-48  64155.90c  1.00000E-48  97249.90c  1.00000E-48
   52128.90c  1.00000E-48  63156.90c  1.00000E-48  97250.90c  1.00000E-48
   53129.90c  1.00000E-48  64156.90c  1.00000E-48  98249.90c  1.00000E-48
   54131.90c  1.00000E-48  64157.90c  1.00000E-48  98250.90c  1.00000E-48
   54132.90c  1.00000E-48  64158.90c  1.00000E-48  98251.90c  1.00000E-48
   54133.90c  1.00000E-48  65159.90c  1.00000E-48  98252.90c  1.00000E-48
C END Burnup
c Zircaloy-4
m2       50112.62c -0.00014065 50114.62c -0.00009425
         50115.62c -0.00004930 50116.62c -0.00210685
         50117.62c -0.00111360 50118.62c -0.00351335
         50119.62c -0.00124555 50120.62c -0.00472555
         50122.62c -0.00067135 50124.62c -0.00083955
         24050.62c -0.00004345 24052.62c -0.00083789
         24053.62c -0.00009501 24054.62c -0.00002365
         26054.62c -0.00012180 26056.62c -0.00192612
         26057.62c -0.00004410 26058.62c -0.00000588
         72174.62c -0.00000016 72176.62c -0.00000521
         72177.62c -0.00001861 72178.62c -0.00002730
         72179.62c -0.00001363 72180.62c -0.00003510
         40090.62c -0.50539335 40091.62c -0.11021406
         40092.62c -0.16846445 40094.62c -0.17072374
         40096.62c -0.02750440
m3       1001.58c 4.71053e-02
         8016.58c 2.35662e-02
c mt3     lwtr.04t
kcode    2000 1.0  100 1000
ksrc     0. 0. 0.
c
=========================================================================
=
c   importances, neutron mode only and keff calculation
c
=========================================================================
=
c Fission products <=========================<
m856  35081.90c             1  $
m857  36082.90c             1  $
m858  36083.90c             1  $
m859  36084.90c             1  $
m860  37085.90c             1  $
m861  37087.90c             1  $
m862  39089.90c             1  $
m863  38090.90c             1  $
m864  40091.90c             1  $
m865  40092.90c             1  $
m866  40093.90c             1  $
m867  40094.90c             1  $
m868  41095.90c             1  $
m869  42095.90c             1  $
m870  40096.90c             1  $
m871  42096.90c             1  $
m872  42097.90c             1  $
m873  42098.90c             1  $
m874  43099.90c             1  $
```

```
m875   42100.90c                1   $
m876   44100.90c                1   $
m877   44101.90c                1   $
m878   44102.90c                1   $
m879   44103.90c                1   $
m880   45103.90c                1   $
m881   44104.90c                1   $
m882   46104.90c                1   $
m883   45105.90c                1   $
m884   46105.90c                1   $
m885   46106.90c                1   $
m886   46107.90c                1   $
m887   46108.90c                1   $
m888   47109.90c                1   $
m889   46110.90c                1   $
m890   48110.90c                1   $
m891   48111.90c                1   $
m892   48112.90c                1   $
m893   48113.90c                1   $
m894   48114.90c                1   $
m895   49115.90c                1   $
m896   51121.90c                1   $
m897   51123.90c                1   $
m898   53127.90c                1   $
m899   52128.90c                1   $
m900   53129.90c                1   $
m901   54131.90c                1   $
m902   54132.90c                1   $
m903   54133.90c                1   $
m904   55133.90c                1   $
m905   54134.90c                1   $
m906   55134.90c                1   $
m907   56134.90c                1   $
m908   54135.90c                1   $
m909   55135.90c                1   $
m910   54136.90c                1   $
m911   55137.90c                1   $
m912   56137.90c                1   $
m913   56138.90c                1   $
m914   57139.90c                1   $
m915   58140.90c                1   $
m916   58141.90c                1   $
m917   59141.90c                1   $
m918   58142.90c                1   $
m919   60142.90c                1   $
m920   59143.90c                1   $
m921   60143.90c                1   $
m922   58144.90c                1   $
m923   60144.90c                1   $
m924   60145.90c                1   $
m925   60146.90c                1   $
m926   60147.90c                1   $
m927   61147.90c                1   $
m928   62147.90c                1   $
m929   60148.90c                1   $
m930   61148.91c                1   $
m931   61148.90c                1   $
m932   62148.90c                1   $
m933   61149.90c                1   $
m934   62149.90c                1   $
m935   60150.90c                1   $
```

```
m936   62150.90c                1   $
m937   62151.90c                1   $
m938   63151.90c                1   $
m939   62152.90c                1   $
m940   62153.90c                1
m941   63153.90c                1   $
m942   62154.90c                1   $
m943   63154.90c                1   $
m944   64154.90c                1   $
m945   63155.90c                1   $
m946   64155.90c                1   $
m947   63156.90c                1   $
m948   64156.90c                1   $
m949   64157.90c                1   $
m950   64158.90c                1   $
m951   65159.90c                1   $
m952   66160.90c                1   $
m953   66161.90c                1
m954   66162.90c                1   $
m955   66163.90c                1   $
m956   68166.90c                1   $
m957   68167.90c                1   $
c Actinides <=======================
m958   90232.90c              1
m959   91231.90c              1
m960   91233.90c              1
m961   92232.90c              1
m962   92233.90c              1   $
m963   92234.90c              1   $
m964   92235.90c              1   $
m965   92236.90c              1   $
m966   92237.90c              1   $
m967   92238.90c              1   $
m968   92239.90c              1   $
m969   93235.90c              1   $
m970   93236.90c              1   $
m971   93237.90c              1   $
m972   93238.90c              1   $
m973   93239.90c              1   $
m974   94236.90c              1   $
m975   94238.90c              1   $
m976   94239.90c              1   $
m977   94240.90c              1   $
m978   94241.90c              1   $
m979   94242.90c              1   $
m980   94243.90c              1   $
m981   95241.90c              1   $
m982   95242.91c              1   $
m983   95242.90c              1   $
m984   95243.90c              1   $
m985   95244.90c              1   $
m986   96242.90c              1   $
m987   96243.90c              1   $
m988   96244.90c              1   $
m989   96245.90c              1
m990   96246.90c              1
m991   96247.90c              1
m992   96248.90c              1
m993   96249.90c              1
m994   97249.90c              1
m995   97250.90c              1
```

```
m996  98249.90c            1
m997  98250.90c            1
m998  98251.90c            1
m999  98252.90c            1
C xxxxxxxxxxxxxxxxxxxxxxxxxxxxxxxxxxxxxxxxxxxxxxxxxxxxxxxxxxxxxxxxxxxxxx
C                          Burnup
C xxxxxxxxxxxxxxxxxxxxxxxxxxxxxxxxxxxxxxxxxxxxxxxxxxxxxxxxxxxxxxxxxxxxxxx
C
@@@@@@@@@@@@@@@@@@@@@@@@@@@@@@@@@@@@@@@@@@@@@@@@@@@@@@@@@@@@@@@@@@@@@@@
FC4 Capture rates
C
@@@@@@@@@@@@@@@@@@@@@@@@@@@@@@@@@@@@@@@@@@@@@@@@@@@@@@@@@@@@@@@@@@@@@@@
F4:n 1
FM4  (1  856  102) (1  857  102) (1  858  102) (1  859  102) (1  860  102)
     (1  861  102) (1  862  102) (1  863  102) (1  864  102) (1  865  102)
     (1  866  102) (1  867  102) (1  868  102) (1  869  102) (1  870  102)
     (1  871  102) (1  872  102) (1  873  102) (1  874  102) (1  875  102)
     (1  876  102) (1  877  102) (1  878  102) (1  879  102) (1  880  102)
     (1  881  102) (1  882  102) (1  883  102) (1  884  102) (1  885  102)
     (1  886  102) (1  887  102) (1  888  102) (1  889  102) (1  890  102)
     (1  891  102) (1  892  102) (1  893  102) (1  894  102) (1  895  102)
     (1  896  102) (1  897  102) (1  898  102) (1  899  102) (1  900  102)
     (1  901  102) (1  902  102) (1  903  102) (1  904  102) (1  905  102)
     (1  906  102) (1  907  102) (1  908  102) (1  909  102) (1  910  102)
     (1  911  102) (1  912  102) (1  913  102) (1  914  102) (1  915  102)
     (1  916  102) (1  917  102) (1  918  102) (1  919  102) (1  920  102)
     (1  921  102) (1  922  102) (1  923  102) (1  924  102) (1  925  102)
     (1  926  102) (1  927  102) (1  928  102) (1  929  102) (1  930  102)
     (1  931  102) (1  932  102) (1  933  102) (1  934  102) (1  935  102)
     (1  936  102) (1  937  102) (1  938  102) (1  939  102) (1  940  102)
     (1  941  102) (1  942  102) (1  943  102) (1  944  102) (1  945  102)
     (1  946  102) (1  947  102) (1  948  102) (1  949  102) (1  950  102)
     (1  951  102) (1  952  102) (1  953  102) (1  954  102) (1  955  102)
     (1  956  102) (1  957  102) (1  958  102) (1  959  102) (1  960  102)
     (1  961  102) (1  962  102) (1  963  102) (1  964  102) (1  965  102)
     (1  966  102) (1  967  102) (1  968  102) (1  969  102) (1  970  102)
     (1  971  102) (1  972  102) (1  973  102) (1  974  102) (1  975  102)
     (1  976  102) (1  977  102) (1  978  102) (1  979  102) (1  980  102)
     (1  981  102) (1  982  102) (1  983  102) (1  984  102) (1  985  102)
     (1  986  102) (1  987  102) (1  988  102) (1  989  102) (1  990  102)
     (1  991  102) (1  992  102) (1  993  102) (1  994  102) (1  995  102)
     (1  996  102) (1  997  102) (1  998  102) (1  999  102)
C
@@@@@@@@@@@@@@@@@@@@@@@@@@@@@@@@@@@@@@@@@@@@@@@@@@@@@@@@@@@@@@@@@@@@@@@
FC14  n2n rates for Actinides
C
@@@@@@@@@@@@@@@@@@@@@@@@@@@@@@@@@@@@@@@@@@@@@@@@@@@@@@@@@@@@@@@@@@@@@@@
F14:n 1
FM14 (1  958  16) (1  959  16) (1  960  16) (1  961  16) (1  962  16)
     (1  963  16) (1  964  16) (1  965  16) (1  966  16) (1  967  16)
     (1  968  16) (1  969  16) (1  970  16) (1  971  16) (1  972  16)
     (1  973  16) (1  974  16) (1  975  16) (1  976  16) (1  977  16)
     (1  978  16) (1  979  16) (1  980  16) (1  981  16) (1  982  16)
     (1  983  16) (1  984  16) (1  985  16) (1  986  16) (1  987  16)
     (1  988  16) (1  989  16) (1  990  16) (1  991  16) (1  992  16)
     (1  993  16) (1  994  16) (1  995  16) (1  996  16) (1  997  16)
     (1  998  16) (1  999  16)
C
@@@@@@@@@@@@@@@@@@@@@@@@@@@@@@@@@@@@@@@@@@@@@@@@@@@@@@@@@@@@@@@@@@@@@@@
FC24  n3n rates for Actinides
C
```

```
@@@@@@@@@@@@@@@@@@@@@@@@@@@@@@@@@@@@@@@@@@@@@@@@@@@@@@@@@@@@@@@@@@@@@@@@@@@@
F24:n 1
FM24 (1  958  17) (1  959  17) (1  960  17) (1  961  17) (1  962  17)
     (1  963  17) (1  964  17) (1  965  17) (1  966  17) (1  967  17)
     (1  968  17) (1  969  17) (1  970  17) (1  971  17) (1  972  17)
     (1  973  17) (1  974  17) (1  975  17) (1  976  17) (1  977  17)
     (1  978  17) (1  979  17) (1  980  17) (1  981  17) (1  982  17)
     (1  983  17) (1  984  17) (1  985  17) (1  986  17) (1  987  17)
     (1  988  17) (1  989  17) (1  990  17) (1  991  17) (1  992  17)
     (1  993  17) (1  994  17) (1  995  17) (1  996  17) (1  997  17)
     (1  998  17) (1  999  17)
C
@@@@@@@@@@@@@@@@@@@@@@@@@@@@@@@@@@@@@@@@@@@@@@@@@@@@@@@@@@@@@@@@@@@@@@@@@@@@
FC34 Fissin rates
C
@@@@@@@@@@@@@@@@@@@@@@@@@@@@@@@@@@@@@@@@@@@@@@@@@@@@@@@@@@@@@@@@@@@@@@@@@@@@
F34:n 1
FM34 (1  958  -6) (1  959  -6) (1  960  -6) (1  961  -6) (1  962  -6)
     (1  963  -6) (1  964  -6) (1  965  -6) (1  966  -6) (1  967  -6)
     (1  968  -6) (1  969  -6) (1  970  -6) (1  971  -6) (1  972  -6)
     (1  973  -6) (1  974  -6) (1  975  -6) (1  976  -6) (1  977  -6)
     (1  978  -6) (1  979  -6) (1  980  -6) (1  981  -6) (1  982  -6)
     (1  983  -6) (1  984  -6) (1  985  -6) (1  986  -6) (1  987  -6)
     (1  988  -6) (1  989  -6) (1  990  -6) (1  991  -6) (1  992  -6)
     (1  993  -6) (1  994  -6) (1  995  -6) (1  996  -6) (1  997  -6)
     (1  998  -6) (1  999  -6)
e34 0.625e-6 20
C
@@@@@@@@@@@@@@@@@@@@@@@@@@@@@@@@@@@@@@@@@@@@@@@@@@@@@@@@@@@@@@@@@@@@@@@@@@@@
FC44 Average fission energy(MeV) & nubar
C
@@@@@@@@@@@@@@@@@@@@@@@@@@@@@@@@@@@@@@@@@@@@@@@@@@@@@@@@@@@@@@@@@@@@@@@@@@@@
F44:n  1   $ fuel cell number
FM44:n (-1  3 -6 ) (-1  3 -6 -7) (-1  3 -6 -8)
C
@@@@@@@@@@@@@@@@@@@@@@@@@@@@@@@@@@@@@@@@@@@@@@@@@@@@@@@@@@@@@@@@@@@@@@@@@@@@
FC54 Two groups flux for burnup calculations
C
@@@@@@@@@@@@@@@@@@@@@@@@@@@@@@@@@@@@@@@@@@@@@@@@@@@@@@@@@@@@@@@@@@@@@@@@@@@@
F54:n 1
E54 6.2500E-07 1.0000E-04 2.0000E+01
C
@@@@@@@@@@@@@@@@@@@@@@@@@@@@@@@@@@@@@@@@@@@@@@@@@@@@@@@@@@@@@@@@@@@@@@@@@@@@
prdmp 150 150 150
print -30 -60 -85 -130 -140
```

```
c ===========================================
c BUCAL1 input file for ThO2-UO2 becnhmark
c ===========================================
* Power
  16.92e+03  38.1347
* Number of active cells
  1
* Number of cells look like active cells
  1
* Volume(cc) and density(g/cc)
  5.35184e+01  9.424
* Number of Burnable elements (in each active cell)
  4
* Material composition in each active cell
* Active cell 01
  90232  1.61215e-02
  92234  8.24518e-06
  92235  1.03615e-03
  92238  4.22957e-02
* Temperatures (Kelvin)
  900.
* Number of Time steps
  6
* Time
  0
  3
  10
  100
  1800
  2000
* Macro time steps
  3
  7
  10
  170
  50
* Refreshment
  0 0
* MCNP name file (maximum 8 characters)
  thor1
* Isotope importance
   35081  1  45103  1  55133  1  62147  1  66160  1  94239  1
   36082  1  44104  1  54134  1  60148  1  66161  1  94240  1
   36083  1  46104  1  55134  1  61148  1  66162  1  94241  1
   36084  1  45105  1  56134  1  61148  1  66163  1  94242  1
   37085  1  46105  1  54135  1  62148  1  68166  1  94243  1
   37087  1  46106  1  55135  1  61149  1  68167  1  95241  1
   39089  1  46107  1  54136  1  62149  1  90232  1  95242  1
   38090  1  46108  1  55137  1  60150  1  91231  1  95242  1
   40091  1  47109  1  56137  1  62150  1  91233  1  95243  1
   40092  1  46110  1  56138  1  62151  1  92232  1  95244  1
   40093  1  48110  1  57139  1  63151  1  92233  1  96242  1
   40094  1  48111  1  58140  1  62152  1  92234  1  96243  1
   41095  1  48112  1  58141  1  62153  1  92235  1  96244  1
   42095  1  48113  1  59141  1  63153  1  92236  1  96245  1
   40096  1  48114  1  58142  1  62154  1  92237  1  96246  1
   42096  1  49115  1  60142  1  63154  1  92238  1  96247  1
   42097  1  51121  1  59143  1  64154  1  92239  1  96248  1
   42098  1  51123  1  60143  1  63155  1  93235  1  96249  1
   43099  1  53127  1  58144  1  64155  1  93236  1  97249  1
   42100  1  52128  1  60144  1  63156  1  93237  1  97250  1
```

44100	1	53129	1	60145	1	64156	1	93238	1	98249	1
44101	1	54131	1	60146	1	64157	1	93239	1	98250	1
44102	1	54132	1	60147	1	64158	1	94236	1	98251	1
44103	1	54133	1	61147	1	65159	1	94238	1	98252	1

```
c ============================================
c       MCNP input file for MOX benchmark
c ============================================
c     Created on: Monday, July 07, 2008 at 18:50
c    cells for High-enriched MOX fuel pin
     1      1 0.069903 -1  u=1 vol=52.8102
     2      4 -5.8736 1 -2  u=1
     3      5 -0.7245 2  u=1
c    cells for Medium-enriched MOX fuel pin
     4      2 0.06983 -1  u=2 vol=52.8102
     5      4 -5.8736 1 -2  u=2
     6      5 -0.7245 2  u=2
c    cells for Low-enriched MOX fuel pin
     7      3 0.069793 -1  u=3 vol=52.8102
     8      4 -5.8736 1 -2  u=3
     9      5 -0.7245 2  u=3
c    cells for guid tube instrument
    10      5 -0.7245 -13  u=4
    11      4 -5.8736 13 -14  u=4
    12      5 -0.7245 14  u=4
    98      0          -6 5 -4 3  u=10 lat=1 $ROW 1
              fill=-8:8 -8:8 0:0
       3 3 2 2 2 2 2 2 2 2 2 2 2 2 3 3  $ROW 1
       3 2 1 1 1 2 1 1 2 1 1 2 1 1 1 2 3  $ROW 2
       2 1 1 1 1 4 1 1 4 1 1 4 1 1 1 1 2  $ROW 3
       2 1 1 4 1 1 1 1 1 1 1 1 1 4 1 1 2  $ROW 4
       2 1 1 1 1 1 1 1 1 1 1 1 1 1 1 1 2  $ROW 5
       2 2 4 1 1 4 1 1 4 1 1 4 1 1 4 2 2  $ROW 6
       2 1 1 1 1 1 1 1 1 1 1 1 1 1 1 1 2  $ROW 7
       2 1 1 1 1 1 1 1 1 1 1 1 1 1 1 1 2  $ROW 8
       2 2 4 1 1 4 1 1 4 1 1 4 1 1 4 2 2  $ROW 9
       2 1 1 1 1 1 1 1 1 1 1 1 1 1 1 1 2  $ROW 10
       2 1 1 1 1 1 1 1 1 1 1 1 1 1 1 1 2  $ROW 11
       2 2 4 1 1 4 1 1 4 1 1 4 1 1 4 2 2  $ROW 12
       2 1 1 1 1 1 1 1 1 1 1 1 1 1 1 1 2  $ROW 13
       2 1 1 4 1 1 1 1 1 1 1 1 1 4 1 1 2  $ROW 14
       2 1 1 1 1 4 1 1 4 1 1 4 1 1 1 1 2  $ROW 15
       3 2 1 1 1 2 1 1 2 1 1 2 1 1 1 2 3  $ROW 16
       3 3 2 2 2 2 2 2 2 2 2 2 2 2 3 3  $ROW 17
    99      0           7 -8 9 -10 11 -12  fill=10
   100      0          -7 :8 :-9 :10 :-11 :12

     1         cz 0.41
     2         cz 0.475
     3         px -0.63
     4         px 0.63
     5         py -0.63
     6         py 0.63
    *7         px -10.71
    *8         px 10.71
    *9         py -10.71
   *10         py 10.71
   *11         pz -50
   *12         pz 50
    13         cz 0.571
    14         cz 0.613

mode  n
imp:n              1 13r         0    $ 1, 100
kcode 2000 1.000000 50 500
ksrc  1.26  0.00 0.00
```

```
      0.00  1.26 0.00
     -1.26  0.00 0.00
      0.00 -1.26 0.00
C Start burnup
C Fuel material number:01
m1    8016.90c    4.6602E-02
C burnable elements
  35081.90c  1.00000E-48  54134.90c  1.00000E-48  66162.90c  1.00000E-48
  36082.90c  1.00000E-48  55134.90c  1.00000E-48  66163.90c  1.00000E-48
  36083.90c  1.00000E-48  56134.90c  1.00000E-48  68166.90c  1.00000E-48
  36084.90c  1.00000E-48  54135.90c  1.00000E-48  68167.90c  1.00000E-48
  37085.90c  1.00000E-48  55135.90c  1.00000E-48  90231.42c  1.00000E-48
  37087.90c  1.00000E-48  54136.90c  1.00000E-48  90232.90c  1.00000E-48
  39089.90c  1.00000E-48  55137.90c  1.00000E-48  90233.90c  1.00000E-48
  38090.90c  1.00000E-48  56137.90c  1.00000E-48  91231.90c  1.00000E-48
  40091.90c  1.00000E-48  56138.90c  1.00000E-48  91232.90c  1.00000E-48
  40092.90c  1.00000E-48  57139.90c  1.00000E-48  91233.90c  1.00000E-48
  40093.90c  1.00000E-48  58140.90c  1.00000E-48  92232.90c  1.00000E-48
  40094.90c  1.00000E-48  58141.90c  1.00000E-48  92233.90c  1.00000E-48
  41095.90c  1.00000E-48  59141.90c  1.00000E-48  92234.90c  2.57180E-07
  42095.90c  1.00000E-48  58142.90c  1.00000E-48  92235.90c  5.37980E-05
  40096.90c  1.00000E-48  60142.90c  1.00000E-48  92236.90c  1.00000E-48
  42096.90c  1.00000E-48  59143.90c  1.00000E-48  92237.90c  1.00000E-48
  42097.90c  1.00000E-48  60143.90c  1.00000E-48  92238.90c  2.11940E-02
  42098.90c  1.00000E-48  58144.90c  1.00000E-48  92239.90c  1.00000E-48
  43099.90c  1.00000E-48  60144.90c  1.00000E-48  93235.90c  1.00000E-48
  42100.90c  1.00000E-48  60145.90c  1.00000E-48  93236.90c  1.00000E-48
  44100.90c  1.00000E-48  60146.90c  1.00000E-48  93237.90c  1.00000E-48
  44101.90c  1.00000E-48  60147.90c  1.00000E-48  93238.90c  1.00000E-48
  44102.90c  1.00000E-48  61147.90c  1.00000E-48  93239.90c  1.00000E-48
  44103.90c  1.00000E-48  62147.90c  1.00000E-48  94236.90c  1.00000E-48
  45103.90c  1.00000E-48  60148.90c  1.00000E-48  94238.90c  5.16770E-05
  44104.90c  1.00000E-48  61148.91c  1.00000E-48  94239.90c  1.12590E-03
  46104.90c  1.00000E-48  61148.90c  1.00000E-48  94240.90c  5.35000E-04
  45105.90c  1.00000E-48  62148.90c  1.00000E-48  94241.90c  1.93920E-04
  46105.90c  1.00000E-48  61149.90c  1.00000E-48  94242.90c  1.46360E-04
  46106.90c  1.00000E-48  62149.90c  1.00000E-48  94243.90c  1.00000E-48
  46107.90c  1.00000E-48  60150.90c  1.00000E-48  95241.90c  1.00000E-48
  46108.90c  1.00000E-48  62150.90c  1.00000E-48  95242.91c  1.00000E-48
  47109.90c  1.00000E-48  62151.90c  1.00000E-48  95242.90c  1.00000E-48
  46110.90c  1.00000E-48  63151.90c  1.00000E-48  95243.90c  1.00000E-48
  48110.90c  1.00000E-48  62152.90c  1.00000E-48  95244.90c  1.00000E-48
  48111.90c  1.00000E-48  62153.90c  1.00000E-48  96242.90c  1.00000E-48
  48112.90c  1.00000E-48  63153.90c  1.00000E-48  96243.90c  1.00000E-48
  48113.90c  1.00000E-48  62154.90c  1.00000E-48  96244.90c  1.00000E-48
  48114.90c  1.00000E-48  63154.90c  1.00000E-48  96245.90c  1.00000E-48
  49115.90c  1.00000E-48  64154.90c  1.00000E-48  96246.90c  1.00000E-48
  51121.90c  1.00000E-48  63155.90c  1.00000E-48  96247.90c  1.00000E-48
  51123.90c  1.00000E-48  64155.90c  1.00000E-48  96248.90c  1.00000E-48
  53127.90c  1.00000E-48  63156.90c  1.00000E-48  96249.90c  1.00000E-48
  52128.90c  1.00000E-48  64156.90c  1.00000E-48  97249.90c  1.00000E-48
  53129.90c  1.00000E-48  64157.90c  1.00000E-48  97250.90c  1.00000E-48
  54131.90c  1.00000E-48  64158.90c  1.00000E-48  98249.90c  1.00000E-48
  54132.90c  1.00000E-48  65159.90c  1.00000E-48  98250.90c  1.00000E-48
  54133.90c  1.00000E-48  66160.90c  1.00000E-48  98251.90c  1.00000E-48
  55133.90c  1.00000E-48  66161.90c  1.00000E-48  98252.90c  1.00000E-48
C Fuel material number:02
m2    8016.90c    4.6553E-02
C burnable elements
  35081.90c  1.00000E-48  54134.90c  1.00000E-48  66162.90c  1.00000E-48
  36082.90c  1.00000E-48  55134.90c  1.00000E-48  66163.90c  1.00000E-48
```

```
   36083.90c  1.00000E-48  56134.90c  1.00000E-48  68166.90c  1.00000E-48
   36084.90c  1.00000E-48  54135.90c  1.00000E-48  68167.90c  1.00000E-48
   37085.90c  1.00000E-48  55135.90c  1.00000E-48  90231.42c  1.00000E-48
   37087.90c  1.00000E-48  54136.90c  1.00000E-48  90232.90c  1.00000E-48
   39089.90c  1.00000E-48  55137.90c  1.00000E-48  90233.90c  1.00000E-48
   38090.90c  1.00000E-48  56137.90c  1.00000E-48  91231.90c  1.00000E-48
   40091.90c  1.00000E-48  56138.90c  1.00000E-48  91232.90c  1.00000E-48
   40092.90c  1.00000E-48  57139.90c  1.00000E-48  91233.90c  1.00000E-48
   40093.90c  1.00000E-48  58140.90c  1.00000E-48  92232.90c  1.00000E-48
   40094.90c  1.00000E-48  58141.90c  1.00000E-48  92233.90c  1.00000E-48
   41095.90c  1.00000E-48  59141.90c  1.00000E-48  92234.90c  2.64360E-07
   42095.90c  1.00000E-48  58142.90c  1.00000E-48  92235.90c  5.53000E-05
   40096.90c  1.00000E-48  60142.90c  1.00000E-48  92236.90c  1.00000E-48
   42096.90c  1.00000E-48  59143.90c  1.00000E-48  92237.90c  1.00000E-48
   42097.90c  1.00000E-48  60143.90c  1.00000E-48  92238.90c  2.17860E-02
   42098.90c  1.00000E-48  58144.90c  1.00000E-48  92239.90c  1.00000E-48
   43099.90c  1.00000E-48  60144.90c  1.00000E-48  93235.90c  1.00000E-48
   42100.90c  1.00000E-48  60145.90c  1.00000E-48  93236.90c  1.00000E-48
   44100.90c  1.00000E-48  60146.90c  1.00000E-48  93237.90c  1.00000E-48
   44101.90c  1.00000E-48  60147.90c  1.00000E-48  93238.90c  1.00000E-48
   44102.90c  1.00000E-48  61147.90c  1.00000E-48  93239.90c  1.00000E-48
   44103.90c  1.00000E-48  62147.90c  1.00000E-48  94236.90c  1.00000E-48
   45103.90c  1.00000E-48  60148.90c  1.00000E-48  94238.90c  3.61280E-05
   44104.90c  1.00000E-48  61148.91c  1.00000E-48  94239.90c  7.87170E-04
   46104.90c  1.00000E-48  61148.90c  1.00000E-48  94240.90c  3.74030E-04
   45105.90c  1.00000E-48  62148.90c  1.00000E-48  94241.90c  1.35570E-04
   46105.90c  1.00000E-48  61149.90c  1.00000E-48  94242.90c  1.02330E-04
   46106.90c  1.00000E-48  62149.90c  1.00000E-48  94243.90c  1.00000E-48
   46107.90c  1.00000E-48  60150.90c  1.00000E-48  95241.90c  1.00000E-48
   46108.90c  1.00000E-48  62150.90c  1.00000E-48  95242.91c  1.00000E-48
   47109.90c  1.00000E-48  62151.90c  1.00000E-48  95242.90c  1.00000E-48
   46110.90c  1.00000E-48  63151.90c  1.00000E-48  95243.90c  1.00000E-48
   48110.90c  1.00000E-48  62152.90c  1.00000E-48  95244.90c  1.00000E-48
   48111.90c  1.00000E-48  62153.90c  1.00000E-48  96242.90c  1.00000E-48
   48112.90c  1.00000E-48  63153.90c  1.00000E-48  96243.90c  1.00000E-48
   48113.90c  1.00000E-48  62154.90c  1.00000E-48  96244.90c  1.00000E-48
   48114.90c  1.00000E-48  63154.90c  1.00000E-48  96245.90c  1.00000E-48
   49115.90c  1.00000E-48  64154.90c  1.00000E-48  96246.90c  1.00000E-48
   51121.90c  1.00000E-48  63155.90c  1.00000E-48  96247.90c  1.00000E-48
   51123.90c  1.00000E-48  64155.90c  1.00000E-48  96248.90c  1.00000E-48
   53127.90c  1.00000E-48  63156.90c  1.00000E-48  96249.90c  1.00000E-48
   52128.90c  1.00000E-48  64156.90c  1.00000E-48  97249.90c  1.00000E-48
   53129.90c  1.00000E-48  64157.90c  1.00000E-48  97250.90c  1.00000E-48
   54131.90c  1.00000E-48  64158.90c  1.00000E-48  98249.90c  1.00000E-48
   54132.90c  1.00000E-48  65159.90c  1.00000E-48  98250.90c  1.00000E-48
   54133.90c  1.00000E-48  66160.90c  1.00000E-48  98251.90c  1.00000E-48
   55133.90c  1.00000E-48  66161.90c  1.00000E-48  98252.90c  1.00000E-48
C Fuel material number:03
m3    8016.90c    4.6529E-02
C burnable elements
   35081.90c  1.00000E-48  54134.90c  1.00000E-48  66162.90c  1.00000E-48
   36082.90c  1.00000E-48  55134.90c  1.00000E-48  66163.90c  1.00000E-48
   36083.90c  1.00000E-48  56134.90c  1.00000E-48  68166.90c  1.00000E-48
   36084.90c  1.00000E-48  54135.90c  1.00000E-48  68167.90c  1.00000E-48
   37085.90c  1.00000E-48  55135.90c  1.00000E-48  90231.42c  1.00000E-48
   37087.90c  1.00000E-48  54136.90c  1.00000E-48  90232.90c  1.00000E-48
   39089.90c  1.00000E-48  55137.90c  1.00000E-48  90233.90c  1.00000E-48
   38090.90c  1.00000E-48  56137.90c  1.00000E-48  91231.90c  1.00000E-48
   40091.90c  1.00000E-48  56138.90c  1.00000E-48  91232.90c  1.00000E-48
   40092.90c  1.00000E-48  57139.90c  1.00000E-48  91233.90c  1.00000E-48
   40093.90c  1.00000E-48  58140.90c  1.00000E-48  92232.90c  1.00000E-48
```

```
  40094.90c  1.00000E-48  58141.90c  1.00000E-48  92233.90c  1.00000E-4
  41095.90c  1.00000E-48  59141.90c  1.00000E-48  92234.90c  2.67890E-0
  42095.90c  1.00000E-48  58142.90c  1.00000E-48  92235.90c  5.60400E-0
  40096.90c  1.00000E-48  60142.90c  1.00000E-48  92236.90c  1.00000E-4
  42096.90c  1.00000E-48  59143.90c  1.00000E-48  92237.90c  1.00000E-4
  42097.90c  1.00000E-48  60143.90c  1.00000E-48  92238.90c  2.20770E-0
  42098.90c  1.00000E-48  58144.90c  1.00000E-48  92239.90c  1.00000E-4
  43099.90c  1.00000E-48  60144.90c  1.00000E-48  93235.90c  1.00000E-4
  42100.90c  1.00000E-48  60145.90c  1.00000E-48  93236.90c  1.00000E-4
  44100.90c  1.00000E-48  60146.90c  1.00000E-48  93237.90c  1.00000E-4
  44101.90c  1.00000E-48  60147.90c  1.00000E-48  93238.90c  1.00000E-4
  44102.90c  1.00000E-48  61147.90c  1.00000E-48  93239.90c  1.00000E-4
  44103.90c  1.00000E-48  62147.90c  1.00000E-48  94236.90c  1.00000E-4
  45103.90c  1.00000E-48  60148.90c  1.00000E-48  94238.90c  2.84730E-0
  44104.90c  1.00000E-48  61148.91c  1.00000E-48  94239.90c  6.20380E-0
  46104.90c  1.00000E-48  61148.90c  1.00000E-48  94240.90c  2.94780E-0
  45105.90c  1.00000E-48  62148.90c  1.00000E-48  94241.90c  1.06850E-0
  46105.90c  1.00000E-48  61149.90c  1.00000E-48  94242.90c  8.06440E-0
  46106.90c  1.00000E-48  62149.90c  1.00000E-48  94243.90c  1.00000E-4
  46107.90c  1.00000E-48  60150.90c  1.00000E-48  95241.90c  1.00000E-4
  46108.90c  1.00000E-48  62150.90c  1.00000E-48  95242.91c  1.00000E-4
  47109.90c  1.00000E-48  62151.90c  1.00000E-48  95242.90c  1.00000E-4
  46110.90c  1.00000E-48  63151.90c  1.00000E-48  95243.90c  1.00000E-4
  48110.90c  1.00000E-48  62152.90c  1.00000E-48  95244.90c  1.00000E-4
  48111.90c  1.00000E-48  62153.90c  1.00000E-48  96242.90c  1.00000E-4
  48112.90c  1.00000E-48  63153.90c  1.00000E-48  96243.90c  1.00000E-4
  48113.90c  1.00000E-48  62154.90c  1.00000E-48  96244.90c  1.00000E-4
  48114.90c  1.00000E-48  63154.90c  1.00000E-48  96245.90c  1.00000E-4
  49115.90c  1.00000E-48  64154.90c  1.00000E-48  96246.90c  1.00000E-4
  51121.90c  1.00000E-48  63155.90c  1.00000E-48  96247.90c  1.00000E-4
  51123.90c  1.00000E-48  64155.90c  1.00000E-48  96248.90c  1.00000E-4
  53127.90c  1.00000E-48  63156.90c  1.00000E-48  96249.90c  1.00000E-4
  52128.90c  1.00000E-48  64156.90c  1.00000E-48  97249.90c  1.00000E-4
  53129.90c  1.00000E-48  64157.90c  1.00000E-48  97250.90c  1.00000E-4
  54131.90c  1.00000E-48  64158.90c  1.00000E-48  98249.90c  1.00000E-4
  54132.90c  1.00000E-48  65159.90c  1.00000E-48  98250.90c  1.00000E-4
  54133.90c  1.00000E-48  66160.90c  1.00000E-48  98251.90c  1.00000E-4
  55133.90c  1.00000E-48  66161.90c  1.00000E-48  98252.90c  1.00000E-4
C END Burnup
m4     40090.62c     0.0198892  $MAT
       40091.62c     0.0043373
       40092.62c     0.0066296
       40094.62c    0.00671856
       40096.62c    0.00108238
       26054.62c   7.7401e-006
       26056.62c     0.0001224
       26057.62c  2.80245e-006
       26058.62c   3.7366e-007
       24050.62c  2.96564e-006
       24052.62c  5.71893e-005
       24053.62c  6.48481e-006
       24054.62c  1.61421e-006
m5     1001.57c       0.048414  $MAT
       8016.57c       0.024213 5010.57c    4.7896e-006 5011.57c
1.9424e-005
mt5    lwtr.04t
C ======================================
C            FISSION PRODUCTS          !
C ======================================
m853   35081.90c             1
m854   36082.90c             1
```

```
m855   36083.90c                1
m856   36084.90c                1
m857   37085.90c                1
m858   37087.90c                1
m859   39089.90c                1
m860   38090.90c                1
m861   40091.90c                1
m862   40092.90c                1
m863   40093.90c                1
m864   40094.90c                1
m865   41095.90c                1
m866   42095.90c                1
m867   40096.90c                1
m868   42096.90c                1
m869   42097.90c                1
m870   42098.90c                1
m871   43099.90c                1
m872   42100.90c                1
m873   44100.90c                1
m874   44101.90c                1
m875   44102.90c                1
m876   44103.90c                1
m877   45103.90c                1
m878   44104.90c                1
m879   46104.90c                1
m880   45105.90c                1
m881   46105.90c                1
m882   46106.90c                1
m883   46107.90c                1
m884   46108.90c                1
m885   47109.90c                1
m886   46110.90c                1
m887   48110.90c                1
m888   48111.90c                1
m889   48112.90c                1
m890   48113.90c                1
m891   48114.90c                1
m892   49115.90c                1
m893   51121.90c                1
m894   51123.90c                1
m895   53127.90c                1
m896   52128.90c                1
m897   53129.90c                1
m898   54131.90c                1
m899   54132.90c                1
m900   54133.90c                1
m901   55133.90c                1
m902   54134.90c                1
m903   55134.90c                1
m904   56134.90c                1
m905   54135.90c                1
m906   55135.90c                1
m907   54136.90c                1
m908   55137.90c                1
m909   56137.90c                1
m910   56138.90c                1
m911   57139.90c                1
m912   58140.90c                1
m913   58141.90c                1
m914   59141.90c                1
m915   58142.90c                1
```

```
m916  60142.90c              1
m917  59143.90c              1
m918  60143.90c              1
m919  58144.90c              1
m920  60144.90c              1
m921  60145.90c              1
m922  60146.90c              1
m923  60147.90c              1
m924  61147.90c              1
m925  62147.90c              1
m926  60148.90c              1
m927  61148.91c              1
m928  61148.90c              1
m929  62148.90c              1
m930  61149.90c              1
m931  62149.90c              1
m932  60150.90c              1
m933  62150.90c              1
m934  62151.90c              1
m935  63151.90c              1
m936  62152.90c              1
m937  62153.90c              1
m938  63153.90c              1
m939  62154.90c              1
m940  63154.90c              1
m941  64154.90c              1
m942  63155.90c              1
m943  64155.90c              1
m944  63156.90c              1
m945  64156.90c              1
m946  64157.90c              1
m947  64158.90c              1
m948  65159.90c              1
m949  66160.90c              1
m950  66161.90c              1
m951  66162.90c              1
m952  66163.90c              1
m953  68166.90c              1
m954  68167.90c              1
C ======================================
C               ACTINIDES              !
C ======================================
m955  90231.42c              1
m956  90232.90c              1
m957  90233.90c              1
m958  91231.90c              1
m959  91232.90c              1
m960  91233.90c              1
m961  92232.90c              1
m962  92233.90c              1
m963  92234.90c              1
m964  92235.90c              1
m965  92236.90c              1
m966  92237.90c              1
m967  92238.90c              1
m968  92239.90c              1
m969  93235.90c              1
m970  93236.90c              1
m971  93237.90c              1
m972  93238.90c              1
m973  93239.90c              1
```

```
m974   94236.90c              1
m975   94238.90c              1
m976   94239.90c              1
m977   94240.90c              1
m978   94241.90c              1
m979   94242.90c              1
m980   94243.90c              1
m981   95241.90c              1
m982   95242.91c              1
m983   95242.90c              1
m984   95243.90c              1
m985   95244.90c              1
m986   96242.90c              1
m987   96243.90c              1
m988   96244.90c              1
m989   96245.90c              1
m990   96246.90c              1
m991   96247.90c              1
m992   96248.90c              1
m993   96249.90c              1
m994   97249.90c              1
m995   97250.90c              1
m996   98249.90c              1
m997   98250.90c              1
m998   98251.90c              1
m999   98252.90c              1
C
xxxxxxxxxxxxxxxxxxxxxxxxxxxxxxxxxxxxxxxxxxxxxxxxxxxxxxxxxxxxxxxxxxxxxxxxxxx
C                              Burnup
C
xxxxxxxxxxxxxxxxxxxxxxxxxxxxxxxxxxxxxxxxxxxxxxxxxxxxxxxxxxxxxxxxxxxxxxxxxxx
C
@@@@@@@@@@@@@@@@@@@@@@@@@@@@@@@@@@@@@@@@@@@@@@@@@@@@@@@@@@@@@@@@@@@@@@@@@@
FC4 Capture rates
C
@@@@@@@@@@@@@@@@@@@@@@@@@@@@@@@@@@@@@@@@@@@@@@@@@@@@@@@@@@@@@@@@@@@@@@@@@@
F4:n (1<98[2 -3 0]<99) (4<98[0 8 0]<99) (7<98[8 7 0]<99)
FM4   (1  853  102) (1  854  102) (1  855  102) (1  856  102) (1  857  102)
      (1  858  102) (1  859  102) (1  860  102) (1  861  102) (1  862  102)
      (1  863  102) (1  864  102) (1  865  102) (1  866  102) (1  867  102)
      (1  868  102) (1  869  102) (1  870  102) (1  871  102) (1  872  102)
      (1  873  102) (1  874  102) (1  875  102) (1  876  102) (1  877  102)
      (1  878  102) (1  879  102) (1  880  102) (1  881  102) (1  882  102)
      (1  883  102) (1  884  102) (1  885  102) (1  886  102) (1  887  102)
      (1  888  102) (1  889  102) (1  890  102) (1  891  102) (1  892  102)
      (1  893  102) (1  894  102) (1  895  102) (1  896  102) (1  897  102)
      (1  898  102) (1  899  102) (1  900  102) (1  901  102) (1  902  102)
      (1  903  102) (1  904  102) (1  905  102) (1  906  102) (1  907  102)
      (1  908  102) (1  909  102) (1  910  102) (1  911  102) (1  912  102)
      (1  913  102) (1  914  102) (1  915  102) (1  916  102) (1  917  102)
      (1  918  102) (1  919  102) (1  920  102) (1  921  102) (1  922  102)
      (1  923  102) (1  924  102) (1  925  102) (1  926  102) (1  927  102)
      (1  928  102) (1  929  102) (1  930  102) (1  931  102) (1  932  102)
      (1  933  102) (1  934  102) (1  935  102) (1  936  102) (1  937  102)
      (1  938  102) (1  939  102) (1  940  102) (1  941  102) (1  942  102)
      (1  943  102) (1  944  102) (1  945  102) (1  946  102) (1  947  102)
      (1  948  102) (1  949  102) (1  950  102) (1  951  102) (1  952  102)
      (1  953  102) (1  954  102) (1  955  102) (1  956  102) (1  957  102)
      (1  958  102) (1  959  102) (1  960  102) (1  961  102) (1  962  102)
      (1  963  102) (1  964  102) (1  965  102) (1  966  102) (1  967  102)
      (1  968  102) (1  969  102) (1  970  102) (1  971  102) (1  972  102)
```

```
     (1  973  102) (1  974  102) (1  975  102) (1  976  102) (1  977  102)
     (1  978  102) (1  979  102) (1  980  102) (1  981  102) (1  982  102)
     (1  983  102) (1  984  102) (1  985  102) (1  986  102) (1  987  102)
     (1  988  102) (1  989  102) (1  990  102) (1  991  102) (1  992  102)
     (1  993  102) (1  994  102) (1  995  102) (1  996  102) (1  997  102)
     (1  998  102) (1  999  102)
C
C#########################################################################################
FC14  n2n rates for Actinides
C
C#########################################################################################
F14:n (1<98[2 -3 0]<99) (4<98[0 8 0]<99) (7<98[8 7 0]<99)
FM14 (1  955  16) (1  956  16) (1  957  16) (1  958  16) (1  959  16)
     (1  960  16) (1  961  16) (1  962  16) (1  963  16) (1  964  16)
     (1  965  16) (1  966  16) (1  967  16) (1  968  16) (1  969  16)
     (1  970  16) (1  971  16) (1  972  16) (1  973  16) (1  974  16)
     (1  975  16) (1  976  16) (1  977  16) (1  978  16) (1  979  16)
     (1  980  16) (1  981  16) (1  982  16) (1  983  16) (1  984  16)
     (1  985  16) (1  986  16) (1  987  16) (1  988  16) (1  989  16)
     (1  990  16) (1  991  16) (1  992  16) (1  993  16) (1  994  16)
     (1  995  16) (1  996  16) (1  997  16) (1  998  16) (1  999  16)
C
C#########################################################################################
FC24  n3n rates for Actinides
C
C#########################################################################################
F24:n (1<98[2 -3 0]<99) (4<98[0 8 0]<99) (7<98[8 7 0]<99)
FM24 (1  955  17) (1  956  17) (1  957  17) (1  958  17) (1  959  17)
     (1  960  17) (1  961  17) (1  962  17) (1  963  17) (1  964  17)
     (1  965  17) (1  966  17) (1  967  17) (1  968  17) (1  969  17)
     (1  970  17) (1  971  17) (1  972  17) (1  973  17) (1  974  17)
     (1  975  17) (1  976  17) (1  977  17) (1  978  17) (1  979  17)
     (1  980  17) (1  981  17) (1  982  17) (1  983  17) (1  984  17)
     (1  985  17) (1  986  17) (1  987  17) (1  988  17) (1  989  17)
     (1  990  17) (1  991  17) (1  992  17) (1  993  17) (1  994  17)
     (1  995  17) (1  996  17) (1  997  17) (1  998  17) (1  999  17)
C
C#########################################################################################
FC34 Fissin rates
C
C#########################################################################################
F34:n (1<98[2 -3 0]<99) (4<98[0 8 0]<99) (7<98[8 7 0]<99)
FM34 (1  955  -6) (1  956  -6) (1  957  -6) (1  958  -6) (1  959  -6)
     (1  960  -6) (1  961  -6) (1  962  -6) (1  963  -6) (1  964  -6)
     (1  965  -6) (1  966  -6) (1  967  -6) (1  968  -6) (1  969  -6)
     (1  970  -6) (1  971  -6) (1  972  -6) (1  973  -6) (1  974  -6)
     (1  975  -6) (1  976  -6) (1  977  -6) (1  978  -6) (1  979  -6)
     (1  980  -6) (1  981  -6) (1  982  -6) (1  983  -6) (1  984  -6)
     (1  985  -6) (1  986  -6) (1  987  -6) (1  988  -6) (1  989  -6)
     (1  990  -6) (1  991  -6) (1  992  -6) (1  993  -6) (1  994  -6)
     (1  995  -6) (1  996  -6) (1  997  -6) (1  998  -6) (1  999  -6)
e34 0.625e-6 20
C
C#########################################################################################
FC44 Average fission energy(MeV) & nubar
C
C#########################################################################################
F44:n  1   $ fuel cell number
FM44:n (-1  1 -6 ) (-1  1 -6 -7) (-1  1 -6 -8)
C
C#########################################################################################
```

```
FC54 Two groups flux for burnup calculations
C
@@@@@@@@@@@@@@@@@@@@@@@@@@@@@@@@@@@@@@@@@@@@@@@@@@@@@@@@@@@@@@@@@@@@@@@@@@
F54:n (1<98[2 -3 0]<99) (4<98[0 8 0]<99) (7<98[8 7 0]<99)
E54 6.2500E-07 1.0000E-04 2.0000E+01
C
@@@@@@@@@@@@@@@@@@@@@@@@@@@@@@@@@@@@@@@@@@@@@@@@@@@@@@@@@@@@@@@@@@@@@@@@@@
print -30 -60 -85 -130 -140
```

```
c ======================================
c BUCAL1 input file for MOX benchmark
c ======================================
* Power
  4.9E+06  38.1
* Number of active cells
  3
* Number of cells look like active cells
  184 68 12
* Volume(cc) and density(g/cc)
  5.2810E+01  10.4539
  5.2810E+01  10.4414
  5.2810E+01  10.4350
* Number of Burnable elements (in each active cell)
  8 8 8
* Material composition in each active cell
* Active cell 01
  92234  2.57180E-07
  92235  5.37980E-05
  92238  2.11940E-02
  94238  5.16770E-05
  94239  1.12590E-03
  94240  5.35000E-04
  94241  1.93920E-04
  94242  1.46360E-04
* Active cell 02
  92234  2.64360E-07
  92235  5.53000E-05
  92238  2.17860E-02
  94238  3.61280E-05
  94239  7.87170E-04
  94240  3.74030E-04
  94241  1.35570E-04
  94242  1.02330E-04
* Active cell 03
  92234  2.67890E-07
  92235  5.60400E-05
  92238  2.20770E-02
  94238  2.84730E-05
  94239  6.20380E-04
  94240  2.94780E-04
  94241  1.06850E-04
  94242  8.06440E-05
* Temperatures (Kelvin)
  900. 900. 900.
* Number of cycles
  3
* Number of Time steps per cycle
  5 5 5
* Time
+ T_Cylce01
  0 10 100 400 420
+ T_Cylce02
  0 10 100 400 420
+ T_Cylce03
  0 10 100 400 420
* Macro time steps per cycle
+ MTS_Cylce01
  10 90 100 20
+ MTS_Cylce02
  10 90 100 20
```

```
+ MTS_Cylce03
  10 90 100 20
* Refreshment
+ R_Cylce01
  30. 10.
+ R_Cylce02
  30. 10.
+ R_Cylce03
  1825. 5.
* MCNP name file (maximum 8 characters)
  moll
* Isotope importance
   35081  1    54134  1   66162  1
   36082  1    55134  1   66163  1
   36083  1    56134  1   68166  1
   36084  1    54135  1   68167  1
   37085  1    55135  1   90231  1
   37087  1    54136  1   90232  1
   39089  1    55137  1   90233  1
   38090  1    56137  1   91231  1
   40091  1    56138  1   91232  1
   40092  1    57139  1   91233  1
   40093  1    58140  1   92232  1
   40094  1    58141  1   92233  1
   41095  1    59141  1   92234  1
   42095  1    58142  1   92235  1
   40096  1    60142  1   92236  1
   42096  1    59143  1   92237  1
   42097  1    60143  1   92238  1
   42098  1    58144  1   92239  1
   43099  1    60144  1   93235  1
   42100  1    60145  1   93236  1
   44100  1    60146  1   93237  1
   44101  1    60147  1   93238  1
   44102  1    61147  1   93239  1
   44103  1    62147  1   94236  1
   45103  1    60148  1   94238  1
   44104  1    61148  1   94239  1
   46104  1    61148  1   94240  1
   45105  1    62148  1   94241  1
   46105  1    61149  1   94242  1
   46106  1    62149  1   94243  1
   46107  1    60150  1   95241  1
   46108  1    62150  1   95242  1
   47109  1    62151  1   95242  1
   46110  1    63151  1   95243  1
   48110  1    62152  1   95244  1
   48111  1    62153  1   96242  1
   48112  1    63153  1   96243  1
   48113  1    62154  1   96244  1
   48114  1    63154  1   96245  1
   49115  1    64154  1   96246  1
   51121  1    63155  1   96247  1
   51123  1    64155  1   96248  1
   53127  1    63156  1   96249  1
   52128  1    64156  1   97249  1
   53129  1    64157  1   97250  1
   54131  1    64158  1   98249  1
   54132  1    65159  1   98250  1
   54133  1    66160  1   98251  1
   55133  1    66161  1   98252  1
```

Appendix E. NEA/OCED codes description and data

In this appendix we give a brief description of the codes used for the validation of our new elaborated burnup code BUCAL1. Also we present the published data for these codes.

I- Codes used for UO2 and UO2-ThO2 benchmarks analysis

CASMO-4 is a deterministic multi-group two-dimensional transport code for standard LWR burnup calculations from Studsvik. It is based on the evaluated data files JEF-2.2 and ENDF/B-VI, which were developed at the OECD/NEA Data Bank and Brookhaven National Nuclear Data Center, respectively.

MCODE is an MCNP4C-ORIGEN2.1 linkage code from MIT (MASSACHUSETTS INSTITUTE of TECHNOLOGY) that uses the matrix exponential method with the predictor-corrector algorithm as integration method. In the transport calculations, the cross sections for most of the isotopes are taken from ENDF/B-V and ENDF/B-VI, while for the others, data from libraries evaluated at different laboratories are taken. In the burnup calculations, the cross sections not provided by MCNP are taken from the ORIGEN one-group cross section library PWRUE.LIB (3-cycle PWR library, thermal spectrum) and the decay data are taken from DECAY.LIB (which comprises a total of 1307 different nuclides, including 129 actinides and 879 fission products).

MOCUP is the MCNP-ORIGEN2 Coupled Utility Program. It employs the MCNP4B generalized-geometry Monte Carlo transport code to produce the neutronics solution and the ORIGEN2 code to compute the time-dependent compositions of the individually selected MCNP cells. All data communication between the two codes is accomplished through the MCNP and ORIGEN2 input/output files. This allows a general material (target, fuel, control, etc.) to be depleted in a neutral particle field, with the accuracy of a transport neutronics solution. Since the MCNP version 4B library does not contain temperature-dependent neutron cross sections of most actinides, a number of libraries from the UTXS compilation were imported. Also for some fission products, the evaluated data files elaborated at Los Alamos National Laboratory were imported via INEEL (Idaho National Engineering & Environmental Laboratory, US). The main features of each code are summarized on Table E-1.

Table E-1. Summary of benchmarking codes.

	MCODE	MOCUP	CASMO-4	BUCAL1
Cross section libraries	ENDF/B-V ENDF/B-VI + other evaluated libraries	ENDF/B-V ENDF/B-VI	ENDF/B-VI, JEF2.2	ENDF/B-VII JEFF-3.1
Code developer	MIT	INEEL	Studsvik	ERSN-LMR
Transport treatment	Monte Carlo	Monte Carlo	KRAM characteristics	Monte Carlo
Resonance treatment	Monte Carlo	Monte Carlo	collision probability	Monte Carlo
Number of energy groups	continuous	continuous	70	continuous
Burnup algorithm	Standard predictor-corrector	Beginning-of-timestep representation	Standard predictor-corrector	Standard predictor-corrector
Actinide representation	39	17	Th231 thru Cf252	45
Fission products	100	41	~200	102

II- Codes used for MOX benchmark analysis

The following is a brief description of nuclear data and analysis codes employed by each participant. Additional comments provided by participants are also included. Table E-2 summarizes the data and codes used by the participants. Table E-3 gives the obtained data by the codes used in the validation process of BUCAL1 using the MOX benchmark.

1) NUPEC, Japan

Institute: Institute for Nuclear Safety, NUPEC, Japan.

Participants: Shungo Sakurai, Susumu Mitake.

Neutron data library: E4LBL70 (L-library), based on ENDF/B-IV.

Neutron data processing code or method: CASLIB.

No. of neutron energy groups: 70 groups for pin cell, finally 16 groups for assembly.

Description of the code system: CASMO-4, a multi-group two-dimensional transport theory code for burn-up calculations on BWR and PWR assemblies. Some characteristics of this code are listed below:

(a) Nuclear data are collected in a library in 70 and 40 groups, and cover the energy range 0 to 10 MeV.

(b) CASMO can accommodate non-symmetric fuel bundles, while half, quadrant, or octant symmetry can be utilized.

(c) The two-dimensional calculation is performed in true heterogeneous geometry.

(d) The calculation sequence starts in a simplified geometry. Energy groups are then collapsed as spatial detail is increased.

(e) A predictor-corrector approach is used in the depletion calculation, which greatly reduces the number of burn-up steps necessary for a given accuracy.

(f) The output is flexible and gives few group cross-sections and reaction rates for any region of the assembly for use in overall reactor calculation.

(g) Discontinuity factors are calculated at the boundary between bundles and for reflector regions.

Geometry modelling: The transport calculation scheme and the corresponding geometry modeling are as follows: One-dimensional pin cell calculation (40 groups) is performed in annular model for each pin type. Each pin type is homogenised, and used for a two-dimensional response matrix (RM) calculation of the assembly in a rectangular geometry, to include the effects of the surroundings. Pin cell spectra are then modified by RM results, and the modified spectra are used for processing a several-group cross-section, with which a two-dimensional heterogeneous calculation of the entire assembly is done for the flux distribution throughout the lattice, by solving the transport equation using the method of characteristics.

Omitted nuclides: 95Mo, 99Tc, 101Ru.

Employed convergence limit for eigenvalue calculations: Convergence tolerance for relative change of flux: 5.0 × 10–5, eigenvalue: 1.0 × 10–4 (default).

Other related information: Machine – SPARC Station 5 (Solaris 2.4).

References to the code system or library:

[1] E. Edenius, B.H. Forssen, C. Gragg, “The Physics Model of CASMO-4”, Proc. Int. Topical Meeting on Advances in Mathematics, Computations and Reactor Physics, Vol. 2, pp. 10-11 1, ANS (1991).

2) CEA, France

Institute: CEA/DRN (France).

Participants: N. Thiollay, B. Roque.

Neutron data library: CEA-93 based on JEF-2.2 evaluations.

Neutron data processing code: Multi-group cross-sections and effective cross-sections processed by NJOY from JEF-2 file.

Neutron energy groups: 172 (X-MAS group structure).

Description of code system: The code system used is the DARWIN package based on the APOLLO2 and PEPIN2 codes. APOLLO2 is the new French code system used for LWRs and HCLWRs. APOLLO2 is a modular code which solves both the Boltzman integral equation

and the integro-differential equation (Sn method). APOLLO2 allows the use of several collision probability methods (exact-2D Pij, and multi-cell Pij based on the interface current method) to solve the integral equation. The PEPIN2 program performs the nuclide depletion calculations.

Different libraries feed this module:

(a) Neutronics data provided by the French transport code APOLLO2. These data are self-shielded cross-sections and neutron spectra.

(b) Nuclear constants (decay data, fission and (α,n) yields) and decay chains.

(c) Complementary cross-sections missing from the transport codes libraries, especially for activation products.

Geometry modelling: Exact heterogeneous geometry, each fuel pin is differentiated, fuel pin divided into four concentric zones. Thus, 36 depletion media are used (9 pins × 4 zones). Self-shielded cross-sections are calculated for every actinide in each concentric zone; powerful and accurate matrix dilution formalism is used for resonant reaction rate calculation.

Omitted or substituted nuclides: The whole nuclides are available in CEA93 library.

Employed convergence limits: External convergence on keff = 1.E-6 dk/k.

Other information: 241Am to 242mAm branching ratio of 0.115 is used.

References:

[1] R. Sanchez, *et al.*, "APOLLO2: A User-oriented, Portable, Modular Code for Multi-group Transport Assembly Calculations", *Nucl. Sci. and Eng.*, 100, 352 (1988).

[2] P. Marimbeau, *et al.*, "The DARWIN Fuel Cycle Package. Procedures for Material Balance Calculation and Qualification", ENC'98, Nice, France, 25-28 October 1998.

3) GRS, Germany

Institute: Gesellschaft für Anlagen- und Reaktorsicherheit GRS, Germany.

Participants: Bernhard Gmal, Ulrich Hesse, Eberhard F. Moser.

Neutron library: JEF-2.2 based library KORLIB-V4 for KENO-5a [2], 2001 standard library for OREST [3], HAMMER [4].

Neutron data processing code and method: Condensing KORLIB-V4 from 292-group library JEF-2.2 [6] by RESMOD code for the infinite dilution case. Resonance treatment is done by the HAMMER code using resonance parameters [7].

No. of neutron energy groups: 83, 32 thermal groups up to 1.13 eV (KENO-5a), PL order is 3.

Description of the code system: KENOREST Version 2001 [1] includes KENO-5a code for 3-D assembly calculations using the Monte Carlo method, coupled with the one-dimensional burn-up code system OREST01 (HAMMER-ORIGEN [5]) for single rod burn-up calculations. The coupling is realized using flux and reaction rate conservation with the FEC method [8] of GRS. The flux spectra and cross-section calculations for the fuel rods are performed by the HAMMER code (THERMOS-HAMLET) using the method of integral Boltzmann neutron transport calculation and Nordheim resonance treatment in the resonance region. The cross-sections are directly fed back to KENO.

Geometry modelling: 3-D for in-core keff calculations by KENO, 1-D for pin cell burn-up calculations.

Used nuclides: All nuclides of ORIGEN library.

Other information: $k\infty$ values are calculated automatically by the code system, taking into account more nuclides than those specified for the benchmark. Fifty-seven (57) nuclides were handled simultaneously. The remaining is treated as long-lived fission products. For 241Am and 242mAm a branching ratio of 0.137 was used.

References:

[1] U. Hesse, *et al.*, "KENOREST – A New Criticality and Inventory System Based on KENO and OREST", ICNC99 Proceedings, Vol. 1, p. 48.

[2] L.M. Petrie, N.F. Landers, "KENO V.a., An Improved Monte Carlo Criticality Program with Supergrouping", NUREG/CR-0200, Vol. 2, Section F11, ORNL, Tennessee 37831, March 1983.

[3] U. Hesse, W. Denk, H. Deitenbeck, "OREST – eine direkte Kopplung von HAMMER und ORIGEN zur Abbrandsimulation von LWR-Brennstoffen", GRS-63 (GRS-erweiterte Version OREST-98), November 1986.

[4] J.E. Suich and H.C. Honeck, "The HAMMER System – Heterogeneous Analysis by Multi-group Methods of Exponentials and Reactors", TID-4500, January 1967.

[5] M.J. Bell, "ORIGEN – The ORNL Isotope Generation and Depletion Code", ORNL-4628, UC 32-Mathematics and Computers (GRS-Version 1990 für NEA Data Bank), May 1973.

[6] W. Bernnat, D. Lutz, J. Kleinert, M. Mattes, "Erstellung und Validierung von Wirkungsquerschnittsbibliotheken auf Basis der evaluierten Dateien JEF-2 und ENDF/B-VI für Kritikalitäts- und Reaktorauslegungs-Rechnungen sowie Störfallanalysen", IKE 6-189, IKE Institut für Kerntechnik und Energiesysteme, Universität Stuttgart, September 1994.

[7] S.F. Mughabghab, "Neutron Resonance Parameters and Thermal Cross-sections", Vol. 1, Brookhaven National Laboratory, Upton, New York, Academic Press, Inc., (1984).

[8] U. Hesse, K. Hummelsheim, “Detaillierte, dreidimensionale Abbrandrechnungen für ein SWR-Atriumbrennelement”, GRS-A-2116, December 1993.

4) PSI, Switzerland

Institute: Paul Scherrer Institute.

Participant: Peter Grimm.

Neutron data library: Cross-sections from JEF-1 (except 155Gd from JENDL-2, zircaloy-2 from ENDF/B-4), processed by ETOBOX (code developed at PSI, Ref. [1]). Fission product yields from JEF-2 for thermal fission. Decay data for fission products are taken from Ref. [3], and for actinides from Ref. [4]. In the decay data 34 actinides (232Th to 248Cm), 55 explicit fission products, two pseudo fission products are taken into account. *Neutron energy group*: 70 groups (69 group WIMS structure + 1 group 10-15 MeV, thermal cut-off 1.3 eV). Point data in resonance range (1.3 eV-907 eV) consists of typically 7 000-8 000 points. Tabulated resonance cross-sections are collapsed to groups for E > 907 eV. Thermal scattering matrix for hydrogen in water is taken from JEF-1 S(α,β) matrix. *Cell, transport and depletion code*:

(a) BOXER – cell and two-dimensional transport and depletion code (developed at PSI, Ref. [2]). Resonance self-shielding: Pointwise two-region collision probability calculation (1.3 eV < E < 907 eV), tabular interpolation versus temperature and equivalent dilution cross-section for E > 907 eV, Dancoff factor corrected for 2-D array geometry by Monte Carlo method.

(b) Cell calculation: One-dimensional integral transport calculation in cylindrical geometry employing white boundary conditions or boundary source from a previously calculated cell. Fundamental mode spectrum (keff = 1) in 70 groups by B1 method for homogenised cell.

(c) Two-dimensional transport calculations: Transmission probability integral transport method in x-y geometry for homogenised cells, using first-order spherical harmonics expansions for mesh surface currents and linear space dependence of surface currents and source within meshes, P1 anisotropic scattering.

(d) Depletion calculation: Taylor series (fixed order), asymptotic densities for nuclides with high destruction rates, predictor-corrector method, density dependent one-group cross-sections within time step for 239Pu and 240Pu (approximated by rational function).

(e) Models and calculational options used: Cell calculation for all pin types (cylindricalised cells) with white boundary condition. Cell calculation for guide tubes with boundary source from high enrichment MOX cell. Cladding composition replaced by zircaloy-2, 3.8859E-2 atoms/barn*cm (sum of number densities for Zr + Fe + Cr in specifications).

(f) Energy group structure for two-dimensional transport calculation: 15 groups, upper boundaries 15, 6.07, 2.23 MeV, 821 keV, 907, 75.5, 16, 4, 1.3, 0.996, 0.625, 0.3, 0.14, 0.05 and 0.02 eV.

(g) Geometric model for 2-D transport calculations: Homogenised pin cells, one mesh per cell. Supercell: 2 × 2 assemblies with translational boundary conditions simulated by 2 × 2 quarter assemblies with reflective boundary.

Employed convergence limits: 1E-4 for fluxes, 1E-5 for eigenvalue.

Other information: Depletion with critical spectrum by search for material buckling at each burn-up step. Burn-up points in each cycle: 0, 0.1, 0.5, 1, 2, 4, 8, 12, 16 GWd/t from BOC (repeated three times).

References:

[1] J.M. Paratte, K. Foskolos, P. Grimm, J.M. Hollard, "ELCOS, The PSI Code System for LWR Core Analysis, Part I: User's Manual for the Library Preparation Code ETOBOX", PSI Report 96-02, January 1996.

[2] J.M. Paratte, P. Grimm, J.M. Hollard, "ELCOS, The PSI Code System for LWR Core Analysis, Part II: User's Manual for the Fuel Assembly Code BOXER", PSI Report 96-08, February 1996.

[3] M.E. Meek, B.F. Rider, "Compilation of Fission Product Yields", NEDO-12154-1, 74NED6 (1974).

[4] W. Seelmann-Eggebert, *et al.*, "Karlsruhe Chart of the Nuclides", 5th edition, Kernforschungszentrum Karlsruhe (1981).

5) BNFL, United Kingdom

Institute: British Nuclear Fuels Ltd (BNFL).

Participants: Gregory O'Connor, Russell Bowden, Peter Thorne.

Neutron data library: 172-group "1997" WIMS library, Version 1, 20th June 1997. Xmas 172 group structure. Nuclear data source – JEF-2.2.

Neutron data processing code or method: WIMS8A processing codes – NJOY & WILT.

Neutron energy groups: 172-group structure condensed to six groups for final CACTUS and BURNUP modules.

Description of code system: WIMS8A, Release 0, is a two-dimensional deterministic code developed by AEA Technology.

Geometry modeling: Geometry modeled according to the benchmark, no simplifications made.

Omitted or substituted nuclides: No nuclides substituted or omitted from the calculations.

Employed convergence limits: None, WIMS8A is a deterministic code.

Other information: Calculations performed on a SunOS 5.7, processor type sun4u using the Solaris 2 operating system. 241Am to 242mAm branching ratio of 0.10 is used.

6) JAERI, Japan (1)

Institute: Japan Atomic Energy Research Institute (JAERI).

Participants: Kenya Suyama, Hiroki Mochizuki and Hiroshi Okuno.

Neutron data library: JENDL-3.2.

Neutron data processing code:

(a) SRAC95 libraries:

– PROF-GROUCH-GII [2] and TIMS-1 [3]: Fast group (10 MeV to 0.41399 eV): 74 groups.

– MCROSS-2 [3]: Resonance (961 eV to 0.41399 eV): 19 500 groups (for ultra fine resonance absorption calculation library).

– GASKET [4] and HEXSCAT [5]: Thermal (3.9279 eV to 1.0E-5 eV) and S(α,β): 48 groups.

(b) SWAT libraries:

– LINEAR, RECENT, SIGMA1 [6] and CRECTJ5 [7]: 147 groups. This SWAT library is for isotopes not included in SRAC95 libraries.

Neutron energy group: 107 groups (for eigenvalue problems). Overlapping groups exists in a resonance region (3.9279 to 0.41399 eV).

Description of code system:

(a) SWAT [8] is an integrated burn-up code system driving SRAC95 and ORIGEN2. In the SWAT calculation, SRAC95 evaluates effective cross-sections dependent on burn-up and burn-up calculation is conducted by ORIGEN2. SWAT includes original cross-section library "SWAT library" for use in burn-up calculation. This library is based on JENDL-3.2. For many isotopes, effective cross-sections are prepared by SRAC95. However, some isotopes are not treated in the SRAC95 calculation. To use the latest cross-section data in JENDL-3.2 for these isotopes, SWAT makes infinite diluted cross-section data from the "SWAT library". This function enables us to perform burn-up calculations using all cross-section data stored in JENDL-3.2. In the SWAT calculation, fission yield and decay constant data are also updated based on JNDC FP Library 2nd version [9].

(b) SRAC [1] is JAERI's Thermal Reactor Standard Code System. It contains many modules for neutronics calculation. SRAC95 is the latest version released in 1996. SRAC has been used for many reactor analyses. SRAC uses collision probability method to calculate group constants. A generalised Dancoff correction factor was introduced for infinite arrays of multi-region cells including several absorber lumps with different nuclide concentrations using the

collision probability method. A fixed boundary source problem is available in the cell calculation using the collision probability method. It can endow a proper spectrum to an isolated cell that cannot have its own spectrum. A remarkable feature of SRAC is its ultra-fine resonance calculation using the collision probability method.

Geometry modelling: Square and cylinder divided by concentric circles (1-D calculation).

Omitted nuclides: None.

Employed convergence limit: 1.0E-5.

Other information: One-hundred seven (107) groups' effective group constants were calculated using the collision probability method in fixed source mode by SRAC95. We then treat the eigenvalue problem with the collision probability method using the constants of the 107 groups. Ultra-fine (15 000 groups) resonance calculation was selected for 961 eV to 3.9279 eV. This sequence is the standard method for calculating eigenvalues using the SRAC system. For 241Am to 242mAm, a branching ratio of 0.11 is used.

References:

[1] K. Okumura, *et al*., JAERI Data/Code 96-015 (1996), see also JAERI-1302 (1986).

[2] S. Hasegawa, JAERI-1248 (1978).

[3] H. Takano *et al*., JAERI-M 4721 (1978).

[4] J.U. Koppel, *et al*., GA-7417 (1966).

[5] Y.D. Naliboff, *et al*., GA-6026 (1964).

[6] D. Cullen, UCRL-50400, Vol. 17, Part B (1979).

[7] T. Nakagawa, JAERI Data/Code 99-41 (2000).

[8] K. Suyama, *et al*., JAERI Data/Code 2000-027 (2000).

[9] K. Tasaka, *et al*., JAERI-1320 (1980).

7) JAERI, Japan (2)

Institute: Japan Atomic Energy Research Institute (JAERI).

Participants: Kenya Suyama, Keisuke Okumura, Hiroshi Okuno and Masaru Ido* (* ITJ Inc.).

Neutron data library: JENDL-3.2.

Neutron data processing code: ART [4] is used to make temperature dependent libraries.

Neutron energy group: Continuous energy.

Description of code system: MVP-BURN [1] is a burn-up code system using the continuous energy Monte Carlo code "MVP" [2] and the burn-up calculation routine of "SRAC95" [3].

Geometry modelling: Two-dimensional modelling specified in the benchmark specification.

Omitted nuclide: In burn-up chain data, 95Mo, 110Ag and 147Sm are not included.

Employed convergence limit: None.

Other information: For 241Am to 242mAm, a branching ratio of 0.116 is used.

History information: Case-1 5000 history/cycle; 50 cycle (include 10 skip).

Case-2 5000 history/cycle; 50 cycle (include 10 skip).

Case-3 10000 history/cycle; 50 cycle (include 10 skip).

Case-4 10000 history/cycle; 50 cycle (include 10 skip).

Case-5 10000 history/cycle; 50 cycle (include 10 skip).

Case-6 10000 history/cycle; 50 cycle (include 10 skip).

Burn-up step: 2 GWd/t per step.

References:

[1] K. Okumura, *et al*., *J. Nucl. Sci. Technol*.,Vol. 32, pp. 128-138 (2000).

[2] T. Mori and M. Nakagawa, JAERI-Data/Code 94-007 (1994).

[3] K. Okumura, *et al*., JAERI Data/Code 96-015(1996), see also JAERI-1302 (1986).

[4] T. Mori, *et al*., Proc. Int. Conf. on Mathematics and Computation (M&C'99), Madrid, Vol. 2, p. 987 (1999).

8) DTLR, United Kingdom

Institute: Department for Transport, Local Government and the Regions (DTLR).

Participant: Gregory O'Connor.

Neutron data library: One-hundred seventy-two (172) group "1996" WIMS library, Version 3. Nuclear data source – JEF-2.2.

Neutron data processing code or method: WIMS pre-processing modules used.

Neutron energy groups: One-hundred seventy-two (172) group structure.

Description of code system: MONK8A, Release Update 1, developed by AEA Technology.

Geometry modelling: Geometry modelled according to the benchmark, no simplifications made.

Omitted or substituted nuclides: Decay chains for 238Pu and Cm isotopes are omitted from the MONK8A code.

Employed convergence limits: Convergence of eigenvalue (keff) to less than 0.0010.

Other information: Three-dimensional Monte Carlo calculation using 1 000 neutrons per stage and 10 super-histories. Calculations performed on a Compaq DeskPro, with Pentium III processor and using WINDOWS-NT Version 4.0 operating system. 241Am to 242mAm branching ratio of 0.12 is used.

9) ORNL, USA

Institute: Oak Ridge National Laboratory.

Participants: Mark D. Hart, Charlotta Sanders.

Neutron data library: scale.rev09.xn238, version 9 of the SCALE 238-group ENDF/B-V library (contains ENDF/B-VI evaluations for O, N, and Eu nuclides).

Neutron data processing code or method: BONAMI/NITAWL.

Neutron energy groups: Two-hundred thirty-eight (238) group structure.

Description of code system: SAS2D is a developmental 2-D depletion sequence in SCALE 5. The final version will be released with SCALE 5 under the name TRITON. SAS2D used NEWT for 2-D transport calculations coupled with ORIGEN-S for independent depletion of each fuel region. NEWT is a generalized-geometry discrete ordinates solver.

Geometry modeling: NEWT employs arbitrary-polygon computational cells; all curved surfaces were approximated by high-order polygons (10 or more sides) with volumes conserved.

Omitted or substituted nuclides: None.

Employed convergence limits: Both flux and eigenvalue convergence limits set to 1E-4. In general, eigenvalues were converged on the order of 1E-6 before spatial convergence was achieved.

Other information: Reported results were obtained from calculations performed on a Compaq Alpha under OSF1 V4.0 compiled with the Compaq FORTRAN 95 compiler. Results were verified on a Macintosh G4-DP running OS X v10.1 and the Absoft F95 compiler. All calculations were performed with controlled but pre-released versions of SCALE 5 modules and data.

Table E-2. Analysis codes and methods.

No.	Country	Institute	Participant	Nuclear data				Calculation			Remarks
				Origin	Library	No. of groups	Processing code	Code	Model	Convergence limits	
1	Japan	NUPEC	Sakurai, Mitake	ENDF/B-IV	E4LBL70 (L-library)	70	CASLIB	CASMO-4	1-D (pin cell, 70 group), 2-D (assembly, 16 group)	Flux: 5.0E-5, k_{eff}: 1.0E-4	CASMO-4: response matrix method
2	France	CEA	Thiollay	JEF-2.2	CEA-93	172	NJOY	DARWIN	2-D	k_{eff}: 1.0E-6	DARWIN code system based on APOLLO2 & PEPIN2 codes
3	Germany	GRS	Gmal, Moser, Hesse	JEF-2.2	KORLIB-V4, 99-standard library	83 (29 thermal)	RESMOD, HAMMER	KENOREST-2000, OREST99	3-D (KENO), 1-D (pin cell burn-up)	NA	No iteration employed to achieve target burn-up
4	Switzerland	PSI	Grimm	JEF-1	BOXLIB	70	ETOBOX	BOXER	2-D	Flux: 1.0E-4, k_{eff}: 1.0E-5	
5	UK	BNFL	O'Connor, Bowden, Thorne	JEF-2.2	"1997" WIMS library	172	NJOY & WILT	WIMS8A	2-D	None	172 group > 6 groups for CACTUS & BURNUP modules; WIMS8A: collision probabilistic method
6	Japan	JAERI (1)	Suyama	JENDL-3.2	MVP94.1	Continuous	LICEM	MVP-BURN	3-D	NA	MVP-BURN: continuous Monte Carlo burn-up code
7	Japan	JAERI (2)	Suyama	JENDL-3.2, JNDCFPV2	SWAT library, SRAC library	147	SWAT: RECENT, LINEAR, SIGMA 1, CRECTJ5, SRAC95: PROFGROUCH	SWAT (SRAC95 & ORIGEN2)	1-D	NA	SRAC95: collision probabilistic method
8	UK	DTLR	O'Connor	JEF-2.2	"1996" WIMS library	172	WIMS pre-processing modules	MONK8A	3-D	k_{eff}: 0.001 less	1 000 neutron per stage, 10 super-histories; decay chains for ^{238}Pu and Cm isotopes are omitted
9	USA	ORNL	De Hart, Sanders	ENDF/B-VI	scale.rev09.xn238	236	BONAMI/NITAWL	SAS2D (NEWT & ORIGEN-S)	2-D	Flux: 1.0E-4, k_{eff}: 1.0E-4	SAS2D is a developmental 2-D depletion sequence in SCALE. The final version will be released with SCALE5 under the name TRITON.

Table E-3. Calulation results for MOX benchmark.

OECD/NEANSC Burnup Credit Benchmark, Phase IV-B (MOX)

Case 3 - First Recycle MOX, Assembly Model

NUPEC (Sakurai)
CASLIB - E4LBL70 (L-libraray), based on ENDF/B-IV

Nuclide	End of Cycle 1	End of Cycle 2	End of Cycle 3	5 Years Cooling
U -234	5.8095E-07	8.3192E-07	1.0211E-06	2.6288E-06
U -235	4.3790E-05	3.4621E-05	2.6722E-05	2.6722E-05
U -236	2.5154E-06	4.4450E-06	5.8461E-06	5.8461E-06
U -238	2.1160E-02	2.0923E-02	2.0675E-02	2.0675E-02
Pu-238	4.1019E-05	3.8424E-05	3.8550E-05	4.0961E-05
Pu-239	8.0416E-04	6.3755E-04	5.0850E-04	5.1029E-04
Pu-240	4.7385E-04	4.4805E-04	4.0953E-04	4.1275E-04
Pu-241	2.1858E-04	2.3660E-04	2.3550E-04	1.8481E-04
Pu-242	1.3785E-04	1.4982E-04	1.6558E-04	1.6558E-04
Np-237	1.5029E-06	2.8860E-06	4.0942E-06	4.0942E-06
Am-241	8.8242E-06	1.5561E-05	1.9061E-05	6.9385E-05
Am-242m	1.3421E-07	3.1898E-07	4.2146E-07	4.1192E-07
Am-243	1.5613E-05	2.7907E-05	3.8034E-05	3.8034E-05
Cm-242	9.7736E-07	2.6204E-06	4.0436E-06	5.0942E-09
Cm-243	1.2992E-08	6.4878E-08	1.3854E-07	1.2340E-07
Cm-244	2.6688E-06	9.2778E-06	1.8435E-05	1.5224E-05
Cm-245	1.2915E-07	8.1985E-07	2.1928E-06	2.1928E-06
Mo-95	No Data	No Data	No Data	No Data
Tc-99	No Data	No Data	No Data	No Data
Ru-101	No Data	No Data	No Data	No Data
Rh-103	2.0509E-05	3.7469E-05	5.1041E-05	5.1041E-05
Ag-109	4.6603E-06	8.0989E-06	1.0524E-05	1.0524E-05
Cs-133	2.3463E-05	4.4403E-05	6.2829E-05	6.2829E-05
Nd-143	1.6594E-05	3.1809E-05	4.5385E-05	4.5385E-05
Nd-145	1.1183E-05	2.1322E-05	3.0386E-05	3.0386E-05
Sm-147	8.2700E-07	2.4742E-06	4.1395E-06	9.9452E-06
Sm-149	4.3945E-07	4.1781E-07	3.7238E-07	4.2796E-07
Sm-150	5.0215E-06	1.0870E-05	1.6535E-05	1.6535E-05
Sm-151	1.5281E-06	1.8767E-06	1.9755E-06	1.8916E-06
Sm-152	2.8187E-06	5.0468E-06	6.4242E-06	6.4242E-06
Eu-153	2.2411E-06	5.4745E-06	8.6655E-06	8.6655E-06
Gd-155	1.6769E-08	2.8935E-08	4.2299E-08	1.0081E-06
k-infinity	1.05978	1.00753	0.961	0.91857
High			50.966	
Medium			41.784	
Low			37.668	
Assembly Ave.			47.996	

OECD/NEANSC Burnup Credit Benchmark, Phase IV-B (MOX)

Case 3 - First Recycle MOX, Assembly Model

CEA (Thiollay)
APOLLO2/PEPIN2 - CEA-93 based on JEF2.2 evaluations

Nuclide	End of Cycle 1	End of Cycle 2	End of Cycle 3	5 Years Cooling
U -234	5.7521E-07	8.2518E-07	1.0179E-06	2.6748E-06
U -235	4.3825E-05	3.4738E-05	2.6937E-05	2.7011E-05
U -236	2.5186E-06	4.4716E-06	5.9179E-06	6.1388E-06
U -238	2.1157E-02	2.0917E-02	2.0667E-02	2.0667E-02
Pu-238	4.1481E-05	3.9171E-05	3.9413E-05	4.1626E-05
Pu-239	8.0714E-04	6.4506E-04	5.1980E-04	5.2156E-04
Pu-240	4.7482E-04	4.5128E-04	4.1647E-04	4.2039E-04
Pu-241	2.1684E-04	2.3304E-04	2.3163E-04	1.8212E-04
Pu-242	1.3389E-04	1.4147E-04	1.5231E-04	1.5231E-04
Np-237	1.2206E-06	2.4144E-06	3.4853E-06	3.8866E-06
Am-241	8.6897E-06	1.5246E-05	1.8687E-05	6.7847E-05
Am-242m	1.3827E-07	3.2226E-07	4.2209E-07	4.1185E-07
Am-243	1.7356E-05	2.9837E-05	3.9436E-05	3.9436E-05
Cm-242	9.5415E-07	2.5215E-06	3.8393E-06	2.7151E-09
Cm-243	1.2966E-08	6.4908E-08	1.3889E-07	1.2375E-07
Cm-244	3.7951E-06	1.2517E-05	2.3817E-05	1.9671E-05
Cm-245	1.9612E-07	1.1882E-06	3.0345E-06	3.0333E-06
Mo-95	1.1834E-05	2.8767E-05	4.4787E-05	5.0765E-05
Tc-99	2.1921E-05	4.2288E-05	6.0943E-05	6.1176E-05
Ru-101	2.3054E-05	4.5186E-05	6.6364E-05	6.6366E-05
Rh-103	2.0064E-05	3.9239E-05	5.4581E-05	5.8014E-05
Ag-109	5.2444E-06	9.4844E-06	1.2993E-05	1.3008E-05
Cs-133	2.3867E-05	4.5475E-05	6.4493E-05	6.5039E-05
Nd-143	1.5508E-05	3.0346E-05	4.3452E-05	4.4325E-05
Nd-145	1.1518E-05	2.2191E-05	3.1988E-05	3.1999E-05
Sm-147	8.0249E-07	2.4525E-06	4.0902E-06	1.0607E-05
Sm-149	3.9254E-07	3.7684E-07	3.4511E-07	3.9940E-07
Sm-150	4.8280E-06	1.0327E-05	1.5706E-05	1.5706E-05
Sm-151	1.4035E-06	1.7138E-06	1.8212E-06	1.7636E-06
Sm-152	2.9820E-06	5.4446E-06	7.1033E-06	7.1049E-06
Eu-153	2.2080E-06	5.3823E-06	8.5860E-06	8.6362E-06
Gd-155	1.2599E-08	2.0400E-08	2.9866E-08	6.1487E-07
k-infinity	1.05624	0.99968	0.94869	0.90715
High			50.910	
Medium			41.960	
Low			37.612	
Assembly Ave.			48.000	

OECD/NEANSC Burnup Credit Benchmark, Phase IV-B (MOX)

Case 3 - First Recycle MOX, Assembly Model

GRS (Gmal)
KENOREST-2001 - KORLIB-V4 based on JEF2.2 evaluations

Nuclide	End of Cycle 1	End of Cycle 2	End of Cycle 3	5 Years Cooling
U -234	5.7410E-07	8.2000E-07	1.0060E-06	2.6800E-06
U -235	4.3720E-05	3.4500E-05	2.6620E-05	2.6690E-05
U -236	2.5730E-06	4.5460E-06	5.9750E-06	6.2030E-06
U -238	2.1160E-02	2.0920E-02	2.0670E-02	2.0670E-02
Pu-238	4.1630E-05	3.9340E-05	3.9530E-05	4.1600E-05
Pu-239	7.9700E-04	6.2980E-04	5.0530E-04	5.0710E-04
Pu-240	4.8300E-04	4.6350E-04	4.2870E-04	4.3260E-04
Pu-241	2.1520E-04	2.3210E-04	2.3200E-04	1.8330E-04
Pu-242	1.3420E-04	1.4200E-04	1.5330E-04	1.5330E-04
Np-237	1.3020E-06	2.5890E-06	3.7460E-06	4.1420E-06
Am-241	8.4140E-06	1.4680E-05	1.7960E-05	6.6320E-05
Am-242m	1.7480E-07	4.1790E-07	5.5400E-07	5.4150E-07
Am-243	1.7340E-05	3.0030E-05	3.9880E-05	3.9880E-05
Cm-242	9.2900E-07	2.4410E-06	3.6990E-06	2.8840E-09
Cm-243	1.1940E-08	5.9910E-08	1.2840E-07	1.1370E-07
Cm-244	3.6100E-06	1.2230E-05	2.3690E-05	1.9570E-05
Cm-245	1.5290E-07	9.7280E-07	2.5940E-06	2.5930E-06
Mo-95	1.1820E-05	2.8660E-05	4.4550E-05	5.0480E-05
Tc-99	2.3060E-05	4.4400E-05	6.3850E-05	6.4090E-05
Ru-101	2.2080E-05	4.3230E-05	6.3400E-05	6.3400E-05
Rh-103	1.9910E-05	3.8470E-05	5.3000E-05	5.6340E-05
Ag-109	5.9460E-06	1.0640E-05	1.4480E-05	1.4490E-05
Cs-133	2.4160E-05	4.5810E-05	6.4660E-05	6.5210E-05
Nd-143	1.5610E-05	3.0560E-05	4.3780E-05	4.4650E-05
Nd-145	1.1440E-05	2.2040E-05	3.1760E-05	3.1770E-05
Sm-147	8.0330E-07	2.4620E-06	4.1200E-06	1.0470E-05
Sm-149	4.0260E-07	3.8580E-07	3.5390E-07	4.0810E-07
Sm-150	4.7960E-06	1.0210E-05	1.5410E-05	1.5410E-05
Sm-151	1.4590E-06	1.7990E-06	1.9340E-06	1.8740E-06
Sm-152	3.1530E-06	5.9850E-06	7.9580E-06	7.9580E-06
Eu-153	2.0380E-06	5.0480E-06	8.2780E-06	8.3280E-06
Gd-155	1.1250E-08	2.1620E-08	3.5120E-08	7.4640E-07
k-infinity	1.05910	0.99909	0.94752	0.90325
High			51.024	
Medium			41.680	
Low			37.377	
Assembly Ave.			47.997	

OECD/NEANSC Burnup Credit Benchmark, Phase IV-B (MOX)

Case 3 - First Recycle MOX, Assembly Model

PSI (Grimm)
BOXER/ETOBOX - JEF-1/JEF-2

Nuclide	End of Cycle 1	End of Cycle 2	End of Cycle 3	5 Years Cooling
U -234	5.7512E-07	8.2480E-07	1.0163E-06	2.6658E-06
U -235	4.3762E-05	3.4601E-05	2.6747E-05	2.6747E-05
U -236	2.5521E-06	4.5243E-06	5.9787E-06	5.9787E-06
U -238	2.1158E-02	2.0917E-02	2.0666E-02	2.0666E-02
Pu-238	4.1593E-05	3.9255E-05	3.9412E-05	4.1388E-05
Pu-239	8.1074E-04	6.4958E-04	5.2512E-04	5.2693E-04
Pu-240	4.7491E-04	4.5167E-04	4.1661E-04	4.2046E-04
Pu-241	2.1629E-04	2.3380E-04	2.3378E-04	1.8365E-04
Pu-242	1.3464E-04	1.4278E-04	1.5439E-04	1.5440E-04
Np-237	1.6560E-06	3.2139E-06	4.5652E-06	4.9848E-06
Am-241	8.7832E-06	1.5571E-05	1.9269E-05	6.9036E-05
Am-242m	1.9036E-07	4.5414E-07	6.0712E-07	5.9239E-07
Am-243	1.6873E-05	2.9412E-05	3.9308E-05	3.9308E-05
Cm-242	8.7154E-07	2.3253E-06	3.5893E-06	3.0594E-09
Cm-243	1.1794E-08	5.8709E-08	1.2551E-07	1.1143E-07
Cm-244	3.4364E-06	1.1486E-05	2.2112E-05	1.8261E-05
Cm-245	1.6672E-07	1.0442E-06	2.7028E-06	2.7017E-06
Mo-95	1.7651E-05	3.4297E-05	4.9929E-05	4.9929E-05
Tc-99	2.1756E-05	4.1811E-05	6.0068E-05	6.0280E-05
Ru-101	2.2850E-05	4.4807E-05	6.5815E-05	6.5815E-05
Rh-103	2.0010E-05	3.9289E-05	5.4843E-05	5.8208E-05
Ag-109	5.2895E-06	9.6113E-06	1.3270E-05	1.3270E-05
Cs-133	2.3804E-05	4.5422E-05	6.4563E-05	6.5015E-05
Nd-143	1.5493E-05	3.0263E-05	4.3346E-05	4.4116E-05
Nd-145	1.1482E-05	2.2157E-05	3.2015E-05	3.2015E-05
Sm-147	8.0328E-07	2.4740E-06	4.1579E-06	1.0734E-05
Sm-149	4.1087E-07	3.8950E-07	3.5594E-07	4.0707E-07
Sm-150	4.9297E-06	1.0740E-05	1.6679E-05	1.6679E-05
Sm-151	1.3420E-06	1.5306E-06	1.5340E-06	1.4779E-06
Sm-152	2.8608E-06	5.0602E-06	6.3335E-06	6.3335E-06
Eu-153	2.2088E-06	5.2837E-06	8.2452E-06	8.2917E-06
Gd-155	1.2702E-08	2.0676E-08	3.0586E-08	6.0623E-07
k-infinity	1.06088	1.00618	0.95837	0.91826
High	17.057	34.053	50.978	
Medium	13.789	27.708	41.776	
Low	12.294	24.805	37.546	
Assembly Ave.	15.999	31.998	47.997	

OECD/NEANSC Burnup Credit Benchmark, Phase IV-B (MOX)

Case 3 - First Recycle MOX, Assembly Model

BNFL (O'Connor, Bowden, Thorne)
WIMS8A - 172-group WIMS '1997' JEF2.2 Nuclear Data Library

Nuclide	End of Cycle 1	End of Cycle 2	End of Cycle 3	5 Years Cooling
U -234	5.8216E-07	8.4354E-07	1.0509E-06	2.7220E-06
U -235	4.3925E-05	3.4893E-05	2.7129E-05	2.7206E-05
U -236	2.4858E-06	4.4215E-06	5.8610E-06	6.0776E-06
U -238	2.1155E-02	2.0911E-02	2.0657E-02	2.0657E-02
Pu-238	4.1519E-05	3.9292E-05	3.9688E-05	4.1989E-05
Pu-239	8.1275E-04	6.5524E-04	5.3435E-04	5.3613E-04
Pu-240	4.7109E-04	4.4499E-04	4.0836E-04	4.1217E-04
Pu-241	2.1962E-04	2.3790E-04	2.3767E-04	1.8687E-04
Pu-242	1.3484E-04	1.4345E-04	1.5546E-04	1.5546E-04
Np-237	1.1137E-06	2.2000E-06	3.1690E-06	3.2112E-06
Am-241	8.7598E-06	1.5505E-05	1.9170E-05	6.9979E-05
Am-242m	1.2244E-07	2.8821E-07	3.8216E-07	3.8216E-07
Am-243	1.6599E-05	2.8469E-05	3.7589E-05	3.7589E-05
Cm-242	9.8523E-07	2.6022E-06	3.9739E-06	1.6887E-09
Cm-243	1.3460E-08	6.7246E-08	1.4425E-07	1.2852E-07
Cm-244	3.7079E-06	1.2184E-05	2.3116E-05	1.9090E-05
Cm-245	1.9252E-07	1.1630E-06	2.9692E-06	2.9692E-06
Mo-95	1.1831E-05	2.8749E-05	4.4723E-05	5.0684E-05
Tc-99	2.2143E-05	4.2478E-05	6.1086E-05	6.1086E-05
Ru-101	2.2911E-05	4.4911E-05	6.5963E-05	6.5963E-05
Rh-103	2.0046E-05	3.9167E-05	5.4464E-05	5.7890E-05
Ag-109	5.2685E-06	9.5331E-06	1.3103E-05	1.3103E-05
Cs-133	2.3862E-05	4.5380E-05	6.4309E-05	6.4769E-05
Nd-143	1.5564E-05	3.0397E-05	4.3537E-05	4.4326E-05
Nd-145	1.1481E-05	2.2101E-05	3.1845E-05	3.1845E-05
Sm-147	8.0039E-07	2.4435E-06	4.0718E-06	1.0589E-05
Sm-149	3.9039E-07	3.7535E-07	3.4617E-07	3.9778E-07
Sm-150	4.7829E-06	1.0197E-05	1.5486E-05	1.5486E-05
Sm-151	1.4076E-06	1.7200E-06	1.8340E-06	1.7758E-06
Sm-152	2.9513E-06	5.3829E-06	7.0072E-06	7.0072E-06
Eu-153	2.1852E-06	5.3132E-06	8.4552E-06	8.5048E-06
Gd-155	1.2846E-08	1.9899E-08	2.7185E-08	6.2682E-07
k-infinity	1.049756	0.996539	0.949737	0.904088
High	17.071	34.069	50.988	
Medium	13.769	27.690	41.778	
Low	12.219	24.696	37.443	
Assembly Ave.	16.000	32.000	48.000	

OECD/NEANSC Burnup Credit Benchmark, Phase IV-B (MOX)

Case 3 - First Recycle MOX, Assembly Model

JAERI (Suyama)
MVP-BURN, JENDL-3.2, Continuous Energy

Nuclide	End of Cycle 1	End of Cycle 2	End of Cycle 3	5 Years Cooling
U-234	5.7489E-07	8.1934E-07	9.9952E-07	2.6318E-06
U-235	4.3905E-05	3.4829E-05	2.7040E-05	2.7116E-05
U-236	2.4930E-06	4.4327E-06	5.8628E-06	6.0806E-06
U-238	2.1161E-02	2.0922E-02	2.0671E-02	2.0671E-02
Pu-238	4.1368E-05	3.8820E-05	3.8846E-05	4.0979E-05
Pu-239	8.0812E-04	6.4771E-04	5.2533E-04	5.2711E-04
Pu-240	4.7323E-04	4.4755E-04	4.1078E-04	4.1461E-04
Pu-241	2.2011E-04	2.3979E-04	2.4058E-04	1.8891E-04
Pu-242	1.3438E-04	1.4244E-04	1.5431E-04	1.5432E-04
Np-237	1.1770E-06	2.3545E-06	3.4219E-06	3.8393E-06
Am-241	8.8762E-06	1.5982E-05	2.0066E-05	7.0845E-05
Am-242m	1.3756E-07	3.3843E-07	4.6346E-07	4.5301E-07
Am-243	1.6980E-05	2.9426E-05	3.8845E-05	3.8826E-05
Cm-242	8.9099E-07	2.4047E-06	3.7415E-06	2.6841E-09
Cm-243	1.1641E-08	6.0687E-08	1.3377E-07	1.1845E-07
Cm-244	3.6913E-06	1.2231E-05	2.3240E-05	1.9193E-05
Cm-245	1.9877E-07	1.2348E-06	3.2335E-06	3.2321E-06
Mo-95	No Data	No Data	No Data	No Data
Tc-99	2.2221E-05	4.2680E-05	6.1468E-05	6.1467E-05
Ru-101	2.1875E-05	4.2980E-05	6.3251E-05	6.3251E-05
Rh-103	2.2642E-05	4.0914E-05	5.5357E-05	5.5357E-05
Ag-109	No Data	No Data	No Data	No Data
Cs-133	2.4597E-05	4.6602E-05	6.6172E-05	6.6172E-05
Nd-143	1.5549E-05	3.0426E-05	4.3648E-05	4.4443E-05
Nd-145	1.1427E-05	2.2143E-05	3.2104E-05	3.2104E-05
Sm-147	No Data	No Data	No Data	No Data
Sm-149	3.9305E-07	3.7427E-07	3.4182E-07	3.9065E-07
Sm-150	4.7807E-06	1.0332E-05	1.5946E-05	1.5946E-05
Sm-151	1.4002E-06	1.6091E-06	1.6197E-06	1.5586E-06
Sm-152	2.9006E-06	5.2213E-06	6.6175E-06	6.6175E-06
Eu-153	2.1559E-06	5.1923E-06	8.1650E-06	8.1650E-06
Gd-155	5.8811E-09	1.0585E-08	1.8072E-08	3.3400E-07
k-infinity	1.05541	0.99749	0.95292	0.91676
High			51.004	
Medium			41.700	
Low			37.577	
Assembly Ave.			47.997	

OECD/NEANSC Burnup Credit Benchmark, Phase IV-B (MOX)

Case 3 - First Recycle MOX, Assembly Model

DTLR (O'Connor)
MONK8A - 172-group WIMS '1997' JEF2.2 Nuclear Data Library

Nuclide	End of Cycle 1	End of Cycle 2	End of Cycle 3	5 Years Cooling
U-234	2.1279E-07	1.7413E-07	1.4169E-07	1.4169E-07
U-235	4.3857E-05	3.4629E-05	2.6596E-05	2.6668E-05
U-236	2.5018E-06	4.4578E-06	5.9076E-06	6.1256E-06
U-238	2.1163E-02	2.0927E-02	2.0678E-02	2.0678E-02
Pu-238	4.0713E-05	3.5013E-05	2.9577E-05	2.8432E-05
Pu-239	8.0065E-04	6.3327E-04	5.0368E-04	5.0542E-04
Pu-240	4.7507E-04	4.5051E-04	4.1309E-04	4.1287E-04
Pu-241	2.1644E-04	2.3299E-04	2.3107E-04	1.8167E-04
Pu-242	1.3502E-04	1.4305E-04	1.5441E-04	1.5441E-04
Np-237	1.0400E-07	3.6114E-07	6.9348E-07	7.0645E-07
Am-241	8.6941E-06	1.5252E-05	1.8616E-05	6.8011E-05
Am-242m	1.4390E-07	3.3587E-07	4.3633E-07	4.3633E-07
Am-243	1.6074E-05	2.7797E-05	3.6793E-05	3.6793E-05
Cm-242	No Data	No Data	No Data	No Data
Cm-243	No Data	No Data	No Data	No Data
Cm-244	No Data	No Data	No Data	No Data
Cm-245	No Data	No Data	No Data	No Data
Mo-95	1.1828E-05	2.8749E-05	4.4743E-05	5.0706E-05
Tc-99	2.2139E-05	4.2498E-05	6.1130E-05	6.1130E-05
Ru-101	2.2897E-05	4.4899E-05	6.5960E-05	6.5960E-05
Rh-103	2.0073E-05	3.9256E-05	5.4560E-05	5.7983E-05
Ag-109	5.2687E-06	9.5091E-06	1.2998E-05	1.2998E-05
Cs-133	2.3866E-05	4.5420E-05	6.4368E-05	6.4828E-05
Nd-143	1.5552E-05	3.0350E-05	4.3375E-05	4.4163E-05
Nd-145	1.1477E-05	2.2103E-05	3.1849E-05	3.1849E-05
Sm-147	8.0403E-07	2.4617E-06	4.1041E-06	1.0635E-05
Sm-149	3.7767E-07	3.5930E-07	3.2302E-07	3.7494E-07
Sm-150	4.7846E-06	1.0201E-05	1.5508E-05	1.5508E-05
Sm-151	1.3972E-06	1.6804E-06	1.7554E-06	1.6976E-06
Sm-152	2.9625E-06	5.3781E-06	6.8758E-06	6.8758E-06
Eu-153	2.1826E-06	5.3538E-06	8.6212E-06	8.6716E-06
Gd-155	1.2499E-08	1.8707E-08	2.4619E-08	6.0517E-07
k-infinity	1.0590	1.0046	0.9510	0.9108
High	17.074	34.090	51.019	
Medium	13.747	27.624	41.689	
Low	12.292	24.747	37.473	
Assembly Ave.	16.000	32.000	48.000	

OECD/NEANSC Burnup Credit Benchmark, Phase IV-B (MO

Case 3 - First Recycle MOX, Assembly Model

ORNL (DeHart, Sanders)
SAS2D - 238-group ENDF/VI based Nuclear Data Library

Nuclide	End of Cycle 1	End of Cycle 2	End of Cycle 3
U-234	5.7170E-07	8.1280E-07	9.9100E-07
U-235	4.3730E-05	3.4590E-05	2.6800E-05
U-236	2.6190E-06	4.6370E-06	6.1140E-06
U-238	2.1160E-02	2.0910E-02	2.0660E-02
Pu-238	4.1300E-05	3.8680E-05	3.8550E-05
Pu-239	8.0920E-04	6.5000E-04	5.2840E-04
Pu-240	4.7570E-04	4.5190E-04	4.1650E-04
Pu-241	2.1670E-04	2.3410E-04	2.3350E-04
Pu-242	1.3480E-04	1.4340E-04	1.5550E-04
Np-237	No Data	No Data	No Data
Am-241	8.7380E-06	1.5530E-05	1.9330E-05
Am-242m	1.7520E-07	3.9650E-07	5.2310E-07
Am-243	1.8260E-05	3.1620E-05	4.2000E-05
Cm-242	8.8600E-07	2.3350E-06	3.5650E-06
Cm-243	1.4560E-08	7.0660E-08	1.4820E-07
Cm-244	3.9610E-06	1.3050E-05	2.4950E-05
Cm-245	1.7670E-07	9.7210E-07	2.2540E-06
Mo-95	1.1690E-05	2.8330E-05	4.3990E-05
Tc-99	2.1760E-05	4.1850E-05	6.0140E-05
Ru-101	2.1640E-05	4.2320E-05	6.1990E-05
Rh-103	1.9630E-05	3.8240E-05	5.2980E-05
Ag-109	5.7460E-06	1.0050E-05	1.3310E-05
Cs-133	2.3870E-05	4.5670E-05	6.5030E-05
Nd-143	1.5350E-05	2.9970E-05	4.2830E-05
Nd-145	1.1260E-05	2.1670E-05	3.1200E-05
Sm-147	7.8960E-07	2.4130E-06	4.0280E-06
Sm-149	4.2340E-07	4.1990E-07	3.8520E-07
Sm-150	5.1050E-06	1.1350E-05	1.7660E-05
Sm-151	1.5140E-06	1.8870E-06	2.0110E-06
Sm-152	2.7790E-06	5.1250E-06	6.7300E-06
Eu-153	2.1290E-06	5.1290E-06	8.1310E-06
Gd-155	4.3940E-09	7.9700E-09	1.3920E-08
k-infinity	1.0627E+00	1.0117E+00	9.6610E-01

Assembly model, first recycle MOX fuel

	Mean				Two Times Relative Standard Deviation (%)				
Nuclide	End of Cycle 1	End of Cycle 2	End of Cycle 3	5 Years Cooling	Nuclide	End of Cycle 1	End of Cycle 2	End of Cycle 3	5 Years Cooling
U-234	5.3087E-07	7.4396E-07	9.0555E-07	2.3439E-06	U-234	48.44	61.95	68.28	75.99
U-235	4.3814E-05	3.4675E-05	2.6824E-05	2.6879E-05	U-235	0.35	0.77	1.45	1.55
U-236	2.5323E-06	4.4920E-06	5.9329E-06	6.0982E-06	U-236	3.62	3.25	2.99	4.77
U-238	2.1159E-02	2.0918E-02	2.0668E-02	2.0668E-02	U-238	0.02	0.05	0.07	0.07
Pu-238	4.1328E-05	3.8499E-05	3.7946E-05	3.9688E-05	Pu-238	1.53	7.52	17.98	23.04
Pu-239	8.0622E-04	6.4353E-04	5.1881E-04	5.2060E-04	Pu-239	1.31	2.79	4.45	4.45
Pu-240	4.7521E-04	4.5118E-04	4.1501E-04	4.1831E-04	Pu-240	1.46	2.45	3.10	3.28
Pu-241	2.1747E-04	2.3504E-04	2.3447E-04	1.8434E-04	Pu-241	1.61	2.33	2.81	2.66
Pu-242	1.3495E-04	1.4355E-04	1.5566E-04	1.5566E-04	Pu-242	1.82	3.65	5.33	5.32
Np-237	1.1537E-06	2.2884E-06	3.3107E-06	3.5521E-06	Np-237	86.81	80.15	75.17	76.59
Am-241	8.7224E-06	1.5416E-05	1.9020E-05	6.8812E-05	Am-241	3.20	4.86	6.50	4.07
Am-242m	1.5209E-07	3.5904E-07	4.7621E-07	4.6744E-07	Am-242m	32.14	31.83	32.50	31.34
Am-243	1.6887E-05	2.9312E-05	3.8985E-05	3.8983E-05	Am-243	9.69	8.60	8.20	8.20
Cm-242	9.2775E-07	2.4643E-06	3.7788E-06	2.9962E-09	Cm-242	9.92	9.76	9.69	68.54
Cm-243	1.2765E-08	6.3857E-08	1.3679E-07	1.2149E-07	Cm-243	16.54	13.53	11.94	12.09
Cm-244	3.5529E-06	1.1854E-05	2.2766E-05	1.8806E-05	Cm-244	23.74	20.70	18.38	18.43
Cm-245	1.7327E-07	1.0564E-06	2.7115E-06	2.7107E-06	Cm-245	29.65	27.95	29.12	29.12
Mo-95	1.2776E-05	2.9592E-05	4.5454E-05	5.0389E-05	Mo-95	37.40	15.62	9.73	1.71
Tc-99	2.2143E-05	4.2572E-05	6.1241E-05	6.1371E-05	Tc-99	4.03	4.09	4.12	4.16
Ru-101	2.2472E-05	4.4048E-05	6.4678E-05	6.4678E-05	Ru-101	5.21	5.29	5.40	5.41
Rh-103	2.0360E-05	3.9006E-05	5.3853E-05	5.6380E-05	Rh-103	9.36	5.16	5.26	8.53
Ag-109	5.3462E-06	9.5610E-06	1.2954E-05	1.2959E-05	Ag-109	15.39	16.10	18.36	18.40
Cs-133	2.3936E-05	4.5523E-05	6.4553E-05	6.4926E-05	Cs-133	2.73	2.66	2.85	2.96
Nd-143	1.5653E-05	3.0515E-05	4.3669E-05	4.4382E-05	Nd-143	4.96	3.60	3.43	2.25
Nd-145	1.1409E-05	2.1966E-05	3.1643E-05	3.1647E-05	Nd-145	2.11	2.80	3.66	3.66
Sm-147	8.0430E-07	2.4544E-06	4.1016E-06	1.0469E-05	Sm-147	2.78	1.74	2.12	5.14
Sm-149	4.0375E-07	3.8735E-07	3.5294E-07	4.0626E-07	Sm-149	9.93	11.05	10.83	10.62
Sm-150	4.8785E-06	1.0528E-05	1.6116E-05	1.6116E-05	Sm-150	5.17	7.98	9.77	9.77
Sm-151	1.4314E-06	1.7271E-06	1.8106E-06	1.7482E-06	Sm-151	8.90	14.39	18.64	18.77
Sm-152	2.9260E-06	5.3305E-06	6.8812E-06	6.8815E-06	Sm-152	7.95	11.47	14.84	14.85
Eu-153	2.1686E-06	5.2721E-06	8.3934E-06	8.4302E-06	Eu-153	5.80	5.34	5.12	5.11
Gd-155	1.1118E-08	1.8599E-08	2.7708E-08	5.9725E-07	Gd-155	72.66	70.68	65.34	79.23